University of Alberta

Thermoelastic dissipation of micro/nano beam resonators

by

Kazi Md. Shammi Tunvir

A thesis submitted to the Faculty of Graduate Studies and Research
in partial fulfillment of the requirements for the degree of

Doctor of Philosophy

Mechanical Engineering

Spring 2013
Edmonton, Alberta

To my parents

Abstract

The work presented in this dissertation offers theoretical analysis of thermoelastic dissipation of micro/nano beam resonators operated with linear small-amplitude vibration or non-linear large-amplitude vibration under adiabatic or isothermal surface conditions. The aim is to find better design and better operating conditions for beam resonators of MEMS/NEMS for less thermoelastic dissipation. The beam resonators studied in this dissertation (which have not been studied in existing literature) include hollow tubular beams, solid beams of elliptical, triangular, or arbitrary rectangular cross-section, layered composite beams of circular and rectangular cross-sections, and stepped-beams of rectangular cross-section. For each case, detailed formulas are derived for quality factor (*Q-factor*) due to thermoelastic dissipation under adiabatic and isothermal surface conditions. In addition, thermoelastic dissipation in beam resonator of rectangular cross-section is analyzed for non-linear large-amplitude vibration under adiabatic or isothermal surface thermal condition with comparison to the results of small-amplitude linear vibration.

The obtained results offer useful guiding ideas for design of beam resonators to achieve higher *Q-factor* with thermoelastic dissipation. For example, the present results show that, to achieve higher *Q-factor*, hollow tubular resonators with isothermal and adiabatic surface conditions are best to operate at low and high

frequencies, respectively, as compared to beam resonators of solid circular or rectangular cross-section. Beam resonators of elliptical and triangular cross-sections are best to operate at high frequencies compared to solid rectangular cross-sections of same cross-sectional area and width irrespective of surface thermal conditions. In case of layered composite beams under either of the two surface thermal conditions, two-layered circular cross-sections is found better at high frequencies than three-layered rectangular cross-section of same material combination and layer sizes. Results for doubly-clamped stepped-beams show that a real beam resonator of rectangular cross-section with an undercut at a clamped end, known as a stepped-beam with single step having a change in cross-sectional size at the step in lateral direction only, provides higher *Q-factor* than a uniform beam of same thickness for all real lengths found in the literature. This dissertation also confirms that non-linear large-amplitude vibration is preferable over linear small-amplitude vibration for doubly-clamped beam resonators under adiabatic surface condition for which the *Q-factor* increases monotonically with amplitude of vibration, while the opposite is true under isothermal surface condition. The large-amplitude effect on thermoelastic dissipation becomes more significant for higher vibration frequencies than lower ones.

Acknowledgements

It has been a long voyage until I have reached to a point where I get the opportunity to thank people for their incessant best wishes, support, and encouragement for all the time. First, I wish to acknowledge gratefully the financial support of the Natural Science and Engineering Research Council of Canada throughout the entire program. I would like to thank my supervisor Professor Dr. C.Q. Ru and co-supervisor Professor Emeritus Dr. A. Mioduchowski for their countless help, support, and encouragement during the course of the research. I appreciate their insightful suggestions and advices and above all confidence that they had in me.

On this occasion, I want to remember my M.Sc. supervisor Dr. Amkee Kim (*late*) *affiliated to Kongju National University, Republic of Korea who died in 2009. His continuous encouragement made me interested in higher education and research.*

I wish to thank my group members Mr. Ming-Zhao Jin, Mr. Jie Chen and Mr. Jian Wu for creating such enjoyable and cooperative environment in the office that helped me to concentrate on the research. I was also fortunate to have made great friends during my stay at University of Alberta. I am grateful to Farzan, Amirreza, Oxana, Mohammad, Kim, Chongbo and Tamran for creating a friendly and supportive atmosphere in the graduate student office.

Specially I want to thank my wife "Nancy" for the mental support, comfort and encouragement that she provided me in the last four years based on which I got the

strength to accomplish this program. She literally gave up everything along with her study and career and came to abroad to be with me and to make my life easy by allowing me the time and space to finish the work without worrying about the reality of life. I hope I can keep the promise that I made to her of a better life. I thank to the Almighty for the miracle that happened in my life during this course of time, the birth of my little angel "Adriyah". She has changed my life, made me a better person, and given me the chance to start thinking about responsibilities of life.

Finally and foremost, my thoughts go to my parents, from whom everything of my life starts and reaches to its destination, who have always supported me in the choices I have made.

Edmonton, AB *Kazi Tunvir*
December 19 2012

Table of Contents

List of Tables

List of Figures

Nomenclatures and Symbols

Nomenclatures

D'_ω	Complex axial rigidity
D''_ω	Complex bending rigidity
$2a$	Major diameter of elliptical cross-section
$2b$	Minor diameter of elliptical cross-section
$2c$	Width of rectangular cross-section
$2d$	Height or thickness of rectangular cross-section
A	Area of the cross-section
C	Perimeter of the cross-section
C_V	Heat capacity per unit volume
D	Outer diameter
d_j	Distance of the outer surface of the j^{th} layer of composite beam of rectangular cross-section from neutral axis
E	Young's modulus
$E(\omega)$	Complex modulus of elasticity
E'	Dissipation (or loss) modulus
$e_n, g_n, k_n, m_n,$ o_n, p_n, q_n	Constant coefficients where n = 1,2,3,……
E_R	Relaxed Young's modulus
E_S	Surface elastic modulus
F	Spatial function for boundary curve of a cross-section
f	Space dependent part of deformation-induced temperature change from the initial uniform temperature
f'	Ordinary frequency (Hz)

G, H	Spatial function of Fourier series in the radial direction for circular cross-section
h	Height of the equilateral triangular cross-section
I	Second moment of cross-sectional area
i	Imaginary constant
I'	Moment of boundary curve C
Im	Imaginary part of a complex quantity
j	Layer number of composite beam
J	Normalizing factor for real amplitude (maximum) of vibration modes
k	Section number of stepped-beam
l	Length of the base of the triangular cross-section
L	Length of the beam
L_k	Length of k^{th} section of stepped-beam
M	Bending moment
M_{o}	Static bending moment
N_{x}	Resultant axial force
P, S, K	Integration constants
Q	Quality factor
r	Spatial coordinate in radial direction of polar coordinate system
R_1	Inner radius of annular cross-section
R_2	Outer radius of annular cross-section
Re	Real number
r_j	Radius of the j^{th} layer of layered composite beam of circular cross-section
s_1, s_2	Two functions of base length (l) and height (h) of triangular cross-section
t	Time
T	Temperature field
T_{o}	Initial uniform temperature
u	Axial displacement of the beam
$U_n, V_n, K'_1, K'_2, K'_3, K'_4,$	Constant functions for any particular mode of vibration that depend on the mode shape factor and mode constant

$K'_5, K'_6, K'_7,$ K'_8	
$u_{\alpha''}$	Components of displacement vector
W	Transverse deflection
W	Real amplitude (maximum) of vibration mode
w_k	Transverse deflection of the k^{th} section of the stepped-beam
w_o	Static transverse deflection
X	x-axis
$x_{\gamma''}$	Position vector
Y	y-axis
Z	z-axis
z	Distance to the neutral Y-axis
ΔT	Deformation-induced temperature change from the initial uniform temperature T_o

Greek Symbols

ϑ_1, ϑ_2	Fourier series index $\vartheta_1 = \vartheta_2 = 1,2,\ldots\ldots,\infty$
$\cdot$	Differential with respect to time
$\Delta\Phi$	Total lost mechanical work
$\Delta\Phi_\varsigma$	Energy loss corresponding to ς dissipation mechanism
α	Thermal expansion coefficient
α'', β'', γ''	Index (α'', β'', γ''= 1,2,3)
β_k	Eigenvalues for k^{th} section of stepped-beam appearing in its vibration in fundamental mode
β_n	Eigenvalue or mode constant appearing in the beam vibration problem corresponding to n^{th} mode of vibration
γ, μ	Normalized lengths of the two sections of the stepped-beam with single step
γ_o	Pre-existing surface tension
Δ	Kronecker delta
ε	Mean strain

ε^*	Residual compressive strain
ε_s	Surface axial strain
ε_{xx}	Axial strain
ε_{yy}	Transverse strain in y direction
ε_{zz}	Transverse strain in z direction
$\varepsilon_{\alpha''\beta''}$	Components of strain
ε_o	Strain under loading of static stress
ζ	Ratio of integration of square of curvatures of the bent sections over the length of the section in a stepped-beam with single step
η_n (n = 1,2,…)	Constant coefficients
Θ	Time dependent part of deformation-induced temperature change from the initial uniform temperature
θ	Spatial coordinate in angular direction of polar coordinate system
θ', α', Φ'	Constants that depends cross-sectional sizes of sections of stepped-beam with single step
κ	Thermal conductivity
λ	A variable that depends on resonant frequency of beam resonator
ν	Poisson's ratio
ξ	Normalized z coordinate over the cross-section
ξ'	Normalized axial coordinate
ρ	Density of the beam material
σ_s	Surface axial stress
σ_{xx}	Uniaxial stress
$\sigma_{\alpha''\beta''}$	Components of stress
σ_o	Static stress
τ	Thermal relaxation time constant
τ_ε	Relaxation time for stress under constant strain
τ_σ	Relaxation time for strain under constant stress
υ_1, υ_2	Indicating mechanics due to stretching and bending of beam respectively
φ	Created curvature of the bent beam
Φ_o	Stored vibrational energy
φ_o	Static created curvature of the bent beam

χ	Thermal diffusivity
ψ	Mode shape factors
ω	Circular frequency (rad sec^{-1})
Ω	Normalized vibration frequency
ω^*	Circular frequency corresponding to maximum dissipation
ω_L	Linear vibration frequency of beam
ω_{NL}	Non-linear vibration frequency of beam
ω_o	Resonant frequency
Γ	A factor of temperature field for layers in a layered composite beam that depends in materials properties, size of the layer and vibration frequency

Chapter 1

Introduction

1.1 Overview

Beam resonators have found broad application in a wide range of MEMS/NEMS as components of filters, oscillators and sensing application (Ekinci and Roukes 2005; Cimalla *et al.* 2007; Li and Hu 2011; Gil-Santos *et al.* 2009). They vibrate to generate resonance frequencies with higher amplitude or waves of specific frequency and can be used to select specific frequencies from a signal. Sizes of resonators in practical applications range from millimeter to nanometer scales with their vibrating capability ranging from MHz to 100 GHz respectively. Resonators of size in millimeter scale can be used in the off chip applications as quartz crystal with vibration in MHz range or of size in micrometer scale can have applications as system-on-chip (SoC) and system-in-package (SiP) with vibration in GHz range, for example, as monolithically integrated AIN switches (Mahameed *et al.* 2008). Nevertheless, at nanometer scale, resonators can be used as distributed sensor networks, single molecule detectors etc. with frequencies in the range of 100 GHz (Piazza 2010). Resonators are more promising for using in the small scale regimes because of their mass sensitivity and ability to detect surface densities based on

change in resonance frequency due to change in mass (Ekinci and Roukes 2005). A resonator of a small size has some advantages such as it becomes more defect free, compact, lighter, faster in response, cheaper to make, and above all, it needs less power to be operated (Lifshitz 2001). On the other hand, selection of material for a resonator based on less structural defects, high thermal and electrical conductivity, required optical properties, etc. is also crucial for high performance. Moreover, high frequency mechanical resonators presenting high performance are important for the development of sensitive devices, for example, a cantilever based resonator in scanning probe microscopy that is used in detecting the ultra small force between a tip and a surface (Kacem *et al.* 2009; Mailly *et al.* 2009; Gil-Santos *et al.* 2009).

However, for all these requirements of high speed, small size, appropriate materials with specific properties etc., sometimes the performance of resonators may have to be compromised. For higher performance, it is desirable to design and construct resonators with little loss of mechanical energy. In resonators, interruption in action or loss of energy during action, known as dissipation of energy, comes from external environmental issues and internal friction of the devices. Some of these external and internal desperados become more active in resonators with decreasing size – even if they are made from pure single crystal materials (Lifshitz and Roukes 2000). Thus for beam resonators, a relevant research topic of current interest is energy dissipation (Yasumura *et al.* 2000; Yang *et al.* 2002; Ekinci and Roukes 2005; Imboden *et al.* 2007) at the micro/nano scale.

Performance of a resonator is determined by *Q-factor* defined as (Yasumura *et al.* 2000; Yang *et al.* 2002)

$$Q = \frac{2\pi \Phi_{\circ}}{\Delta \Phi} \tag{1.1}$$

where Φ_o is the stored vibration energy and $\Delta\Phi$ is the total loss of mechanical energy per cycle of vibration given by $\Delta\Phi = \sum_{\varsigma} \Delta\Phi_{\varsigma}$. Here, $\Delta\Phi_{\varsigma}$ represents the energy loss due to various dissipation mechanisms. Energy loss mechanisms in resonator can be from many sources and are divided into two general classes such as extrinsic and intrinsic losses. Losses due to clamping of the beam structures, surrounding medium, gas damping etc. constitute the extrinsic losses while the intrinsic losses are occurred due to phonon-phonon interaction, phonon-electron interaction, thermoelastic effect, surface elasticity, surface defects etc. Thus, total dissipation or the summation of the inverse of *Q-factor*s due to different dissipation processes is given as (Yasumura *et al.* 2000; Yang *et al.* 2002)

$$\left(\frac{1}{Q}\right)_{Total} = \frac{1}{Q_{Medium}} + \frac{1}{Q_{Support}} + \frac{1}{Q_{TED}} + \frac{1}{Q_{Surface}} + \frac{1}{Q_{Other}} \tag{1.2}$$

Surrounding medium affects energy dissipation by creating barrier to heat transfer between resonator surface and the medium, for example, air, or gas (Blom *et al.* 1992). Loss due to surrounding medium increases rapidly as the resonator's surface-to-volume ratio increases. As the dissipation is directly related to the air or gas pressure, the pressure range (from high vacuum to atmospheric) can be divided into intrinsic, molecular and viscous regions. Negligible damping takes place in the intrinsic region, which is formally known as vacuum environment. In the molecular region, the dissipation is caused by independent collision of non-interacting air or gas molecules with the moving surface of the vibrating resonator (Blom *et al.* 1992). In the viscous region, air or gas acts as viscous fluid.

In high vacuum, i.e. the intrinsic region mentioned above, the energy dissipation due to a mechanical support could be significant. Mechanical coupling of the resonator structure with its supports causes the wave to propagate from the

device structure to the support, which is known as clamping, or support loss to the resonators. It is directly proportional to the width of the beam resonator while inversely proportional to the length of the resonators (Judge *et al.* 2007; Hosaka *et al.* 1995).

As an intrinsic loss mechanism, surface of the resonator structure can be a dominating part in energy dissipation that originates from the disruption of atomic lattice at the surface or due to thin layer of surface contamination (Ru 2009a; Yasumura *et al.* 2000; Lu *et al.* 2008; Seoánez *et al.* 2008). It has been seen from the literature that dissipation due to surface becomes significant if surface to volume ratio of the structure becomes very high, in other words, if the size of the structure goes down to nano scale (Yasumura *et al.* 2000; Seoánez *et al.* 2008; Ru 2009a). The size dependence of the elastic behavior and properties of solids at nano scale also arises due to this surface effect, which is the consequence of the imperfection of the coordination number in surface atoms compared to those that lie within the materials in bulk (Nix and Gao 1998) which, in turn, relax the remaining bonds of lower coordinated surface atoms. Coordination number of an central atom in a crystal or molecule is the number of nearest neighbor atoms and thus an imperfection in coordination number at the surface points to the termination of lattice periodicity (Guo and Zhao 2007). The percentage of surface atoms and therefore the percentage of atoms that have reduced coordination number increases with the increasing of surface area to volume ratio. The more the atoms with reduced coordination number or surface contamination on the surface of the structure, the structure is more susceptible to surface dissipation.

Dissipation due to phonon interactions can be categorized by the acoustic wave interactions with the thermal phonons and the mobile charges (Ayazi *et al.*

2011; Akhieser 1939; Landau and Rumer 1937). Interaction of an acoustic wave propagating in the resonator with the thermal lattice motions i.e. thermal phonons is known as phonon-phonon interaction. On the other hand, interaction of an acoustic wave propagating in semiconductors and metals with the mobile charges or electron is known as phonon-electron interaction. The process of restoring thermal equilibrium to the phonon gas is accompanied by energy dissipation from the acoustic wave. However acoustic dissipation due to phonon-phonon or phonon-electron interaction strongly depends on temperature and at low temperature where lattice vibrations are small, the resulting energy dissipation is negligible.

Thermoelastic dissipation is a major and inevitable dissipation mechanism among various intrinsic dissipation mechanisms in beam resonators (Lifshitz and Roukes 2000; Imboden *et al.* 2007). It occurs in any elastic material subjected to cyclic deformation, especially when the period of a cycle is approximately equal to the material's thermal relaxation time (Zener 1937). For example when an elastic flexural beam vibrates, most of the mechanical work is converted to elastic energy and some part of the work goes into thermal energy. While the elastic energy is always recoverable, the thermal energy is lost due to irreversible thermal conductivity. The lost thermal energy defines thermoelastic dissipation.

While dissipation due to support, surrounding medium, phonon-phonon and phonon-electron interaction in the resonator structures can be controlled by proper choice of the environment, materials, size, and careful design, thermoelastic dissipation and surface dissipation are often inevitable as they arise from the interior material defects/friction. Surface dissipation is essentially size dependent and becomes dominating at nano scale as seen in the literature (Yasumura *et al.* 2000). However, thermoelastic dissipation is always present in resonators of size

ranging from macro to nano scale (Yang *et al.* 2002), even if they are made from pure single crystal materials (Lifshitz and Roukes 2000).

In this dissertation, the author aims to study thermoelastic dissipation in beam resonators through the explorations of innovative geometries based on real structure under various practical operating conditions that suitable for next generation resonators in MEMS/NEMS with high quality factor due to thermoelastic dissipation.

1.2 Literature Review

1.2.1 Literatures on General Solutions of Thermoelastic Dissipation

In the last two decades, thermoelastic dissipation has been identified as a major dissipation mechanism for energy loss in a wide range of micro/nano mechanical resonators of MEMS/NEMS. Zener (1937) initiated the analysis of thermoelastic dissipation where stress-induced heat transfer in thermoelastic materials was discovered to be the main responsible factor for the loss of mechanical energy. In a series of analytical and experimental studies (Zener 1937, 1938, 1948), Zener investigated thermoelastic friction in thin structures based on one-dimensional theory of standard anelastic solid. However, the theory developed by Zener (1937, 1938) cannot describe the thermoelastic behavior of bodies of arbitrary form (Alblas 1961). Realizing the necessity of generalization of Zener's work (Zener 1937, 1938) for new evolving area of MEMS, Alblas (1961) developed a method for the solution of thermoelastic loss of three-dimensional problem based on the linear theory of elasticity where the conversion of mechanical energy into heat was

considered. Later Alblas extended his earlier works (Alblas 1961) for several boundary value problems of vibrating beams (Alblas 1981) and found that effects of thermoelastic dissipation are best observed in bars and wires. By the time Alblas published both of his works (Alblas 1961, 1981), following Zener's work, theory of thermoelastic dissipation has been developed by many other researchers by constructing exact solutions to the coupled equations of linear thermoelasticity in simpler geometries of infinite and semi-infinite thermoelastic bodies (Biot 1956; Deresiewicz 1957; Chadwick and Sneddon 1958; Lockett 1958), and analyzing thermoelastic waves in an infinite thin plate (Daimaruya and Naitoh 1987) or infinite rods of circular cross-section (Daimaruya and Naitoh 1982). Just after two decades of Alblas's study, Lifshitz and Roukes (2000) reinvestigated the problem of thermoelastic dissipation for thin resonator beams under flexure and developed exact solution to the coupled heat equation of linear thermoelasticity. Their results showed that the simplified classical results of Zener (1937, 1938) are very close to the exact solution under reasonably fair conditions.

Following Zener's work, most of the previous works on thermoelastic dissipation of elastic beam structures were limited to the resonators of thin-walled rectangular cross-section with a large width-to-thickness ratio. Few approximate solutions for thermoelasticity of beams with various cross-sectional shapes were developed such as for circular cross-section (Copper and Pilkey 2002; Jones 1966), however, dissipation due to thermoelastic effect was not considered in these approximate solutions. Their analysis ignored the role of thermal boundary conditions and simply could not satisfy a thermal surface condition prescribed along the boundary curve of the cross-section. Very recently, Ru (2009b) has developed a closed form solution of thermoelastic dissipation for thin beam resonators through

an approximate method by which thermoelastic dissipation can be calculated for different thermal surface conditions prescribed along the boundary curve of the cross-section.

1.2.2 Finite Element Modeling of Thermoelastic Dissipation

In recent years, following the exact solution of thermoelastic dissipation of Lifshitz and Roukes (2000) for thin flexure beams of rectangular cross-section, several finite element models (Choi *et al.* 2010; Ardito *et al.* 2008; Serra and Bonaldi 2009; Basak *et al.* 2011; Duwel *et al.* 2006) of thermoelastic dissipation for structures with arbitrary geometries have been developed using the complex frequency method in which thermoelastic dissipation is expressed in terms of a complex resonant frequency (Lifshitz and Roukes 2000). Among them, Choi *et al.* (2010), Ardito *et al.* (2008), and Serra and Bonaldi (2009) applied the finite element model to the flexural straight beams of rectangular cross-section, while Basak *et al.* (2011) analyzed the tapered and triangular beams for thermoelastic dissipation using the developed finite element models of Choi *et al.* (2010), Ardito *et al.* (2008), and Serra and Bonaldi (2009). Duwel *et al.* (2006) sought solution for thermoelastic dissipation in two different approaches called “fully coupled” and “weakly coupled” thermomechanical approaches. In the first approach, they solved the fully coupled thermomechanical equations that evaluate thermoelastic dissipation in both two and three-dimensions for arbitrary structures while the weakly coupled approach uses the eigenvalues and eigenvectors of the uncoupled thermal and mechanical dynamic equations to calculate damping. Both the approaches were implemented in finite element solver and were used to calculate thermoelastic dissipation for beams in flexural, longitudinal and torsional modes. However, implementing large

numerical models of FE analysis based on complex frequency method in finite element solver is computationally expensive for calculating thermoelastic dissipation. As a remedy of this issue, Hao *et al.* (2009) have suggested a finite element model based on the thermal energy method where the generation of thermal energy per cycle of the vibration is sought. As compared to the complex frequency method, the thermal energy method does not involve complex-frequencies and thus can be implemented easily in commercial FE tools and can be used with fast speed.

1.2.3 Application of Thermoelastic Dissipation Models to Various Specific Problems

For the last decade, many researchers have studied thermoelastic dissipation in MEMS/NEMS resonators of various specific geometries, that used in particular applications, employing the previously mentioned exact solution method (Lifshitz and Roukes 2000) or classical solution (Zener 1937, 1938), or finite element methods (Choi *et al.* 2010; Ardito *et al.* 2008; Serra and Bonaldi 2009; Basak *et al.* 2011; Duwel *et al.* 2006). Such geometries include resonator of thin ring structure (Wong *et al.* 2004; Yi 2008; Kim 2010), tunable MEMS mirrors (Tang *et al.* 2008), inextensional hemispherical shell (Choi *et al.* 2009), thin rectangular and circular plate structures (Norris and Photiadis 2005; Sun and Tohmyoh 2009; Li *et al.* 2012), cylindrical shell structures with application to tubular oscillator structures (Lu 2008), micro/nano scaled anisotropic beams (Sharma 2011), resonators with proof mass and a network of suspension beam (Li and Hu 2011), and so on. Houston *et al.* (2002) proposed a simple model for MEMS/NEMS

oscillators based on Zener's classical model (Zener 1937, 1938) and successfully predicted the internal friction of a high *Q-factor* microscopic oscillator based on the observation that resonant modes of oscillator structures always contain some flexural components. Prabhakar and Vengallatore (2008) used the method of exact solution (Lifshitz and Roukes 2000) of thermoelastic dissipation with consideration of two-dimensional heat conduction for beam resonators. However, effect of two-dimensional heat conduction on thermoelastic dissipation compared to one-dimensional heat conduction (Lifshitz and Roukes 2000) is found to be negligible for the thin flexural structure for a wide range of frequencies. Ardito and Comi (2009) modified the linear thermoelastic model with a nonlocal strain term incorporating internal characteristic material lengths and proposed a solution for thermoelastic dissipation of thin beams following the exact method of Lifshitz and Roukes (2000). The size-effects on the *Q-factor* of thin beams are explored using two constants such as a mechanical internal characteristic length and a thermal internal characteristic length in the formulations of the nonlocal moment of inertia and a coefficient respectively.

Among different resonator structures, beam resonators have been studied heavily because of their promising applications in MEMS/NEMS, structural simplicity, ease of handling and high *Q-factor* depending on size. However, development in the design of beam resonators for higher *Q-factor* continues. Few research groups explored for innovative designs of beam resonators to achieve components of high *Q-factor* of their MEMS/NEMS devices through the experiment and FE modeling. For example, introduction of trench, slots or channels have been considered in the design of micro/nano beam structures in order to alter their mechanical and thermal transport behaviors. Specifically, internal channels were

designed in the beam resonators to achieve a change in resonance frequency (Thomas *et al.* 2007) and slots were introduced in micromechanical beam resonators to alter the coupling between mechanical and thermal eigenmodes (Candler *et al.* 2006). Following these experiments, some approximate analytical solutions and FE modeling of thermoelastic dissipation have been offered for the aforementioned beam resonators (Abdolvand *et al.* 2003, 2006; Sairam and Vengallatore 2009). In specific, Abdolvand *et al.* (2003, 2006) modified Zener's thermoelastic dissipation model (Zener 1937, 1938) of transversely vibrating structures to extend its applicability towards flexure modes of trench-refilled resonators. Sairam and Vengallatore (2009) developed FE models to compute thermoelastic dissipation in flexure beam resonators containing structural discontinuities in the form of channels and slots. Their results showed that trenching in structures can shift the resonance frequency and slots in the beams can enhance the *Q-factor* by 3∼4 time. However, the process of trenching and slotting in beam structures of micro/nano scale were found challenging and expensive.

On the other hand, it has been seen that homogeneous thin beam resonators in MEMS/NEMS are often coated with the highly conductive metals. It is basically done so to enhance the optical and electrical properties of resonators (Ekinci and Roukes 2005; Cimalla 2007). However, at the same time coating or lamination may be proved undesirable for particular behaviors. Such results are found in the literature when thermoelastic dissipation is measured (Yoneoka *et al.* 2010) and numerically calculated (Bishop and Kinra 1993, 1994, 1997; Vengallatore 2005; Prabhakar and Vengallatore 2007) for such composites beam/plate resonators of MEMS devices considering them as layered composite structures with a perfect thermal contact between adjacent layers. Bishop and Kinra (1993) initiated the

study of thermoelastic dissipation in layered composite beam through exact theoretical solutions for beams under flexure and extension. Later they generalized their theory for thin flexural structures in (Bishop and Kinra 1994, 1997) and applied to the numerical analysis of thin plate under bending deformation. Later, Vengallatore (2005) and Prabhakar and Vengallatore (2007) used the developed theory of (Bishop and Kinra 1994, 1997) for the numerical analysis of thermoelastic dissipation in metal coated ceramic composite beam structures. In the theoretical analysis of Bishop and Kinra (1993, 1994, 1997), a perfect thermal contact between layers was assumed. Their results (Bishop and Kinra 1993, 1994, 1997; Vengallatore 2005; Prabhakar and Vengallatore 2007) showed that layered composite beam/plates experience higher thermoelastic dissipation than homogeneous structure, which is attributed to the interface dissipation.

1.2.4 Studies of Thermoelastic Dissipation under Various Loadings

Various types of loads that either produced naturally in resonator structure during fabrication (such as axial residual stress) or intentionally applied on resonator structures (such as static tensile force in axial direction) have been found to contribute in the reduction of thermoelastic dissipation of resonator structure (Verbridge *et al.* 2006; Kumar and Haque 2010; Vahdat and Rezezadeh 2011). An axial static stress on beam resonators does not reduce the loss of mechanical energy; however, the total stored energy and hence the resonance frequencies of the structure increase with the application of axial static stress along the axial direction. Axial loading also appears in electrostatically actuated clamped-clamped

beam/plate structure where midplane of the structure is stretched due to large-deformation induced by the attractive force of capacitive voltage as seen from the studies of Nayfeh and Younis (2004), Vahdat and Rezazadeh (2011), De and Aluru (2006), Hajnayeb *et al.* (2011), Zamanian and Khadem (2010), etc. In addition to the nonlinearity due to applied electrostatic charge, geometrical non-linearity is produced in the doubly-clamped structure due to large static deflection which in result produces an axial stretch in the beam due to the boundary condition. Nayfeh and Younis (2004) studied the effect of electrostatic magnitude on the *Q-factor* of the system by considering the electrostatic actuation as a linear function of microbeam deflection, while they neglected the midplane stretching due to large-deflection. In a similar study to Nayfeh and Younis (2004), De and Aluru (2006) considered the non-linear effect of electrostatic actuation, but neglected the midplane stretching term. Later, Vahdat and Rezazadeh (2011) carried out similar works for beam resonators but with the consideration of a static pre-stretching of the midplane. Analysis of thermoelastic dissipation in these works was carried out based on linearized small-amplitude vibration around the largely deflected static equilibrium position. The effect of the midplane stretching on thermoelastic dissipation in (Vahdat and Rezazadeh 2011) was found very small. All these works concluded that *Q-factor* due to thermoelastic dissipation in electrostatically actuated beam resonator decreases with the increase of actuating voltage. Zamanian and Khadem (2010) studied the same problem for the solution of thermoelastic dissipation in two-layered beam structure, however, without considering any thermal contact between the beam layers. Following Zamanian and Khadem (2010), Hajnayeb *et al.* (2011) studied thermoelastic dissipation in electrostatically actuated carbon nanotube (DWNT) resonators based on the linearized small-amplitude

vibration around a largely deflected static equilibrium position. Méndez *et al.* (2009) studied non-linear large-deflection effect on resonance frequencies and the decay rate of amplitude of some thermoelastically under-damped cantilever microbeams through FE modeling, without studying the effect of large-vibration on thermoelastic dissipation.

1.2.5 Experimental Studies of Thermoelastic Dissipation

In the last two decades, various resonator structures from simple beams to designed complex network of beam/plates have been subjected to the experimental analysis for the measurement of mechanical/electrical properties and thermoelastic dissipation of resonators. However, measurement of thermoelastic dissipation even with the most careful experimental setup is not an easy job. Because even if the measurements are done in sufficient vacuum environment and at room temperature with slender and thin structure to control dissipations due to air/gas, support, phonon-phonon interaction, phonon-electron interaction etc., dissipation due to thermoelastic effect combines with the surface dissipation and presents a total $1/Q$ as mentioned in Eq. (1.2). However, some experimental studies are worth of mentioning because the measurements in them were carried out with sufficient care for external environment, size and structure made of absolute pure material. For example, *Q-factor* due to thermoelastic dissipation or due to combined effect of several dissipation processes are measured in experimental works for micron and submicron thick cantilevers (Yasumura *et al.* 2000), for chemically etched single crystal silicon beam (Roszhart 1990), for micromechanical resonators of resonant frequencies from 500KHz to 10MHz (Candler *et al.* 2003), for doubly-clamped silicon beam (Yi *et al.* 2009), for micro scale resonators (Houston *et al.* 2004), for

GaAs micromechanical resonators (Okamoto *et al.* 2008), for Si-Ge alloy MEMS gyros (Duwel *et al.* 2003), for silicon tuning fork resonator under electrostatic actuation (Muller *et al.* 2009), for ultra thin single crystal silicon cantilevers (Yang *et al.* 2002), for silicon based micro-cantilevers (Lu *et al.* 2008), for Si flexural beam resonators (Foulgoc *et al.* 2006a, b), etc. For increasing *Q-factor* in experimental results with the decreasing size of resonator, the loss mechanism was assumed to be thermoelastic dissipation. On the other hand, decrease in *Q-factor* with decreasing thickness was thought to be dominated by surface loss mechanism. From most experimental studies of micro beam/plate resonators, at high vacuum, thermoelastic dissipation is found to be the dominating dissipation source with *Q-factor* up to 10^4 (Sepulveda *et al.* 2006). One important observation by Yang *et al.* (2002) is that the ultrathin cantilever beam resonators with thickness < 500 nm and length > 10 μm are not limited by thermoelastic loss while dissipation in cantilever beams of thicker than 500 nm and shorter than 10 μm are dominated by thermoelastic dissipation.

1.3 Justification of the Dissertation

1.3.1 Limitations in the Literatures – To the Date

For the last two decades, studies on thermoelastic dissipation based on the analytical modeling, FE modeling, experimental and numerical analyses have been accomplished for various resonator structures as observed from the aforementioned literature review. Among different resonator structures, slender beam resonators have been studied heavily and found to be the most popular resonator structure in MEMS/NEMS because of their simplicity, ease of handling and

availability through micromachining and various fabrication processes of MEMS/NEMS.

Thermoelastic dissipation in beam resonator has been studied heavily so far for thin rectangular cross-sectional geometry. Very few works can be found in the literatures that offer innovative ideas for modification of the existing beam resonators, or innovative designs for beam geometries that can replace the existing beams, or effective operating conditions for existing beam resonators that contribute in the reduction of thermoelastic dissipation in them. However, worth to mention, modification in beam resonators of rectangular cross-section such as introduction of internal channels or trench (Thomas 2007) and slots (Candler *et al.* 2006) were considered before in the body of micro/nano beam structures to change the resonance frequency and to alter the coupling between mechanical and thermal eigenmodes. High expense and complicacy involved in the design process of channels, slots in beams at micro/nano scale could not be justified against the achieved results. Therefore, existing literature has the deficiency in offering a simple design for next generation high frequency beam resonators that contribute to a significant reduction in thermoelastic dissipation.

In the endeavor, it has been noticed that the effect of cross-sectional shape of beam resonators on thermoelastic dissipation has never been studied before. Thermoelastic dissipation in a beam resonators is solely due to the evolved thermal field that occurs over a cycle of its vibration while the thermal field in a beam resonator is essentially dependent to the cross-sectional size and shape of the beam. Interestingly, micro and nano beams with elliptical, triangular, or rectangular cross-sections have been reported in the literature, for example, in (Hu *et al.* 2003; Yuan *et al.* 2006; Urban *et al.* 2008; Gradečak *et al.* 2005; Nam *et al.* 2006; Bi *et al.* 2010;

Liang *et al.* 2010). Moreover, as grown solid circular and thick-wall hollow tubular micro/nano beam structures are also present in the literature, for example, in (Stan *et al.* 2007; Zhou *et al.* 2009; Cheng *et al.* 2009; Zhao and Lei 2009). However, the analysis of thermoelastic dissipation in these beam structures of different cross-sectional shapes has never been a topic for study in the literature. Besides the homogeneous beams, layered composite beams of doubly-symmetric rectangular cross-section and axi-symmetric circular cross-section at micro and nano scale also have been reported in the literature (Czekalla *et al.* 2009; Kim *et al.* 2008; Senthil *et al.* 2009; Wang and Adhikari 2011). Nevertheless, very recently stepped-beams, produced by various micromachining techniques, are already found in real applications as resonator in MEMS/NEMS devices, for example, in (Mamin 2007; Behreyni and Shafai 2006; Wang *et al.* 2006; etc.). Besides that, beam resonators with an undercut at the clamped end, which are distinguished as stepped-beams, have been found to be produced due to isotropic itching of the supporting substrate during fabrication as a release process of the beam (Gavan *et al.* 2009a, b; Herrera-May *et al.* 2011). Despite their technical relevancies, till to date, no systematic study of thermoelastic dissipation has been carried out for layered composite beam resonators of circular cross-section, and stepped-beams.

On the other hand, application of axial static stress on beam resonators or a naturally occurred axial residual stress in the structure during fabrication reduces thermoelastic dissipation in beam resonators as seen from the studies of Verbridge *et al.* (2006), Kumar and Haque (2010) and Vahdat and Rezezadeh (2011). The amount of tensile force that applied to these micro/nano beam structures in the numerical examples (Kumar and Haque 2010; Vahdat and Rezezadeh 2011) had no experimental validation. Moreover, it may not be always possible to apply axial

tensile force on the beam resonator in a compact design of MEMS/NEMS devices. On the other hand, axial stretch of the midplane of a clamped-clamped beam resonator can also be produced in the beam during non-linear large-amplitude vibration. Moreover, in next generation ultrahigh-frequency resonators of MEMS/NEMS, non-linear large-deflection vibration is practically evident (Peng *et al.* 2006; Bunch 2007; Masmanidis *et al.* 2007; Eom *et al.* 2011) which may contribute in a reduction of thermoelastic dissipation of the beam. In addition, recent finding also confirms that mass detection sensitivity of micro/nano beam resonator can be increased by non-linear large vibration (Eom *et al.* 2011). However, no systematic study on thermoelastic dissipation under non-linear vibration with large-deflection has been found so far in the literature.

Surface thermal condition is one of the most important factors, which controls thermoelastic dissipation in a beam resonator. However, only adiabatic surface thermal condition has been used so far in the analysis of thermoelastic dissipation of beam resonator. An isothermal surface condition which can be expected for a denser external medium has never been considered in the studies of thermoelastic dissipation of resonators.

1.3.2 Goals of the Dissertation

A high *Q-factor* is the primary demand for uninterrupted performances of a beam resonator. A high frequency resonator (Husain *et al.* 2003) with high performance at micro/nano scale is appropriate for the next generation sensitive applications. The objective of the thesis is to explore for innovative designs or new geometries and effective operating conditions for next generation beam resonators based on the available real structures and practical operating conditions that offer a

high *Q-factor* due to thermoelastic dissipation. The following goals are set for this dissertation:

i. Thermoelastic dissipation in hollow tubular beams

Hollow tubular beams (Stan *et al.* 2007; Zhou *et al.* 2009) at micro/nano scales are available in the literature, which are produced through various fabrication processes or micromachining techniques. The hollowed section in a hollow tubular beam is through the axial direction. Thermal field of a hollow tubular beam will be much different from a beam of solid cross-section because of its inner and outer surfaces. Moreover, resonance frequency of a hollow beam is much higher than a solid beam of same outer size for any mode of vibration and the resonance frequencies of hollow tubular beams increase as the wall thickness decreases. Therefore, thermoelastic dissipation in a hollow tubular beam resonator will be studied in this dissertation with comparison to the results of thermoelastic dissipation in beam resonators of solid circular and solid rectangular cross-section.

ii. Effect of cross-sectional shapes on thermoelastic dissipation

In this dissertation, effect of cross-sectional shape and size of beam resonator on thermoelastic dissipation will be investigated based on practically available beam geometries. The available beam geometries of different cross-sectional shapes at micro/nano scales would include micro/nanowires elliptical cross-sections (Hu *et al.* 2003; Yuan *et al.* 2006; Urban *et al.* 2008), micro/nanowires of triangular cross-sections (Gradečak *et al.* 2005; Nam *et al.* 2006; Agrawal *et al.* 2009), micro/nanowires of rectangular cross-section with moderate width-to-thickness ratio (Bi *et al.*

2010; Liang *et al.* 2010). Elastic bending deflection and vibration analysis of these beam resonators of symmetric or doubly symmetric cross-sections can be studied assuming the Eular-Bernoulli beam model. However, the thermal fields in each beam that coupled to the deformation field will be different from other due to different cross-sectional shapes for the beams. Therefore, thermoelastic dissipation in beam resonators of elliptical, triangular, and arbitrary rectangular cross-sections will be studied with comparison to the results for thin rectangular cross-section of equivalent size.

iii. Thermoelastic dissipation of layered composite beams

Investigation of cross-sectional effect on thermoelastic dissipation has been extended to layered composite beam resonators too. For the last two decades, metal coated beam resonators, known as layered composite beams (Bishop and Kinra 1993, 1994, 1997; Vengallatore 2005; Prabhakar and Vengallatore 2007), have come into discussion for their enhanced optical and electrical properties and applications (Ekinci and Roukes 2005; Cimalla 2007). Results from various experimental (Yoneoka *et al.* 2010) and analytical (Bishop and Kinra 1993, 1994, 1997; Vengallatore 2005; Prabhakar and Vengallatore 2007) works on thermoelastic dissipation of layered composite beams showed that they experience higher thermoelastic dissipation than homogeneous beam of same size, which is attributed to interface dissipation. However, rectangular cross-section have been considered so far for all of these layered composite beam resonators. In this case, this dissertation introduces the layered composite beam of circular cross section based on real structures (Czekalla *et al.* 2009; Kim *et al.* 2008; Arslan *et al.* 2008; Liu *et al.* 2010; Senthil *et al.* 2009; Huang *et al.* 2006;

Wang and Adhikari 2011) as the next generation high frequency member of beam resonators. Therefore, thermoelastic dissipation in layered composite beams of circular cross-section will be studied here with comparison to the layered composite beam resonators of rectangular cross-section assuming a perfect thermal contact between adjacent layers of both the cross-sections.

iv. Thermoelastic dissipation in stepped-beams

Cross-sectional size in slender beam can be varied in two different ways such as continuous variation of cross-sectional size along the length and variation of cross-sectional size at different locations along the length of the beam. The latter one is known as stepped-beam. Recently beam resonators of rectangular cross-section with stepped configuration have become very popular in MEMS/NEMS for their enhanced properties and real applications, for example, in sensing mechanical motion to allow MEMS sensors to be capable of measuring high frequency (Mamin 2007), in estimation of material properties (Behreyni and Shafai 2006), in detecting protein (Varshney *et al.* 2009), and viruses (Ilic *et al.* 2004) as MEMS/NEMS resonators, etc. Besides the designed stepped-beam resonators, beam resonators of rectangular cross-section with an undercut at the clamped end have also been characterized as stepped-beams in the literatures (Gavan *et al.* 2009a, b; Herrera-May *et al.* 2011). An undercut in a beam resonator of MEMS/NEMS is produced during fabrication when supporting substrate is isotropically etched as a part of release process of the beam. Resonance frequency as well as modal shape of a stepped-beam is different from that of a beam of uniform cross-section and they vary with the number and positions of steps along the beam length. Thus, it is to be interesting to find

optimum step positions and best orientation of rectangular cross-section at the step in respect of high *Q-factor* due to thermoelastic dissipation. Therefore, thermoelastic dissipation of stepped-beam resonator of rectangular cross-section will be studied with an emphasis on the effect of step position and orientation of cross-section at the step on thermoelastic dissipation.

v. Thermoelastic dissipation under non-linear large-vibration

Non-linear large-deflection vibration is practically evident in the next generation in ultrahigh-frequency resonators of MEMS/NEMS (Peng *et al.* 2006; Bunch 2007; Masmanidis *et al.* 2007; Eom *et al.* 2011). Non-linear effects in micro/nano beam resonators can arise from different sources including large-deflection (geometrical non-linear effect), material non-linear effect, etc. Due to geometrical non-linear effect, an axial stretching of the midplane is occurred in doubly-clamped beam resonators during non-linear large-deflection. The axial stretching of the beam resonator will be constant along the beam length, but will vary with time or the amplitudes of vibration. Therefore, the effect of amplitude of non-linear large-vibration on thermoelastic dissipation will be investigated in this thesis with comparison to thermoelastic dissipation of beam resonators under linear small vibration.

vi. Effect of surface thermal conditions on thermoelastic dissipation

Moreover, each aforementioned problem of thermoelastic dissipation will be solved separately for both adiabatic and isothermal surface conditions. Surface thermal conditions depend on heat transfer between the beam and the surrounding medium. An adiabatic condition can be expected in vacuum (ignoring radiation losses) while isothermal condition can be expected for a

denser external medium. In isothermal surface condition, temperature remains constant on the surface of the beam, while the adiabatic surface condition requests that normal gradient of temperature field vanishes on the surface.

1.4 References

Abdolvand R., Ho G. K., Erbil A. and Ayazi F. 2003. Thermoelastic damping in trench-refilled polysilicon resonators. *Transducer '03: The 12th International Conference on Solid State Sensors, Actuators and Micro Systems* 324-327.

Abdolvand R., Johari H., Ho G. K., Erbil A. and Ayazi F. 2006. Quality factor in trench-refilled polysilicon beam resonators. *Journal of Microelectromechanical Systems* **15** 471-478.

Agrawal B. K., Pathak A., Agrawal S. 2009. Abs initio study of [001] GaN nanowires. *Journal of Nanoparticle Research* **11** 841-859.

Akhieser A. 1939. On the absorption of sound in solids. *Journal of Physics* **4** 277-287.

Alblas J. B. 1961. On the general theory of thermo-elastic friction. *Applied Science Research* **10** 349-362.

Alblas J. B. 1981. A note on the theory of thermoelastic damping. *Journal of Thermal Stresses* **4** 333-355.

Ardito R., Comi C. 2009. Nonlocal thermoelastic damping in microelectromechanical resonators. *Journal of Engineering Mechanics* **135** 214-220.

Ardito R., Comi C., Corigliano A., Frangi A. 2008. Solid damping in micro electro mechanical systems. *Meccanica* **43** 419-428.

Arslan I., Talin A. A., Wang G. T. 2008. Three-dimensional visualization of surface defects in core-shell nanowires. *Journal of Physical Chemistry C* **112** 11093-11097.

Ayazi F., Sorenson L., Tabrizian R. 2011. Energy dissipation in micromechanical resonators. Proceedings of SPIE: *Micro- and Nanotechnology Sensors, Systems and Appication III* **8031** 803119.

Basak A. Nandakumar K., Chatterjee A. 2011. Decoupled three-dimensional finite element computation of thermoelastic damping using Zener's approximation. *Meccanica* **46** 371-381.

Behreyni B., Shafai C. 2006. Application of twin-beam structures for estimation of material properties and sensor fabrication. *Canadian Journal of Electronics and Computer Engineering* **31** 85-88.

Bi Y., Hu H., Lu G. 2010. Highly ordered rectangular silver nanowire monolayers: water-assisted synthesis and galvanic replacement reaction with HAuCl4. *Chemical Communications* **46** 598-600.

Biot M. 1956. Thermoelasticity and irreversible thermodynamics. *Journal of Applied Physics* **27** 240-253.

Bishop J. E. and Kinra V. K. 1993. Thermoelastic damping of a laminated beam in flexure and extension. *Journal of Reinforced Plastics and Composites* **12** 210.

Bishop J. E. and Kinra V. K. 1994. Elastothermodynamic damping in composite materials. *Mechanics of Composite Materials and Structures* **1** 75-93.

Bishop J. E. and Kinra V. K. 1997. Elastothermodynamic damping in laminated composites. *International Journal of Solids and Structures* **34** 1075-1092.

Blom F. R., Bouwstra S., Elwenspoek M., Fluitman J. H. J. 1992. Dependence of the quality factor of micromachined silicon beam resonators on pressure and geometry. *Journal of Vacuum Science and Technology* **B10** 19-26.

Bunch J. S. 2007. Electromechanical resonators from graphene sheets. *Science* **315** 490.

Candler R. N., Li H., Markuz L., Park W.-T., Partridge A., Yama G., Kenny T. W. 2003. Investigation of energy loss mechanisms in micromechanical resonators.

Transducer 03: the 12th International Conference on Solid State Sensors, Actuators and Microsystems 332-334.

Candler R. N.., Amy D., Mathew V., Saurabh A. C., Matthew A. H., Woo-Tae P., Bongsang K., Gary Y., Aaron P., Markus L. and Thomas W. K. 2006. Impact of geometry on thermoelastic dissipation in micromechanical resonant beams. *Journal of Microelectromechanical Systems* **15** 927-934.

Chadwick P. and Sneddon I. 1958. Plane waves in an elastic solid conducting heat. *Journal of Mechanics and Physics of Solids* **6** 223-230.

Cheng Y., Zhang J., Zhang Y., Chen X., Wang Y., Ma H. and Cao X. 2009. Preparation of hollow carbon and silicon carbide fibers with different cross-sections by using electrospun fibers as templates. *European Journal of Inorganic Chemistry* **28** 4248-4254.

Choi J., Cho M., Rhim J. 2010. Efficient prediction of the quality factors of micromechanical resonators. *Journal of Sound and Vibration* **329** 84-95.

Choi S. Y., Na Y. H. and Kim J. H. 2009. Thermoelastic damping of inextensional Hemispherical shell. *World Academy of Science, Engineering and Technology* **56** 198-203.

Cimalla V., Niebelschütz F., Tonisch K., Foerster Ch., Brueckner K., Cimalla I., Friedrich T., Pezoldt J., Stephan R., Hein M., Ambacher O. 2007. Nanoelectromechanical devices for sensing applications. *Sensors and Actuators B* **126** 24-34.

Copper C. D., Pilkey W. D. 2002. Thermoelasticity solutions for straight beams. Transaction of the ASME. *Journal of Applied Mechanics* **69** 224-229.

Czekalla C., Sturm C, Schmidt-Grund R, Cao B., Zúñiga Pérez J., Lorenz M., and GrundmannM. 2009. Optical characterization of zinc oxide microlasers and

microwire core-shell heterostructures. *Journal of Vacuum Science Technology B* **27** 1780-1783.

Daimaruya M. and Naitoh M. 1982. Dispersion and energy dissipation of thermoelastic waves in a circular cylinder. *Acustica* **51** 2 124-130.

Daimaruya M. and Naitoh M. 1987. Dispersion and energy dissipation of thermoelastic waves in a plate. *Journal of Sound and Vibration* **117** 511-518.

De S. K. and Aluru N. R. 2006. Theory of thermoelastic damping in electrostatically actuated microstructures. *Physical Review B* **74** 14305.

Deresiewicz H. 1957. Plane waves in a thermoelastic solid. *The Journal of the Acoustical Society of America* **29** 204-209.

Duwel A., Candler R. N., Kenny T. W., Varghese M. 2006. Engineering MEMS resonators with low thermoelastic damping. *Journal of Microelectromechanical Systems* **15** 1437-1445.

Duwel A., Gorman J., Weinstein M., Borenstein J., Ward P. 2003. Experimental study of thermoelastic damping in MEMS gyros. *Sensors and Actuators A* **103** 70-75.

Ekinci K. L., Roukes M. L. 2005. Nanoelectromechanical systems. *Review of Scientific Instruments* **76** 061101.

Eom K., Park H. S., Yoon D. S. and Kwon T. 2011. Nanomechanical resonators and their applications in biological/chemical detection: nanomechanics principles. *Physics Reports* **503** 115-163.

Foulgoc B L, Traon O., Masson S., Parent A., Bourouina T., Marty F., Bosseboeuf A., Parrain F., Mathias H., Gilles J. P. 2006b. High-Q silicon flexural resonators for vibrating inertial sensors: investigation of the limiting damping mechanisms. *IEEE Sensors* 1365-1368.

Foulgoc B., Bourouina T., Traon O., Bosseboeuf A., Marty F., Breluzeun C., Grandchamp J. P., Masson S. 2006a. Highly decoupled single-crystal silicon resonators: an approach for the intrinsic quality factor. *Journal of Micromechanics and Microengineering* **16** S45.

Gavan K. B., Drift E. W. J. M. van der, Venstra W. J., Zuiddam M. R., Zant H. S. J. van der 2009a. Effect of undercut on the resonant behavior of silicon nitride cantilevers. *Journal of Micromechanics and Microengineering* **19** 035003.

Gavan K. B., Westra H. J. R., Drift E. W. J. M. van der, Venstra W. J., Zant H. S. J. van der 2009b. Impact of fabrication technology on flexural resonances of silicon nitride cantilevers. *Microelectronics Engineering* **86** 1216-1218.

Gil-Santos E., Ramos D., Jana A., Calleja M., Raman A. and Tamayo J. 2009. Mass sensing based on deterministic and stochastic responses of elastically coupled nanocantilevers. *Nano Letters* **9** 4122-4127.

Gradečak S., Qian F., Li Y., Park H. G., Lieber C. M. GaN nanowire lasers with low lasing thresholds. *Applied Physics Letters* **87** 173111.

Guo J. G., Zhao Y. P. 2007. The size dependent bending elastic properties of nanobeams with surface effects. *Nanotechnology* **18** 295701.

Hajnayeb A., Khadem S. E., Zamanian M. 2011. Thermoelastic damping of a double-walled carbon nanotube under electrostatic force. *Micro & Nano Letters* **6** 698-703.

Hao Z., Xu Y., Durgam K. 2009. A thermal-energy method for calculating thermoelastic damping in micromechanical resonators. *Journal of Sound and Vibration* **322** 870-882.

Herrera-May A. L., García-Ramírez P. J., Aguilera-Cortés L. A., Plascencia-Mora H., García-González L., Manjarrez E., Narducci M., Figueras E. 2011. Analytical

Modeling for the Bending Resonant Frequency of Sensors Based on Micro and Nanoresonators With Complex Structural Geometry. *IEEE Journal of Sensors* **11** 1361.

Hosaka H., Itao K., Kuroda S. 1995. Damping characteristics of beam-shaped micro oscillators. *Sensors and Actuator A* **49** 87-95.

Houston B. H., Photiadis D. M., Marcus M. H., Bucaro J. A., Liu X., Vignola J. F. 2002. Thermoelastic loss in microscale oscillators. *Applied Physics Letters* **80** 1300-1302.

Houston B. H., Photiadis D. M., Vingola J. F., Marcus M. H., Liu X., Czaplewski D., Sekarik L., Butler J., Pehrsson P., Bucaro J. A. 2004. Loss due to transverse thermoelastic currents in microscale resonators. *Materials Science and Engineering A* **370** 407-411.

Hu J., Bando Y., Liu Z., Sekiguchi T., Golberg D., Zhan J. 2003. Epitaxial Heterostructures: Side-to-Side Si–ZnS, Si–ZnSe Biaxial Nanowires, and Sandwichlike ZnS–Si–ZnS Triaxial Nanowires. *Journal of American Chemical Society* **125** 11306-11313.

Huang L., Lau S. P., Yang H. Y., Yu S. F. 2006. Local measurement of secondary electron emission from ZnO-coated carbon nanotubes. *Nanotechnology* **17** 1564-1567.

Husain A., Hone J., Henk W., Ch. Postma, Huang X. M. H., Drake T., Barbic M., Scherer A., Roukes M. L. 2003. Nanowire-based very-high-frequency electromechanical resonator. *Applied Phyiscs Letters* **83**(6), 1241.

Ilic B., Yang Y., Craighead H. G. 2004. Virus detection using nanoelectromechanical devices. *Applied Physics Letters* **85** 2604.

Imboden M., Mohanty P., Gaidarzhy A., Rankin J., Sheldon B. W. 2007. Scaling of dissipation in megahertz-range micromechanical diamond oscillators. *Applied Physics Letters* **90** 173502.

Jones J. P. 1966. Thermoelastic vibration of a beam. *The Journal of the Acoustical Society of America* **39** 542-548.

Judge J. A., Photiadis D. M., Vignola J. F., Houston B. H., Jarzynski J. 2007. Attachment loss of micromechanical and nanomechanical resonators in the limits of thick and thin support structures. *Journal of Applied Physics* **101**(1) 013521.

Kacem N., Hentz S., Pinto D., Reig B. and Nguyen V. 2009. Non-linear dynamics of nanomechanical beam resonators: improving the performance of NEMS-based sensors. *Nanotechnology* **20** 275501.

Kim S.-B., Na Y.-H., Kim J.-H. 2010. Thermoelastic damping effect on in-extensional vibration of rotating thin ring. *Journal of Sound and Vibration* **329** 1227-1234.

Kim W. H., Lee W. J. and Shim S. H. 2008. Composite nanowires with MgO/ZnO core-sheath structures: study of thin ZnO shell layers. *Journal of Physics and Chemistry of Solids* **69** 1491-1494.

Kumar S., Haque M. A. 2010. Stress-dependent thermal relaxation effects in micro-mechanical resonators. *Acta Mechanica* **212** 83-91.

Landau L. D. and Rumer G. 1937. On the absorption of sound in solids. *Physics Z. Sowjetunion* **4** 277-287.

Li P., Fang Y., Hu R. 2012. Thermoelastic damping in rectangular and circular microplate resonators. *Journal of Sound and Vibration* **331** 721-733.

Li P., Hu R. 2011. Thermoelastic damping in micromechanical resonators with a proof mass and a network of suspension beams. *Japanese Journal of Applied Physics* **50** 077202.

Liang G., Huang W., Koong C. S., Wang J. S., Lan J. 2010. Geometry effects on thermoelectric properties of silicon nanowires based on electronic band structures. *Journal of Applied* Physics **107** 014317.

Lifshitz R. 2001. Nanomechanics: What is it all about? *Nanotechnology Forum* 16-18

Lifshitz R. and Roukes M. L. 2000. Thermoelastic damping in micro- and nanomechanical systems. *Physical Review B* **61** 5600-5609.

Liu J., Wang C., Xie Q., Cai J., Zhang J. 2010. Hierarchical Cd_4SiS_6/SiO_2 heterostructures nanowire arrays. *Nanoscale Research Letters* **5** 231-236.

Lockett F. 1958. Effect of thermal properties of a solid on the velocity of Rayleigh waves. *Journal of Mechanics and Physics of Solids* **7** 71-75.

Lu J., Ikehara T., Zhang Y., Mihara T., Maeda R. 2008. Mechanical quality factor of microcantilevers for mass sensing applications. *Proceedings of SPIE* **6800** 68991Y1.

Lu P., Lee H. P., Lu C., Chen H. B. 2008. Thermoelastic damping in cylindrical shells with application to tubular oscillator structures. *International Journal of Mechanical Sciences* **50** 501-512.

Mahameed R., Sinha N., Pisani M. B., Piazza G. 2008. Dual-Beam Actuation of Piezoelectric AlN RF MEMS Switches Monolithically Integrated with AlN Contour-Mode Resonators. *Journal of Micromechanics and Microengineering* **18** (10) 105011

Mailly F., Dumas N., Pous N., Latorre L., Garel O., Martincic E., Verjus F., Pellet C., Dufour-Gergam E. and Nouet P. 2009. Pirani pressure sensor for smart wafer-level packaging. *Sensors and Actuators A* **156** 201-207.

Mamin J. 2007. Nanosensors: small strains, big gains. *Nature Nanotechnology* **2** 81-82.

Masmanidis S. C., Rassul B. K., Iwijn D. V., Gustaaf B., Mark R. F. and Roukes M. L. 2007. Multifunctional nanomechanical systems via tunably coupled piezoelectric actuation. *Science* **317** 780.

Méndez C., Paquay S., Klapka I. and Raskin J. P. 2009. Effect of geometrical non-linearity on MEMS thermoelastic damping. *Non-linear Analysis: Real World Applications* **10** 1579-1588.

Muller C., Baborowski J., Pezous A., Dubois M.-A. 2009. Experimental evidence of thermoelastic damping in silicon tuning fork. *Procedia Chemistry* **1** 1395-1398.

Nam C. Y., Jaroenapibal P., Tham D., Luzzi D. E., Evoy S., Fischer J. E. 2006. Diameter-dependent electromechanical properties of GaN nanowires. *Nano Letters* **6** 153-158.

Nayfeh A. H., Younis M. I. 2004. Modeling and simulations of thermoelastic damping in microplates. *Journal of Micromechanics and Microengineering* **14** 1711.

Nix W. D., Gao H. 1998. An atomistic interpretation of interface stress. *Scripta Materialia* **39(12)** 1653-1661.

Norris A. N., Photiadis D. M. 2005. Thermoelastic relaxation in elastic structures, with applications to thin plates. *Q. JI. Mechanics and Applied Mathematics* **58** 143-163.

Okamoto H., Ito D., Onomitsu K., Yamaguchi H. 2008. Thermoelastic damping in GaAs micromechanical resonators. *Physica Status Solidi C* **5** 2920-2922.

Peng H. B., Chang C. W., Aloni S., Yuzvinsky T. D. and Zettl A. 2006. Ultrahigh frequency nanotube resonators. *Physical Review Letters* **97** 087203.

Piazza G. 2010. Alumimun nitride piezoelectric NEMS resonators and switches. *Proc. SPIE 7679, Micro- and Nanotechnology Sensors, Systems, and Applications II*, 76791L. doi:10.1117/12.849989.

Prabhakar S. and Vengallatore S. 2007. Thermoelastic damping in bilayered micromechanical beam resonators. *Journal of Micromechanics and Microengineering* **17** 532-538.

Prabhakar S., Vengallatore S. 2008. Theory of thermoelastc damping in micromechanical resonators with two-dimensional heat conduction. *Journal of Microelectromechanical Systems* **17** 492-502.

Roszhart T. V. 1990. The effect of thermoelastic internal friction on the Q of micromachined silicon resonators. *IEEE Sensors* 13-16.

Ru C. Q. 2009a. Size effect of dissipative surface stress on quality factor of microbeams. *Applied Physics Letters* **94(5)** 051905.

Ru C. Q. 2009b. Thermoelastic dissipation of nanowire resonators with surface stress. *Physica E* **41** 1243-1248.

Sairam P. and Vengallatore S. 2009. Thermoelastic damping in hollow and slotted microresonators. *Journal of Microelectromechanical Systems* **18** 725-735.

Senthil K., Tak Y., Seol M., Yong K. 2009. Synthesis and characterization of ZnO nanowire-CdO composite nanostructures. *Nanoscale Research Letters* **4** 1329-1334.

Seoánez C., Guinea F., Castro Neto A. H. 2008. Surface dissipation in nanoelectromechanical systems: Unified description with the standard tunneling model and effects of metallic electrodes. Physical Review B **77** 125107.

Sepulveda N., Aslam D., Sullivan J. P. 2006. Polycrystalline diamond MEMS resonator technology for sensor applications. *Diamond Related Materials* **15** 398-403.

Serra E., Bonaldi M. 2009. A finite element formulation for thermoelastic damping analysis. *International Journal o Nuemrical Methods in Engineering* **78** 671-691.

Sharma J. N. 2011. Thermoelastic damping and frequency shift in Micro/Nanoscale anisotropic beams. *Journal of Thermal Stresses* **34** 650-666.

Stan G., Ciobanu C. V., Parthangal P. M. and Cook R. F. 2007. Diameter-dependent radial and tangential elastic moduli of ZnO nanowires. *Nano Letters* **7** 3691-3697.

Sun Y., Tohmyoh H. 2009. Thermoelastic damping of the axi-symmetric vibration of circular plate resonators. *Journal of Sound and Vibration* **319** 392-405.

Tang H., Yi Y. B., Matin M. A. 2008. Predictive modeling of thermoelastic energy dissipation in tunable MEMS mirrors. *Journal of Micro/nanolithography. MEMS MOEMS* **7** 023004.

Thomas P. B., Michel G., Scott M. K., Wenjiang S., Greg C., John S. F., Ken B. and Scott R. M. 2007. Weighing of biomolecules, single cells and single nanoparticles in fluid. *Nature letters* **446** 1066.

Urban D. F., Bürki J., Zhang C. H., Stafford C. A., Grabert H. 2008. Jahn-Teller distortions and the supershell effect in metal nanowires. *Physical Review Letters* **93** 186403.

Vahdat A. S. and Rezazadeh G. 2011. Effect of axial and residual stresses on thermoelastic damping in capacitive micro-beam resonators. *Journal of the Franklin Institute* **348** 622-639.

Varshney M., Waggoner P. S., Montagna R. A., Craighead H. J. 2009. Prion protein detection in serum using micromechanical resonator arrays. *Talanta* **80** 593-599.

Vengallatore S. 2005. Analysis of thermoelastic damping in laminated composite micromechanical beam resonators. *Journal of Micromechanics and Microengineering* **15** 2398-2404.

Verbidge S. S., Parpia J. M., Reichenbach R. B., Bellan L. M., Craighead H. G. 2006. High quality factor resonance at room temperature with nanostrings under high tensile stress. *Journal of Applied physics* **99** 124304.

Wang C. Y. and Adhikari S. 2011. ZnO-CNT composite nanotubes as nanoresonators. *Physics Letters A* **375** 2171-2175.

Wang L., Phillips S. M., Branicky M. S., Bayraktar B. 2006. Nano-resonators for RF-enabled networked-control. *J of Physics: Conference Series* **38** 158-162.

Wong S. J., Fox C. H. J., McWilliam S., Fell C. P., Eley R. 2004. A preliminary investigation of thermo-elastic damping in silicon ring. *Journal of Micromechanics and Microengineering* **14** S108-S113.

Yang J., Ono T., Esashi M. 2002. Energy dissipation in submicrometer thick single-crystal silicon cantilevers. *Journal of Microelectromechanical Systems* **11** 775-783.

Yasumura K. Y., Stowe T. D., Chow E. M., Pfafman T., Kenny W. T., Stipe B. C., Rugar D. 2000. Quality factor in micros- and submicron-thick cantilevers. *Journal of Microelectromechanical Systems* **9** 117-125.

Yi Y.-B. 2008. Geometric effects on thermoelastic damping in MEMS resonators. *Journal of Sound and Vibration* **309** 588-599.

Yi Y.-B., Rhafrooz A., Pourkamali S. 2009. Modeling and testing of the collective effects of thermoelastic and fluid damping on Silicon MEMS resonators. *Journal Micro/Nanolithographic MEMS/MOEMS* **8** 023010.

Yoneoka S., Roper C.S., Candler R.N., Chandorkar S.A., Graham A.B., Provine J., Maboudian R., Howe R.T., Kenny T.W. 2010. Characterization of encapsulated micromechanical resonators sealed and coated with polycrystalline SiC. *Journal of Microelectromechanical Systems* **19** 357-366.

Yuan G. H., Wang P., Zhang D., Jiao X., Ming H. 2006. Extraordinary transmission through elliptical gold nanowire grating under s-polarization excitation. *International Symposium on Biophotonics, Nanophotonics and Metamaterials* 370-372.

Zamanian M. and Khadem S. E. 2010. Analysis of thermoelastic damping in microresonators by considering the stretching effect. *International Journal of Mechanical Sciences* **52** 1366-1375.

Zener C. 1937. Internal friction in solids. I. Theory of internal friction in reeds. *Physical Review* **52** 230-235.

Zener C. 1938. Internal friction in solids II. General theory of thermoelastic internal friction. *Physical Review* **53** 90-99.

Zener C. 1948. Elasticity and anelasticity of metals. *The University of Chicago Press*, Chicago, Illinois.

Zhou S. M., Wan P., Li S., Zhang B., Gong H. C. and Zhang X. T. 2009. Superconducting single crystalline MgB_2 nanotubes. *Materials Letters* **63** 1680-1682.

Zhao Y. and Lei J. 2009. Hollow micro/nanomaterials with multilevel interior structures. *Advanced Materials* **21** 3621-3638.

Chapter 2

Background and Existing Theories

2.1 Thermoelastic Dissipation

In thermoelastic solids, the strain and temperature fields are coupled. Due to the change in temperature, volume changes, when the volume changes due to the elastic deformation, the temperature changes. Thermal expansion coefficient is the constant that relates the change in length to the change in temperature of a material. When a body is elastically deformed (with volume change), thus increasing its potential energy, and is allowed to oscillate freely, the body gradually loses its potential energy and return to its stable equilibrium even if it does not exchange energy with the environment for example by air drag, friction etc. One fundamental mechanism that responsible for this dissipation is known as thermoelastic dissipation wherein the potential energy is converted to heat. If the body is thermally isolated from its surroundings, thermoelastic dissipation leads to an increase in its temperature. Thermoelastic dissipation can be discussed from some different but equivalent standpoints, such as –

i. Firstly, a view that is related to the loss of mechanical energy (Zener 1937; Roszhart 1990) of solid structure. In general, the stress field in a vibrating body is non-uniform and hence some regions become hotter relative to others due to temperature-deformation coupling which generates a temperature gradient into the material. The deviation of temperature from a standard reference temperature in a thermoelastic material is related to two parameters such as stress and strain where strain or deformation in an thermoelastic material depends on stress and temperature. The generated temperature gradient produces a thermal strain field that is out of phase with the applied stress field. The thermal strain field is due to the temperature-deformation coupling represented by the coefficient of thermal expansion of the material. This phase difference in applied stress and strain is used to estimate the conversion of mechanical energy into heat. This particular energy conversion process is irreversible and is manifested as a loss of mechanical work. This process of energy dissipation is known as thermoelastic dissipation.

ii. Secondly, the above-mentioned description of thermoelastic dissipation is actually the process of entropy generation due to strictly internal irreversibility in a system of vibrating body (Kinra and Milligan 1994). Due to inhomogenities in the stress field during vibration, local temperature gradients are created in the body, which leads to an irreversible heat conduction from regions of high temperature to regions of low temperature. In the process, defined by the second law of thermodynamics, entropy is generated which is manifested as a conversion of useful mechanical energy into heat (Kinra and Milligan 1994). As the total energy of the system

remains constant, this increase in entropy has to come at the cost of potential (strain)/kinetic energy of the system. The resulting dissipation mechanism is known as thermoelastic dissipation.

In general, a thermoelastic problem consists of sixteen unknown functions of position $x_{\gamma''}$.and time t such as six-stress components $\sigma_{\alpha''\beta''}$, six strain components $\varepsilon_{\alpha''\beta''}$, three components of the displacement vector $u_{\alpha''}$, and the temperature T. Four sets of equations governing these quantities are (Kovalenko 1969)

i. the six stress-strain relations

$$\sigma_{\alpha''\beta''} = \frac{E}{1+\nu}\varepsilon_{\alpha''\beta''} + \left[\frac{\nu E \varepsilon_{\gamma''\gamma''}}{(1+\nu)(1-2\nu)} - \frac{E\alpha(T-T_\circ)}{(1-2\nu)}\right]\delta_{\alpha''\beta''} \tag{2.1}$$

ii. the six strain-deformation relations

$$\varepsilon_{\alpha''\beta''} = \frac{1}{2}\left[u_{\alpha'',\beta''} + u_{\beta'',\alpha''}\right] \tag{2.2}$$

iii. three equations of motion

$$\sigma_{\alpha''\beta'',\beta''} = \rho\ddot{u}_{\alpha''} \tag{2.3}$$

iv. the heat conduction equation

$$C_V\dot{T} + \alpha T\dot{\sigma}_{\gamma''\gamma''} = \kappa T_{,\alpha''\alpha''} \tag{2.4}$$

where $\sigma_{\gamma''\gamma''} = \sigma_{xx} + \sigma_{yy} + \sigma_{zz}$ is the hydrostatic stress, T is the temperature field given by $T(x,y,z,t) = T_\circ + \Delta T(x,y,z,t)$, ΔT is the deformation-induced temperature change from the initial uniform temperature $T_\circ$, C_V is the heat capacity per unit volume, κ is the thermal conductivity, α is the thermal expansion coefficient, and E and ν are the Young's modulus and Poisson's ration of the bulk material. Thus, sixteen unknowns are determined by the sixteen equations (Eqs. (2.1)-(2.4)). The vibration mode is determined by the equation of motion upon application of end conditions of the structure.

Temperature-deformation coupling that responsible for thermoelastic dissipation is governed by the coupled heat conduction equation (Eq. (2.4)). The coupled heat conduction equation (Eq. (2.4)) can also be expressed in terms of mean strain produced due to the applied stress $\sigma_{\gamma''\gamma''}$ as follows (Bishop and Kinra 1993, 1997; Lifshitz and Roukes 2000; Ru 2009)

$$C_V \dot{T} + \frac{E\alpha T}{1-2\nu}\dot{\varepsilon}_{\gamma''\gamma''} = \kappa T_{,\alpha''\alpha''} \tag{2.5}$$

where $\varepsilon_{\gamma''\gamma''} = \varepsilon_{xx} + \varepsilon_{yy} + \varepsilon_{zz}$ is the mean strain. The first term on the left hand side is the rate of change of stored thermal energy in the system while the second term on the left hand side represents the volumetric rate of thermal energy generation or a heat source in the system. Without this term the rest of the equation is just linear heat conduction equation of Fourier Law. The term on the right hand side of Eq. (2.5) represents the rate of energy transfer into a unit volume by conduction at any point in the system. According to Eq. (2.5), the stress field affects the temperature field, and in result temperature field affects the stress field. However, the relative temperature change resulting from the thermoelastic effect is very small in most crystalline solids and thus the thermal stress produced by these small changes in temperature can be assumed negligible compared to the applied stress (Bishop and Kinra 1993, 1997). Therefore, following Bishop and Kinra (1993, 1997), the stress field is assumed to be independent of temperature. In what follows, T of the temperature-deformation coupling term (second term on the left hand side) in Eq. (2.5) is replaced with $T_\circ$ and the heat equation is changed to

$$C_V \dot{T} + \frac{E\alpha T_\circ}{1-2\nu}\dot{\varepsilon}_{\gamma''\gamma''} = \kappa T_{,\alpha''\alpha''} \tag{2.6}$$

By doing so, the non-linear coupled heat conduction equation converts into linear one-way coupled heat conduction equation; thereby reduce the algebraic complicacy of heat conduction equation.

Thermoelastic dissipation is essentially controlled by the surface thermal condition over the structure. The thermal boundary condition associated with the thermoelastic problem may be adiabatic or isothermal depending on the condition of heat transfer with the surrounding environment. An adiabatic condition can be expected in vacuum (ignoring radiation losses) while isothermal condition can be expected for a denser external medium. In isothermal surface condition temperature remains constant on the surface of the beam, while the adiabatic surface condition requests that normal gradient of temperature field vanishes on the surface.

2.2 Complex Modulus Method

Dissipation in mechanical systems is defined by the inverse of *Q-factor*, which is the ratio of mechanical energy lost per cycle to total stored elastic (strain) energy such as (Zener 1937)

$$\frac{1}{Q}=\frac{1}{2\pi}\frac{(Energy\ loss)/cycle}{Total\ elastic\ energy} \tag{2.7}$$

The loss of energy in each cycle can be calculated by analyzing the required energy supply for each cycle for a perfect periodic motion. In this dissertation, the dissipation due to internal friction or material dissipation is calculated through “complex-modulus” method. The complex modulus method is briefly discussed here for an infinitesimal material element which is vibrating with circular frequency ω. It has been assumed that a periodical stress is needed to apply on the material

element for a real periodical strain such that $\sigma(t)=\sigma_\circ e^{-i\omega t}$ and $\varepsilon(t)=\varepsilon_\circ e^{-i\omega t}$, where $\varepsilon_\circ$ (x) is a real number and ω is the circular frequency. The required energy supply for each cycle (between $t=0$ and $t=2\pi/\omega$) for a perfect periodic motion over the volume of the material element is (Zener 1937, 1938)

$$Energy\ \ loss\ per\ cycle=\int_0^{2\pi/\omega} Re[\sigma]Re\left[\frac{d\varepsilon}{dt}\right]dt \tag{2.8}$$

Under the condition of static loading, the modulus of elasticity is defined as $E=\sigma_\circ/\varepsilon_\circ$. When dynamic loading in the form of vibration is applied, the internal friction resists the exciting force. The resisting internal friction causes a phase shift between stress and strain under steady state vibration condition. Thus, the elastic modulus, $E(\omega)$ depends on frequency, ω and holds a complex form such that $E(\omega)=E+iE'$ where $E(\omega)$ is the complex modulus of elasticity, E is the elastic (or storage) modulus i.e. the conventional (real valued) Young's modulus and E' is the dissipation (or loss) modulus (Zener 1937, 1938). The revised stress-strain relation is $\sigma_\circ=[E+iE']\varepsilon_\circ$ where $\sigma_\circ$ is a complex quantity. This means that the stress will include a component that is 90 degree out of phase with strain, which is responsible for the internal dissipation and thus represents an energy loss

$$\int_0^{2\pi/\omega} Re[\sigma]Re\left[\frac{d\varepsilon}{dt}\right]dt=-\pi\, Im[E(\omega)]\,\varepsilon_\circ^{\,2} \tag{2.9}$$

This indicates that the imaginary part of complex modulus of elasticity $E(\omega)$ determines the energy loss per cycle of vibration. Defining the total elastic energy over the volume of the material element as $Re[E(\omega)]\,\varepsilon_\circ^{\,2}/2$, the inverse of the *Q-factor* given by Eq. (2.7) can be expressed as the ratio of imaginary to real part of the complex modulus such that

$$\frac{1}{Q}=-\frac{Im[E(\omega)]}{Re[E(\omega)]} \tag{2.10}$$

2.3 Surface Thermal Conditions

The temperature field in the body of a resonator can be obtained form the heat conduction equation (Eq. (2.6)) upon satisfying the physical conditions existing on the boundary surface of the body. Surface thermal conditions depend on heat transfer between the body and the surrounding medium. Two typical cases of surface thermal conditions, adiabatic and isothermal conditions are considered in this dissertation. An adiabatic condition can be expected in vacuum (ignoring radiation losses) while isothermal condition can be expected for a denser external medium. An adiabatic surface condition requests that normal gradient of the temperature field ΔT vanishes on all surfaces such that

$$\left.\frac{\partial \Delta T}{\partial n}\right|_{Along\ the\ boundary\ surface} = 0 \tag{2.11}$$

For isothermal surface condition, temperature field ΔT remains constant on all the surfaces of the body such that

$$\left.\Delta T\right|_{Along\ the\ boundary\ surface} = 0 \tag{2.12}$$

2.4 Existing Theories of Thermoelastic Dissipation in Beams

Thermoelastic dissipation is a major dissipation mechanism for energy loss in a large range of micro/nano mechanical resonators (Zener 1937, 1938; Lifshitz and Roukes 2000; Yasumura *et al.* 2000; Mohanty *et al.* 2002; Yang *et al.* 2002; Imboden *et al.* 2007). Two most popular and heavily cited solutions (Zener 1937, 1938; Lifshitz and Roukes 2000) of thermoelastic dissipation for beam resonators of thin

rectangular cross-section will be described briefly in this chapter. Zener (1937, 1938) was the first to realize the importance of thermoelastic dissipation in vibrating reeds, wires etc. and introduced the concept of relaxation time, τ through an anelastic model of stress-strain. In his work, it was assumed that the interior dissipation in deformable solids is associated essentially with a difference in the phases between applied stress and resulting strain, which is described best by the relaxation time τ. A simple model for interior dissipation based on a generalized stress-strain relation of standard linear solid was offered (Zener 1937, 1938)

$$\sigma + \tau_{\varepsilon} \frac{d\sigma}{dt} = E_R \left[\varepsilon + \tau_{\sigma} \frac{d\varepsilon}{dt} \right] \tag{2.13}$$

where E_R is the relaxed Young's modulus, τ_{ε} is the relaxation time for stress under the condition of constant strain, and τ_{σ} is the relaxation time for strain under constant stress. Detailed identification of these two relaxation times depends on the physical mechanism of dissipation, for example, for the present case of thermoelastic dissipation, they are represented by thermal relaxation time constants that are needed to allow the temperature gradient in the body of the structure to relax. In Zener's approach, the governing heat conduction equation is solved for one-dimensional heat conduction. For a beam of thickness 2d, operated at resonance frequency ω, the classical closed form formula for thermoelastic dissipation given by Zener (1937, 1938) is

$$\left(\frac{1}{Q}\right)_{Zener\,(1937,\,1938)} = \frac{E\alpha^2 T_{\circ}}{C_V} \frac{\Omega}{1+\Omega^2} \tag{2.14}$$

where Ω is the normalized frequency given by $\Omega = \left(4\omega d^2 C_V\right)/\left(\pi^2 \kappa\right)$, C_V is the heat capacity per unit volume, α is the thermal expansion coefficient, E is the Young's modulus of the bulk material and κ is the thermal conductivity, ω is the fundamental vibration frequency and d is the half of the beam thickness.

Following Zener's works, Kinra and Milligan (1994) and Lifshitz and Roukes (2000), in recent past, have independently developed exact solution which is equivalent to the closed form solution of Zener (1937, 1938). The most cited closed form expression from exact solution for thermoelastic dissipation in flexural beam resonator of thin rectangular cross-section of thickness 2*d* is given as (Lifshitz and Roukes 2000)

$$\left(\frac{1}{Q}\right)_{\text{Lifshitz \& Roukes (2000)}} = \frac{E\alpha^2 T_\circ}{C_V}\left[\frac{6}{\lambda^2} - \frac{6}{\lambda^3}\frac{\sinh\lambda + \sin\lambda}{\cosh\lambda + \cos\lambda}\right] \tag{2.15}$$

where $\lambda = d\sqrt{(2\omega_\circ C_V)/\kappa}$ and $\omega_\circ$ is the frequency corresponding to normal mode of vibration. To calculate the effect of thermoelastic coupling on the vibration of a thin beam in flexure, they solved the coupled thermoelastic equations such as equation of motion (Eq. (2.2)) and heat conduction equation (Eq. (2.6)) for the case of harmonic vibration. Specifically for harmonic vibration, they calculated the two dimensional temperature field along the boundary of the rectangular cross-section using the heat equation and then solved the equation of motion using the obtained temperature profile. The normal mode of vibration and corresponding frequencies were sought where the real part of the complex frequencies represents new eigen-frequencies of the beam in the presence of thermoelastic coupling and the imaginary part gives attenuation of vibration. Their results showed that the simplified classical results of Zener (1937, 1938) are very close to the exact solution of Lifshitz and Roukes (2000) under reasonably fair conditions.

In the theoretical analyses of Zener (1937, 1938), thermal field is obtained as a function of thickness coordinate while temperature field in Lifshitz and Roukes (2000) is the function of both axial and thickness coordinates. Both models are found to be reasonable for beam of thin doubly symmetric rectangular cross-section.

However, they may not be suitable for thermal fields in other doubly and non-doubly symmetric cross-sections such as elliptical, triangular, and arbitrary rectangular, etc. Both the analyses are based on adiabatic surface thermal condition, thus lag ability to offer solution for thermoelastic dissipation with other important thermal boundary conditions such as isothermal condition. Lifshitz and Roukes (2000) derived their exact solution of thermoelastic dissipation for only clamped-clamped and clamped-free boundary conditions of the beam. Moreover, theories developed in Zener (1937, 1938) and Lifshitz and Roukes (2000) are only for thermoelastic dissipation under small linear vibration and do not have the scope for analysis of thermoelastic dissipation in beam resonators under non-linear large-vibration.

However, obtained results of thermoelastic dissipation in this dissertation, especially for thin beams of rectangular cross-section under small linear vibration and adiabatic surface thermal condition, are frequently compared with the results of Zener (1937, 1938) and Lifshitz and Roukes (2000) for validation.

2.5 References

Bishop J. E. and Kinra V. K. 1993. Thermoelastic damping of a laminated beam in flexure and extension. *Journal of Reinforced Plastics and Composites* **12** 210.

Bishop J. E. and Kinra V. K. 1997. Elastothermodynamic damping in laminated composites. *International Journal of Solids and Structures* **34** 1075-1092.

Imboden M., Mohanty P., Gaidarzhy A., Rankin J., Sheldon B. W. 2007. Scaling of dissipation in megahertz-range micromechanical diamond oscillators. *Applied Physics Letters* **90** 173502.

Kinra V. K. and Milligan K. B. 1994. A second-law analysis of thermoelastic damping. *Journal of Applied Mechanics* **61** 71-76.

Kovalenko A. D. 1969. Thermoelastcity: basic theory and applications. *Wolters-Noordhoff Publishing Groningen*, The Netherlands.

Lifshitz R. and Roukes M. L. 2000. Thermoelastic damping in micro- and nanomechanical systems. *Physical Review B* **61** 5600-5609.

Mohanty P., Harrington D. A., Ekinci K. L., Yang Y. T., Murphy M. J., Roukes M. L. 2002. Intrinsic dissipation in high-frequency micromechanical resonators. *Physical Review B* **66** 085416.

Paul H., Hill W. 1989. The art of electronics. *Cambridge University Press*. Canbridge (England), NewYork.

Roszhart T. V. 1990. The effect of thermoelastic internal friction on the *Q* of micromachined silicon resonators. *IEEE Sensors* 13-16.

Ru C. Q. 2009b. Thermoelastic dissipation of nanowire resonators with surface stress. *Physica E* **41** 1243-1248.

Yang J., Ono T., Esashi M. 2002. Energy dissipation in submicrometer thick single-crystal silicon cantilevers. *Journal of Microelectromechanical Systems* **11** 775-783.

Yasumura K. Y., Stowe T. D., Chow E. M., Pfafman T., Kenny W. T., Stipe B. C., Rugar D. 2000. Quality factor in micros- and submicron-thick cantilevers. *Journal of Microelectromechanical Systems* **9** 117-125.

Zener C. 1937. Internal friction in solids. I. Theory of internal friction in reeds. *Physical Review* **52** 230-235.

Zener C. 1938. Internal friction in solids II. General theory of thermoelastic internal friction. *Physical Review* **53** 90-99.

Chapter 3

Thermoelastic Dissipation of Hollow Tubular Beam Resonators[1]

3.1 Overview

Solid and hollow tubular structures of circular cross-section at micro/nano scale are practically present in the literature, for example, as ZnO nanowires (Stan *et al.* 2007), super conducting single crystalline MgB_2 nanotubes (Zhou *et al.* 2009), etc. This chapter[1] contains thermoelastic dissipation in tubular beam resonators of circular cross-section. Detailed formulas are derived for inverse of *Q-factor* for thin elastic hollow tubular beam under adiabatic and isothermal surface condition. *Q-factor* is calculated for hollow tubes at size scale ranging from millimeter to nanometer with single or mixed thermal boundary conditions on surface. It is found that hollow geometry of tubular resonators has a surprising frequency-dependent effect on the *Q-factor*, which can change the *Q-factor* by almost two orders of

[1]*A version of this chapter has been published. Tunvir K., Ru C. Q., Mioduchowski A. 2010. Physica E 42 2341-2352.*

magnitude as compared to a solid beam of circular or rectangular cross-section of same outer size. In particular, the effect of hollow geometry on the *Q-factor* is opposite for high or low frequencies, and the effect of isothermal surface condition is almost one order of magnitude stronger than that of adiabatic surface condition especially for hollow tubes of thinner wall-thickness. This analysis suggests that, to achieve a higher *Q-factor*, hollow tubular resonators with isothermal surface condition are best to operate at low frequencies, while hollow tubular resonators with adiabatic surface condition are best to operate at high frequency making them suitable member for the next generation gigahertz resonators. For a doubly-clamped thin-walled tubular resonator vibrating at its lower natural frequencies, it can be suggested that adiabatic surface thermal condition is favorable at millimeter scale while isothermal surface condition is favorable at nanometer scale.

3.2 Introduction

Resonators have found broad and spreading application in a wide range of MEMS/NEMS (Arcamone *et al.* 2006; Rinaldi *et al.* 2007; Chen *et al.* 2008; Gil-Santos *et al.* 2009; Kacem *et al.* 2009; Mailly *et al.* 2009; Memarian and Mansour 2009; Yi *et al.* 2009). For their optimum usage it is desirable to design and construct resonators with little loss of mechanical energy as energy dissipation could increase significantly with size decreasing – even if they are made from pure single-crystal materials (Lifshitz and Roukes 2000). In particular, thermoelastic dissipation has been identified to be mainly responsible for observed energy loss in a large range of micro/nano mechanical resonators (Zener 1937, 1938; Lifshitz and Roukes 2000; Mohanty *et al.* 2002).

Analysis of thermoelastic dissipation of flexural beam resonators was initiated by Zener in 1937 where damping in some mechanical resonators was found to be mainly due to thermoelastic relaxation. Following Zener's work, theory of thermoelastic dissipation has been developed by many other researchers by constructing exact solutions to the coupled equations of linear thermoelasticity in simpler geometries of infinite and semi-infinite thermoelastic bodies (Biot 1956; Deresiewicz 1957; Chadwick and Sneddon 1958; Lockett 1958), and analyzing thermoelastic waves in an infinite thin plate (Daimaruya and Naitoh 1987) or infinite rods of circular cross-section (Daimaruya and Naitoh 1982). Recently, Lifshitz and Roukes (2000) have studied exact solution of thermoelastic dissipation for resonator beams of solid thin rectangular cross section with interesting comparison to Zener's classical results. In addition, a simple 1D surface stress-strain model has been proposed in (Ru 2009) to study surface stress effects on thermoelastic dissipation of NWs (nanowires) of solid rectangular or circular cross-section, together with many other recent works on thermoelastic dissipation of beam resonators (Cross and Lifshitz 2001; Srikar and Senturia 2002; De and Aluru 2006; Sun 2006; Wong *et al.* 2006; Yi and Matin 2007; Boukai *et al.* 2008; Yun and Park 2008). However, recent progress in design of micro/nano resonators introduced trench, voids, slots and channels in beam structure, in order to alter their thermal transport behavior. For example, internal channels were designed in beam resonators to change resonance frequency (Thomas 2007), slots were introduced in micromechanical resonators to alter the coupling between mechanical and thermal eigenmodes (Rob *et al.* 2006). Following these experiments, some approximate solutions have been offered to estimate the thermoelastic dissipation of the aforementioned resonators. For example, Abdolvan *et al.* (2006) modified Zener's

thermoelastic dissipation model of transversely resonating structures to extend its applicability towards flexure modes of trench-refilled resonators; Sairam and Vengallatore (2009) developed a model to compute thermoelastic dissipation in flexure beam resonators containing structural discontinuities in the form of channels and slots. Besides the slotted and channeled rectangular micro machined beams, as grown solid and hollow tubular nano-structures with thick-walled circular cross-section are synthesized and can be used as the superior resonators in MEMS/NEMS as discussed in the present study. Such solid and hollow tubular structures of circular cross-section are ZnO nanowires (Stan *et al.* 2007), super conducting single crystalline MgB_2 nanotubes (diameter D = ~ 90 nm and wall thickness = ~ 30 nm (Zhou *et al.* 2009)), hollow carbon nanofibers (D = 80 - 450 nm and wall thickness= 10-20 nm (Cheng *et al.* 2009)), hollow silicon carbide fibers (D = ~ 385 nm and wall thickness= ~ 45 nm (Cheng *et al.* 2009)), Au nanotubes (Zhao and Lei 2009) and ZnO nanotubes (Jiang *et al.* 2006; Zhao and Lei 2009). Despite their practical existence and possible potential usefulness, till to date, no systematic study of thermoelastic dissipation for hollow micro/nano mechanical tubular resonators has been available in the existing literature.

In this chapter, it has been attempted to analyze thermoelastic dissipation of hollow beam resonators of circular cross-section. Various possible surface thermal conditions are considered in the calculation, with an emphasis on the effect of hollow tubular geometry on thermoelastic dissipation as compared to a solid beam of circular cross-section with same outer diameter. The basic thermoelasticity model and formulations for thermoelastic dissipation are described in section 3.3. Thermal field for hollow tubular beams under various surface thermal conditions are analyzed in 3.4. Numerical results for thermoelastic dissipation in hollow

tubular beams are presented and described in section 3.5. Finally, all results are summarized in section 3.6.

3.3 Theoretical Model

3.3.1 Basic Thermoelasticity Model

Thermoelastic dissipation is a relevant dissipation mechanism in beam resonators when the size of the structure scales down to smaller scales such as submicron and nanometer scales (Lifshitz and Roukes 2000). Thermoelastic dissipation occurs in any material that is subjected to cyclic loading, especially when the period of cyclic loading is approximately equal to a structure's thermal relaxation time constant. Here the energy dissipation due to thermoelasticity in hollow tubular beam resonators has been modeled through a continuum modeling approach. A continuum model, where dissipation depends on the geometry of the structure as well as elastic and thermodynamic properties of the material, is expected to work well for hollow tubular structures of the above mentioned dimensions.

For an elastic beam, having the *X*-axis along its axial direction and the *Y* and *Z*-axes in two perpendicular axes of symmetry on its cross-section, following the simple Eular-Bernoulli beam model, the axial strain for bending in the *X*-*Z* plane is $\varepsilon_{xx} = \varepsilon^* + z\varphi$ (Ru 2009) where $\varphi = \partial^2 w / \partial x^2$. Here z is the distance to the neutral *Y*-axis, $w(x,t)$ and $\varphi(x,t)$ are transverse deflection and the created curvature of the bent beam, ε^* is the residual compressive strain caused by the pre-existing surface tension γ_o. The uniaxial stress in the bulk beam is given by

$$\sigma_{xx} = E(\varepsilon_{xx} - \alpha \Delta T) \tag{3.1}$$

and the axial stress due to the surface is given by (Ru 2009)

$$\sigma_s = \gamma_\circ + E_s(\varepsilon_s - \alpha \Delta T) \tag{3.2}$$

where σ_{xx} is the uniaxial stress in bulk beam, σ_s is the surface axial stress, E_s is the surface elastic modulus, ε_s is surface axial strain, ΔT is the deformation-induced temperature change from the initial uniform temperature $T_\circ$. The bending moment contributed by both the bulk material and the surface is given by (Ru 2009)

$$M = \int_A \sigma_{xx}\, z\, dA + \int_C \sigma_s\, z\, dl \tag{3.3}$$

where A and C are the area and perimeter of the cross-section. The temperature field $T(x,y,z,t) = T_\circ + \Delta T(x,y,z,t)$ is coupled with the deformation by (Zener 1937, 1938; Landau and Lifshitz 1959; Lifshitz and Roukes 2000)

$$C_V \frac{\partial T}{\partial t} + \frac{E\alpha T_\circ}{1-2\nu}\frac{\partial \varepsilon}{\partial t} = \kappa \nabla^2 T \tag{3.4}$$

where C_V is the heat capacity per unit volume, $\varepsilon = \varepsilon_{xx} + \varepsilon_{yy} + \varepsilon_{zz}$ is the mean strain, κ is the thermal conductivity, α is the thermal expansion coefficient, and E and ν are the Young's modulus and Poisson's ration of the bulk material. Heat conduction along axial direction is usually negligible as the axial wave-length of temperature/deformation is much larger than the dimension of the cross-section. For uniaxial stress-state, the two lateral strains of the beam are $\varepsilon_{yy} = \varepsilon_{zz} = -(\nu \sigma_{xx}/E) + \alpha \Delta T$. Because the axial wave-length of bending deformation is usually much larger than the dimension of the cross-section, heat conduction along axial x-direction is negligible (Lifshitz and Roukes 2000). Thus Eq. (3.4) becomes

$$C_V\left[1 + \frac{2(1+\nu)}{(1-2\nu)}\frac{E\alpha^2 T_\circ}{C_V}\right]\frac{\partial(\Delta T)}{\partial t} + E\alpha T_\circ z\frac{\partial \varphi(x,t)}{\partial t} = \kappa\left(\frac{\partial^2}{\partial y^2} + \frac{\partial^2}{\partial z^2}\right)\Delta T \tag{3.5}$$

Here, $(E\alpha^2 T_\circ)/C_V$ is negligible compared to unity (Lifshitz and Roukes 2000).

3.3.2 Thermoelastic Dissipation of Hollow Tubular Beams

Thermoelastic dissipation, defined by the ratio of energy loss per cycle to total strain energy stored, can be calculated by the required energy supply per cycle for a perfect periodic harmonic motion (Zener 1937, 1938). Assuming $M(x,t)=M_\circ(x)e^{-i\omega t}$ and $\varphi(x,t)=\varphi_\circ(x)e^{-i\omega t}$, where $\varphi_\circ(x)$ is a real quantity and ω is the (circular) vibration frequency. It is seen from Eq. (3.5) that the temperature field ΔT must have the form $\Delta T(x,y,z,t) = \Theta(x,t)f(y,z)$. It follows from Eqs. (3.3) and (3.5) that

$$\begin{aligned} &M=(EI+E_sI'-\nu\gamma_\circ I')\varphi-\alpha\left[ES+\{E_s-(1+\nu)\gamma_\circ\}K\right]\Theta(x,t);\\ &C_VS\frac{\partial\Theta}{\partial t}+E\alpha T_\circ I\frac{\partial\varphi}{\partial t}+\kappa P\Theta(x,t)=0 \end{aligned} \tag{3.6}$$

where S, K, P, I and I' are defined as

$$\begin{aligned} &S\equiv\int_A z\,f(y,z)dA\\ &K\equiv\int_C z\,f(y,z)dl\\ &P\equiv-\int_A z\left(\frac{\partial^2}{\partial y^2}+\frac{\partial^2}{\partial z^2}\right)f(y,z)dA\\ &I\equiv\int_A z^2\,dA\\ &I'\equiv\int_C z^2\,dl \end{aligned} \tag{3.7}$$

The required energy supply for an infinitesimal bending element dx of the beam located at a point x over a period, $t=0\sim 2\pi/\omega$, is equal to the work done by the external force, $dx\int_0^{2\pi/\omega} Re[M]Re[d\varphi/dt]dt$. Since the total strain energy stored is $Re[M_\circ]\varphi_\circ dx/2$, it can be verified that thermoelastic dissipation or the inverse of the *Q-factor* is given by (Ru 2009)

$$\frac{1}{Q}=\frac{(energy\ loss)/cycle}{2\pi(total\ energy)}=\frac{PEIT_\circ\kappa\omega\alpha^2\left[ES+\{E_s-(1+\nu)\gamma_\circ\}K\right]}{(EI+E_sI'-\nu\gamma_\circ I')\left(P^2\kappa^2+\omega^2C_V{}^2S^2\right)} \tag{3.8}$$

Therefore, for calculating the dissipation $1/Q$, it is enough to calculate the three constants S, K and P defined by the integrals (Eq. (3.7)) of the temperature field ΔT, without knowing the temperature field exactly. The validity of this method was confirmed by excellent agreement with the well-known classical results (Zener 1937, 1938; Lifshitz and Roukes 2000) for thin-wall rectangular and circular cross-sections under adiabatic surface condition (Ru 2009).

3.4 Temperature Field

As mentioned, there is no solution in the existing literature for thermoelastic dissipation of tubular elastic beams of hollow circular cross-section. To derive the desired solution, let's consider hollow tubular beam having inner and outer radii as R_1 and R_2 respectively, as shown in Fig. 3.1. In polar coordinate the Y-Z plane can be expressed as $y = r\cos\theta$ and $z = r\sin\theta$ where $R_1 \le r \le R_2$ and $0 \le \theta \le 2\pi$. To calculate the dissipation $1/Q$, it is necessary to calculate the three constants P, S and K defined by $f(y,z)$ based on Eq. (3.7). For this end, let us find an approximate solution for heat equation (Eq. (3.5)). Neglecting heat conduction in axial direction as explained before, Eq. (3.5) for a circular cross-section can be written as

$$C_V \frac{\partial \Delta T}{\partial t} + \alpha E T_\circ r \sin\theta \frac{\partial \varphi}{\partial t} = \kappa \left(\frac{\partial}{\partial r^2} + \frac{1}{r}\frac{\partial}{\partial r} + \frac{1}{r^2}\frac{\partial}{\partial \theta^2} \right) \Delta T \tag{3.9}$$

For harmonic vibration ΔT must have the form $\Delta T(x,y,z,t) = \Theta(x,t) f(r,\theta)$, where the function $f(r,\theta)$ is periodic in θ and can be expanded into a Fourier series in the variable θ such as $f(r,\theta) = \sum_{\vartheta_1=1}^{\infty} G_{\vartheta_1}(r)\sin\vartheta_1\theta + \sum_{\vartheta_2=0}^{\infty} H_{\vartheta_2}(r)\cos\vartheta_2\theta$. For an annular cross-section with zero thermal conditions for ΔT at the inner and outer surfaces (such as adiabatic, isothermal surface conditions, or a combination of them), substitution of

the above Fourier series into Eq. (3.9) leads to the conclusion that $G_{\vartheta_1}(r) \equiv 0$ when $\vartheta_1 \neq 1$ and $H_{\vartheta_2}(r) \equiv 0$ for any ϑ_2 and then $f(r,\theta) = \sin\theta G(r)$ (where the subscript 1 has been dropped for $G(r)$). Obviously, $f(r, \theta)$ given by this expression is always odd in z because it is an odd function in θ. Here, it follows from Eq. (3.9) that $G(r)$ is determined by an equation of the form

$$G(r) + e_1 r = e_2 \left(\frac{\partial^2}{\partial r^2} + \frac{1}{r}\frac{\partial}{\partial r} - \frac{1}{r^2} \right) G(r) \tag{3.10}$$

where e_1 and e_2 represent two parameters independent of r and θ. The series solution of Eq. (3.10) determined using numerical code (Maple 13.0) is of the following form

$$G(r) = e_3 \left[r + \frac{r^3}{8e_2} + \frac{r^5}{192{e_2}^2} + O\left(r^7\right) \right] + e_4 \left[-\frac{2}{r} + \frac{3r^3}{32{e_2}^2} + O\left(r^5\right) + ln(r) \left\{ -\frac{r}{e_2} - \frac{r^3}{8{e_2}^2} + O\left(r^5\right) \right\} \right] + e_1 \left[\frac{r^3}{8e_2} + \frac{r^5}{192{e_2}^2} + O\left(r^6\right) \right] \tag{3.11}$$

where e_3 and e_4 are two arbitrary coefficients while the third part is a particular solution. For the present method, simple approximate form of $G(r)$ can be obtained based on a truncation of the series solution Eq. (3.11). For example, for a solid circular cross-section, coefficient e_4 must be zero and coefficient e_3 is to be determined by the single surface boundary condition. Therefore, it follows from Eq. (3.11) that a simple approximate solution for $G(r)$ can be assumed to be an odd polynomial up to the third power of r (in which, without losing the generality, the coefficient of r has been chosen as unity). For an annular circular-cross section, however, two surface conditions are requested and therefore coefficient e_4 cannot be zero. Thus, taking the leading lowest-order term $1/r$ in the e_4-related part of Eq.

(3.11), a simple approximate solution of $G(r)$ for cross-section of a hollow tubular beam is given by

$$G(r) = \frac{e_5}{r} + r + e_6 r^3 \tag{3.12}$$

where, without losing the generality, the coefficient of r for $G(r)$ has been chosen as unity, and e_5 and e_6 are two constants to be determined by two thermal surface conditions at the inner and outer surfaces. Thus the three constants P, S and K defined by Eq. (3.7) can be calculated in terms of the coefficients e_5 and e_6 as

$$\begin{aligned}
P &= -\int_A r\sin\theta\left(\frac{\partial^2}{\partial r^2} + \frac{1}{r}\frac{\partial}{\partial r} - \frac{1}{r^2}\right) f(r,\theta)\,dA = -2\pi e_6\left(R_2{}^4 - R_1{}^4\right) \\
S &= \int_A r\sin\theta\; f(r,\theta)\,dA = \pi\left(R_2{}^2 - R_1{}^2\right)\left[\frac{e_5}{2} + \frac{R_1{}^2 + R_2{}^2}{4} + \frac{e_6\left(R_1{}^4 + R_1{}^2 R_2{}^2 + R_2{}^4\right)}{6}\right] \\
K &= \int_{C|_{r=R_1}} r\sin\theta\, f(r,\theta)\,dl + \int_{C|_{r=R_2}} r\sin\theta\, f(r,\theta)\,dl = = \pi\left[e_5\left(R_1 + R_2\right) + \left(R_1{}^3 + R_2{}^3\right) + e_6\left(R_1{}^5 + R_2{}^5\right)\right]
\end{aligned} \tag{3.13}$$

Thermoelastic dissipation Eq. (3.8) for different thermal surface conditions is discussed below.

3.4.1 Adiabatic Surface Condition

An adiabatic surface condition requires that normal derivative of ΔT vanishes on all surfaces such that $\partial \Delta T/\partial r = 0$ at $r = R_1$ and $r = R_2$. Satisfying adiabatic surface condition, $e_5 = R_1{}^2 R_2{}^2/\left(R_1{}^2 + R_2{}^2\right)$ and $e_6 = -1/\left[3\left(R_1{}^2 + R_2{}^2\right)\right]$ are obtained Thus constants P, S and K are given by

$$\begin{aligned}
P &= \frac{2}{3}\pi\left(R_2{}^2 - R_1{}^2\right) \\
S &= \frac{1}{36}\pi\left[\frac{\left(R_2{}^2 - R_1{}^2\right)\left(7R_1{}^4 + 34R_1{}^2R_2{}^2 + 7R_2{}^4\right)}{R_1{}^2 + R_2{}^2}\right] \\
K &= \frac{2}{3}\pi\left[\frac{\left(R_1{}^5 + R_2{}^5\right) + 3R_1{}^2R_2{}^2\left(R_1 + R_2\right)}{R_1{}^2 + R_2{}^2}\right]
\end{aligned} \tag{3.14}$$

Thus the thermoelastic dissipation $1/Q$ given by Eq. (3.8) under adiabatic thermal surface condition is

$$\frac{1}{Q}=\frac{\omega E\alpha^2 IT_\circ\left[E\frac{\left(7R_1^{\,4}+34R_1^{\,2}R_2^{\,2}+7R_2^{\,4}\right)}{24\left(R_1^{\,2}+R_2^{\,2}\right)}+\{E_s-(1+\nu)\gamma_\circ\}\frac{\left\{\left(R_1^{\,5}+R_2^{\,5}\right)+3R_1^{\,2}R_2^{\,2}(R_1+R_2)\right\}}{R_2^{\,4}-R_1^{\,4}}\right]}{\kappa\left(EI+E_sI'-\nu\gamma_\circ I'\right)\left[1+\omega^2\left\{\frac{C_V\left(7R_1^{\,4}+34R_1^{\,2}R_2^{\,2}+7R_2^{\,4}\right)}{24\kappa\left(R_1^{\,2}+R_2^{\,2}\right)}\right\}^2\right]} \tag{3.15}$$

It follows from Eqs. (3.8) and (3.15) that maximum dissipation occurs at

$$\omega=\frac{\kappa P}{C_V S}=\frac{24\kappa\left(R_1^{\,2}+R_2^{\,2}\right)}{C_V\left(7R_1^{\,4}+34R_1^{\,2}R_2^{\,2}+7R_2^{\,4}\right)} \tag{3.16}$$

and the corresponding value of the maximum $1/Q$ is given by

$$\left(\frac{1}{Q}\right)_{max}=\frac{E\alpha^2 IT_\circ\left[E+\{E_s-(1+\nu)\gamma_\circ\}\frac{24\left\{\left(R_1^{\,5}+R_2^{\,5}\right)+3R_1^{\,2}R_2^{\,2}(R_1+R_2)\right\}}{\left(7R_1^{\,4}+34R_1^{\,2}R_2^{\,2}+7R_2^{\,4}\right)\left(R_2^{\,2}-R_1^{\,2}\right)}\right]}{2C_V\left(EI+E_sI'-\nu\gamma_\circ I'\right)} \tag{3.17}$$

In the absence of surface stress effect (i.e. for E_s = γ_o = 0), thermoelastic dissipation $1/Q$ Eq. (3.15) for annular tube with adiabatic thermal surface condition is

$$\frac{1}{Q}=\frac{\omega E\alpha^2 T_\circ\left[\frac{7R_1^{\,4}+34R_1^{\,2}R_2^{\,2}+7R_2^{\,4}}{R_1^{\,2}+R_2^{\,2}}\right]}{24\kappa\left[1+\left\{\frac{C_V\omega\left(7R_1^{\,4}+34R_1^{\,2}R_2^{\,2}+7R_2^{\,4}\right)}{24\kappa\left(R_1^{\,2}+R_2^{\,2}\right)}\right\}^2\right]} \tag{3.18}$$

3.4.2 Isothermal Surface Condition

An isothermal surface condition requests ΔT vanishes on all surfaces such that ΔT = 0 at $r=R_1$ and $r=R_2$. Satisfying isothermal surface condition, $e_5=-R_1^{\,2}R_2^{\,2}/\left(R_1^{\,2}+R_2^{\,2}\right)$ and $e_6=-1/\left(R_1^{\,2}+R_2^{\,2}\right)$ are obtained and therefore

$$P = 2\pi\left(R_2^{\,2} - R_1^{\,2}\right)$$
$$S = \frac{1}{12}\pi\frac{\left(R_2^{\,2} - R_1^{\,2}\right)^3}{R_1^{\,2}+R_2^{\,2}} \tag{3.19}$$
$$K = 0$$

In the absence of surface stress effect (E_s = γ_o = 0), thermoelastic dissipation $1/Q$ given by Eq. (3.8) for annular tube with isothermal surface condition is

$$\frac{1}{Q} = \frac{\omega E\alpha^2 T_\circ \frac{\left(R_2^{\,2}-R_1^{\,2}\right)^2}{R_1^{\,2}+R_2^{\,2}}}{24\kappa\left[1+\omega^2 C_V^{\,2}\left\{\frac{\left(R_2^{\,2}-R_1^{\,2}\right)^2}{24k\left(R_1^{\,2}+R_2^{\,2}\right)}\right\}^2\right]} \tag{3.20}$$

3.4.3 Isothermal at Inner and Adiabatic at Outer surface

Due to different surrounding media inside and outside the tubular resonator, it is possible to have mixed thermal surface conditions at the inner and outer surfaces. First, let us consider the case in which the inner surface is isothermal while the outer surface is adiabatic. An isothermal condition at $r = R_1$ requests ΔT = 0 at $r = R_1$, while as an adiabatic surface condition at $r = R_2$ requires that $\partial\Delta T/\partial r$ = 0 at $r = R_2$. Satisfying the two conditions, $e_5 = \left[R_1^{\,2}R_2^{\,2}\left(R_1^{\,2} - 3R_2^{\,2}\right)\right]/\left(R_1^{\,4}+3R_2^{\,4}\right)$ and $e_6 = -\left(R_1^{\,2}+R_2^{\,2}\right)/\left(R_1^{\,4}+3R_2^{\,4}\right)$ are obtained. Thus

$$P = 2\pi\frac{\left(R_1^{\,2}+R_2^{\,2}\right)\left(R_2^{\,4} - R_1^{\,4}\right)}{R_1^{\,4}+3R_2^{\,4}}$$
$$S = \frac{1}{12}\pi\frac{\left(7R_2^{\,8} - R_1^{\,8}\right)+18R_1^{\,4}R_2^{\,4} - 4R_1^{\,2}R_2^{\,2}\left(R_1^{\,4}+5R_2^{\,4}\right)}{R_1^{\,4}+3R_2^{\,4}} \tag{3.21}$$
$$K = 2\pi\frac{R_2^{\,3}\left(R_1^{\,2} - R_2^{\,2}\right)^2}{R_1^{\,4}+3R_2^{\,4}}$$

In the absence of surface stress effect (E_s = γ_o = 0), thermoelastic dissipation $1/Q$ given by Eq. (3.8) becomes

$$\frac{1}{Q}=\frac{\omega E\alpha^2 T_\circ\left[\left(7R_2^{\,8}-R_1^{\,8}\right)+18R_1^{\,4}R_2^{\,4}-4R_1^{\,2}R_2^{\,2}\left(R_1^{\,4}+5R_2^{\,4}\right)\right]}{24\kappa\left(R_1^{\,2}+R_2^{\,2}\right)\left(R_2^{\,4}-R_1^{\,4}\right)\left[1+\omega^2 C_V^{\,2}\left\{\frac{\left(7R_2^{\,8}-R_1^{\,8}\right)+18R_1^{\,4}R_2^{\,4}-4R_1^{\,2}R_2^{\,2}\left(R_1^{\,4}+5R_2^{\,4}\right)}{24\kappa\left(R_1^{\,2}+R_2^{\,2}\right)\left(R_2^{\,4}-R_1^{\,4}\right)}\right\}^2\right]} \tag{3.22}$$

3.4.4 Adiabatic at Inner and Isothermal at Outer surface

Finally, let us consider the case in which the inner surface is adiabatic while the outer surface is isothermal. An adiabatic surface condition at $r=R_1$ and isothermal thermal condition at $r=R_2$ requires $\partial\Delta T/\partial r$ = 0 at $r=R_1$ and ΔT = 0 at $r=R_2$ respectively Satisfying the two conditions, $e_5 = \left[R_1^{\,2}R_2^{\,2}\left(R_2^{\,2}-3R_1^{\,2}\right)\right]/\left(3R_1^{\,4}+R_2^{\,4}\right)$, $e_6 = -\left(R_1^{\,2}+R_2^{\,2}\right)/\left(3R_1^{\,4}+R_2^{\,4}\right)$ are obtained and

$$\begin{aligned}
P&=2\pi\frac{\left(R_1^{\,2}+R_2^{\,2}\right)\left(R_2^{\,4}-R_1^{\,4}\right)}{3R_1^{\,4}+R_2^{\,4}}\\
S&=\frac{1}{12}\pi\frac{\left(R_2^{\,8}-7R_1^{\,8}\right)-18R_1^{\,4}R_2^{\,4}+4R_1^{\,2}R_2^{\,2}\left(5R_1^{\,4}+R_2^{\,4}\right)}{3R_1^{\,4}+R_2^{\,4}}\\
K&=2\pi\frac{R_1^{\,3}\left(R_1^{\,2}-R_2^{\,2}\right)^2}{3R_1^{\,4}+R_2^{\,4}}
\end{aligned} \tag{3.23}$$

In the absence of surface stress effect (E_s = γ_o = 0), thermoelastic dissipation $1/Q$ Eq. (3.8) becomes

$$\frac{1}{Q}=\frac{\omega E\alpha^2 T_\circ\left[\left(R_2^{\,8}-7R_1^{\,8}\right)-18R_1^{\,4}R_2^{\,4}+4R_1^{\,2}R_2^{\,2}\left(5R_1^{\,4}+R_2^{\,4}\right)\right]}{24\kappa\left(R_1^{\,2}+R_2^{\,2}\right)\left(R_2^{\,4}-R_1^{\,4}\right)\left[1+\omega^2 C_V^{\,2}\left\{\frac{\left(R_2^{\,8}-7R_1^{\,8}\right)-18R_1^{\,4}R_2^{\,4}+4R_1^{\,2}R_2^{\,2}\left(5R_1^{\,4}+R_2^{\,4}\right)}{24\kappa\left(R_1^{\,2}+R_2^{\,2}\right)\left(R_2^{\,4}-R_1^{\,4}\right)}\right\}^2\right]} \tag{3.24}$$

It can be verified that, in the absence of surface stress effect, the maximum dissipation for any of the above all four thermal surface conditions become

$$\left(\frac{1}{Q}\right)_{max}=\frac{E\alpha^2 T_\circ}{2C_V} \tag{3.25}$$

which implies that in the absence of surface stress effect, the maximum thermoelastic dissipation is determined by the material constants alone, independent of the size and shape of the cross-section and the thermal surface conditions (Ru 2009).

3.5 Results and Discussions

Now let us examine the dependence of thermoelastic dissipation on the wall-thickness of hollow tubular resonators and the surface thermal conditions. Surface thermal conditions depend on heat transfer between the beam and the surrounding medium. Here two typical cases of surface thermal conditions, adiabatic and isothermal conditions, and their mixed combinations are considered. An adiabatic condition can be expected in vacuum (ignoring radiation losses) while isothermal condition can be expected in a denser external medium. In isothermal surface condition temperature remains constant on the surfaces of the beam, while the adiabatic surface condition requests that normal gradient of temperature field vanishes on the surfaces. In what follows, the formulas derived in the above section will be used to examine the dependence of thermoelastic dissipation on the ratio of two radii of hollow tubular beams for all four possible surface thermal conditions:

i. adiabatic on all surfaces

ii. isothermal on all surfaces

iii. isothermal on inner surface and adiabatic on outer surface

iv. adiabatic on inner surface and isothermal on outer surface.

3.5.1 Effect of Hollow Geometry at Micron Scale

Calculation of thermoelastic dissipation is carried out for polysilicon beams of hollow circular cross-section. The material constants are taken from (Srikar and Senturia 2002): coefficient of thermal expansion, α = 2.6×10^{-6} K^{-1}, bulk elastic modulus, E = 160×10^{9} Nm^{-2}, thermal conductivity, κ = 148 Wm^{-1}K^{-1} and heat capacity per unit volume, C_V = 1.66×10^{6} Jm^{-3}K^{-1}. In Figs. 3.2 and 3.3, the effect of tubular geometry on the *Q-factor* of a hollow beam of given outer diameter D = 1 μm and various inner diameter is demonstrated for adiabatic and isothermal surface conditions respectively. The reference or equilibrium temperature is set to T_o = 300 K. Normalized *Q-factor*, defined by the ratio of *Q-factor* for the hollow tube to *Q-factor* for a solid beam of circular cross-section of same outer diameter under otherwise identical conditions, is plotted with respect to vibration frequency ω in the absence of surface stress. Hollow geometry of the beam is given in terms of the ratio of the inner radius to the outer radius (R_1/R_2) for the given outer radius R_2. The vibration frequency is assumed to be in a range of $10^5 \sim 10^{14}$ rad sec^{-1}, which covers the operating frequencies of most micro/nano resonators found in the literature.

For adiabatic surface condition (Fig. 3.2), thinner beams show lower *Q-factor* for vibration frequencies not higher than a certain value approximately of 10^9 rad sec^{-1}, while thinner beams show higher *Q-factor* when vibration frequency is higher than 10^9 rad sec^{-1} till 10^{12} rad sec^{-1}. It is seen from Fig. 3.2 that the *Q-factor* varies significantly only within a frequency range of $10^8 \sim 10^{10}$ rad sec^{-1}. Indeed, the *Q-factor* is almost frequency-independent for frequency below 10^8 rad sec^{-1} or above 10^{10} rad sec^{-1}. In particular, thinner beams show larger and steeper change in the *Q-factor* within this frequency range, and the normalized ratio $Q_{Hollow\ tubular}/Q_{Solid\ tubular}$ is larger or smaller than unity by a factor up to four. On the other hand, similar but

opposite behavior of the *Q-factor* is observed for hollow tubes having isothermal surface condition (Fig. 3.3). It is seen from Fig. 3.3 that thinner tubes have higher *Q-factor* up to a certain frequency within the range of 10^{10} -10^{11} rad sec^{-1}, while thinner tubes have lower *Q-factor* for frequencies higher than 10^{11} rad sec^{-1}. The *Q-factor* is almost frequency-independent for frequencies lower than 10^{9} rad sec^{-1} or higher than 10^{12} rad sec^{-1}. Most remarkably, thinner beams with isothermal surface condition show very large and steep change in the *Q-factor* within the frequency range of 10^{9} -10^{12} rad sec^{-1}, and the normalized ratio $Q_{Hollow\ tubular}/Q_{Solid\ tubular}$ for isothermal surface condition is larger or smaller than unity by a factor up to fifty.

In summary, combined with different thermal surface conditions, hollow geometry of tubular resonators has a surprising frequency-dependent effect on the *Q-factor*, which can change the *Q-factor* by almost two orders of magnitude as compared to a solid beam of same outer diameter under otherwise identical conditions. In particular, the hollow geometry has opposite effect for high or low frequencies. The present analysis indicates that, to achieve a higher *Q-factor*, hollow tubular resonators with isothermal surface condition are best to operate at low frequencies, while hollow tubular resonators with adiabatic surface condition are best to operate at high frequencies. Unfortunately, due to the lack of relevant known data in the existing literature, it is not possible to compare the theoretical predictions with any available experimental or simulation results.

3.5.2 Effect of Hollow Geometry at Nano Scale

Essentially similar results can be obtained for tubular resonators at nano scale. To study the thermoelastic dissipation at nano scale, the outer diameter of tubes is changed to D = 50 nm. The behaviors of *Q-factor* for adiabatic and isothermal

surface condition are showed in Fig. 3.4 and Fig. 3.5, respectively. It is seen from Figs. 3.4 and 3.5 that sharp change in *Q-factor* occurs for frequency between $10^{10} \sim 3\times10^{12}$ rad sec^{-1} for adiabatic surface conditions, or for frequency between $3\times10^{11} \sim 10^{15}$ rad sec^{-1} for isothermal surface condition.

3.5.3 Effect of Mixed Thermal Surface Condition

It is seen from Figs. 3.2-3.5 that the effect of isothermal surface condition is almost one order of magnitude stronger than that of adiabatic surface condition especially for hollow tubes of larger radius ratio (such as R_1/R_2 > 0.3-0.4). Therefore, it is expected that the overall effect of a mixed thermal surface condition for hollow tubes of larger radius ratio will be dominated by the isothermal surface condition, and therefore similar to those of an isothermal surface condition showed in Figs. 3.3 and 3.5. To verify this, the effect of hollow tubular geometry on thermoelastic dissipation is showed in Figs. 3.6 and 3.7 for a mixed surface thermal condition in which the inner surface is isothermal while the outer surface is adiabatic, at micron and nano scales respectively. As expected, the curves in Figs. 3.6 and 3.7 are similar to those of Figs. 3.3 and 3.5 obtained for isothermal surface condition. Here it should be noted that the range of ω in which the sharp change of thermoelastic dissipation takes place depends on the size of the hollow tubes (Figs. 3.6 and 3.7).

On the other hand, the results for an otherwise mixed thermal condition are showed in Figs. 3.8 and 3.9 in which the inner surface is adiabatic while the outer surface is isothermal, for micron and nano scales respectively. Having adiabatic thermal condition at the inner surface, the trend of the curves ($Q_{Hollow\ tubular}/Q_{Solid\ tubular}$ versus ω) for tubes of $R_1/R_2 = 0 \sim 0.4$ in both the figures. (see magnified inset of Figs. 3.8 and 3.9) are similar to those for adiabatic surface condition showed in

Figs. 3.2 and 3.4, while for tubes of R_1/R_2 = 0.5 ~ 0.9, the curves are similar with those for isothermal surface condition plotted in Figs. 3.3 and 3.5. Thus, isothermal surface condition indeed has a dominant effect over adiabatic surface condition on thermoelastic dissipation of hollow tubes of thinner wall-thickness.

3.5.4 Thermoelastic Dissipation of a Hollow Tubular Beam Resonator at Its Natural Frequencies

Thermoelastic dissipation for hollow tubes at their natural frequencies is of greater interest for designing of resonators. The *Q-factor* at first three natural frequencies is shown in Figs. 3.10-3.13 for doubly-clamped hollow tubes of different dimension under adiabatic or isothermal surface condition. The sizes of the tubes are at millimeter or nanometer scale. At millimeter scale for adiabatic surface condition, the thinnest tubular resonator shows the highest *Q-factor* (Fig. 3.10) and the maximum dissipation occurs in a solid beam, while for isothermal surface condition (Fig. 3.11), a solid beam has a highest *Q-factor* and the maximum dissipation occurs for tubes of R_1/R_2 = 0.7 ~ 0.8. On the other hand, at nano scale, opposite behavior of *Q-factor* is obtained for adiabatic and isothermal surface conditions, as shown in Figs. 3.12 and 3.13 respectively. It is suggested that for a doubly-clamped thin-walled tubular resonator vibrating at its lower natural frequencies, the adiabatic surface thermal condition is favorable at millimeter scale while isothermal surface condition is favorable at nanometer scale. Calculation of this study showed that similar results are true for cantilever tubular resonators.

3.5.5 The Maximum Dissipation $(1/Q)_{max}$

It is known that, in the absence of surface stress effect (E_s = γ_o = 0), the maximum dissipation is determined by the material constants alone, independent of the size and shape of the cross-section and the thermal surface condition (Eq. (3.25)). Therefore, to study the dependence of the maximum dissipation on hollow geometry of tubular resonators, surface stress effect should be taken into account. Since surface stress becomes important only at small scale, the effect of hollow geometry on the maximum dissipations is shown in Fig. 3.14 at nano scale for different surface thermal conditions. Surface stress constants for Si beam resonator are taken from (Zhang 2009; Miller and Shenoy 2000). It is seen from Fig. 3.14 that the maximum thermoelastic dissipation of a hollow tubular resonator is essentially lower than that of a solid one for any surface thermal condition. In particular, for isothermal surface condition, the maximum dissipation in a hollow tube goes down rapidly with increasing radius ratio R_1/R_2. However, the maximum dissipation of a hollow tube with adiabatic or mixed thermal condition can be slightly larger than that of a solid beam for geometries of R_1/R_2 = 0.3 $\sim$ 0.7 (as shown in the magnified inset of Fig. 3.14), but eventually lower than that of a solid beam when R_1/R_2 becomes larger than 0.7.

3.5.6 Comparison of Hollow Tube with Beam Resonator of Solid Rectangular Cross-Section

Noticing the numerous applications of beam resonators of rectangular cross-section in literatures, thermoelastic dissipation of hollow beam resonator at submicron scale is compared with that in beam resonator of solid rectangular cross-section (described in Chapter 4) of same cross-sectional area and width under adiabatic

surface condition (Fig. 3.15) and isothermal surface condition (Fig. 3.16). Interestingly, behavior of these two cross-sections in respect of *Q-factor* of beam resonator is different for low and high frequencies. Under adiabatic surface condition (Fig. 3.15), hollow tubular beam resonators for any wall thickness suffer much less thermoelastic dissipation than solid rectangular cross-section for high frequencies such as $f \geq 10^8$ Hz. It is clear that under adiabatic surface condition, a hollow tubular beam resonator is a better member for gigahertz resonators (Peng *et al.* 2006; Gaidarzhi *et al.* 2007; Husain *et al.* 2003) than a beam resonator of solid rectangular cross-section. On the other hand, under isothermal surface condition (Fig. 3.16), hollow tubular beam resonators always suffer less thermoelastic dissipation than solid rectangular cross-section of same size, however, under low operating frequencies ($f \leq 10^{10}$ Hz) and particularly for thin walls ($R_1/R_2 \geq 0.5$). However, for thick wall thicknesses ($R_1/R_2 = 0.25$) the opposite result is evident under isothermal surface condition.

3.6 Summary

To meet the need of estimating thermoelastic dissipation of hollow tubular resonators at micro/nano scale, for the first time in the literature, the present work offers a systematic analysis of the effect of hollow geometry on the *Q-factor* of tubular beam resonators. The present analysis showed that thermoelastic dissipation strongly depends on the hollow geometry and surface thermal conditions, and hollow geometry can change the *Q-factor* by almost two orders of magnitude as compared to a solid circular beam of same outer diameter under otherwise identical conditions. The present results predict that the effect of isothermal surface condition on thermoelastic dissipation is almost one order of

magnitude stronger than the effect of adiabatic surface condition especially for hollow tubes of thinner wall-thickness, and thin-walled hollow tubes with isothermal surface condition are preferable to achieve a high *Q-factor* for frequencies not higher than 10^{10} rad sec^{-1} at micron scale or for frequencies not higher than 10^{13} rad sec^{-1} at nano scale. The present analysis indicates that, to achieve a higher *Q-factor*, hollow tubular resonators with adiabatic surface condition are best to operate at high frequencies, while hollow tubular resonators with isothermal surface condition are best to operate at low frequencies. The results obtained for a doubly-clamped thin-walled tubular resonator vibrating at its lower natural frequencies suggest that adiabatic surface thermal condition is favorable at millimeter scale while isothermal surface condition is favorable at nanometer scale. It is also concluded that tubular beam resonators are promising members for next generation gigahertz resonators.

3.7 Figures and Illustrations

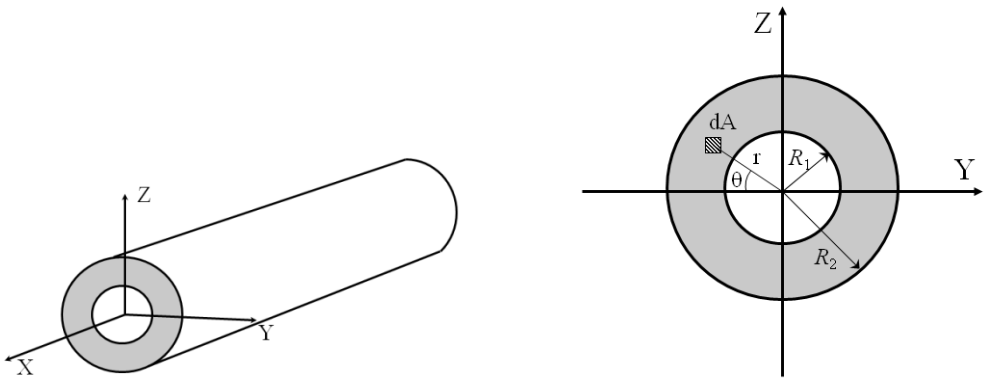

(a) (b)

Fig. 3.1 (a) Schematic diagram of a typical hollow cylindrical tube and (b) Schematic diagram of cross-sectional geometry.

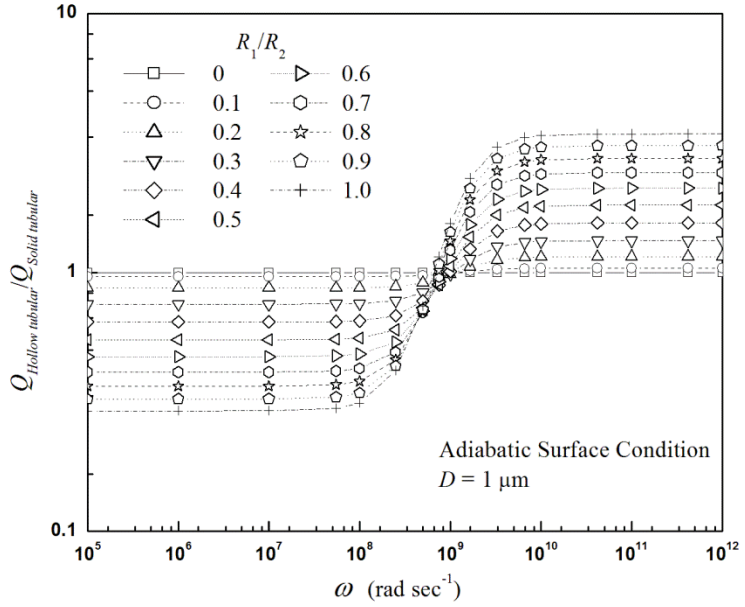

Fig. 3.2 Normalized *Q-factor* vs. ω vibration frequencies for annular tube with different R_1/R_2 under adiabatic surface condition (D = 1 μm).

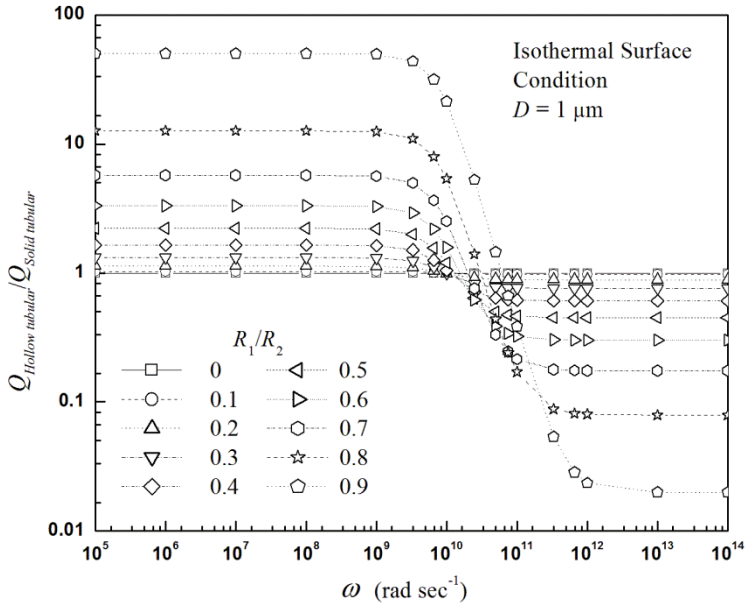

Fig. 3.3 Normalized *Q-factor* vs. vibration frequencies for annular tube with different R_1/R_2 under isothermal surface condition (D = 1 μm).

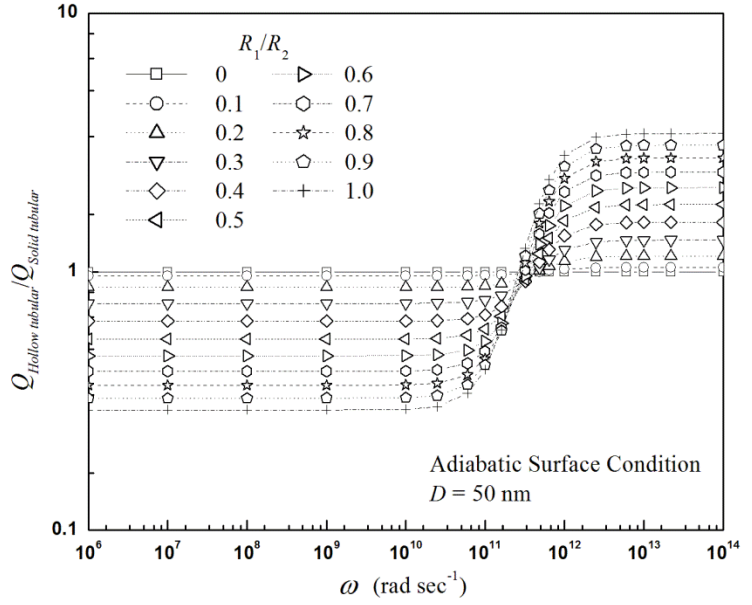

Fig. 3.4 Normalized *Q-factor* vs. vibration frequencies for annular tube with different R_1/R_2 under adiabatic surface condition (D = 50 nm).

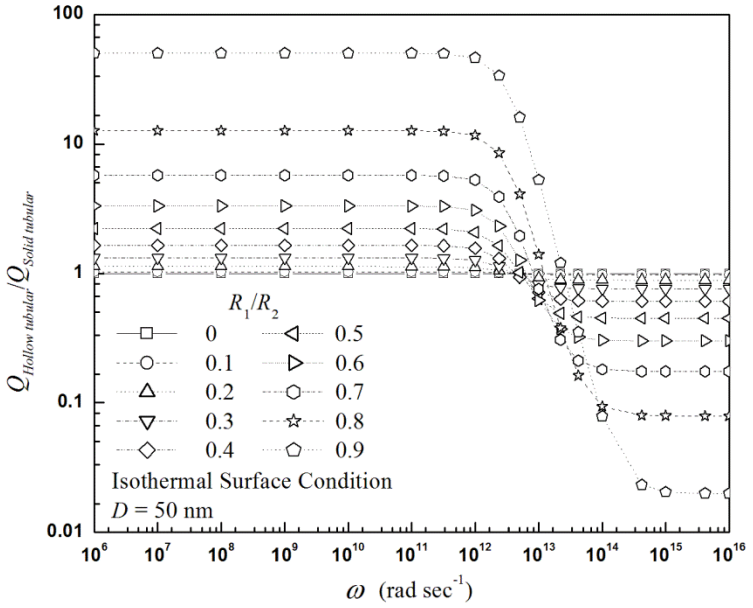

Fig. 3.5 Normalized *Q-factor* vs. vibration frequencies for annular tube with different R_1/R_2 under isothermal surface condition (D = 50 nm).

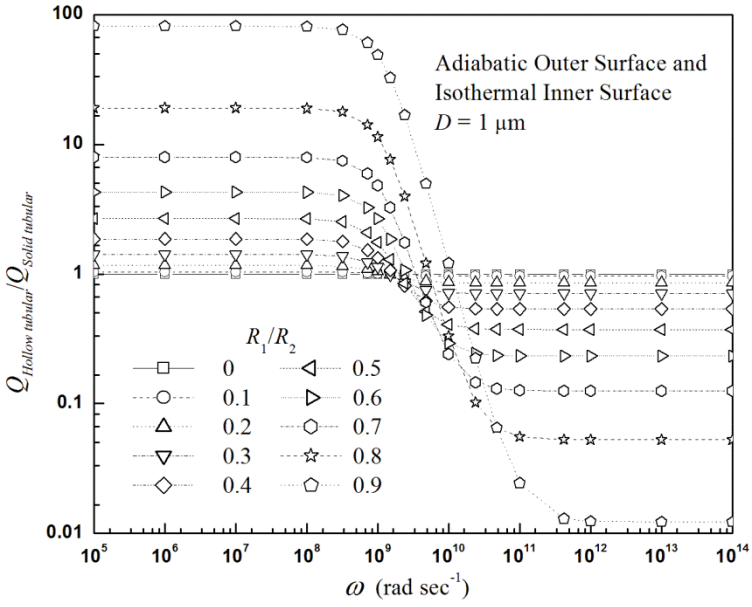

Fig. 3.6 Normalized *Q-factor* vs. vibration frequencies for annular tube with different R_1/R_2 having isothermal inner surface and adiabatic outer surface (D = 1 μm).

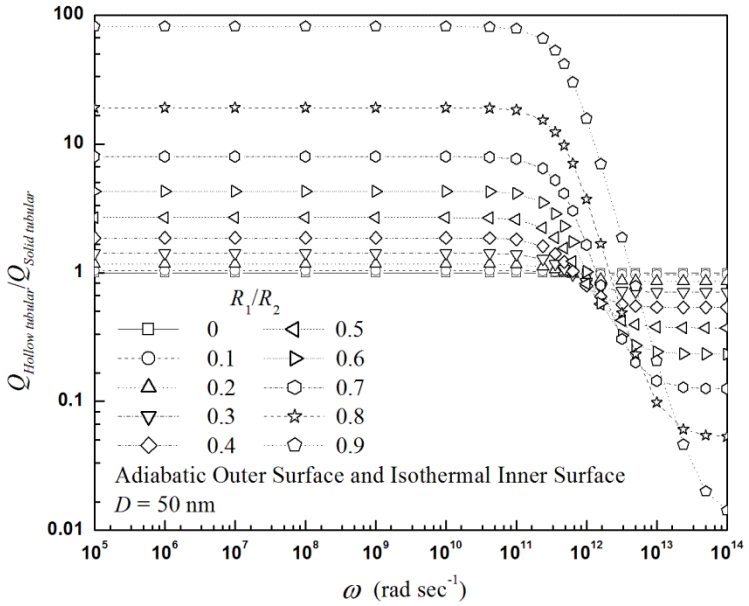

Fig. 3.7 Normalized *Q-factor* vs. vibration frequencies for annular tube with different R_1/R_2 having isothermal inner surface and adiabatic outer surface (D = 50 nm).

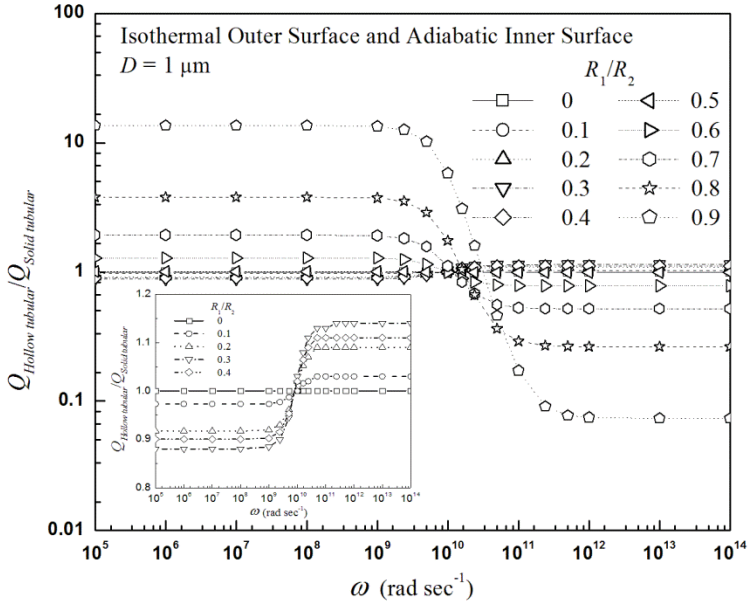

Fig. 3.8 Normalized *Q-factor* vs. vibration frequencies for annular tube with different R_1/R_2 having adiabatic inner surface and isothermal outer surface (D = 1 μm).

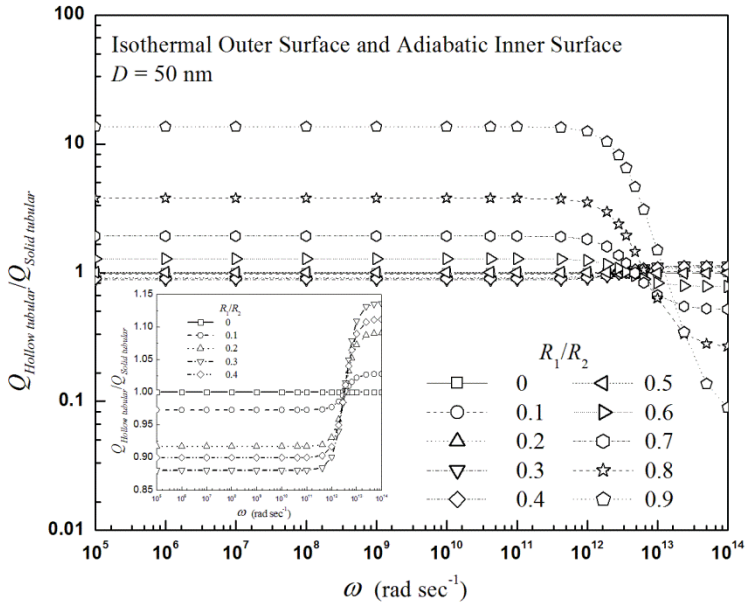

Fig. 3.9 Normalized *Q-factor* vs. vibration frequencies for annular tubes with different R_1/R_2 having adiabatic inner surface and isothermal outer surface (D = 50 nm).

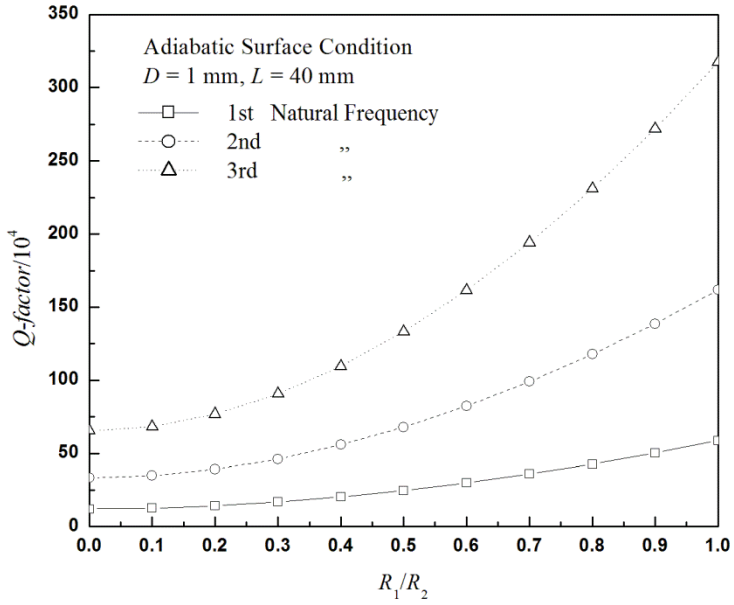

Fig. 3.10 *Q-factor* vs. R_1/R_2 for a doubly-clamped annular tube at its first three natural frequencies with adiabatic thermal surface condition (D = 1 mm and L = 40 mm).

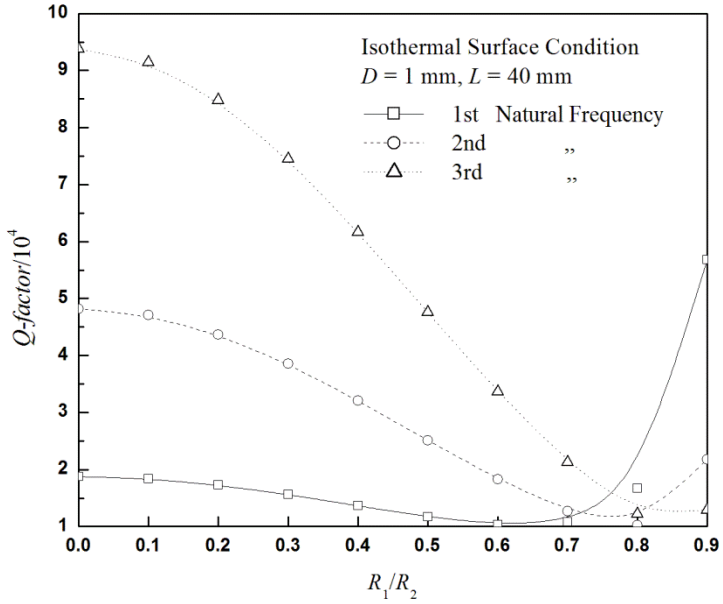

Fig. 3.11 *Q-factor* vs. R_1/R_2 for a doubly-clamped annular tube at its first three natural frequencies with isothermal surface condition (D = 1 mm and L = 40 mm).

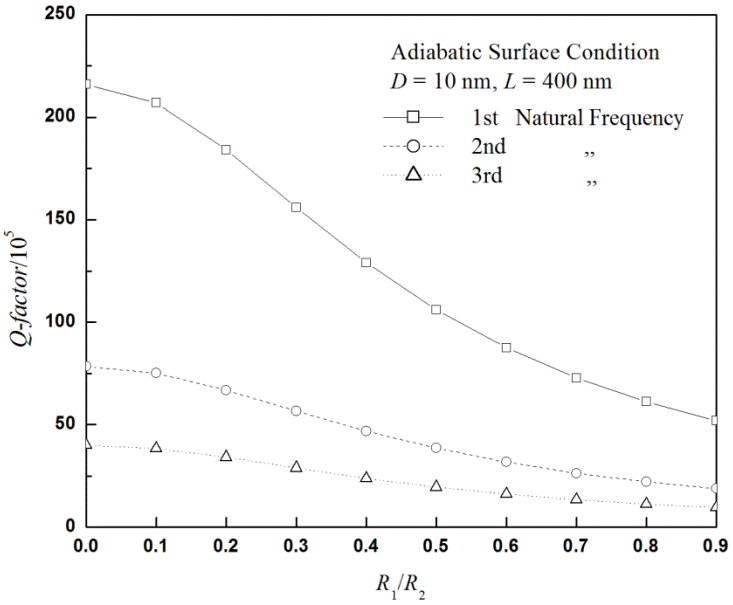

Fig. 3.12 *Q-factor* vs. R_1/R_2 for a doubly-clamped annular tube at its first three natural frequencies with adiabatic surface condition (D = 10 nm and L = 400 nm).

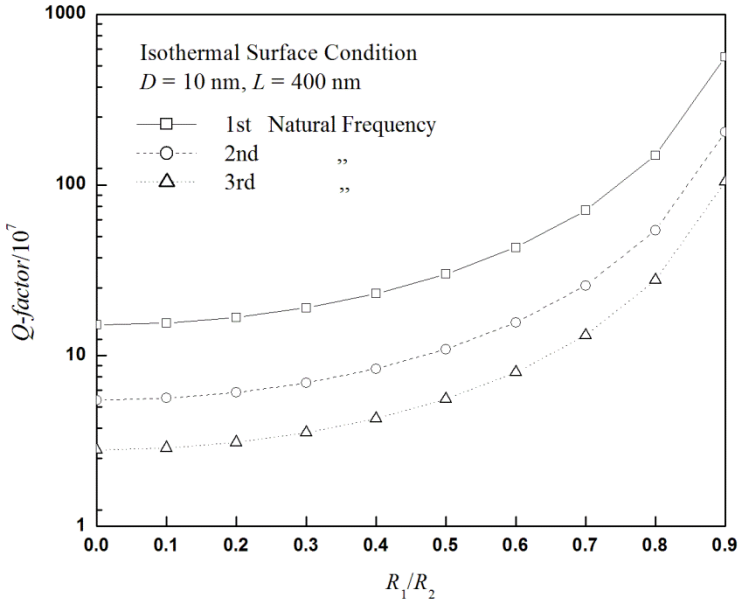

Fig. 3.13 *Q-factor* vs. R_1/R_2 for a doubly-clamped annular tube at its first three natural frequencies with isothermal surface condition (D = 10 nm and L = 400 nm).

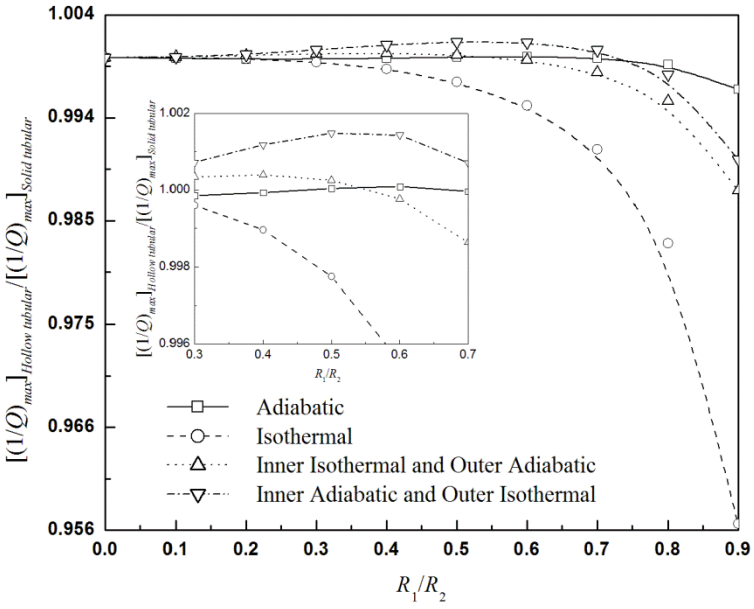

Fig. 3.14 Normalized $(1/Q)_{max}$ vs. R_1/R_2 for hollow tubular beams with surface stress effects and different thermal surface conditions (surface elastic modulus, E_s = 11.7 Nm^{-1} (Zhang 2009; Miller and Shenoy 2000), surface tension, γ_o = 1.12 Nm^{-1} (Miller and Shenoy 2000) and bulk elastic modulus, E = 160×10^9 Nm^{-2} (Srikar and Senturia 2002) for silicon tube of D = 50 nm).

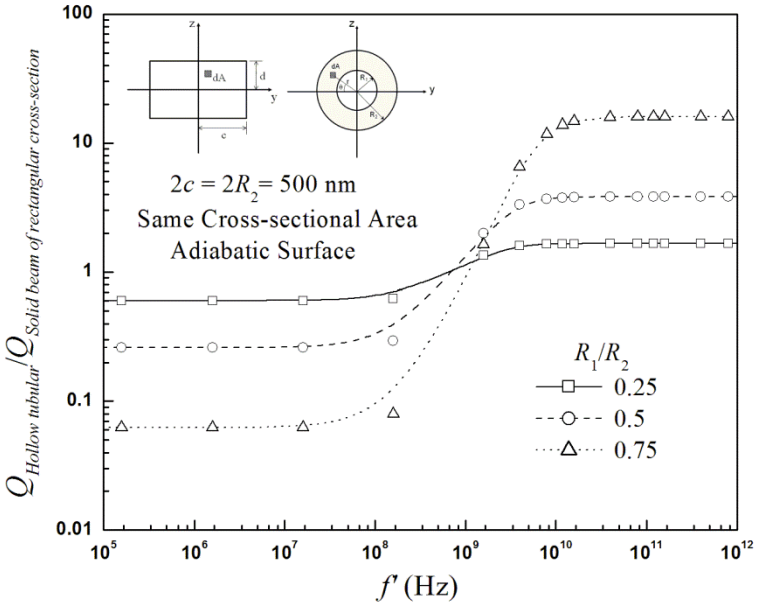

Fig. 3.15 Comparison between beam resonators of solid rectangular cross-section and hollow tubular beam resonator of same size under adiabatic surface condition in respect of *Q-factor*.

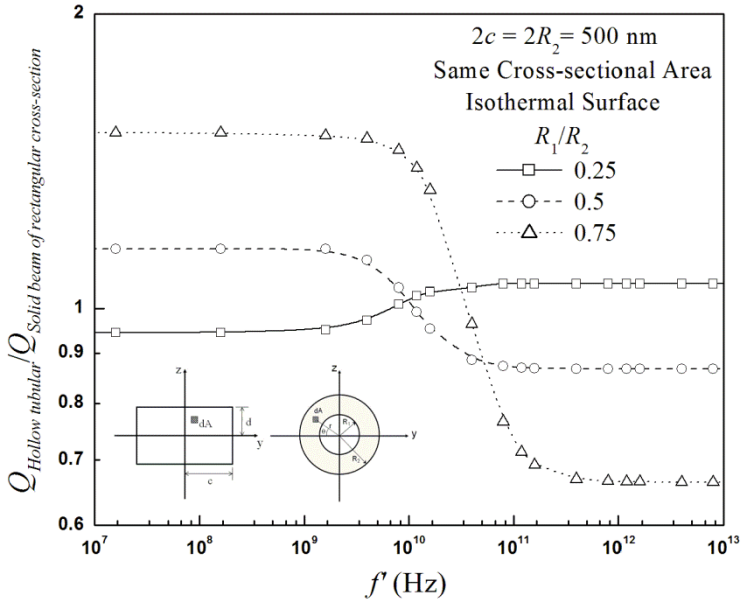

Fig. 3.16 Comparison between beam resonators of solid rectangular cross-section and hollow tubular beam resonator of same size under isothermal surface condition in respect of *Q-factor*.

3.8 References

Abdolvan R., Johari H., Ho G. K., Erbil A. and Ayazi F. 2006. Quality factor in trench-refilled polysilicon beam resonators. *Journal of Microelectromechanical Systems* **15** 471-478.

Arcamone J., Rius G., Abadal G., Teva J., Barniol N. and Pe´rez-Murano F. 2006. Micro/nanomechanical resonators for distributed mass sensing with capacitive detection. *Microelectronic Engineering* **83** 1216-1220.

Biot M. 1956. Thermoelasticity and irreversible thermodynamics. *Journal of Applied Physics* **27** 240-253.

Boukai A. I., Bunimovich Y., Kheli J. T., Yu J. K., Goddard III W. A. and Heath J. R. 2008. Silicon nanowires as efficient thermoelectric materials. *Nature* **451** 168.

Candler R. N.., Amy D., Mathew V., Saurabh A. C., Matthew A. H., Woo-Tae P., Bongsang K., Gary Y., Aaron P., Markus L. and Thomas W. K. 2006. Impact of geometry on thermoelastic dissipation in micromechanical resonant beams. *Journal of Microelectromechanical Systems* **15** 927-934.

Chadwick P. and Sneddon I. 1958. Plane waves in an elastic solid conducting heat. *Journal of Mechanics and Physics of Solids* **6** 223-230.

Chen C., Ma Z. and Anada T. 2008. Synthesis of ultrawideband bandpass filter by multisection of commensurate stepped-impedance resonators. *Microwave and Optical Technology Letters* **50** 2635-2639.

Cheng Y., Zhang J., Zhang Y., Chen X., Wang Y., Ma H. and Cao X. 2009. Preparation of hollow carbon and silicon carbide fibers with different cross-sections by using electrospun fibers as templates. *European Journal of Inorganic Chemistry* **28** 4248-4254.

Cross M. C. and Lifshitz R. 2001. Elastic wave transmission at an abrupt junction in a thin plate with application to heat transport and vibrations in mesoscopic systems. *Physical Review B* **64** 085324.

Daimaruya M. and Naitoh M. 1982. Dispersion and energy dissipation of thermoelastic waves in a circular cylinder. *Acustica* **51** 2 124-130.

Daimaruya M. and Naitoh M. 1987. Dispersion and energy dissipation of thermoelastic waves in a plate. *Journal of Sound and Vibration* **117** 511-518.

De S. K. and Aluru N. R. 2006. Theory of thermoelastic damping in electrostatically actuated microstructures. *Physical Review B* **74** 144305.

Deresiewicz H. 1957. Plane waves in a thermoelastic solid. *The Journal of the Acoustical Society of America* **29** 204-209.

Gaidarzhy A**.,** Imboden M., Mohanty P.,Rankin J., Sheldon B. W. 2007**.** High quality factor gigahertz frequencies in nanomechanical diamond resonators. *Applied Physics Letters* **91** 203503.

Gil-Santos E., Ramos D., Jana A., Calleja M., Raman A. and Tamayo J. 2009. Mass sensing based on deterministic and stochastic responses of elastically coupled nanocantilevers. *Nano Letters* **9** 4122-4127.

Husain A., Hone J., Henk W., Ch. Postma, Huang X. M. H., Drake T., Barbic M., Scherer A., Roukes M. L. 2003. Nanowire-based very-high-frequency electromechanical resonator. *Applied Phyiscs Letters* **83**(6), 1241.

Jiang L., Feng X. J., Zhai J., Jin M. H., Song Y. L. and Zhu D. B. 2006. High-yield self-assembly of flower-like ZnO nanostructures. *Journal of Nanoscience and Nanotechnology* **6** 1830-1832.

Kacem N., Hentz S., Pinto D., Reig B. and Nguyen V. 2009. Non-linear dynamics of nanomechanical beam resonators: improving the performance of NEMS-based sensors. *Nanotechnology* **20** 275501.

Landau L. and Lifshitz E. 1959. *Theory of Elasticity*. Pergamon Press, Oxford

Lifshitz R. and Roukes M. L. 2000. Thermoelastic damping in micro- and nanomechanical systems. *Physical Review B* **61** 5600-5609.

Lockett F. 1958. Effect of thermal properties of a solid on the velocity of Rayleigh waves. *Journal of Mechanics and Physics of Solids* **7** 71-75.

Mailly F., Dumas N., Pous N., Latorre L., Garel O., Martincic E., Verjus F., Pellet C., Dufour-Gergam E. and Nouet P. 2009. Pirani pressure sensor for smart wafer-level packaging. *Sensors and Actuators A* **156** 201-207.

Maple 13.0 software, *Maplesoft*

Memarian M. and Mansour R. R. 2009. Quad-mode and dual-mode dielectric resonator filters. *IEEE Transaction on Microwave Theory and Techniques* **57**(12) 3418-3426.

Miller R. E. and Shenoy V. B. 2000. Size-dependent elastic properties of nanosized structural elements. *Nanotechnology* **11** 139.

Mohanty P., Harrington D. A., Ekinci K. L., Yang Y. T., Murphy M. J. and Roukes M. L. 2002. Intrinsic dissipation in high-frequency micromechanical resonators. *Physical Review B* **66** 085416.

Peng H. B., Chang C.W., Aloni S., Yuzvinsky T. D., Zettl A. 2006. Ultrahigh frequency nanotube resonators. *Physical Review Letters* **97** 087203.

Rinaldi G., Packirisamy M. and Stiharu I. 2007. Tuning the dynamic behaviour of cantilever MEMS based sensors and actuators. *Sensors Review* **27** 142-150.

Ru C. Q. 2009. Thermoelastic dissipation of nanowire resonators with surface stress. *Physica E* **41** 1243-1248.

Sairam P. and Vengallatore S. 2009. Thermoelastic damping in hollow and slotted microresonators. *Journal of Microelectromechanical Systems* **18** 725-735.

Srikar V. T. and Senturia S. D. 2002. Thermoelastic damping in fine-grained polysilicon flexural beam resonators. *Journal of Microelectromechanical Systems* **11** 499-504.

Stan G., Ciobanu C. V., Parthangal P. M. and Cook R. F. 2007. Diameter-dependent radial and tangential elastic moduli of ZnO nanowires. *Nano Letters* **7** 3691-3697.

Sun Y., Fang D. and Soh A. K. 2006. Thermoelastic damping in micro-beam resonators. *International Journal of Solids and Structures* **43** 3213-3229.

Thomas P. B., Michel G., Scott M. K., Wenjiang S., Greg C., John S. F., Ken B. and Scott R. M. 2007. Weighing of biomolecules, single cells and single nanoparticles in fluid. *Nature letters* **446** 1066.

Wong S. J., Fox C. H. J. and McWilliam S. 2006. Thermoelastic damping of the in-plane vibration of thin silicon rings. *Journal of Sound and Vibration* **293** 266-285.

Yi Y. B. and Matin M. A. J. 2007. Eigenvalue solution of thermoelastic damping in beam resonators using a finite element analysis. *Vibration and Acoustics* **129** 478-483.

Yi Y., Rahafrooz A. and Pourkamali S. 2009. Modeling and testing of the collective effects of thermoelastic and fluid damping on silicon MEMS resonators. *Journal of Micro/Nanolithography in MEMS and MOEMS* **8** 023010.

Yun. G. and Park H. S. 2008. A multiscale, finite deformation formulation for surface stress effects on the coupled thermomechanical behavior of nanomaterials. *Computational Methods in Applied Mechanics and Engineering* **197** 3337-3350.

Zener C. 1937. Internal friction in solids. I. Theory of internal friction in reeds. *Physical Review* **52** 230-235.

Zener C. 1938. Internal friction in solids II. General theory of thermoelastic internal friction. *Physical Review* **53** 90-99.

Zhang J. H., Huang Q. A., Yu H. and Wang J. 2009. The influence of surface effects on size-dependent mechanical properties of silicon nanobeams at finite temperature. *Journal of Physics D: Applied Physics* **42** 045409.

Zhao Y. and Lei J. 2009. Hollow micro/nanomaterials with multilevel interior structures. *Advanced Materials* **21** 3621-3638.

Zhou S. M., Wan P., Li S., Zhang B., Gong H. C. and Zhang X. T. 2009. Superconducting single crystalline MgB_2 nanotubes. *Materials Letters* **63** 1680-1682.

Chapter 4

Effect of Cross-Sectional Shape on Thermoelastic Dissipation[2]

4.1 Overview

In spite of practical relevance, little effort has been made to analyze the effect of geometrical shape of cross-section on thermoelastic dissipation of micro/nano beams under different surface thermal condition. The present chapter contains the study thermoelastic dissipation of micro/nano beams of elliptical, triangular or arbitrary rectangular cross-section with accurate satisfaction of the surface thermal condition. Detailed formulas are derived for *Q-factor* of beams of the above-mentioned cross-sections. Results of this study show that for all cross-section discussed, thermoelastic dissipation is a non-monotonic function of the absolute size of the cross-section provided the beam length is fixed, and the maximum dissipation appears at a specific size which is of the order of a few hundreds of nanometers for examples discussed. These results suggest that thermoelastic dissipation could increase with decreasing cross-sectional size within the micron scale, while it could

[2]*A version of this chapter has been published. Tunvir K., Ru C. Q., Mioduchowski A. 2012. International Journal of Mechanical Sciences* ***62*** *77-88.*

decrease with decreasing cross-sectional size within the nano scale. In general, for all beams of the above-mentioned cross-sections, the *Q-factor* for isothermal surface is always higher than the *Q-factor* for adiabatic surface under otherwise identical conditions at micro/nano scales. The present analysis also indicates that, to achieve a high *Q-factor*, beam resonators with elliptical or triangular cross-sections are best to operate at higher frequencies while beams of rectangular cross-sections are best to operate at lower frequencies.

4.2 Introduction

Beam resonators have broad application in a wide range of MEMS/NEMS (Ekinci and Roukes 2005; Cimalla *et al.* 2007; Li *et al.* 2007; Gil-Santos *et al.* 2009). A relevant research topic of current interest is energy dissipation of beam resonators at the micro/nano scale (Yasumura *et al.* 2000; Yang *et al.* 2002; Ekinci and Roukes 2005; Imboden *et al.* 2007). In particular, thermoelastic dissipation has been identified as a major dissipation mechanism for energy loss in a large range of micro/nano mechanical resonators (Zener 1937, 1938; Lifshitz and Roukes 2000; Yasumura *et al.* 2000; Mohanty *et al.* 2002; Yang *et al.* 2002; Imboden *et al.* 2007).

Analysis of thermoelastic dissipation of flexural beam resonators was initiated by Zener (1937, 1938) where damping in some mechanical resonators of rectangular cross-section was attributed to thermoelastic relaxation. Following Zener's work, most of previous works of thermoelastic dissipation were limited to resonators of thin-walled rectangular cross-section with a large width-to-thickness ratio. Although few approximate solutions for thermoelastic loss of beam resonators with various cross-sectional shapes were developed (Jones 1966; Copper and Pilkey 2002), these approximate solutions ignored the role of surface thermal condition

and simply cannot satisfy thermal surface condition prescribed along the boundary curve of the cross-section. Recently, Lifshitz and Roukes (2000) studied exact solution of thermoelastic dissipation for resonator beams of thin rectangular cross section, and their results showed that the simplified classical results of Zener (1937, 1938) is very close to the exact solution under reasonably fair conditions. Their study has stimulated a renewed interest on thermoelastic dissipation of beam resonators (Srikar and Senturia 2002; Houston *et al.* 2004; De and Aluru 2006; Foulgoc *et al.* 2006; Sun *et al.* 2006; Kar and Kanoria 2007; Lu *et al.* 2008; Yun and Park 2008; Ru 2009; Zamanian and Khadem 2010), with a specific concern about small scale effects of thermoelastic dissipation. Very recently, an analysis of thermoelastic dissipation for hollow tubular beam resonators has been offered by Tunvir *et al.* (2010) where a hollow circular cross-section is found to be superior over solid circular cross-section in many cases, in order to achieve higher *Q-factor*. The results suggest that the cross-sectional shape could have a significant impact on thermoelastic dissipation of beam resonators.

Micro and nano beams with elliptical, triangular, or rectangular cross-sections have been reported in the literature. The examples of nanowires of elliptical cross-sections include biaxial Si-ZnS nanowires (of major diameter $2a$ = 124.3 nm and minor diameter, $2b$ = 98.6 nm (Hu *et al.* 2003)), triaxial ZnS-Si-ZnS nanowires (of major diameter $2a$ = 124.3 nm and minor diameter $2b$ = 96.4 nm, (Hu *et al.* 2003)), and Au nanowire (of major diameter $2a$ = 3 μm and minor diameter 2b = 2 μm (Yuan *et al.* 2006)). In particular, in terms of stability against thermal and electrical energy, most stable aspect ratios of elliptical cross-section are not greater than 1.6 (Urban *et al.* 2008). On the other hand, nanowires of triangular cross-sections are produced by various chemical synthesis processes, such as GaN

nanowire of base l = 84 nm (Gradečak *et al.* 2005; Nam *et al.* 2006). An *ab initio* study was carried out in (Agrawal *et al.* 2009) for structural, electronic and optical properties of triangular nanowires. In addition, nanowires of rectangular cross-section with moderate width-to-thickness ratio are also reported in the literature. For example Au nanowires (Bi *et al.* 2010), and Si nanowires (Liang *et al.* 2010) etc are considered as good candidates as resonators for application in MEMS/NEMS. Despite their technical relevance, till to date, no systematic study of thermoelastic dissipation has been carried out for beam resonators of elliptical, triangular or arbitrary rectangular cross-sections. Indeed, to the best of author's knowledge, detailed solution is not available for thermoelastic dissipation of elastic beams of the above-mentioned cross-sectional shapes under adiabatic or isothermal surface condition.

In the present chapter, it has been attempted to analyze thermoelastic dissipation of beam resonators having an elliptical, triangular, or arbitrary rectangular cross-section. Adiabatic or isothermal surface condition is considered, with an emphasis on the effect of geometrical shape of cross-sections on thermoelastic dissipation. The basic thermoelasticity model is described in section 4.3. Theoretical formulation of thermoelastic dissipation and numerical results are given in section 4.4, 4.5 and 4.6, respectively, for beam resonators of arbitrary rectangular, elliptical and triangular cross-sections. In section 4.7, a comparative study is given for thermoelastic dissipation of beam resonators having different cross-sectional shapes. Finally, all results are summarized in section 4.8.

4.3 Theoretical Model

4.3.1 Basic Thermoelasticity Model

Thermoelastic dissipation is a relevant dissipation mechanism in beam resonators at smaller scales (Lifshitz and Roukes 2000). Thermoelastic dissipation occurs in any elastic material subjected to cyclic deformation, especially when the period of cycle is approximately equal to the material's thermal relaxation time constant (Zener 1937, 1938). Here the thermoelastic dissipation has been modeled through a continuum modeling approach. Continuum models are expected to work well for thermoelastic dissipation of beam resonators at micro/nano scales.

For an elastic beam, having the *X*-axis along its axial direction and the *Y* and Z-axes in two perpendicular principal axes of its cross-section, axial strain for bending in the *X*-*Z* plane is $\varepsilon_{xx} = \varepsilon^* + z\varphi$ where $\varphi = \partial^2 w / \partial x^2$. Here, z is the distance to the neutral *Y*-axis, $w(x,t)$ and $\varphi(x,t)$ are transverse deflection and the created curvature of the bent beam respectively, ε^* is residual compressive strain due to a pre-existing surface tension γ_o and is constant throughout the entire beam. The pre-existing surface tension γ_o will not cause any pre-existing bending of the beam of cross-section having two perpendicular axes of symmetry (Ru 2009). In addition to initial surface tension γ_o, surface deformation caused by the bending of the beam structure can lead to additional surface stress. The uniaxial stress in bulk beam, the axial stress in the surface (Ru 2009) and bending moment (Ru 2009) contributed by both the bulk material and the surface are given by

$$\begin{aligned} \sigma_{xx} &= E(\varepsilon_{xx} - \alpha \Delta T) \\ \sigma_s &= \gamma_\circ + E_s(\varepsilon_s - \alpha \Delta T) \\ M &= \int_A \sigma_{xx} z dA + \int_C \sigma_s z dl \end{aligned} \tag{4.1}$$

where σ_{xx} is uniaxial stress in bulk beam, σ_s is the surface axial stress, E_s is the surface elastic modulus, ε_s is surface axial strain, ΔT is the deformation-induced temperature change from the initial uniform temperature T_o, and A and C are the area and perimeter of the cross-section. The temperature field $T(x,y,z,t) = T_o + \Delta T(x,y,z,t)$ is coupled with the deformation by (Zener 1937, 1938; Landau and Lifshitz 1959; Lifshitz and Roukes 2000)

$$C_V \frac{\partial T}{\partial t} + \frac{E\alpha T_\circ}{1-2\nu}\frac{\partial \varepsilon}{\partial t} = \kappa \nabla^2 T \tag{4.2}$$

where C_V is the heat capacity per unit volume, $\varepsilon = \varepsilon_{xx} + \varepsilon_{yy} + \varepsilon_{zz}$ is the mean strain, κ is the thermal conductivity, α is the thermal expansion coefficient, and E and ν are the Young's modulus and Poisson's ration of the bulk material. For uniaxial stress-state, the two lateral strains of the beam are $\varepsilon_{yy} = \varepsilon_{zz} = -(\nu \sigma_{xx}/E) + \alpha \Delta T$. Because the axial wave-length of bending deformation is usually much larger than the dimension of the cross-section, heat conduction along axial x-direction is negligible (Lifshitz and Roukes 2000). Thus Eq. (4.2) becomes

$$\left[C_V + 2(1+\nu)\frac{E\alpha^2 T_\circ}{1-2\nu}\right]\frac{\partial(\Delta T)}{\partial t} + E\alpha T_\circ z \frac{\partial \varphi(x,t)}{\partial t} = \kappa\left(\frac{\partial^2}{\partial y^2} + \frac{\partial^2}{\partial z^2}\right)\Delta T \tag{4.3}$$

4.3.2 Thermoelastic Dissipation of Solid Uniform Beams

Thermoelastic dissipation, defined by the ratio of mechanical energy loss per cycle to total strain energy stored, can be calculated by the net mechanical work per cycle for a periodic harmonic motion (Zener 1937, 1938). Assuming $M(x,t) = M_\circ(x)e^{-i\omega t}$ and $\varphi(x,t) = \varphi_\circ(x)e^{-i\omega t}$, where $\varphi_o(x)$ is a real quantity and ω is the (circular) vibration frequency. It is seen from Eq. (4.3) that the temperature field ΔT must have the form $\Delta T(x,y,z,t) = \Theta(x,t)f(y,z)$. It follows from Eqs. (4.1), (4.2) and (4.3) that

$$M = (EI + E_s I' - \nu\gamma_\circ I')\varphi - \alpha[ES + \{E_s - (1+\nu)\gamma_\circ\}K]\Theta(x,t);$$
$$C_V S\frac{\partial\Theta}{\partial t} + E\alpha T_\circ I\frac{\partial\varphi}{\partial t} + \kappa P\Theta(x,t) = 0 \tag{4.4}$$

where S, K, P, I and I' are defined as

$$S \equiv \int_A z\, f(y,z)dA$$
$$K \equiv \int_C z\, f(y,z)dl$$
$$P \equiv -\int_A z\left(\frac{\partial^2}{\partial y^2} + \frac{\partial^2}{\partial z^2}\right) f(y,z)dA \tag{4.5}$$
$$I \equiv \int_A z^2\, dA$$
$$I' \equiv \int_C z^2\, dl$$

The required energy supply for an infinitesimal bending element dx of the beam located at a point x over a period, $t = 0 \sim 2\pi/\omega$, is equal to the work done by the external force, $dx\int_0^{2\pi/\omega} Re[M]Re[d\varphi/dt]dt$. Since the total strain energy stored in element dx is $Re[M_\circ]\varphi_\circ dx/2$, it can be verified that thermoelastic dissipation or the inverse of the *Q-factor* is given by (Ru 2009)

$$\frac{1}{Q} = \frac{(energy\ loss)/cycle}{2\pi(total\ energy)} = \frac{PEIT_\circ\kappa\omega\alpha^2[ES + \{E_s - (1+\nu)\gamma_\circ\}K]}{(EI + E_s I' - \nu\gamma_\circ I')(P^2\kappa^2 + \omega^2 C_V{}^2 S^2)} \tag{4.6}$$

Therefore, for calculating the dissipation $1/Q$, it is enough to calculate the three constants S, P and K defined by the integrals in Eq. (4.5) of the temperature field ΔT, even without knowing the exact temperature field. The validity of this method was confirmed by excellent agreement with the well-known classical results (Lifshitz and Roukes 2000; Zener 1937, 1938) for thin-wall rectangular and circular cross-sections under adiabatic surface condition (Ru 2009).

4.4 Beams of Rectangular Cross-Section

Rectangular cross-sections of arbitrary width-to-height ratio can be found in the literature such as Au nanowires (Bi *et al.* 2010), Si nanowires (Liang *et al.* 2010) etc which are considered as good candidates as resonators in MEMS/NEMS. Most of previous theoretical analysis on rectangular beams such as (Lifshitz and Roukes 2000; Ru 2009) has been limited to thin-walled rectangular beams with a large width-to-height ratio. To the best of author's knowledge, thermoelastic dissipation of rectangular beams with variable width-to-height ratio and different surface thermal conditions has not been well studied in the existing literature.

4.4.1 Theoretical Analysis of Temperature Field for Rectangular Cross-Section

Let's consider a beam having rectangular cross-section of width $2c$ and height $2d$ respectively, with Y axis in the direction of width, as shown in Fig. 4.1-a. Equation of the rectangular curve with arbitrary aspect ratio c/d can be written as

$$F(y,z)=\left(y^2-c^2\right)\left(z^2-d^2\right)=0 \tag{4.7}$$

Since the rectangular cross-section is doubly symmetric, $f(y,z)$ in Eqs. (4.3) and (4.5) must be odd in z and even in y. Thus the general form of $f(y,z)$ up to the fifth degree is given by

$$f(y,z)=z\left[1+g_1y^2+g_2z^2+g_3y^4+g_4y^2z^2+g_5z^4\right] \tag{4.8}$$

where g_1, g_2, g_3, g_4 and g_5 are constants to be determined. The degree of approximate function $f(y,z)$ is simply decided in such a way that the number of independent coefficients is equal to the number of conditions and therefore all

independent coefficients can be determined uniquely by satisfying all required conditions.

4.4.1.1 Adiabatic Surface Condition

Let us first consider adiabatic surface condition which requires that normal derivative $\partial\Delta T/\partial n$ (or $\partial f/\partial n$) vanishes along the given boundary curve $F(y,z) = 0$ of the cross-section in the Y-Z plane. It can be easily verified that ($\partial f/\partial n = 0$) along a given boundary curve $F(y,z) = 0$ means that

$$\left(\frac{\partial f}{\partial y}\frac{\partial F}{\partial y}+\frac{\partial f}{\partial z}\frac{\partial F}{\partial z}\right)\Big|_{F(y,z)=0}=0 \tag{4.9}$$

On using Eqs. (4.7)-(4.9), adiabatic surface condition gives

$$\begin{aligned} &g_1=g_3=g_4=0;\\ &1+3g_2d^2+5g_5d^4=0 \end{aligned} \tag{4.10}$$

Therefore $f(y,z)$ should be independent of y. Keeping the solution in a lower order of z and choosing $g_5=0$, $g_2 = -1/(3d^2)$ is obtained Therefore $f(y,z)$ for a rectangular cross-section under adiabatic surface thermal condition is given by

$$f(y,z)=z\left[1-\frac{z^2}{3d^2}\right] \tag{4.11}$$

The integrals P, S and K of Eq. (4.5) can thus be derived as

$$\begin{aligned} P&=\frac{8}{3}cd\\ S&=\frac{16}{15}cd^3\\ K&=\frac{8d^2}{3}\left[c-\frac{2d}{5}\right] \end{aligned} \tag{4.12}$$

Thus using P, S and K in Eq. (4.6) one can calculate energy dissipation $1/Q$ for a rectangular beam of arbitrary width-to-height ratio under adiabatic surface thermal condition. In the case of $c >> d$, the above results reduce to

$$\begin{aligned} P &= \frac{8}{3}cd \\ S &= \frac{16}{15}cd^3 \\ K &= \frac{8cd^2}{3} \end{aligned} \tag{4.13}$$

in agreement with Ru (2009) for thin-walled rectangular cross-sections.

4.4.1.2 Isothermal Surface Condition

Next, let us consider isothermal surface which requests $\Delta T = 0$ along the given curve $F(y,z) = 0$ in the Y-Z plane. Thus, since $f(y,z)$ must be odd in z, up to the lowest order of z and y, the solution $f(y,z)$ is given by

$$f(y,z) = z\left(y^2 - c^2\right)\left(z^2 - d^2\right) \tag{4.14}$$

and the integrals P, S and K of Eq. (4.5) can thus be derived as

$$\begin{aligned} P &= \frac{16}{3}c^3d^3 + \frac{16}{15}cd^5 \\ S &= \frac{16}{45}c^3d^5 \\ K &= 0 \end{aligned} \tag{4.15}$$

It is noted that the integral values P and S in Ru (2009) under isothermal surface condition for thin rectangular cross-section ($c >> d$) are

$$\begin{aligned} P &= 8cd \\ S &= \frac{8}{15}cd^3 \end{aligned} \tag{4.16}$$

Since S, P and K defined in Eq. (4.5) are all proportional to a constant factor of $f(y,z)$, it is seen from Eq. (4.6) that *Q-factor* does not depend on any constant factor of $f(y,z)$

and therefore $f(y,z)$ is arbitrary within to a constant factor. Evidently, as expected, Eq. (4.15) reduce to Eq. (4.16) with a common constant factor, which does not cause any difference in *Q-factor* because $f(y,z)$ is arbitrary within to a constant factor.

4.4.2 Numerical Results and Discussion for Rectangular Cross-Section

What is of greater interest for rectangular cross-sections is to find out the effect of aspect ratio (c/d) on thermoelastic dissipation. For this reason, the *Q-factor* of rectangular beams, as compared to a beam of square cross-section with same cross-sectional area, is demonstrated for varying aspect ratio in Figs. 4.2 and 4.3, for adiabatic and isothermal surface conditions respectively. Thus, the normalized *Q-factor*, defined by the ratio of Q for the rectangular beam to Q for the square beam of same cross-sectional area, is plotted against vibration frequency ω in the absence of surface stress-effect. Aspect ratio of the rectangular cross-section (c/d) varies from 1 to 10. Calculations of thermoelastic dissipation in this study are carried out for equilibrium temperature T_o = 300 K and for material constants that taken from (Srikar and Senturia 2002): coefficient of thermal expansion, $\alpha = 2.6\times10^{-6}$ K^{-1}, bulk elastic modulus, $E = 160\times10^{9}$ Nm^{-2}, thermal conductivity, $\kappa = 148$ $Wm^{-1}K^{-1}$ and heat capacity per unit volume, $C_V = 1.66\times10^{6}$ $Jm^{-3}K^{-1}$.

4.4.2.1 Adiabatic Surface Condition

Under adiabatic surface thermal condition, it is seen from Fig. 4.2 that for an aspect ratio of c/d = 10, *Q-factor* of a rectangular beam is 9 times higher than that of a square beam of same cross-sectional area for vibration frequencies below 10^7 rad

sec^{-1}, while the former is 9 times lower than the latter for vibration frequency higher than 4×10^8 rad sec^{-1}. The normalized *Q-factor* varies significantly only within a limited frequency range of $10^7 \sim 10^{10}$ rad sec^{-1}, which means that the normalized *Q-factor* is almost frequency-independent for frequencies higher than 4×10^8 rad $sec^{-1}$and for frequencies below 10^7 rad sec^{-1}. Moreover, Fig. 4.2 shows that effects of cross-sectional shapes on *Q-factor* are different for low and high frequencies. This behavior is due to the dependency of thermoelastic dissipation on thermal relaxation time (Zener 1937, 1938; Lifshitz and Roukes 2000) and operating frequency, ω. Thermal relaxation time is the time that is needed to allow the temperature gradient of the beam to relax. In the absence of surface stress effect ($E_s = \gamma_o = 0$), Eq. (4.6) can be rearranged as

$$\frac{1}{Q} = \frac{E\alpha^2 T_\circ}{C_V}\left[\frac{\omega\tau}{1+(\omega\tau)^2}\right] \tag{4.17}$$

where $\tau = (C_V S)/(\kappa P)$. Comparing with Zener's formula for thermoelastic dissipation in (Zener 1937, 1938; Lifshitz and Roukes 2000), τ is the thermal relaxation time of a beam of given cross-section. Thus thermal relaxation time of the given cross-section depends on the cross-sectional size and shape and thermal diffusivity of the material, $\chi = \kappa/C_V$. It can be realized from Eq. (4.17) that maximum dissipation occurs when vibration frequency is on the order of the system's thermal relaxation rate ($1/\tau$). For example, thermal relaxation rates for rectangular (c/d = 10) and square cross-sections of same cross-sectional area are 8.92×10^8 sec^{-1} and 8.92×10^7 sec^{-1} respectively which indicates that maximum dissipations in rectangular (c/d = 10) and square beams of same cross-sectional area occur at different frequencies. Dissipation decreases gradually as the operating frequency ω goes away from the frequency at which maximum dissipation occurs. Thus different thermal relaxation

rates for square and rectangular cross-sectional shapes of same cross-sectional area cause their *Q-factors* to be different at low and high frequencies.

4.4.2.2 Isothermal Surface Condition

Similar behavior of normalized *Q-factor* for beams of rectangular cross-section can be observed for isothermal surface condition, except that the range of frequency in which *Q-factor* varies significantly is $10^7 \sim 10^{11}$ rad sec^{-1} (Fig. 4.3) for isothermal surface condition. For an aspect ratio of $c/d = 10$, say, *Q-factor* of a rectangular beam can be higher than that of a square beam of same cross-sectional area by a factor of more than 8. Under isothermal surface condition, thermal relaxation rates for rectangular ($c/d = 10$) and square cross-sections of same cross-sectional area are 5.36×10^9 sec^{-1} and 6.42×10^8 sec^{-1} respectively which are higher than those under adiabatic surface condition. For rectangular and square cross-sections, temperature gradient in beam relaxes quicker under isothermal surface than under adiabatic surface condition. Effects of these cross-sections on *Q-factors* are also different at low and high frequencies because of their different thermal relaxation times.

4.4.2.3 Dissipation at Natural Frequencies

Thermoelastic dissipation of beams at their natural frequencies is of greater interest for designing of resonators. The normalized *Q-factor*s at fundamental frequency are shown in Fig. 4.4 for doubly-clamped beam of rectangular cross-section under adiabatic or isothermal surface condition. The fundamental frequency of an elastic beam is calculated by

$$\omega = \sqrt{\frac{\beta^4 EI}{L^4 \rho A}} \tag{4.18}$$

where ρ = density of the material, A = cross-sectional area, β = 4.73 for fundamental frequency of beam with clamped ends, and L = length of the beam. Here the ratio of length (L) to width ($2c$) of the beam is always kept as 40. The validity of the present approach is evident from the solution for arbitrary rectangular cross-section of this study as they are identical to the solution for thin walled structure (Zener 1937; Ru 2009) as c/d tends to infinity (Fig. 4.3). Nevertheless, classical solution of Zener (1937) is also used to normalize the *Q-factor*s for rectangular cross-section of the present solution to assess the validity of the present approach. Under adiabatic surface thermal condition at any scale (Fig. 4.4), the present result matches the solutions of Zener (1937) with reasonable accuracy. *Q-factors* for rectangular cross-section under isothermal surface condition are also normalized by the solution of Zener (1937) to assess the merit of the present approach. It is also observed from Fig. 4.4 that *Q-factors* under isothermal surface condition are higher than those under adiabatic condition for any aspect ratio (c/d) at both micro and nano scales. At macro scale, *Q-factors* under isothermal surface condition is lower than those under adiabatic surface condition only until c/d = 2.2.

4.4.2.4 Maximum Dissipation

Finally, let us examine the dependence of the maximum dissipation on rectangular cross-section. It follows from Eq. (4.6) that the maximum dissipation $(1/Q)_{max}$ for given cross-section occurs at a frequency of

$$\omega^* = \frac{1}{\tau} = \frac{\kappa P}{C_V S} \tag{4.19}$$

which along with Eq. (4.6) shows that in the absence of surface stress effect (E_s = γ_o = 0), the maximum dissipation is determined by the material constants alone, independent of the size and shape of the cross-section and the thermal surface condition (Ru 2009; Tunvir *et al.* 2010), as given by

$$\left.\frac{1}{Q}_{max}\right|_{E_s=\gamma_o=0} = \frac{E\alpha^2 T_o}{2C_V} \tag{4.20}$$

Therefore, to study the dependence of the maximum dissipation on rectangular cross-section, surface stress effect should be taken into account. Surface stress constants for Si beam resonator are taken from (Miller and Shenoy 2000; Zhang 2009): surface tension, γ_o = 1.12 Nm^{-1}, surface elastic modulus, E_s = 11.7 Nm^{-1}. The effect of these surface stresses on thermoelastic dissipation depends on the size of the cross-section, but is independent of operating frequency ω. For example, for E = 160 Nm^{-2}, γ_o = 1.12 Nm^{-1} and E_s = 11.7 Nm^{-1}, the surface stress effect reduces thermoelastic dissipation of rectangular beam (c/d = 10) by only about 0.33% and 1.3% under adiabatic and isothermal surface conditions respectively if thickness ($2d$) goes down to 30nm from 1 μm. It must be mentioned here that the difference between the entire cross-sectional area and the bulk material cross-sectional area has been neglected in this calculation. Effect of rectangular cross-section on the maximum dissipation of a beam resonator is shown in Fig. 4.5 for micro/nano scale, compared to the maximum dissipation of a square beam of same cross-sectional area. It is seen that at nanometer scale the maximum dissipation for a rectangular beam is always lower than the maximum dissipation of a square cross-section of same cross-sectional area under adiabatic or isothermal surface condition. Somewhat surprisingly, at micro scale (Fig. 4.5), the maximum thermoelastic

dissipation is almost same for both cross-sections irrespective of aspect ratio and thermal surface condition.

4.5 Beams of Elliptical Cross-Section

As mentioned before, nanowires of elliptical cross-sections are reported in the literature (Hu *et al.* 2003; Yuan *et al.* 2006). Most stable cross-sectional aspect ratios for nanowires of elliptical cross-section are found to be not greater than 1.6 (Urban *et al.* 2008). Despite their technical relevance, however, effect of the aspect ratio of elliptical cross-sections on thermoelastic dissipation has not been studied previously, which has raised an interesting problem for research of thermoelastic dissipation.

4.5.1 Theoretical Analysis of Temperature Field for Elliptical Cross-Section

No solution is available in the existing literature for thermoelastic dissipation of elastic beams of elliptical cross-section under different surface thermal conditions. To derive the desired solution, let us consider an elliptical cross-section of major and minor radii a and b respectively, as shown in Fig. 4.1-b. The axial direction of the beam is in the x-direction while the cross-section is on the Y-Z plane. Equation of the elliptical boundary curve of the cross-section can be written as

$$F(y,z)=\frac{y^2}{a^2}+\frac{z^2}{b^2}-1=0 \tag{4.21}$$

It should be stated here that for any doubly symmetric cross-section of two perpendicular axes of symmetry (such as elliptical or rectangular), it can be verified

from Eq. (4.3) that $f(y,z)$ must be odd in z and even in y (Ru 2009; Tunvir *et al.* 2010). Thus, up to the second-degree, the general form of $f(y,z)$ can be given as a polynomial of y and z as follows

$$f(y,z)=z\left[1+m_1y^2+m_2z^2\right] \tag{4.22}$$

where m_1, m_2 are constants to be determined.

4.5.1.1 Adiabatic Surface Condition

Adiabatic surface condition requires that normal derivative ($\partial\Delta T/\partial n$) vanishes along the boundary curve of the elliptical cross-section (see Eq. (4.9)). On using Eqs. (4.9), (4.21) and (4.22), adiabatic surface condition gives

$$m_1=-\frac{1}{a^2+2b^2},\quad m_2=-\frac{1}{3b^2} \tag{4.23}$$

Therefore $f(y,z)$, which exactly meets the adiabatic surface condition, is given by

$$f(y,z)=z\left[1-\frac{y^2}{a^2+2b^2}-\frac{z^2}{3b^2}\right] \tag{4.24}$$

The integrals P, S and K of Eq. (4.5) can be derived as

$$\begin{aligned}
P&=\frac{\pi}{2}ab\left[1+\frac{b^2}{a^2+2b^2}\right]\\
S&=\frac{\pi}{24}ab^3\left[5-\frac{a^2}{a^2+2b^2}\right]\\
K&=\frac{\pi}{7680\left(a^2b+2b^3\right)}\begin{bmatrix}a^2b^2\left(4005\,b^2-2505\,a^2\right)+\left(14805\,b^6-945\,a^6\right)\\+\pi^2\left(2400\,a^6+800\,a^2b^4+6240\,a^4b^2-9440\,b^6\right)\\+\pi^4\left(1536\,b^6+3584\,a^2b^4-3584\,a^4b^2-1536\,a^6\right)\end{bmatrix}
\end{aligned} \tag{4.25}$$

Thus using P, S and K in Eq. (4.6) one can calculate energy dissipation $1/Q$ for a beam of elliptical cross-section under adiabatic surface condition. It can be verified easily that the present results with $a = b$ in Eq. (4.25) reduce to those of a solid circular cross-section under adiabatic surface thermal condition given in (Ru 2009).

4.5.1.2 Isothermal Surface Condition

Now let us consider isothermal surface which requests ΔT vanishes on the elliptical boundary curve of the cross-section. Thus, since $f(y,z)$ must be odd in z, it follows from Eqs. (4.21) and (4.22), up to the lowest order of z and y, $f(y,z)$ is obtained as

$$f(y,z)\big|_{F(y,z)=0} = z\left[1 + m_1 y^2 + m_2 z^2\right] = 0 \tag{4.26}$$

which gives $m_1 = -1/a^2$ and $m_2 = -1/b^2$. Therefore $f(y,z)$, which exactly meets the isothermal surface condition, is given by

$$f(y,z) = z\left[1 - \frac{y^2}{a^2} - \frac{z^2}{b^2}\right] \tag{4.27}$$

The integrals P, S and K defined by Eq. (4.5) can thus be derived as

$$\begin{aligned} P &= \frac{\pi}{2} b\left[3a + \frac{b^2}{a}\right] \\ S &= \frac{\pi}{12} a b^3 \\ K &= 0 \end{aligned} \tag{4.28}$$

This result for $a = b$ is in agreement with Ru (2009) for solid circular cross-sections under isothermal surface condition.

4.5.2 Numerical Results and Discussion for Elliptical Cross-Section

Let us examine the dependence of thermoelastic dissipation on the elliptical cross-section and surface thermal conditions. In Figs. 4.6 and 4.7, the effect of elliptical cross-section on the *Q-factor* is demonstrated for adiabatic and isothermal surface conditions respectively. In general, since solution for an elliptical cross-section is

not available, one may use a rectangular cross-section to approximately replace an elliptical cross-section. In doing so, it is of interest to find out possible error caused by such a replacement. For this reason, normalized *Q-factor*, defined by the ratio of Q for the elliptical beam to Q for a rectangular beam (discussed previously in section 3) of same cross-section area and width under otherwise identical condition, is plotted against vibration frequency ω in the absence of surface stress effect (E_s = γ_0 = 0). It is to be noted here that the choice of rectangular cross-section of same cross-sectional area and width as the normalizing structure is made so that the rectangular beam has smaller bending rigidity in *X-Z* plane for all aspect ratio. Aspect ratio (a/b) varies from 1 to 10 with fixed width $2a$. Rectangular cross-section is chosen for normalization also due to its popular usage in MEMS/NEMS. Vibration frequency considered are in a range of 10^3-10^{14} rad sec^{-1}, which covers the operating frequencies of most resonators reported in the literature.

4.5.2.1 Adiabatic Surface Condition

Under adiabatic surface condition (Fig. 4.6), compared to a rectangular beam of same cross-sectional area and width, the *Q-factor* for elliptical beam is lower than that for the rectangular beam for vibration frequencies lower than10^7 rad sec^{-1}, while the former is higher than the latter for vibration frequencies higher than 10^9 rad sec^{-1}. The normalized *Q-factor* varies significantly only within a restricted frequency range of 10^6-10^{10} rad sec^{-1}. Indeed, the normalized *Q-factor* is almost frequency-independent for frequencies below 10^6 rad sec^{-1} or for frequencies above 10^{10} rad sec^{-1}. In addition, the elliptical beams of larger aspect ratio (a/b) show steeper change in the normalized *Q-factor*, and the normalized ratio $Q_{elliptical}/Q_{rectangular}$ is bigger or smaller than unity by a factor up to 1.4. It is also

revealed that for the most stable aspect ratio of elliptical cross-sections ($1 \leq a/b \leq 2$) in nanowire resonators (Urban *et al.* 2008), the *Q-factor* for an elliptical cross-section depends on the operating frequency and can be as high as 1.3 times that for a rectangular cross-section of same cross-sectional area and width. As expected, for example, thermal relaxation rates for elliptical cross-section (a/b = 2) is 4.61×10^{7} sec^{-1}, while thermal relaxation rates for rectangular cross-section of same cross-sectional area and width is 5.79×10^{7} sec^{-1}.

4.5.2.2 Isothermal Surface Condition

Similar behavior of the normalized *Q-factor* is observed for isothermal surface condition (Fig. 4.7). Unlike the result for adiabatic surface condition, however, the normalized *Q-factor* for isothermal surface varies significantly within a frequency range of 10^{7} rad sec^{-1} to 6×10^{10} rad sec^{-1}. Plotted curve for the aspect ratio a/b = 1 under isothermal surface condition shows that, *Q-factor* of a beam resonator of circular cross-section can be 13% higher or lower than that of a rectangular cross-section of same width and cross-sectional area. In summary, the elliptical geometry has a moderate effect on the *Q-factor* as compared to a rectangular cross-section of same width and cross-sectional area, and this effect is opposite for high and low frequencies. This moderate effect can also be described by the small difference between thermal relaxation rates of the two cross-sections. For example, under isothermal surface condition, thermal relaxation rates for elliptical (a/b = 2) and rectangular cross-sections of same cross-sectional area and width are 2.78×10^{8} sec^{-1} and 3.58×10^{8} sec^{-1} respectively which are also higher than those under adiabatic surface condition. Replacing an elliptical beam by a rectangular beam of same cross-

sectional area and width can cause up to a few tens of percentages in relative error. The present analysis also suggests that, to achieve a higher *Q-factor*, beam resonators of elliptical cross-section are best to operate at high frequencies (>10^7 rad sec^{-1}) for both adiabatic and isothermal surface thermal conditions.

4.5.2.3 Dissipation at Natural Frequencies

Fig. 4.8 shows *Q-factors* at fundamental frequencies of elliptical beams of various aspect ratios where the ratio of length (L) to major axis ($2a$) of the cross-section is always kept as 40. The cross-section sizes of the beams considered are at millimeter, micrometer and nanometer scales. It is seen from Fig. 4.8 that *Q-factor* for elliptical beams for isothermal surface condition is always higher than the *Q-factor* for adiabatic surface condition at micrometer and nanometer scales. In addition, the *Q-factor* is increased with increasing cross-sectional aspect ratio, and the increase in *Q-factor* can be more than a few orders of magnitude when the aspect ratio (a/b) increases from 1 to 10. For any aspect ratio (a/b), *Q-factor*s at nanometer scale are always higher than those at micro and millimeter scales.

4.5.2.4 Maximum Dissipation

The maximum dissipation of an elliptical beam under different surface thermal conditions, normalized by the maximum dissipation of a rectangular beam of equal width and cross-sectional area, is shown in Fig. 4.9 in the presence of surface stress at micro and nano scales. It is seen from Fig. 4.9 that the maximum thermoelastic dissipation in the elliptical beam is always lower than that for a rectangular beam of equal cross-sectional area and width. In addition, the maximum dissipations at

nanometer scale is always less than that at micrometer scale for any aspect ratio of the elliptical cross-section under both adiabatic and isothermal surface thermal conditions. In particular, under isothermal surface condition, the maximum dissipation in beam resonators of elliptical cross-section goes down rapidly with increasing aspect ratio (a/b) of the elliptical cross-section.

4.6 Beams of Triangular (Isosceles) Cross-Section

Nanowires of triangular cross-section are reported in the literature, for example, in Gradečak *et al.* 2005; Nam *et al.* 2006 where the cross-sections are usually close to an equilateral triangle. To the best of author's knowledge, thermoelastic dissipation of triangular beams has not been studied previously.

4.6.1 Theoretical Analysis of Temperature Field for Triangular (Isosceles) Cross-Section

Let's consider an isosceles triangular beam of base l and height h respectively, as shown in Fig. 4.1-c where the Y-Z coordinate system is centered at the centroid of the triangular cross-section with Y-axis parallel to the base of the isosceles triangle. In this section, in order to avoid surface tension induced pre-bending of beams of triangular cross-section which are non-symmetric about the neutral Y-axis, the problem has been confined to the case when surface stress are absent ($E_s = \gamma_o = 0$). Furthermore, to simplify the derivation of the polynomial solution $f(y,z)$, let us introduce another Y'-Z' system whose Y'-axis is parallel to the Y-axis so that the origin of the Y'-Z' system is located at the top vertex of the triangle as shown in Fig.

4.1-c. Thus the equations of the three sides of the triangle in the Y'-Z' system are given by

$$z' = \frac{s_1}{s_2} y';\ z' = \frac{-s_1}{s_2} y';\ z' = -h \tag{4.29}$$

where

$$s_1 = \frac{h}{\sqrt{h^2 + (l/2)^2}};\ s_2 = \frac{l/2}{\sqrt{h^2 + (l/2)^2}};\ z' = z - \frac{2h}{3};\ y' = y \tag{4.30}$$

Since the problem is symmetric about the Z'-axis, $f(y',z')$ is even in y' and its general form, up to the fourth order, is given by

$$f(y',z') = p_1 + p_2 z' + p_3 z'^2 + p_4 z'^3 + p_5 z'^4 + y'^2\left[p_6 + p_7 z' + p_8 z'^2\right] + p_9 y'^4 \tag{4.31}$$

where p_1, p_2, p_3, p_4, p_5, p_6, p_7, p_8 and p_9 are constants to be determined, and one of the nine constants can be chosen arbitrarily, as it can be seen from Eq. (4.6) that $f(y',z')$ is arbitrary within to a constant factor. As shown below, the degree of approximate function $f(y',z')$ is simply decided in such a way that the number of independent coefficients is equal to the number of conditions and therefore all independent coefficients can be determined uniquely by satisfying all required conditions. It should be stated here that for any doubly symmetric cross-section of two perpendicular axes of symmetry (such as elliptical or rectangular), it can be verified from Eq. (4.3) that $f(y',z')$ must be odd in z' and even in y' (Ru 2009; Tunvir *et al.* 2010), which satisfies the zero-axial resultant force condition $\int_A \Delta T dA = 0$ (Ru 2009) and is compatible with heat Eq. (4.3). For a non-doubly symmetric cross-section such as triangular one discussed now, the zero-axial resultant force condition $\int_A \Delta T dA = 0$ requests that any approximate solution $f(y',z')$ should satisfy

$$\int_A f(y',z') dA = 0 \tag{4.32}$$

Furthermore, $f(y',z')$ is also requested to meet heat equation Eq. (4.3) approximately. For this reason, $f(y',z')$ is requested to meet the zero-order average form of Eq. (4.3) obtained by integration of Eq. (4.3) over the cross-section as

$$\int_A \nabla^2 f(y',z')\,dA = 0 \tag{4.33}$$

In addition, $f(y',z')$ will be requested to meet first-order average form of Eq. (4.3) i.e. 2nd equation in Eq. (4.4) which is obtained by multiplying Eq. (4.3) by z' and integrating over the cross-section. In other words, instead of satisfying exact heat equation (Eq. (4.3)), the approximate solution $f(y',z')$ is requested to meet the condition Eq. (4.4) and two extra integral conditions (Eqs. (4.32) and (4.33)). Evidently the two integral conditions (Eqs. (4.32) and (4.33)) are met automatically when the cross-section is doubly symmetrical and $f(y',z')$ is odd in z'.

4.6.1.1 Adiabatic Surface Condition

An adiabatic surface condition requires that normal derivative ($\partial\Delta T/\partial n$) vanishes along all three sides of the isosceles triangular curve shown in Fig. 4.1-c. Substitution of Eq. (4.31) into the adiabatic surface condition similar to Eq. (4.9), on using Eqs. (4.29) and (4.30), it can be verified that

$$\begin{aligned}
&p_2 - 2p_3 h + 3p_4 h^2 - 4p_5 h^3 = 0\\
&p_7 - 2p_8 h = 0\\
&p_2 = 0\\
&p_6 = p_3\\
&(3p_4 - 2p_7)\frac{{s_1}^2}{s_2} + p_7 s_2 = 0\\
&(2p_8 - 4p_5)\frac{{s_1}^3}{{s_2}^2} + 2s_1(2p_9 - p_8) = 0
\end{aligned} \tag{4.34}$$

Note that $p_2 = 0$, it is seen from Eqs. (4.31) and (4.34) that five, out of total eight constants, p_4, p_5, p_6, p_8 and p_9, can be uniquely determined in terms of the

remaining three arbitrary constants p_1, p_3 and p_7. Since $f(y',z')$ is arbitrary within a constant factor, one can choose one of the three arbitrary constants (p_1, p_3 and p_7), say p_7 = 1, and thus the remaining two constants (p_1 and p_3) are determined uniquely by the two integral conditions of Eqs. (4.32) and (4.33). In doing so, it can be verified that $f(y,z)$ for an isosceles triangular cross-section under adiabatic surface thermal condition is given by

$$\begin{aligned} f(y,z) = p_1 + p_3\left(z-\frac{2h}{3}\right)^2 + \left(\frac{2}{3}-\frac{s_2^{\,2}}{3s_1^{\,2}}\right)\left(z-\frac{2h}{3}\right)^3 + \left(\frac{2s_1^{\,2}-s_2^{\,2}}{4s_1^{\,2}h}-\frac{p_3}{2h^2}\right)\left(z-\frac{2h}{3}\right)^4 \\ + y^2\left(z-\frac{2h}{3}\right) + \frac{y^2}{2h}\left(z-\frac{2h}{3}\right)^2 + p_3y^2 + \left(\frac{s_1^{\,2}}{4s_2^{\,2}h}-\frac{s_1^{\,2}p_3}{2s_2^{\,2}h^2}\right)y^4 \end{aligned} \tag{4.35}$$

where

$$p_1 = \frac{1}{2880s_1^{\,2}h}\left[s_1^{\,2}l^4 - 4l^2h^2s_1^{\,2} - 20l^2h^2s_2^{\,2} - 192h^4s_1^{\,2} - 304s_2^{\,2}h^4\right]$$

$$p_3 = \frac{h\left(3s_1^{\,2}+s_2^{\,2}\right)}{6s_1^{\,2}}$$

It is seen from Eq. (4.6) that the integral K defined by Eq. (4.5) does not affect $1/Q$ when the surface stress is absent. The integrals P and S of Eq. (4.5) can be derived as

$$\begin{aligned} P &= -\frac{lh^3\left(3s_1^{\,2}+7s_2^{\,2}\right)}{180s_1^{\,2}} \\ S &= \frac{lh}{30240s_1^{\,2}}\left[s_1^{\,2}l^4 + 2l^2h^2s_1^{\,2} - 184h^4s_2^{\,2} - 14s_2^{\,2}h^2l^2 - 72s_1^{\,2}h^4\right] \end{aligned} \tag{4.36}$$

Thus using P and S in Eq. (4.6), one can calculate energy dissipation $1/Q$ for a beam resonator of triangular cross-section under adiabatic surface condition.

4.6.1.2 Isothermal Surface Condition

Here let us consider isothermal surface condition which requests that ΔT vanishes along all three sides of the isosceles triangular curve. Equation of the triangular boundary curve in the *Y*-*Z* plane is

$$F(y,z)=\left(z-\frac{2h}{3}+\frac{s_1 y}{s_2}\right)\left(z-\frac{2h}{3}-\frac{s_1 y}{s_2}\right)\left(z+\frac{h}{3}\right)=0 \tag{4.37}$$

Since the problem is symmetric about the *Z*-axis, $f(y,z)$ is even in y. Thus, because $f(y,z)$ is arbitrary within a constant factor, up to the lowest order, the general form of $f(y,z)$ is

$$f(y,z)=\left(p_{10}+z+p_{11}z^2\right)\left(z-\frac{2h}{3}+\frac{s_1 y}{s_2}\right)\left(z-\frac{2h}{3}-\frac{s_1 y}{s_2}\right)\left(z+\frac{h}{3}\right) \tag{4.38}$$

where p_{10} and p_{11} are constants to be determined. Similar to the adiabatic case, $f(y,z)$ of Eq. (4.38) has to satisfy $\int_A f(y,z)dA=0$ and $\int_A \square^2 f(y,z)dA=0$. Thus constants p_{10} and p_{11} can be found as

$$p_{10}=\frac{10h}{3}\left[\frac{3s_1^{\,2}l^2+4h^2s_1^{\,2}\quad 24h^2s_2^{\,2}}{21s_1^{\,2}l^2\quad 600h^2s_2^{\,2}\quad 116h^2s_1^{\,2}}\right]$$

$$p_{11}=\frac{105}{h}\left[\frac{3s_1^{\,2}l^2+4h^2s_1^{\,2}-24h^2s_2^{\,2}}{21s_1^{\,2}l^2-600h^2s_2^{\,2}-116h^2s_1^{\,2}}\right]$$

Thus the integrals *P* and *S* of Eq. (4.5) can be derived as

$$\begin{aligned}P&=\frac{lh^2}{20s_2^{\,2}}\left[\frac{21s_1^{\,4}l^4+8h^4s_1^{\,4}+106s_1^{\,4}h^2l^2-240h^4s_2^{\,4}-222s_1^{\,2}h^2l^2s_2^{\,2}-1208s_1^{\,2}h^4s_2^{\,2}}{21s_1^{\,2}l^2-600h^2s_2^{\,2}-116h^2s_1^{\,2}}\right]\\ S&=-\frac{lh^4}{1120s_2^{\,2}}\left[\frac{1440h^4s_2^{\,4}+7l^4s_1^{\,4}+144s_1^{\,2}h^4s_2^{\,2}-204s_1^{\,2}h^2l^2s_2^{\,2}-12s_1^{\,4}h^2l^2}{21s_1^{\,2}l^2-600h^2s_2^{\,2}-116h^2s_1^{\,2}}\right]\end{aligned} \tag{4.39}$$

4.6.2 Numerical Results and Discussion for Triangular Cross-Section

Numerical results of thermoelastic dissipation of triangular beams are demonstrated in this section in the absence of surface stress effect. In Figs. 4.10 and 4.11, the effect on the *Q-factor* of triangular cross-section with different base-to-height ratio, l/h, is demonstrated for adiabatic and isothermal surface conditions respectively. Since solution for a triangular cross-section is not available in the literature, one could use a rectangular cross-section to approximately replace a triangular cross-section. In doing so, it is of interest to find out possible error caused by such a rough replacement. For this reason, normalized *Q-factor* is defined by the ratio of Q for the triangular beam to Q for a rectangular beam (discussed previously in section 3) of same base (l = width of the rectangle = $2c$) and cross-sectional area, where the aspect ratio l/h of the triangular cross-section varies from 1 to 10.

4.6.2.1 Adiabatic Surface Condition

Most of triangular cross-sections of nanowires reported in the literature are close to an equilateral triangle (Gradečak *et al.* 2005; Nam *et al.* 2006; Agrawal *et al.* 2009). An equilateral triangle holds a relation $h=\left(\sqrt{3}/2\right)l$, which implies l/h = 1.154. Since the present analysis assumes that the beam will be bent in the *X-Z* plane, having a smaller bending rigidity in the *X-Z* plane is the main interest. Therefore, for triangular cross-sections, the problem has been kept confined with $l/h \geq 1.154$. It can be seen that (Fig. 4.10), under adiabatic condition, behavior of normalized *Q-factor* for l/h = 1 and l/h = 1.154 are quite same. For l/h = 1 or 1.154, *Q-factor* of an equilateral triangular beam is about 6 times that of a rectangular beam of same

cross-sectional area and base for vibration frequency below 10^6 rad sec^{-1}, but is about 6 times lower than that of the rectangular beam for vibration frequency above 10^{10} rad sec^{-1}. Different effects of cross-sectional shape on *Q-factor* for low and high frequencies are due to the dependency of thermoelastic dissipation on thermal relaxation time. As expected, for example, thermal relaxation rate for triangular cross-section (l/h = 1.154) is 7.88×10^6 sec^{-1}, while thermal relaxation rate for rectangular cross-section of same cross-sectional area and width is 4.75×10^7 sec^{-1}. *Q-factor* changes significantly within a frequency range of 10^6 rad sec^{-1} to 10^{10} rad sec^{-1}. Remarkably, it is observed (Fig. 4.10) that for a large aspect ratio of l/h = 10, *Q-factor* of triangular beam under adiabatic surface conditions can be as large as 40 times that for a rectangular beam of same cross-sectional area and base, although such an unusually large aspect ratio has probably no practical relevance for micro/nano beams.

4.6.2.2 Isothermal Surface Condition

Effect of bending rigidity of the beam on the *Q-factor* is quite remarkable in case of isothermal surface condition as shown in Fig. 4.11. Normalized *Q-factor* for $l/h \geq 2$ is much different from that for $l/h \leq 1.154$. For a large aspect ratio of l/h = 10, the normalized *Q-factor*s of triangular beam are about 4 times those of rectangular beam of same cross-sectional area and base for vibration frequencies above 10^{11} rad sec^{-1}, but 9.3 times lower than the latter for vibration frequencies below 10^8 rad sec^{-1}. Indeed, within the transition frequency range of 10^8 – 10^{11} rad sec^{-1}, the normalized *Q-factor*s vary significantly. As expected, for example, under isothermal surface condition, thermal relaxation rates for triangular cross-section (l/h = 1.154) is 2.0×10^8 sec^{-1}, while thermal relaxation rates for rectangular cross-section of same

cross-sectional area and width is 2.96×10^{8} sec^{-1} which are higher than those under adiabatic surface condition.

4.6.2.3 Dissipation at Natural Frequencies

Fig. 4.12 shows the dependence of *Q-factor* on the aspect ratio l/h (varying between 1 and 10) at the fundamental frequency of beams of triangular cross-sections. The ratio of length (L) to base (l) is always kept as 40. An interesting result obtained from Fig. 4.12 is that *Q-factor* under isothermal surface condition is higher than that under adiabatic surface condition for nano and micro scale while for millimeter scale *Q-factor* under isothermal surface condition is higher than that under adiabatic surface condition for aspect ratios $l/h > 2.5$ and the former is always lower than the latter for $l/h < 2.5$. Moreover for micro/nano scales, the *Q-factor* at the fundamental frequency increases with increasing aspect ratio (l/h), and the increase in *Q-factor* can be more than one order of magnitude when the aspect ratio increases from 1 to 10. In particular, at millimeter scale only under adiabatic surface condition the *Q-factor* at the fundamental frequency is observed to decrease with increasing aspect ratio.

4.7 Comparative Study of Beams with Different Cross-Sectional Shapes

Present analysis shows that, depending on surface thermal condition, geometrical parameters and operating frequency, *Q-factor* due to thermoelastic dissipation of beams of elliptical or triangular cross-section can be higher or lower than that of a rectangular cross-section of same cross-sectional area and width. A topic of current

interest is the size-dependence of dissipation at small scales. Of course, such a size-dependence should depend on the specific nature of different dissipation mechanisms. Some recent experimental results (Ekinci and Roukes 2005; Carr *et al.* 1999; Ardito *et al.* 2008; Gaspar *et al.* 2004; Smith *et al.* 2008) suggested that, for some dissipation mechanisms (such as surface dissipation), the *Q-factor* could vary significantly with the cross-sectional size of nanowires. For example, maximum attainable *Q-factor* in mono-crystalline mechanical resonators are seemed to scale downward from 10^9 to 10^3 with linear dimension i.e. volume-to-surface ratio as size of the cross-sections goes down to nano scale from macro scale (Ekinci and Roukes 2005). This effect has also been observed by other groups in suspended Si nanowires (Carr *et al.* 1999; Ardito *et al.* 2008), a-Si:H-based microstructures (Gaspar *et al.* 2004) and Ge nanowires (Smith *et al.* 2008). Therefore, it is of interest to study the size-dependence of thermoelastic *Q-factor* for various cross-sections, and to find out the minimum thermoelastic *Q-factor* against frequency and the beam-length.

4.7.1 Size-dependence of Thermoelastic Dissipation

Thermoelastic dissipation is believed to be a significant dissipation mechanism for beam resonators in MEMS/NEMS. For example, thermoelastic dissipation is found to make a significant contribution to energy dissipation for beams thicker than 500 nm and shorter than 10 μm (Yang *et al.* 2002). Fig. 4.13 shows thermoelastic *Q-factor* versus absolute sizes of elliptical, triangular and rectangular cross-sections at their respective fundamental frequencies. For comparison, based on the most practical geometrical shapes reported in the literature (Lifshitz and Roukes 2000; Gradečak *et al.* 2005; Nam *et al.* 2006; Urban *et al.* 2008; Ru 2009), aspect ratio for elliptical,

triangular and arbitrary rectangular cross-sections are considered to be a/b = 1.3, l/h = 1.154 and c/d = 10 respectively. Results of Fig. 4.13 are obtained by varying the cross-sectional dimension (as defined by the ratio of area to perimeter of the cross-section) with a common constant length of beams of 10 μm in the absence of surface stress effect. It is seen from Fig. 4.13 that for all of the three cross-sections, thermoelastic dissipation is a non-monotonic function of the absolute size of the cross-section for beams of given constant length. Actually, there is a specific "transition size" for each of the three cross-sections, below which the *Q-factor* decreases with increasing size and above which the *Q-factor* increases with increasing size. Dissipation becomes maximal when vibration frequency is of the order of relaxation rate (Zener 1937, 1938; Lifshitz and Roukes 2000). The transition size is of the order of a few hundreds of nanometers for examples showed in Fig. 4.13, which implies that thermoelastic dissipation could increase with decreasing size within the micron scale while it could decrease with decreasing size within the nano scale. The size for maximum dissipation agrees with the results of Yang *et al.* (2002) who suggested that size limits for beam resonator that susceptible to thermoelastic dissipation for ultrathin cantilever beam resonators are thickness > 500 nm and length < 10 μm. Unfortunately, due to lack of relevant known data in the existing literature on the section size-dependence of thermoelastic dissipation, it is not possible to compare these results with any available experimental or simulation results. Moreover, the lowest *Q-factor* for all three cross-sections under adiabatic or isothermal surface condition is about 10^4, which is almost the minimum *Q-factor* requested for many applications to MEMS/NEMS (Sepulveda *et al.* 2006).

4.7.2 Dependence of Q-factor on Length

Although thermoelastic *Q-factor* given by (Eq. (4.6)) does not explicitly depend on length (L) of the beam, the length of beam can influence thermoelastic dissipation by changing the fundamental or higher-order natural frequencies of beam. Thus it is of interest to see the dependence of thermoelastic dissipation on length (L) of beams of various cross-sections (rectangular, elliptical and triangular). Comparison is made among various cross-sections having constant cross-sectional sizes. For absolute sizes of the cross-sections, the most probable geometrical shapes reported in the literature have been considered (Lifshitz and Roukes 2000; Gradečak *et al.* 2005; Nam *et al.* 2006; Urban *et al.* 2008; Ru 2009) such as rectangular (c/d = 10), elliptical (a/b = 1.3) and triangular (l/h = 1.154 for equilateral triangles) cross sections. It is noted here that the cross-sectional areas of the three cross-sections are kept same in the calculation : c = 5 μm, d = 0.5 μm, a = 2.03 μm, b = 1.57 μm, l = 4.8 μm and h = 4.16 μm. Fig. 4.14 shows the effect of length on *Q-factors* of beam resonators of given cross-sectional sizes at their natural frequencies under both adiabatic and isothermal surface conditions. The minimum *Q-factors* all the beams under both surface thermal conditions is about 10^4, which is almost the minimum *Q-factor* requested for many applications to MEMS/NEMS (Sepulveda *et al.* 2006). Surprisingly, *Q-factors* for triangular and elliptical cross-section under isothermal surface condition are quite similar for all the lengths considered. As expected, *Q-factors* from Zener (1937) coincide with those of thin rectangular cross-section under adiabatic surface thermal conditions (Fig. 4.14). For the given cross-sectional sizes, the minimum *Q-factor* occurs for beams of lengths between 2 and 70 μm. In case of designing a beam of particular cross-section and under any surface thermal condition, the length should be chosen accordingly to achieve higher *Q-factor*.

4.8 Summary

The total dissipation of mechanical devices in MEMS/NEMS includes dissipation due to extrinsic causes such as surrounding environment, clamping etc. and intrinsic causes such as thermoelasticity, surface dissipation. While dissipation due extrinsic causes can be avoided by proper choice of environment and improved design of the device, thermoelastic dissipation, surface dissipation etc. are inevitable as they arise from interior material defects. Thermoelastic loss is considered as the fundamental intrinsic dissipation mechanism in microbeam bending resonators. Surface dissipation, attributed to surface lattice defect-induced interior friction and time-dependent surface stress, could become essential usually only when the size of the device goes down to nano scale.

The present work analyzes the effects of various shape of cross-section on thermoelastic dissipation of micro/nano beam resonators. Arbitrary rectangular, elliptical and triangular cross-sections are studied with an emphasis on comparison between different shapes of cross-section and the role of surface thermal conditions. Most interesting results obtained in this work include

i. elliptical geometry of cross-section has a moderate effect on the *Q-factor* as compared to a rectangular cross-section of same cross-sectional area and width. Replacing a beam of elliptical cross-section by a rectangular beam of same cross-sectional area and width can cause a few tens of percentages in relative error for the cross-sectional aspect ratio up to 10.

ii. in general for all the beams, the *Q-factor* at fundamental frequency for isothermal surface condition is always higher than the *Q-factor* for adiabatic surface condition at micro/nano scales. At millimeter scale, *Q-factor* at fundamental frequency for beams under isothermal surface

condition are higher than those under adiabatic surface condition for aspect ratio larger than 2.5 while formers are always lower than the latter for aspect ratio less than 2.5. In addition, at micro/nano scales and under adiabatic or isothermal surface thermal condition, the *Q-factor* at fundamental frequency always increases with increasing cross-sectional aspect ratio. Moreover, the increase in *Q-factor* can be more than a few orders of magnitude when the cross-sectional aspect ratio increases from 1 to 10.

iii. for all beams discussed, in general, the highest *Q-factor* is achieved at nanometer scale while the lowest occurs at millimeter scale. The present analysis also indicates that, to achieve a high *Q-factor*, beam resonators with elliptical or triangular cross-sections are best to operate at higher frequencies while beams of rectangular cross-sections are best to operate at lower frequencies.

iv. for beams of constant length, obtained results show that thermoelastic dissipation is a non-monotonic function of the absolute size of the cross-section, and the maximum dissipation appears at a specific size of the order of a few hundreds of nanometers. Therefore, at least for examples discussed, thermoelastic dissipation increases with decreasing cross-sectional size within the micron scale while it decreases with decreasing size within the nano scale.

v. under any surface thermal condition, as the cross-sectional aspect ratio increases, the maximum dissipation of a beam of elliptical cross-section goes down more rapidly than a beam of rectangular cross-section.

4.9 Figures and Illustrations

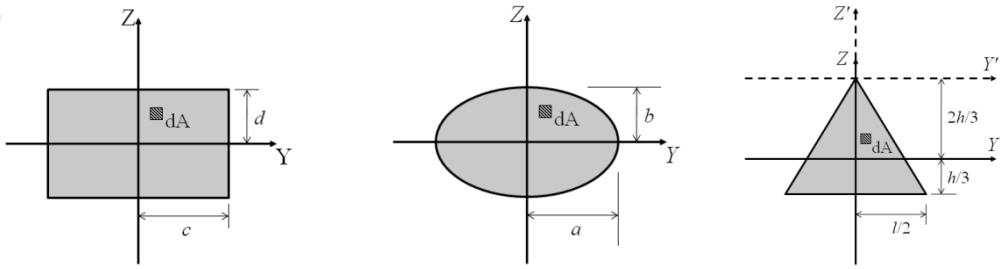

(a) (b) (c)

Fig. 4.1 Schematic diagram of cross-sections of beam resonators (a) rectangular, (b) elliptical and (c) triangular (isosceles).

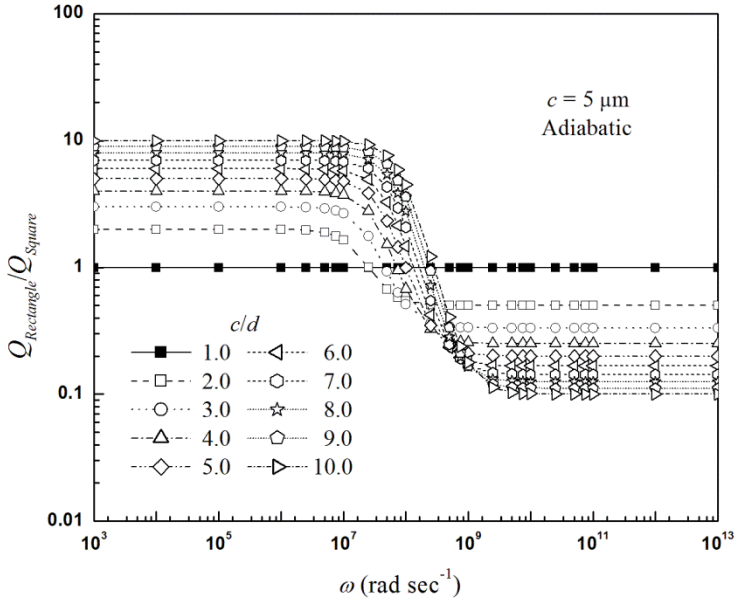

Fig. 4.2 Normalized *Q-factor* vs. vibration frequency ω for beams of rectangular cross-section under adiabatic surface condition, with c = 5 μm (normalized by *Q-factor* for a square beam of same cross-sectional area).

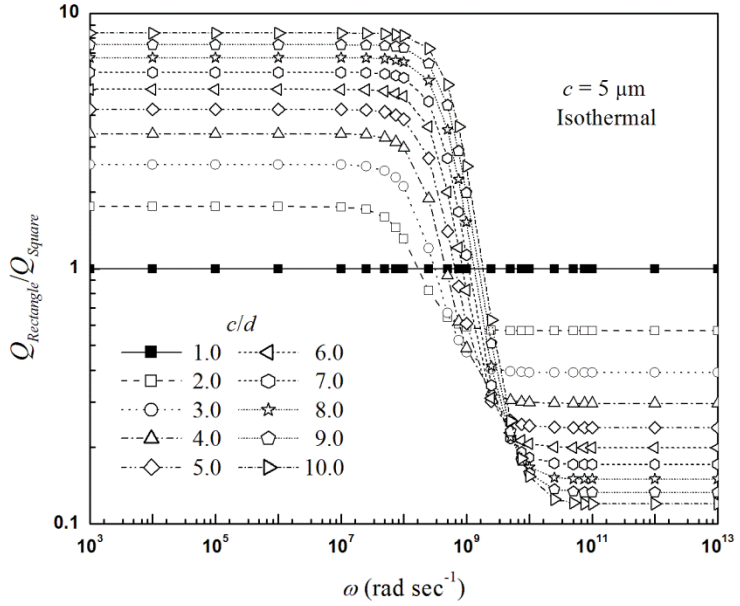

Fig. 4.3 Normalized *Q-factor* vs. vibration frequency ω for beams of rectangular cross-section under isothermal surface condition, with c = 5 μm (normalized by *Q-factor* for a square beam of same cross-sectional area).

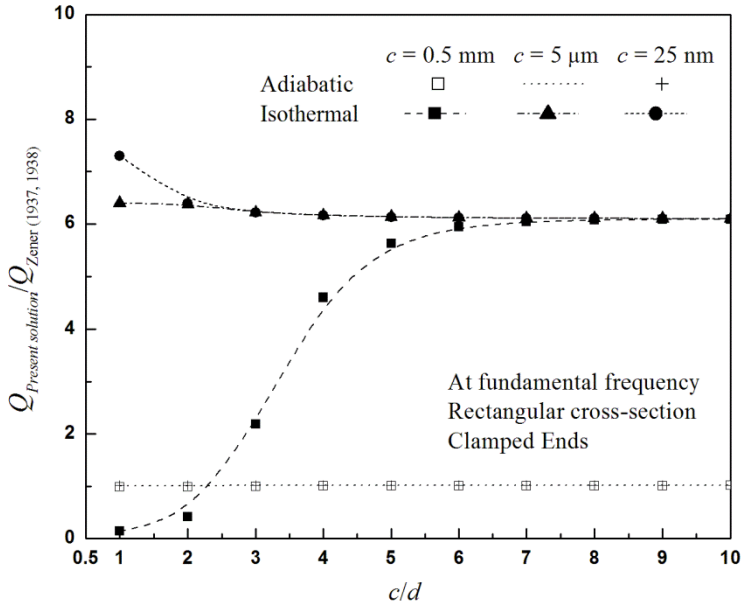

Fig. 4.4 Normalized *Q-factor* vs. c/d for a doubly-clamped beam of rectangular cross section at its fundamental frequency ($L/2c$ = 40). (Normalized by classical solutions from Zener (1937) for a rectangular beam of same cross-sectional area).

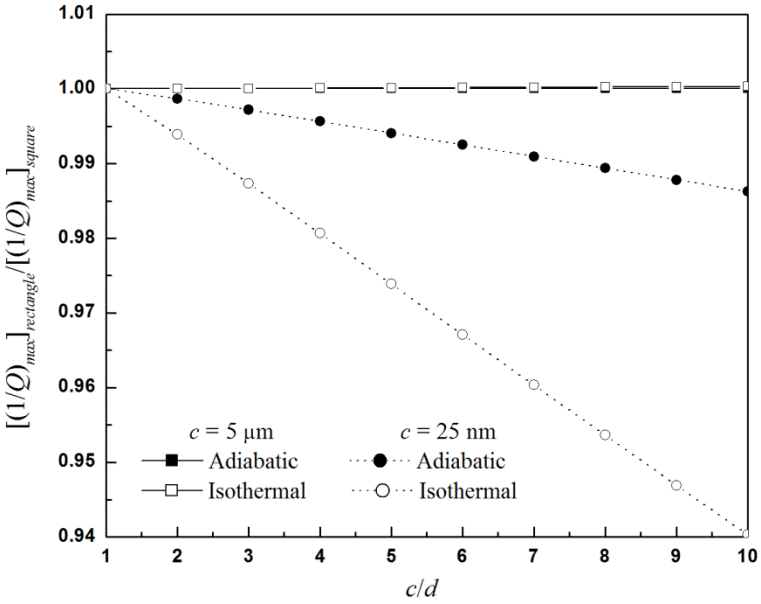

Fig. 4.5 Normalized $(1/Q)_{max}$ vs. c/d for beams of rectangular cross-section with surface stress effect (surface elastic modulus, E_s = 11.7 Nm^{-1} (Miller and Shenoy 2000), surface tension, γ_o = 1.12 Nm^{-1} (Miller and Shenoy 2000) and bulk elastic modulus, E = 160×10^9 Nm^{-2} (Srikar and Senturia 2002) for polysilicon beam).

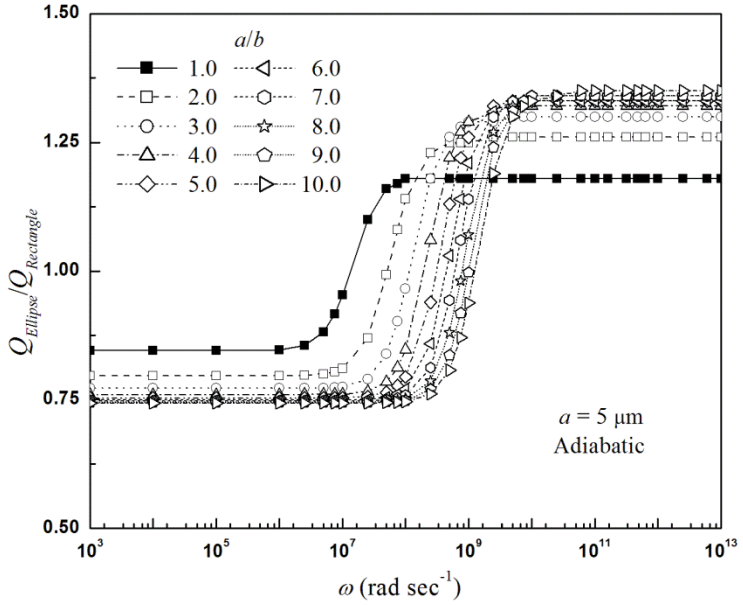

Fig. 4.6 Normalized *Q-factor* vs. vibration frequency ω for beams of elliptical cross-section under adiabatic surface condition, with a = 5 μm (normalized by *Q-factor* for a rectangular beam of same cross-sectional area and width such that $2a$ = width of rectangle $2c$).

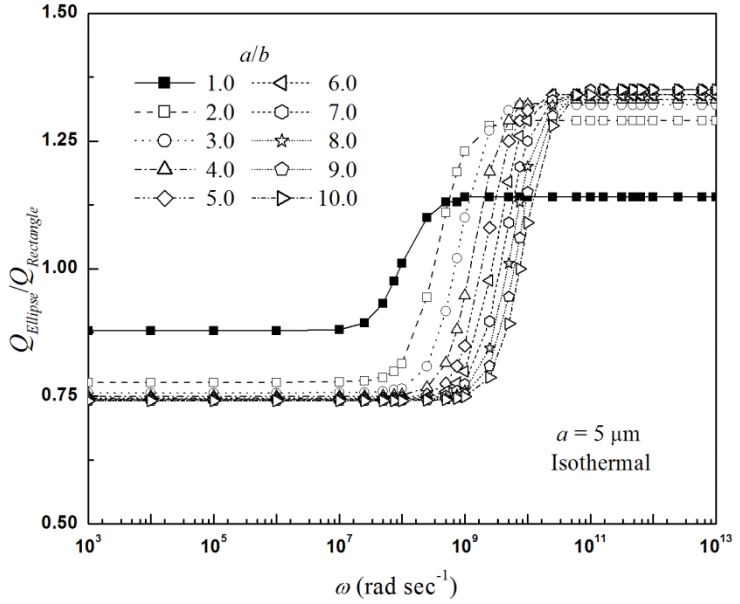

Fig. 4.7 Normalized *Q-factor* vs. vibration frequency ω for beams of elliptical cross-section under isothermal surface condition, with a = 5 μm (normalized by *Q-factor* for a rectangular beam of same cross-sectional area and width such that $2a$ = width of rectangle $2c$).

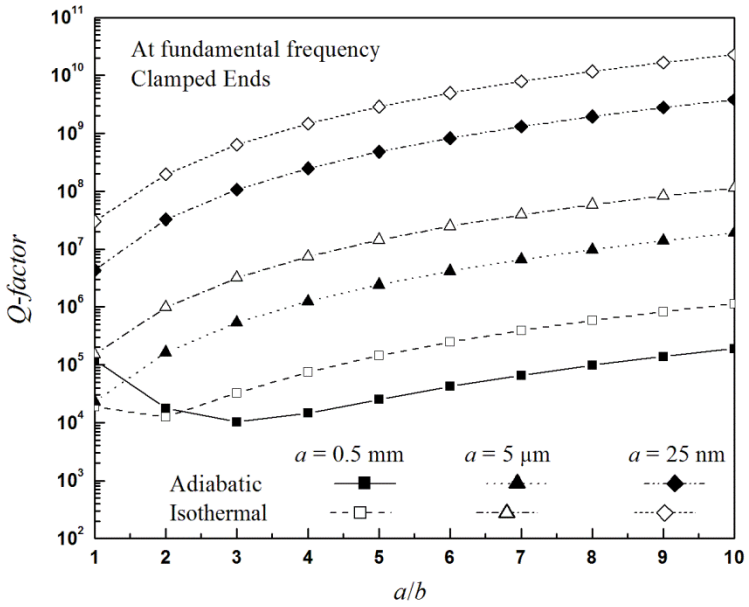

Fig. 4.8 *Q-factor* vs. a/b for a doubly-clamped beam of elliptical cross section at its fundamental frequency ($L/2a$ = 40).

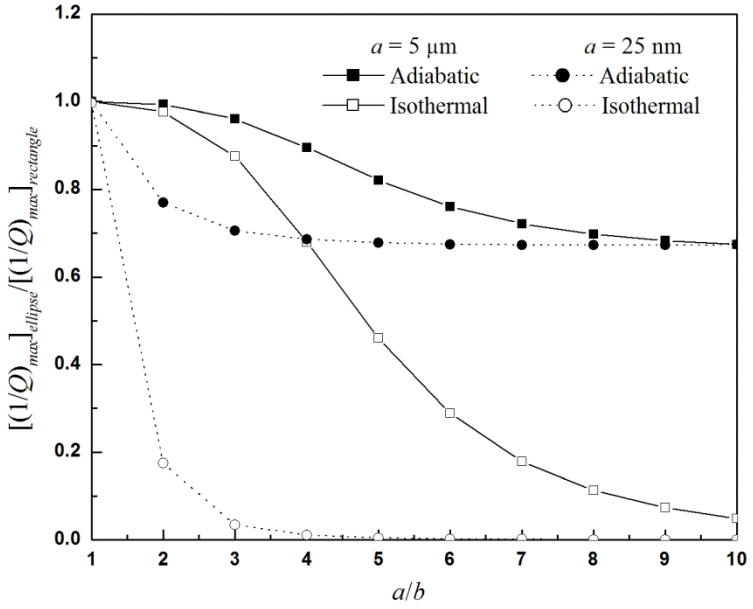

Fig. 4.9 Normalized $(1/Q)_{max}$ vs. a/b for beams of elliptical cross-section with surface stress effect (surface elastic modulus, E_s = 11.7 Nm^{-1} (Miller and Shenoy 2000), surface tension, γ_o = 1.12 Nm^{-1} (Miller and Shenoy 2000) and bulk elastic modulus, E = 160×10^9 Nm^{-2} (Srikar and Senturia 2002) for polysilicon beam).

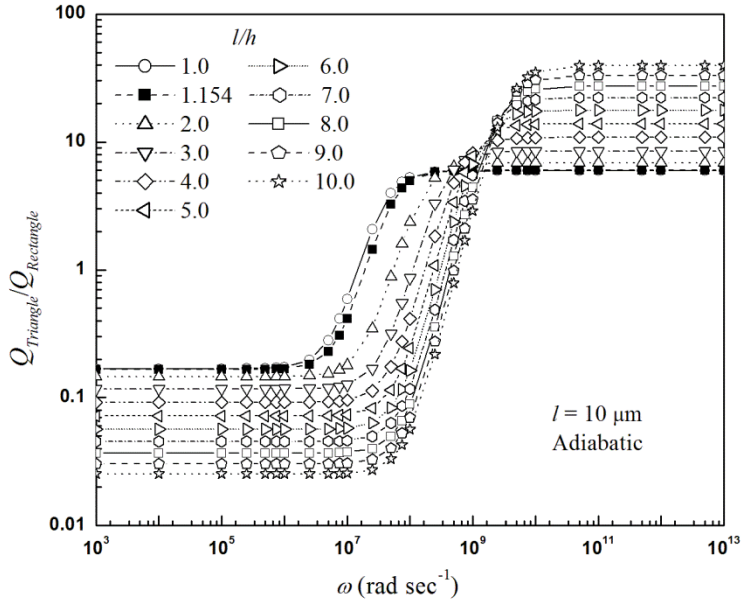

Fig. 4.10 Normalized *Q-factor* vs. vibration frequency ω for beams of triangular cross-section under adiabatic surface condition, with l = 10 μm (normalized by *Q-factor* for a rectangular beam of same cross-sectional area and width such that l = width of rectangle 2c).

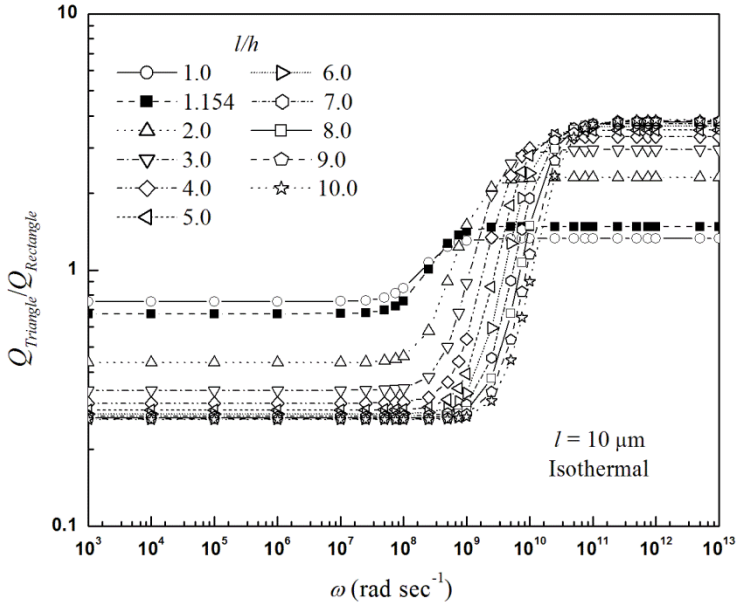

Fig. 4.11 Normalized *Q-factor* vs. vibration frequency ω for beams of triangular cross-section under isothermal surface condition, with l = 10 μm (normalized by *Q-factor* for a rectangular beam of same cross-sectional area and width such that l = width of rectangle 2c).

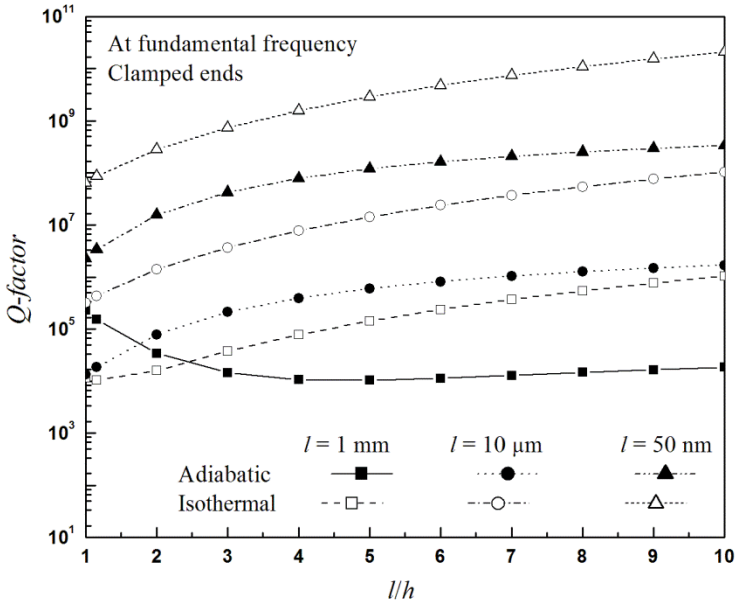

Fig. 4.12 *Q-factor* vs. l/h for a doubly-clamped beam of triangular cross section at its fundamental frequency (L/l = 40).

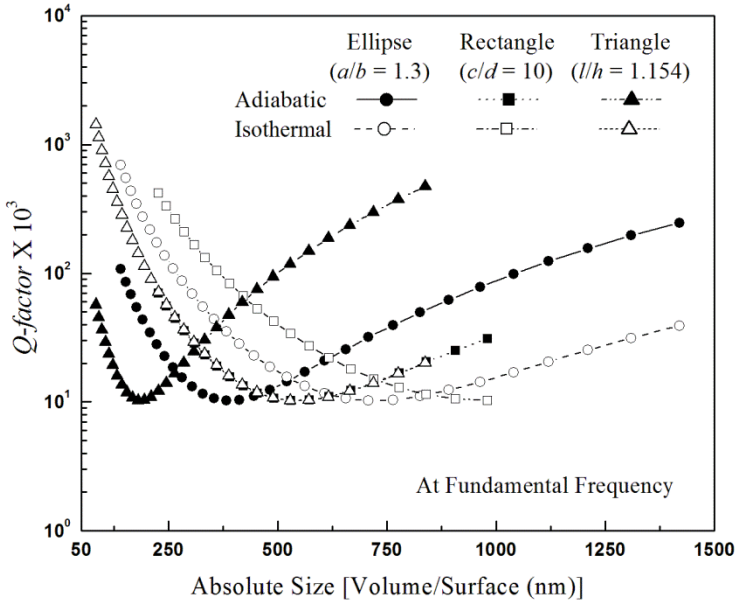

Fig. 4.13 *Q-factor* at the fundamental frequency as a function of absolute size (ratio of volume to surface) of the cross-section (constant length L = 10 μm for all beams).

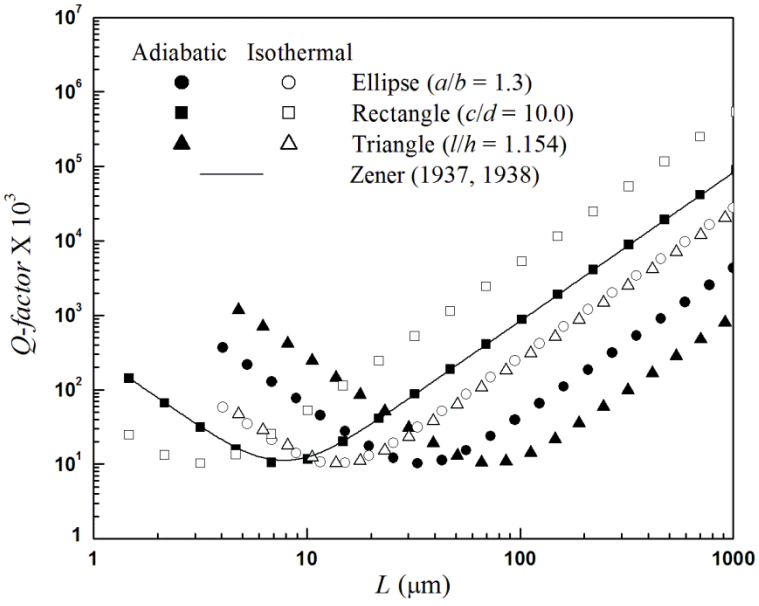

Fig. 4.14 *Q-factor*s for polysilicon clamped beams with respect to length (L) of the beam providing the cross-sectional size for respective beam is kept constant (c = 5 μm, d = 0.5 μm, a = 2.03 μm, b = 1.57 μm, l = 4.8 μm. h = 4.16 μm).

4.10 References

Agrawal B. K., Pathak A., Agrawal S. 2009. Ab initio study of [001] GaN nanowires. *Journal of Nanoparticle Research* **11** 841-859.

Ardito R., Comi C., Corigliano A., Frangi A. 2008. Solid damping in micro electro mechanical Systems. *Meccanica* **43** 419-428.

Bi Y., Hu H., Lu G. 2010. Highly ordered rectangular silver nanowire monolayers: water-assisted synthesis and galvanic replacement reaction with HAuCl4. *Chemical Communications* **46** 598-600.

Carr D. W., Evoy S., Sekaric L., Craighead H. G., Parpia J. M. 1999. Measurement of mechanical resonance and losses in nanometer scale silicon wires. *Applied Physics Letters* **75** 920.

Cimalla V., Niebelschütz F., Tonisch K., Foerster Ch., Brueckner K., Cimalla I., Friedrich T., Pezoldt J., Stephan R., Hein M., Ambacher O. 2007. Nanoelectromechanical devices for sensing applications. *Sensors and Actuators B* **126** 24-34.

Copper C. D., Pilkey W. D. 2002. Thermoelasticity solutions for straight beams. Transaction of the ASME. *Journal of Applied Mechanics* **69** 224-229.

De S. K., Aluru N. R. 2006. Theory of thermoelastic damping in electrostatically actuated Microstructures. *Physical Review B* **74** 144305.

Ekinci K. L., Roukes M.L. 2005. Nanoelectromechanical systems. *Review of Scientific Instruments* **76** 061101.

Foulgoc B., Bourouina T., Traon O., Bosseboeuf A., Marty F., Breluzeun C., Grandchamp J. P., Masson S. 2006. Highly decoupled single-crystal silicon resonators: an approach for the intrinsic quality factor. *Journal of Micromechanics and Microengineering* **16** S45.

Gaspar J., Chu V., Conde J. P. 2004. Amorphous silicon electrostatic microresonators with high quality factors. *Applied Physics Letters* **84** 622.

Gil-Santos E., Ramos D., Jana A., Calleja M., Raman A., Tamayo J. 2009. Mass sensing based on deterministic and stochastic responses of elastically coupled nanocantilevers. *Nano Letters* **9** 4122-4127.

Gradečak S., Qian F., Li Y., Park H. G., Lieber C. M. GaN nanowire lasers with low lasing thresholds. *Applied Physics Letters* **87** 173111.

Houston B. H., Photiadis D. M., Vignola J. F., Marcus M. H., Liu X., Czaplewski D., Sekaric L., Butler J., Pehrsson P., Bucaro J. A. 2004. Loss due to transverse thermoelastic currents in microscale resonators. *Materials Science and Engineering A* **370** 407-411.

Hu J., Bando Y., Liu Z., Sekiguchi T., Golberg D., Zhan J. 2003. Epitaxial Heterostructures: Side-to-Side Si–ZnS, Si–ZnSe Biaxial Nanowires, and Sandwichlike ZnS–Si–ZnS Triaxial Nanowires. *Journal of American Chemical Society* **125** 11306-11313.

Imboden M., Mohanty P., Gaidarzhy A., Rankin J., Sheldon B. W. 2007. Scaling of dissipation in megahertz-range micromechanical diamond oscillators. *Applied Physics Letters* **90** 173502.

Jones J. P. 1966. Thermoelastic vibration of a beam. *The Journal of the Acoustical Society of America* **39** 542-548.

Kar A., Kanoria M., 2007. Thermo-elastic interaction with energy dissipation in an unbounded body with a spherical hole. *International Journal of Solids and Structures* **44** 2961-2971.

Landau L., Lifshitz R. 1959. Theory of Elasticity. Pergamon Press, Oxford.

Li M., Tang H. X., Roukes M. L. 2007. Ultra-sensitive NEMS-based cantilevers for sensing, scanned probe and very high-frequency applications. *Nature Nanotechnology* **2** 114-120.

Liang G., Huang W., Koong C. S., Wang J. S., Lan J. 2010. Geometry effects on thermoelectric properties of silicon nanowires based on electronic band structures. *Journal of Applied* Physics **107** 014317.

Lifshitz R., Roukes M. L. 2000. Thermoelastic damping in micro- and nanomechanical systems. *Physical Review B* **61** 5600-5609.

Lu P., Lee H. P., Lu C., Chen H. B. 2008. Thermoelastic damping in cylindrical shells with application to tubular oscillator structures. *International Journal of Mechanical Sciences* **50** 501-512.

Miller R. E., Shenoy V. B. 2000. Size dependent elastic properties of nanosized structural elements. *Nanotechnology* **11** 139.

Mohanty P., Harrington D. A., Ekinci K. L., Yang Y. T., Murphy M. J., Roukes M. L. 2002. Intrinsic dissipation in high-frequency micromechanical resonators. *Physical Review B* **66** 085416.

Nam C. Y., Jaroenapibal P., Tham D., Luzzi D. E., Evoy S., Fischer J. E. 2006. Diameter-dependent electromechanical properties of GaN nanowires. *Nano Letters* **6** 153-158.

Ru C. Q. 2009. Thermoelastic dissipation of nanowire resonators with surface stress. *Physica E* **41** 1243-1248.

Sepulveda N., Aslam D., Sullivan J. P. 2006. Polycrystalline diamond MEMS resonator technology for sensor applications. *Diamond and Related Materials* **15** 398-403.

Smith D. A., Holmberg V. C., Lee D. C., Korget B. A. 2008. Young's modulus and size-dependent mechanical quality factor of nanoelectromechanical germanium nanowire resonators. *Journal of Physical Chemistry C* **112** 10725.

Srikar V. T., Senturia S. D. 2002. Thermoelastic damping in fine-grained polysilicon flexural beam Resonators. *Journal of Microelectromechanical Systems* **11** 499-504.

Sun Y., Fang D., Soh A. K. 2006. Thermoelastic damping in micro-beam resonators. *International Journal of Solids and Structures* **43** 3213-3229.

Tunvir K., Ru C. Q., Mioduchowski A. 2010. Thermoelastic dissipation of hollow micromechanical Resonators. *Physica E*; **42** 2341-2352.

Urban D. F., Bürki J., Zhang C. H., Stafford C. A., Grabert H. 2008. Jahn-Teller distortions and the supershell effect in metal nanowires. *Physical Review Letters* **93** 186403.

Yang J., Ono T., Esashi M. 2002. Energy dissipation in submicrometer thick single-crystal silicon cantilevers. *Journal of Microelectromechanical Systems* **11** 775-783.

Yasumura K. Y., Stowe T. D., Chow E. M., Pfafman T., Kenny W. T., Stipe B. C., Rugar D. 2000. Quality factor in micros- and submicron-thick cantilevers. *Journal of Microelectromechanical Systems* **9** 117-125.

Yuan G. H., Wang P., Zhang D., Jiao X., Ming H. 2006. Extraordinary transmission through elliptical gold nanowire grating under s-polarization excitation. *International Symposium on Biophotonics, Nanophotonics and Metamaterials* 370-372.

Yun G., Park H. S. 2008. A multiscale, finite deformation formulation for surface stress effects on the coupled thermomechanical behavior of nanomaterials.

Computational Methods in Applied Mechanics and Engineering **197** 3337-3350.

Zamanian M., Khadem S. E. 2010. Analysis of Thermoelastic Damping in Microresonators by Considering the Stretching Effect. *International Journal of Mechanical Sciences* **52** 1366-1375.

Zener C. 1937. Internal Friction in Solids. I. Theory of Internal Friction in Reeds. *Physical Review* **52** 230-235.

Zener C. 1938. Internal Friction in Solids II. General Theory of Thermoelastic Internal Friction. *Physical Review* **53** 90-99.

Zhang J. H., Huang Q. A., Yu H., Wang J. 2009. The influence of surface effects on size-dependent mechanical properties of silicon nanobeams at finite temperature. *Journal of Physics D: Applied Physics* **42** 045409.

Chapter 5

Thermoelastic Dissipation of Layered Composite Beam Resonators[3]

5.1 Overview

This chapter provides studies on thermoelastic dissipations of metal (Cu, Al, Ag, Au) coated ceramic (Si) composite beams of thin symmetric three-layered rectangular cross-section and axi-symmetric two-layered circular cross-section under adiabatic and isothermal surface conditions. Comparison between cross-sectional shapes in respect of thermoelastic dissipation and the effects of volume fractions of outer layer on thermoelastic dissipation for two different cross-sections are numerically evaluated where total size of composite beams is kept fixed. Results of this study show that effects of cross-sectional shapes on thermoelastic dissipation of composite beams are different for low and high frequencies. Under both surface thermal conditions, composite beams of three-layered rectangular cross-section are

[3]*A version of this chapter has been submitted for publication. Tunvir K., Ru C. Q. and Mioduchowski A. 2012. Composites Part B: Engineering* (*Under Review*).

found best to be operated at low frequencies while composite beams of two-layered circular cross-sections of same material combination are preferable to be operated at high frequencies if inner layers as well as outer layers of the two cross-sections have same size. Irrespective of surface thermal conditions, for both the cross-sections the maximum thermoelastic dissipation increases and the frequency corresponding to maximum dissipation decreases in Al coated Si beams as the volume fraction of outer layer increases. However, for constant volume fraction of outer layer, the frequencies corresponding to maximum dissipations under adiabatic condition are always smaller than under isothermal condition in composite beams of both cross-sections.

5.2 Introduction

Beam resonators have broad application in a wide range of MEMS/NEMS (Ekinci and Roukes 2005; Cimalla 2007). A relevant research topic of current interest is energy dissipation of beam resonators at the micro/nano scale (Imboden 2007). Total dissipation of mechanical devices in MEMS/NEMS includes dissipation due to extrinsic causes (such as surrounding environment, clamping etc.) and intrinsic causes such as thermoelasticity and surface dissipation. While dissipation due extrinsic causes can be avoided by proper choice of environment and improved design, intrinsic thermoelastic dissipation and surface dissipation etc. are often inevitable as they arise from interior material defects. Among various dissipation processes, thermoelastic dissipation has been identified as a major dissipation mechanism for energy loss in a large range of micro/nano mechanical resonators (Yasumura *et al.* 2000; Mohanty *et al.* 2002; Sairam and Vengallatore 2009).

As time goes and new technologies evolve for designing MEMS/NEMS resonators, advanced geometries such as beam resonators of various cross-sections (Tunvir *et al.* 2012) and advanced structures such as layered composite materials (Bishop and Kinra 1993, 1994, 1997; Vengallatore 2005; Prabhakar and Vengallatore 2007) have come into discussion for their enhanced properties and applications. Composite beam resonator is usually defined as layered structures with different constituent materials for different layers. For example, in MEMS/NEMS, ceramic substrates, such as Si and SiC, are always coated or laminated with more conductive metallic layers such as Al, Cu, Ag, Au etc. (Vengallatore 2005; Prabhakar and Vengallatore 2007) for particular applications. Coating or lamination on thin devices is basically done to enhance the optical and electrical properties of resonators (Ekinci and Roukes 2005; Cimalla 2007). However, at the same time coating or lamination may be proved undesirable for particular behaviors. Such results are found when thermoelastic dissipation is measured (Yoneoka *et al.* 2010) and calculated (Bishop and Kinra 1993, 1994, 1997; Vengallatore 2005; Prabhakar and Vengallatore 2007) for laminated or coated composites of MEMS devices.

Analysis of thermoelastic dissipation of flexural beam resonators was initiated by Zener (Zener 1937) and followed by many research groups, for example, see recent works (Lifshitz and Roukes 2000; Yasumura *et al.* 2000; Yang *et al.* 2002) in the last two decades. Among them, Lifshitz and Roukes (2000) studied exact solution of thermoelastic dissipation for resonator beams of thin rectangular cross section, and their results showed that the simplified classical results of Zener (1937) is very close to the exact solution under reasonably fair conditions. However, all these works were limited to homogeneous beams. Bishop and Kinra (Bishop and Kinra 1993) first studied thermoelastic dissipation of layered composite beam for

beams under flexure and extension through exact solution method. Later their theory was generalized for thin flexural structures in (Bishop and Kinra 1994, 1997) and was applied to the numerical analysis of thin plate under bending deformation. The developed theory in (Bishop and Kinra 1994, 1997) was used by (Vengallatore 2005; Prabhakar and Vengallatore 2007) for the analysis of thermoelastic dissipation in real composite beam structures. In theoretical analysis of (Bishop and Kinra 1993, 1994, 1997), a perfect thermal contact between layers was assumed, but deformation due to Poisson's ratio was ignored. Their results (Bishop and Kinra 1993, 1994, 1997; Vengallatore 2005; Prabhakar and Vengallatore 2007) showed that layered composite beams experience higher thermoelastic dissipation than homogeneous beam, which is attributed to interface dissipation. Following Bishop's work (Bishop and Kinra 1993, 1994), most previous works on thermoelastic dissipation of composite beams have been limited to resonators of thin walled rectangular cross-section characterized by a large width-to-thickness ratio. In addition, studies in (Bishop and Kinra 1993, 1994, 1997; Vengallatore 2005) were carried out only for adiabatic thermal condition on outer surface, thus leaving a question for other surface thermal condition such as isothermal surface conditions.

Here the effect of two different cross-sectional shapes (rectangular and circular) on thermoelastic dissipation in composite beams with adiabatic or isothermal surface condition on outer surface have been studied based on models developed in (Ru 2009; Tunvir *et al.* 2010, 2012). Obtained results (Ru 2009; Tunvir *et al.* 2010, 2012) suggested that the cross-sectional shape could have a significant impact on thermoelastic dissipation of beam resonators. Relevance of composite beams of rectangular cross-section in practical applications is already found in literature (Bishop and Kinra 1993, 1994, 1997; Vengallatore 2005; Prabhakar and

Vengallatore 2007). Nevertheless, composite beams of axi-symmetric circular cross-section at micro and nano scale have been reported in the literature, for example, MgZnO-ZnO core-shell micro wires (of outer diameter = 7 μm (Czekalla *et al.* 2009)), MgO-ZnO core-sheath nanowires (outer diameter = 50∼100 nm and thickness of outer layer = 15∼25 nm, (Kim *et al.* 2008)), GaN-AlN core-shell beam structure (Arslan *et al.* 2008), Cd_4SiS_6-SiO_2 core-shell beam structure (outer diameter = 1 μm (Liu *et al.* 2010)), ZnO NW-CdO core shell beam structure (Senthil *et al.* 2009) and ZnO-CNT composite nanotube as nano resonators (Huang *et al.* 2006; Wang and Adhikari 2011). Despite their technical relevance, till to date, no systematic study of thermoelastic dissipation has been carried out for composite layered beam resonators of circular and rectangular cross-sections. To the best of author's knowledge, detailed solution is not available for thermoelastic dissipation of composite elastic beams of the above-mentioned cross-sectional shapes under adiabatic or isothermal surface condition.

The basic thermoelasticity model and formulation for thermoelastic dissipation of layered elastic composite beam are described in section 5.3. Boundary and interface conditions are described in sections 5.4. Approximate solutions for thermal field of composite beam of both three-layered rectangular and two-layered circular cross-section are given in section 5.5. Numerical results and discussion of thermoelastic dissipation are presented in section 5.6. Effect of individual material layers and interface between them on fluctuating temperature field and lost mechanical works over the cross-section are discussed in section 5.7. Finally, all results are summarized in section 5.8.

5.3 Theoretical Model

5.3.1 Basic Thermoelasticity Model for Layered Composite Beam

Here thermoelastic dissipation in thin layered composite beams are analyzed through a continuum modeling approach. Continuum models are expected to work well for thermoelastic dissipation of beam resonators at micro/nano scales. Let us consider a thin, elastic, symmetric three-layered Eular-Bernoulli composite beam, having the *X*-axis along its axial direction and the *Y* and *Z*-axes in two perpendicular principal axes of its cross-section (Fig. 5.1-a). The beam is symmetric in respect of cross-sectional geometry as well as materials of layers. Thus the neutral *Y*-axis coincides the centroidal axis of the composite beam. The axial strain for bending in the *X*-*Z* plane is $\varepsilon_{xx} = z\varphi$ where $\varphi = \partial^2 w / \partial x^2$, z is the distance to the neutral *Y*-axis, $w(x,t)$ and $\varphi(x,t)$ are transverse deflection and the created curvature of the bent beam respectively. Assuming each layer of the composite beam as isotropic, homogeneous thermoelastic material, the bending moments contributed by all layers of the composite beam is given by (Ru 2009)

$$M = \sum_{j=1}^{n} \int_{A_j} \sigma_j z dA$$
$$\sigma_j = E_j \left[\varepsilon_{xx} - \alpha_j \Delta T_j \right] \tag{5.1}$$

Where j is the identification number for particular layer, σ_j is uniaxial stress in j^{th} layer of the composite beam, ΔT_j is the deformation-induced temperature change from the initial uniform temperature T_o of the j^{th} layer, and A_j is the cross-sectional area of the j^{th} layer. The temperature field $T_j(x,y,z,t) = T_o + \Delta T_j(x,y,z,t)$ is coupled with the deformation (Bishop and Kinra 1993) by

$$(C_V)_j \frac{\partial T_j}{\partial t} + \frac{E_j \alpha_j T_\circ}{1-2\nu_j} \frac{\partial \varepsilon}{\partial t} = \kappa_j \nabla^2 T_j \tag{5.2}$$

where $(C_V)_j$ is the heat capacity per unit volume of the j^{th} layer, $\varepsilon = (1 - 2\nu_j)\varepsilon_{xx}$ is the mean strain (Bishop and Kinra 1993), κ_j is the thermal conductivity, α_j is the thermal expansion coefficient, and E_j and ν_j are the Young's modulus and Poisson's ration of the j^{th} layer. Because the axial wave-length of bending deformation is usually much larger than the dimension of the cross-section, heat conductions along axial x-direction is negligible (Lifshitz and Roukes 2000). Thus, Eq. (5.2) becomes

$$(C_V)_j \frac{\partial(\Delta T_j)}{\partial t} + E_j \alpha_j T_\circ z \frac{\partial \varphi(x,t)}{\partial t} = \kappa_j \left[\frac{\partial^2}{\partial y^2} + \frac{\partial^2}{\partial z^2} \right] (\Delta T_j) \tag{5.3}$$

5.3.2 Thermoelastic Dissipation in Layered Composite Beam

Thermoelastic dissipation in layered composite beam, defined by the ratio of lost mechanical work per cycle to total stored strain energy, can be calculated by the net mechanical work per cycle in all layers for a periodic harmonic motion (Vengallatore 2005; Prabhakar and Vengallatore 2007). It is seen from Eq. (5.3) that for harmonic vibration the temperature field ΔT_j must have the form $\Delta T_j(x,y,z,t) = \Theta_j(x,t) f_j(y,z)$. It follows from Eqs. (5.1) and (5.3) that

$$\begin{aligned} M &= \sum_{j=1}^{n} \left[E_j I_j \varphi(x,t) - \alpha_j E_j S_j \Theta_j(x,t) \right] \\ (C_V)_j S_j \frac{\partial}{\partial t} \Theta_j(x,t) &+ E_j \alpha_j T_\circ I_j \frac{\partial \varphi(x,t)}{\partial t} + \kappa_j \Theta_j(x,t) P_j = 0 \end{aligned} \tag{5.4}$$

where S_j, P_j and I_j are defined for the j^{th} layer as

$$S_j \equiv \int_{A_j} z f_j(y,z)\,dA$$
$$P_j \equiv -\int_{A_j} z\left(\frac{\partial^2}{\partial y^2}+\frac{\partial^2}{\partial z^2}\right) f_j(y,z)\,dA \tag{5.5}$$
$$I_j \equiv \int_{A_j} z^2\,dA$$

Here the second equation of Eq. (5.4) is the simplified first order average form of Eq. (5.3) over the cross-section. Assuming $M(x,t)=M_\circ(x)e^{-i\omega t}$ and $\varphi(x,t)=\varphi_\circ(x)e^{-i\omega t}$, where $\varphi_\circ(x)$ is a real quantity and ω is the (circular) vibration frequency, $M(x,t)$, in view of Eq. (5.4), can be given by

$$M(x,t)=\sum_{j=1}^{n}\left[E_j I_j+\frac{\omega^2(C_V)_j E_j^{\,2}\alpha_j^{\,2}S_j^{\,2}I_j T_\circ}{P_j^{\,2}\kappa_j^{\,2}+\omega^2(C_V)_j^{\,2}S_j^{\,2}}-\frac{i\omega\kappa_j E_j^{\,2}\alpha_j^{\,2}P_j S_j I_j T_\circ}{P_j^{\,2}\kappa_j^{\,2}+\omega^2(C_V)_j^{\,2}S_j^{\,2}}\right]\varphi(x,t) \tag{5.6}$$

In view of Eqs. (5.4) and (5.6), ΔT_j can be expressed as

$$\Delta T_j(x,y,z,t)=\Gamma_j\,\varphi(x,t)f_j(y,z) \tag{5.7}$$

where

$$\Gamma_j=\frac{iE_j\alpha_j T_\circ I_j\kappa_j P_j\omega-E_j\alpha_j T_\circ I_j\omega^2(C_V)_j S_j}{P_j^{\,2}\kappa_j^{\,2}+\omega^2(C_V)_j^{\,2}S_j^{\,2}}$$

The required energy supply for an infinitesimal bending element dx of the beam located at a point x over a period, $t=0\sim 2\pi/\omega$, is equal to the work done by the external force (stress) over a period. Notifying that the cross-section is symmetric about z and ΔT_j is anti-symmetric about z (Eq. (5.3)), it can be verified from Eq. (5.1) that the stress work on the element dx over a period is $dx\int_0^{2\pi/\omega} Re[M]Re[d\varphi/dt]dt$. The total strain energy stored in element dx is $Re[M_\circ]\varphi_\circ dx/2$. Thus using Eqs. (5.4), (5.5) and (5.6), total lost energy per cycle and strain energy in layered composite beam can be given as

$$\sum_{j=1}^{n}\left[(Lost\ mechanical-energy)/cycle\right]_j=\sum_{j=1}^{n}\pi\frac{\omega\kappa_j E_j^{\,2}\alpha_j^{\,2}P_j S_j I_j T_\circ}{P_j^{\,2}\kappa_j^{\,2}+\omega^2(C_V)_j^{\,2}S_j^{\,2}}\varphi_\circ^{\,2}(x)dx \tag{5.8}$$

$$\sum_{j=1}^{n}\left[Total\ Stored\ Strain\ Energy\right]_j=\frac{1}{2}\sum_{j=1}^{n}\left[E_j I_j+\frac{\omega^2(C_V)_j E_j^{\,2}\alpha_j^{\,2}S_j^{\,2}I_j T_\circ}{P_j^{\,2}\kappa_j^{\,2}+\omega^2(C_V)_j^{\,2}S_j^{\,2}}\right]\varphi_\circ^{\,2}(x)dx \tag{5.9}$$

Since $\left[E_j\alpha_j^{\,2}T_\circ\right]/\left[C_V\right]_j$ is negligible compared to unity, thermoelastic dissipation or the inverse of the *Q-factor* for the composite beam is given by

$$\left[\frac{1}{Q}\right]_{Layered\ Composite}=\frac{1}{2\pi}\frac{\sum_{j=1}^{n}\left[(Lost\ energy)/cycle\right]_j}{\sum_{j=1}^{n}\left[Total\ Stored\ Strain\ Energy\right]_j}=\frac{\sum_{j=1}^{n}\frac{E_j^{\,2}\alpha_j^{\,2}I_j T_\circ}{(C_V)_j}\frac{\Omega_j}{1+\Omega_j^{\,2}}}{\sum_{j=1}^{n}E_j I_j} \tag{5.10}$$

where $\Omega = [\omega_j(C_V)_j S_j]/P_j\kappa_j$ is the normalized frequency of the j^{th} layer. With the present method, for calculating the dissipation $1/Q$, it is enough to calculate the two constants S_j and P_j in all layers defined by the integrals in Eq. (5.5) in terms of $f_j(y,z)$. The validity of this method was confirmed by excellent agreement with the well-known classical results (Lifshitz and Roukes 2000; Zener 1937) for homogeneous thin-wall rectangular cross-section (Tunvir *et al.* 2012) under adiabatic surface condition.

5.4 Boundary and Interface Conditions

Heat conduction in the beam is responsible for thermoelastic dissipation. In this work, a perfect thermal contact (Bishop and Kinra 1993) is assumed between the layers while thermal boundary conditions are applied to the outer surface of the cross-section. Outer surface thermal conditions depend on heat transfer between the beam and the surrounding medium. Here two typical surface thermal conditions, adiabatic and isothermal conditions are considered for the outer surface. An adiabatic condition (Cimalla *et al.* 2007) can be expected in vacuum (ignoring

radiation losses) while isothermal condition can be expected for a denser external medium. Adiabatic surface condition requests that normal gradient of temperature field vanishes on the surface, while isothermal surface condition requests that temperature remains constant on the surface. Thus for adiabatic surface condition, normal derivative $\partial \Delta T/\partial n$ vanishes along the surface $F(y,z) = 0$ of the cross-section in the *Y-Z* plane which means that

$$\frac{\partial \Delta T_j}{\partial z}\Big|_{F(y,z)=0} = 0 \qquad \text{at} \qquad z = z_{Outer\ surface} \tag{5.11}$$

On the other hand, an isothermal surface requests $\Delta T = 0$ along the surface $F(y,z) = 0$ in the *Y-Z* plane such that

$$\Delta T_j\big|_{F(y,z)=0} = 0 \qquad \text{at} \quad z = z_{Outer\ surface} \tag{5.12}$$

The interface between two consecutive layers is assumed thermally perfect, which requires that the temperature and heat flux are continuous across the interface. Then the interface conditions can be expressed as

$$\Delta T_j = \Delta T_{j+1} \qquad \text{at} \quad z = z_{Interface} \tag{5.13}$$

$$\kappa_j \frac{\partial(\Delta T_j)}{\partial z} = \kappa_{j+1} \frac{\partial(\Delta T_{j+1})}{\partial z} \qquad \text{at} \quad z = z_{Interface} \tag{5.14}$$

5.5 Approximate Solution for Temperature Field

In this study, three-layered composite beam of symmetric rectangular cross-section and two-layered composite beam of axi-symmetric circular cross-section are analyzed. Both the beams are symmetric in both material properties and geometry. In the following subsections, approximate solutions for $f_j(y,z)$ of above mentioned cross-sections are analyzed upon application of the boundary and interface conditions described in section 5.4.

5.5.1 Symmetric Three-layered Rectangular Cross-Section

Let us consider a three-layered symmetric rectangular cross-section as shown in Figs. 5.1-a and 5.1-b. The outer layers are of same material and numbered as layer 1 (j =1), while the inner layer carries subscript j = 2. The height and width of the cross-section is $2d_1$ and $2c$ where $c >> d_1$. The inner layer has a thickness of $2d_2$ and the outer layers have the same thickness ($d_1 - d_2$). The volume fraction of the outer layer is

$$[V_f]_{rect} = \frac{Volume\ of\ outer\ layers}{Volume\ of\ the\ beam} = 1 - \frac{d_2}{d_1} \tag{5.15}$$

Since σ_j in Eq. (5.1) is an odd function of z and the operator in Eq. (5.3) is symmetric in z, $f_j(y,z)$ must be odd in z and even in y. However, as the beam cross-section is thin in Z-direction ($c >> d_1$) and thus heat conduction along y-direction is ignored, the general form of $f_j(y,z)$ can be approximated by a polynomial in z which contains only odd power of z. Moreover as the problem is symmetric about the neutral Y-axis, it is sufficient to consider only the upper half ($z > 0$) of the cross-section. Thus considering adiabatic or isothermal surface condition on outer surface and temperature and heat continuity at the interface of the layers, $f_1(y,z)$ and $f_2(y,z)$ are assumed as

$$f_1(y,z) = g_6 z + g_7 z^3 + g_8 z^5 \tag{5.16}$$

$$f_2(y,z) = g_9 z + g_{10} z^3 \tag{5.17}$$

where g_6, g_7, g_8, g_9 and g_{10} are constants to be determined. The degree of approximate function $f_j(y,z)$ is simply decided in such a way that the number of independent coefficients is equal to the number of interface and surface conditions and therefore all independent coefficients can be determined uniquely by the

interface and surface conditions. Since both $f_1(y,z)$ and $f_2(y,z)$ are arbitrary within a constant factor, one can choose $g_6 = g_9 = 1$.

5.5.1.1 Adiabatic Outer Surface

Upon application of adiabatic boundary condition (Eq. (5.11)) on the outer surface ($z = b$) and conditions for perfect thermal contact (Eqs. (5.13), (5.14)) at the interface ($z = a$) to $f_1(y,z)$, three, out of total five constants, say g_7, g_8 and g_{10} of Eq. (5.16) and Eq. (5.17), can be uniquely determined in terms of the remaining two arbitrary constants g_6 and g_9. Thus, with $g_6 = g_9 = 1$, the three constants g_7, g_8 and g_{10} are

$$g_7 = -\frac{1}{3}\frac{5\kappa_1\left(d_1^{\,4}-d_2^{\,4}\right)+3\kappa_2\left(d_2^{\,4}-5d_1^{\,4}\right)}{d_1^{\,2}d_2^{\,2}\left[5\kappa_1\left(d_1^{\,2}-d_2^{\,2}\right)+\kappa_2\left(3d_2^{\,2}-5d_1^{\,2}\right)\right]}-\frac{10}{3}\frac{\kappa_2 d_1^{\,2}\Gamma_2}{d_2^{\,2}\left[5\kappa_1\left(d_1^{\,2}-d_2^{\,2}\right)+\kappa_2\left(3d_2^{\,2}-5d_1^{\,2}\right)\right]\Gamma_1}$$

$$g_8 = \frac{\kappa_1\left(d_1^{\,2}-d_2^{\,2}\right)+\kappa_2\left(d_2^{\,2}-3d_1^{\,2}\right)}{d_1^{\,2}d_2^{\,2}\left[5\kappa_1\left(d_1^{\,2}-d_2^{\,2}\right)+\kappa_2\left(3d_2^{\,2}-5d_1^{\,2}\right)\right]}+\frac{2\kappa_2\Gamma_2}{d_2^{\,2}\left[5\kappa_1\left(d_1^{\,2}-d_2^{\,2}\right)+\kappa_2\left(3d_2^{\,2}-5d_1^{\,2}\right)\right]\Gamma_1}$$

$$g_{10} = \frac{1}{3}\frac{15\kappa_1\left(d_2^{\,2}-d_1^{\,2}\right)+\kappa_2\left(5d_1^{\,2}-3d_2^{\,2}\right)}{d_2^{\,2}\left[5\kappa_1\left(d_1^{\,2}-d_2^{\,2}\right)+\kappa_2\left(3d_2^{\,2}-5d_1^{\,2}\right)\right]}+\frac{2}{3}\frac{\kappa_1\left(d_2^{\,4}+5d_1^{\,4}-6d_2^{\,2}d_1^{\,2}\right)\Gamma_1}{d_2^{\,2}d_1^{\,2}\left[5\kappa_1\left(d_1^{\,2}-d_2^{\,2}\right)+\kappa_2\left(3d_2^{\,2}-5d_1^{\,2}\right)\right]\Gamma_2}$$

In what follows, P_j and S_j can be determined from Eq. (5.5) by using respective $f_j(y,z)$. A useful check on the theoretical formulation and numerical analysis is to verify that the $f_2(y,z)$ reduce to the polynomial form for a solid homogeneous beam (Ru 2009; Tunvir *et al.* 2012) in the limit of an infinitesimally thin outer layer (limit $V_f \to 0$ i.e. $z_{Interface} \to z_{Outer\ surface}$). Indeed, it can be verified that for limit $d_2 \to d_1$, $f_2(y,z)$ reduces to

$$\lim_{d_2 \to d_1} f_2(y,z) = z - \frac{1}{3}\frac{z^3}{d_1^{\,2}} \tag{5.18}$$

in agreement with (Ru 2009; Tunvir *et al.* 2012) for thin-walled ($c >> d_1$) rectangular cross-sections under adiabatic surface thermal condition. It is also

verified that P_1 and S_1 vanish and P_2 and S_2 reduce to the forms which are in agreement with (Ru 2009; Tunvir *et al.* 2012) for the limit $d_2 \to d_1$ It is also mentioned here that for the condition $d_2 \to d_1$, P_2 and S_2 become independent of operating frequency.

5.5.1.2 Isothermal Outer Surface

Applying isothermal boundary condition (Eq. (5.12)) on the outer surface ($z = d_1$) and conditions for perfect thermal contact (Eqs. (5.13), (5.14)) at the interface ($z = d_2$), with $g_6 = g_9 = 1$, the three constants g_7, g_8 and g_{10} are

$$g_7 = -\frac{\kappa_1\left(d_1^{\,4} - 5d_2^{\,4}\right) + 3\kappa_2\left(d_2^{\,4} - d_1^{\,4}\right)}{d_2^{\,2}d_1^{\,2}\left[\kappa_1\left(3d_1^{\,2} - 5d_2^{\,2}\right) + 3\kappa_2\left(d_2^{\,2} - d_1^{\,2}\right)\right]} - \frac{2\kappa_2 d_1^{\,2}\Gamma_2}{d_2^{\,2}\left[\kappa_1\left(3d_1^{\,2} - 5d_2^{\,2}\right) + 3\kappa_2\left(d_2^{\,2} - d_1^{\,2}\right)\right]\Gamma_1}$$

$$g_8 = \frac{\kappa_1\left(d_1^{\,2} - 3d_2^{\,2}\right) + 3\kappa_2\left(d_2^{\,2} - d_1^{\,2}\right)}{d_2^{\,2}d_1^{\,2}\left[\kappa_1\left(3d_1^{\,2} - 5d_2^{\,2}\right) + 3\kappa_2\left(d_2^{\,2} - d_1^{\,2}\right)\right]} + \frac{2\kappa_2\Gamma_2}{d_2^{\,2}\left[\kappa_1\left(3d_1^{\,2} - 5d_2^{\,2}\right) + 3\kappa_2\left(d_2^{\,2} - d_1^{\,2}\right)\right]\Gamma_1}$$

$$g_{10} = \frac{\kappa_1\left(5d_2^{\,2} - 3d_1^{\,2}\right) + \kappa_2\left(d_1^{\,2} - d_2^{\,2}\right)}{d_2^{\,2}\left[\kappa_1\left(3d_1^{\,2} - 5d_2^{\,2}\right) + 3\kappa_2\left(d_2^{\,2} - d_1^{\,2}\right)\right]} + \frac{2\kappa_1\left(d_2^{\,4} + d_1^{\,4} - 2d_2^{\,2}d_1^{\,2}\right)\Gamma_1}{d_2^{\,2}d_1^{\,2}\left[\kappa_1\left(3d_1^{\,2} - 5d_2^{\,2}\right) + 3\kappa_2\left(d_2^{\,2} - d_1^{\,2}\right)\right]\Gamma_2}$$

Thus, P_j and S_j can be determined from Eq. (5.5) by using respective $f_j(y,z)$. To check the validity of the theoretical formulation and numerical analysis under isothermal outer surface, $f_2(y,z)$ should reduce to the polynomial form for a solid homogeneous beam (Ru 2009; Tunvir *et al.* 2012) in the limit of an infinitesimally thin outer layer (limit $V_f \to 0$ i.e. $z_{Interface} \to z_{Outer\ surface}$), such that, for limit $d_2 \to d_1$, $f_2(y,z)$ reduces to

$$\lim_{d_2 \to d_1} f_2(y,z) = z - \frac{z^3}{d_1^{\,2}} \tag{5.19}$$

in agreement with (Ru 2009; Tunvir *et al.* 2012) for thin-walled ($c >> d_1$) rectangular cross-sections under isothermal surface condition. It is also verified that

P_1 and S_1 vanish and P_2 and S_2 reduce to the forms that are in agreement with (Ru 2009; Tunvir *et al.* 2012) for the limit $d_2 \to d_1$.

5.5.2 Axi-symmetric Two-layered Circular Cross-Section

A two-layered axi-symmetric circular cross-section is shown in Figs. 5.1-a and 5.1-c. The outer layer is numbered as layer 1 (j = 1), while the inner layer carries subscript j = 2. The radiuses of outer and inner layers are R_1 and R_2 respectively. The volume fraction of the outer layer can be calculated as

$$\left[V_f\right]_{cir} = 1 - \frac{r_2^{\,2}}{r_1^{\,2}} \tag{5.20}$$

In polar coordinate the *Y-Z* plane can be expressed as $y = r\cos\theta$ and $z = r\sin\theta$ where $0 \le r \le r_1$ and $0 \le \theta \le 2\pi$. To find an approximate solution for heat equation (Eq. (5.3)), neglecting heat conduction in axial direction as explained before, Eq. (5.3) for a circular cross-section can be written as

$$(C_V)_j \frac{\partial \Delta T_j}{\partial t} + \alpha_j E_j T_o r \sin\theta \frac{\partial \varphi}{\partial t} = \kappa_j \left(\frac{\partial}{\partial r^2} + \frac{1}{r}\frac{\partial}{\partial r} + \frac{1}{r^2}\frac{\partial}{\partial \theta^2} \right) \Delta T_j \tag{5.21}$$

For harmonic vibration ΔT_j must have the form $\Delta T_j(x,y,z,t) = \Theta_j(x,t) f_j(r,\theta)$, where the function $f_j(r,\theta)$ is periodic in θ and can be expressed (Tunvir *et al.* 2010) as $f_j(r,\theta) = \sin\theta\ G_j(r)$ Obviously, $f_j(r,\theta)$ given by this expression is always odd in z because it is an odd function in θ. Here, it follows from Eq. (5.21) that $G_j(r)$ is determined by an equation of the form

$$G_j(r) + e_7 r = e_8 \left(\frac{\partial^2}{\partial r^2} + \frac{1}{r}\frac{\partial}{\partial r} - \frac{1}{r^2} \right) G_j(r) \tag{5.22}$$

where e_7 and e_8 represent two parameters independent of r and θ. The series solution of Eq. (5.22) is of the following

$$G_j(r)=e_9\left[r+\frac{r^3}{8e_8}+\frac{r^5}{192e_8^{\,2}}+O\left(r^7\right)\right]+e_{10}\left[-\frac{2}{r}+\frac{3r^3}{32e_8^{\,2}}+O\left(r^5\right)+ln(r)\left\{-\frac{r}{e_8}-\frac{r^3}{8e_8^{\,2}}+O\left(r^5\right)\right\}\right]$$
$$+e_7\left[\frac{r^3}{8e_8}+\frac{r^5}{192e_8^{\,2}}+O\left(r^6\right)\right] \tag{5.23}$$

where e_9 and e_{10} are two arbitrary coefficients while the third part is a particular solution. For the present method, simple approximate form of $G(r)$ can be obtained based on a truncation of the series solution (Eq. (5.23)). For example, for a solid circular cross-section, coefficient e_{10} must be zero and coefficient e_9 is to be determined by the single surface boundary condition. For an annular circular-cross section, two surface conditions are requested and therefore coefficient e_{10} cannot be zero. Thus a two-layered composite of axi-symmetric circular cross-section can be assumed as combination of one solid circular cross-section and an annular circular cross-section with a perfect elastic and thermal contact between the surface of solid section and inner surface of the annular section. Considering adiabatic or isothermal surface condition on the outer surface and temperature and heat flux continuity at the interface, $G_1(r)$ and $G_2(r)$ can be approximated as

$$G_1(r)=\frac{e_{11}}{r}+e_{12}\,r+e_{13}\,r^3 \tag{5.24}$$

$$G_2(r)=e_{14}\,r+e_{15}\,r^3 \tag{5.25}$$

where e_{11}, e_{12}, e_{13}, e_{14} and e_{15} are constant coefficients to be determined. The degree of approximate function $G_j(r)$ is simply decided in such a way that the number of independent coefficients is equal to the number of conditions and therefore all independent coefficients can be determined uniquely by satisfying all required conditions. Since both $f_1(r,\theta)$ and $f_2(r,\theta)$ are arbitrary within a constant factor, one can choose $e_{12} = e_{14} = 1$.

5.5.2.1 Adiabatic Outer Surface

For adiabatic boundary condition (Eq. (5.11)) on the outer surface ($r = r_1$) and conditions for perfect thermal contact (Eqs. (5.13), (5.14)) at $r = r_2$, three, out of total five constants, e_{11}, e_{13} and e_{15} of Eqs. (5.24) and (5.25), can be uniquely determined in terms of the remaining two arbitrary constants e_{12} and e_{14}. Thus, with $e_{12} = e_{14} = 1$, e_{11}, e_{13} and e_{15} are

$$e_{11} = \frac{r_1^{\,2} r_2^{\,2}\left[\kappa_1\left(r_1^{\,2} - r_2^{\,2}\right) + \kappa_2\left(r_2^{\,2} - 3r_1^{\,2}\right)\right]}{\kappa_1\left(r_1^{\,4} - r_2^{\,4}\right) + \kappa_2\left(3r_1^{\,4} + r_2^{\,4}\right)} + \frac{2\kappa_2 r_1^{\,4} r_2^{\,2} \Gamma_2}{\left[\kappa_1\left(r_1^{\,4} - r_2^{\,4}\right) + \kappa_2\left(3r_1^{\,4} + r_2^{\,4}\right)\right]\Gamma_1}$$

$$e_{13} = \frac{\kappa_1\left(r_2^{\,2} - r_1^{\,2}\right) - 3\kappa_2\left(r_1^{\,2} + r_2^{\,2}\right)}{3\left[\kappa_1\left(r_1^{\,4} - r_2^{\,4}\right) + \kappa_2\left(3r_1^{\,4} + r_2^{\,4}\right)\right]} + \frac{2\kappa_2 r_2^{\,2} U_2}{3\left[\kappa_1\left(r_1^{\,4} - r_2^{\,4}\right) + \kappa_2\left(3r_1^{\,4} + r_2^{\,4}\right)\right]\Gamma_1}$$

$$e_{15} = -\frac{3\kappa_1\left(r_1^{\,4} - r_2^{\,4}\right) + \kappa_2\left(3r_1^{\,4} + r_2^{\,4}\right)}{3\left[\kappa_1\left(r_1^{\,4} - r_2^{\,4}\right) + \kappa_2\left(3r_1^{\,4} + r_2^{\,4}\right)\right]} - \frac{2\kappa_1\left(2r_1^{\,2} r_2^{\,2} + r_2^{\,4} - 3r_1^{\,4}\right)\Gamma_1}{3\left[\kappa_1\left(r_1^{\,4} - r_2^{\,4}\right) + \kappa_2\left(3r_1^{\,4} + r_2^{\,4}\right)\right]\Gamma_2}$$

Thus, P_j and S_j in Eq. (5.5) can be determined using respective $f_j(r,\theta)$. Similar to rectangular cross-section, $G_2(r)$ reduces to the polynomial form for a solid circular cross-section in the limit of an infinitesimally thin outer layer (limit $V_f \to 0$ i.e. $z_{Interface} \to z_{Outer\ surface}$), such that for $r_2 \to r_1$, as

$$\lim_{r_2 \to r_1} G_2(r) = r - \frac{1}{3}\frac{r^3}{r_1^{\,2}} \tag{5.26}$$

in agreement with (Ru 2009) for solid circular cross-sections under adiabatic surface thermal condition. It is also verified that P_1 and S_1 vanish and P_2 and S_2 under adiabatic surface thermal condition reduce to the forms that are in agreement with (Ru 2009) for the limit $r_2 \to r_1$.

5.5.2.2 Isothermal Outer Surface

Upon application of isothermal boundary condition (Eq. (5.12)) on the outer surface ($r = r_1$) and conditions for perfect thermal contact (Eqs. (5.13), (5.14)) at the interface ($r = r_2$), with $e_{12} = e_{14} = 1$, constant coefficients e_5, e_7 and e_9 are

$$e_{11} = -\frac{r_1^{\,2} r_2^{\,2}\left[\kappa_1\left(r_1^{\,2} - 3r_2^{\,2}\right) + 3\kappa_2\left(r_2^{\,2} - r_1^{\,2}\right)\right]}{3\kappa_2\left(r_2^{\,4} - r_1^{\,4}\right) - \kappa_1\left(r_1^{\,4} + 3r_2^{\,4}\right)} - \frac{2\kappa_2 r_1^{\,4} r_2^{\,2}\,\Gamma_2}{\left[3\kappa_2\left(r_2^{\,4} - r_1^{\,4}\right) - \kappa_1\left(r_1^{\,4} + 3r_2^{\,4}\right)\right]\Gamma_1}$$

$$e_{13} = \frac{\left[\kappa_1\left(r_1^{\,2} + r_2^{\,2}\right) + 3\kappa_2\left(r_1^{\,2} - r_2^{\,2}\right)\right]}{3\kappa_2\left(r_2^{\,4} - r_1^{\,4}\right) - \kappa_1\left(r_1^{\,4} + 3r_2^{\,4}\right)} + \frac{2\kappa_2 r_2^{\,2}\Gamma_2}{\left[3\kappa_2\left(r_2^{\,4} - r_1^{\,4}\right) - \kappa_1\left(r_1^{\,4} + 3r_2^{\,4}\right)\right]\Gamma_1}$$

$$e_{15} = -\frac{\kappa_2\left(r_2^{\,2} - r_1^{\,2}\right) - \kappa_1\left(r_1^{\,4} + 3r_2^{\,4}\right)}{r_2^{\,2}\left[3\kappa_2\left(r_2^{\,4} - r_1^{\,4}\right) - \kappa_1\left(r_1^{\,4} + 3r_2^{\,4}\right)\right]} - \frac{2\kappa_1\left(r_1^{\,2} - r_2^{\,2}\right)^2\Gamma_1}{r_2^{\,2}\left[3\kappa_2\left(r_2^{\,4} - r_1^{\,4}\right) - \kappa_1\left(r_1^{\,4} + 3r_2^{\,4}\right)\right]\Gamma_2}$$

Thus, P_j and S_j in Eq. (5.5) can be determined using respective $f_j(r,\theta)$. Similar to rectangular cross-section, $G_2(r)$ reduces to the polynomial form for a solid circular cross-section in the limit of an vanishing outer layer (limit $V_f \to 0$ i.e. $z_{Interface} \to z_{Outer\ surface}$), such that for $r_2 \to r_1$, as

$$\lim_{r_2 \to r_1} G_2(r) = r - \frac{r^3}{r_1^{\,2}} \tag{5.27}$$

in agreement with (Ru 2009) for solid circular cross-sections under isothermal surface condition. It is also verified that P_1 and S_1 vanish and P_2 and S_2 under isothermal surface condition reduce to the forms given in (Ru 2009) for the limit $r_2 \to r_1$.

5.6 Numerical Results and Discussion

Eqs. (5.5) and (5.10) are used to calculate the dependency of thermoelastic dissipation on frequency, volume fraction of the outer layer, cross-sectional shapes and surface thermal conditions. The representative materials used in the numerical

analysis of composite beams are metals and ceramics where highly conductive metals like Al, Cu, Ag, Au are used to coat ceramics Si beam in micromechanical devices (Prabhakar and Vengallatore 2007). Thermoelastic dissipation in composite beams (Bishop and Kinra 1993, 1994, 1997; Vengallatore 2005; Prabhakar and Vengallatore 2007) has been limited to rectangular cross-section under adiabatic surface thermal condition so far. In this section, first, thermoelastic dissipations in composite beams of symmetric three-layered rectangular cross-sections and axi-symmetric two-layered circular cross-section (Huang *et al.* 2006; Arslan *et al.* 2008; Kim *et al.* 2008; Czekalla *et al.* 2009; Senthil *et al.* 2009; Liu *et al.* 2010; Wang and Adhikari 2011) under both adiabatic and isothermal surface conditions are analyzed for constant cross-sectional sizes of layers of the two cross-sections and compared with each other. Furthermore, thermoelastic dissipation in composite beams of symmetric three-layered rectangular cross-sections under adiabatic surface condition is compared with the existing results in literature. Second, dependency of thermoelastic dissipation in composite beams of these two cross-sections on volume fraction of outer layers and surface thermals conditions are discussed. Material and thermal properties of the constituent layers of composite beams are taken from (Vengallatore 2005). Thermoelastic dissipations ($1/Q$) of composite beams are discussed against the normalized frequency of the inner Si layer. In all the numerical calculations, equilibrium temperature of the composite beams is considered to be 300 K and the total size of composite beam in the bending direction for both the cross-sections is kept fixed such that $2d_1 = 2r_1 = 2.22$ μm.

5.6.1 Comparison between Composite Beams of Rectangular and Circular Cross-Section

Composite beams of symmetric three-layered rectangular cross-section are compared with composite beams of axi-symmetric two-layered circular cross-section under adiabatic surface thermal condition having constant sizes for corresponding layers in the two cross-sections. Metal (Cu, Al, Ag and Au) coated Si composite beams are used for this comparison. Noting the sole dependency of thermoelastic dissipation on the size of beam along bending direction (Lifshitz and Roukes 2000; Ru 2009; Tunvir *et al.* 2010, 2012), in this comparison the sizes of inner and outer layers of composite beams for the two cross-sections are kept same such that $r_2 = d_2 = 1$ μm and $(r_1 - r_2) = (d_1 - d_2) = 0.11$ μm. Figs. 5.2 and 5.3 are showing thermoelastic dissipations $(1/Q)$ against a wide range of Ω_{Si} for Cu, Al, Ag and Au coated Si composite beams of rectangular and circular cross-sections respectively under adiabatic surface thermal conditions. Thermoelastic dissipations for homogeneous Si beams of same size as composite beam under adiabatic surface condition are included in Figs. 5.2 and 5.3 to compare with the results of composite beams. Moreover, thermoelastic dissipations for homogeneous Si beam of rectangular cross-section calculated from Zener (1937) are included in Fig. 5.2 to verify the accuracy of the present model. Significant thermoelastic dissipation can take place in composite beams of rectangular cross-section compared to homogeneous beam for adiabatic surface thermal condition (Fig. 5.2) for even volume fraction as low as $V_f = 0.1$ (calculated using Eq. (5.15) for rectangular cross-section for the above mentioned sizes of layers). It is seen in Fig. 5.2 that composite beams of rectangular cross-section with Cu and Al as outer layer create very high

dissipation compared to that with Ag or Au. Maximum dissipations in all composite beams of rectangular cross-sections occur at a normalized frequency of Ω_{Si} = 1 (Fig. 5.2). No significant change is observed in the frequencies corresponding to maximum dissipations in various composite beams of rectangular cross-section (Fig. 5.2).

The results of Cu/Si/Cu, Al/Si/Al, Ag/Si/Ag and Au/Si/Au composite and homogeneous Si beam of rectangular cross-sections under adiabatic condition of present study (Fig. 5.2) can be compared with the results in (Vengallatore 2005) as they are given for same composite beams of same sizes of layers in bending direction. It must be mentioned here that thermoelastic dissipations ($1/Q$) of composite and homogeneous beams from the present study should be multiplied by 2π because of a different expression for $1/Q$ in (Vengallatore 2005). Moreover equivalent normalized frequency Ω_{Si} as described in (Vengallatore 2005) is about 2.46 times that of the present study. For all the composite beams (Fig. 5.2), the relative error between $1/Q$ from the present study and those found in (Vengallatore 2005) are less than 10%.

On the other hand, composite beams of axi-symmetric circular cross-section also experience significant thermoelastic dissipation compared to homogeneous Si beams of same size in the bending direction as composite beams (Fig. 5.3). Similar to composite beams of rectangular cross-section of Fig. 5.2, thermoelastic dissipations in Ag/Si and Au/Si are smaller than those in Al/Si and Cu/Si (Fig. 5.3). However, unlike rectangular cross-section (Fig. 5.2), significant changes in frequencies corresponding to maximum dissipations are observed in composite beams of circular cross-section compared to homogeneous Si beam.

Relative comparison between results composite beams of symmetric three-layered rectangular cross-section (Fig. 5.2) and two-layered circular cross-section (Fig. 5.3) under adiabatic surface condition is shown in Fig. 5.4 against operating frequency ω. It is revealed that under adiabatic surface thermal conditions, thermoelastic dissipations in circular cross-section are higher than those in rectangular cross-section for operating frequencies lower than approximately 10^9 rad sec^{-1}, while opposite is true for higher frequencies than 10^9 rad sec^{-1}. Similar results can be observed in the comparison between composite beams of rectangular and circular cross-sections under isothermal surface condition (Fig. 5.5). In particular, under isothermal surface condition (Fig. 5.5) thermoelastic dissipations in circular cross-section can differ by two orders of magnitude from thermoelastic dissipation in rectangular cross-section for both low and high frequencies. However, different results may be obtained for other sizes of layers and material combinations of composite beams.

5.6.2 Effect of Volume Fraction of Outer Layer and Surface Thermal Conditions on Thermoelastic Dissipation

Metallization or coating (outer layer) of small thickness on thin beam like structures of micro-mechanical devices provides enhanced optical properties (Ekinci and Roukes 2005; Cimalla 2007; Kim *et al.* 2008). However, it has been seen from Figs. 5.2-5.5 that for even very small volume fraction significant thermoelastic dissipation can take place in composite beams compared to homogeneous beam for both surface thermal conditions. Thus, it is of interest to see the extent of the effect of different volume fractions of outer layer on thermoelastic dissipation in composite

beams. Figs. 5.6 and 5.7 are showing thermoelastic dissipations ($1/Q$) of Al/Si/Al composite beam of rectangular cross-section for different volume fractions (V_f) of the outer layer under adiabatic and isothermal conditions respectively. Thicknesses for the outer layers corresponding to different volume fractions (V_f) are calculated using (Eq. (5.15)) for fixed total thickness of composite beam, $2d_1$ = 2.22 μm. For both surface thermal conditions, thermoelastic dissipation increases with volume fraction of the outer layer for a wide range of frequencies indicating a strong dependency of thermoelastic dissipation on the position of interface from neutral axis of the composite beam. For both surface thermal conditions, composites with higher volume fraction of the outer layer experience maximum dissipations, $(1/Q)_{max}$, at lower frequencies. Surprisingly, for constant volume fraction the amount of maximum dissipation for adiabatic and isothermal surface conditions are similar which is quite different than the behavior seen in case of homogeneous beam of rectangular cross-section (Tunvir *et al.* 2012) for different surface thermal conditions. This may be due to the fact that interfaces play much stronger role on thermoelastic dissipation in composite beam. However, for constant volume fraction of the outer layer in composite beam of rectangular cross-section, the frequencies corresponding to maximum dissipation under isothermal surface condition are always higher than those under adiabatic outer surface.

On the other hand, thermoelastic dissipations in composite beams of axi-symmetric two-layered circular cross-section (Al/Si) for different volume fractions of outer layer are shown in Figs. 5.8 and 5.9 for adiabatic and isothermal surface conditions respectively. Thicknesses for the outer layer for circular cross-sections corresponding to different volume fractions (V_f) are calculated using (Eq. (5.20)) for fixed total thickness of composite beams $2r_1$ = 2.22 μm. Similar to rectangular cross-

section, for both surface thermal conditions thermoelastic dissipations increase with volume fraction of outer layer (Figs. 5.8 and 5.9). For a constant volume fraction, the amounts of maximum dissipations for adiabatic and isothermal surface conditions are similar in Al coated Si of circular cross-section beams while frequencies corresponding to maximum dissipation under isothermal surface condition are higher than those under adiabatic outer surface (Figs. 5.8 and 5.9). It is also revealed from Figs. 5.6-5.9 that under adiabatic or isothermal surface condition, the frequencies corresponding to maximum dissipations in Al coated Si beams of circular cross-section are always smaller than those for rectangular cross-section provided that the volume fraction of outer layer is constant in the two cross-sections.

5.7 Effect of Interface on Temperature Field and Lost Mechanical Work of Layered Composite Beam

Thermoelastic dissipation in a thermoelastic beam is solely due to the fluctuating temperature field, ΔT, over the cross-section, which is a result of applied cyclic stress (Ru 2009). However, temperature fluctuations and the resulting heat conduction in a composite beam interact with interface. Thus, a spatial analysis of ΔT_j and lost mechanical work over the cross-section of a composite beam is helpful to understand the effect of interface and material combinations for layers.

5.7.1 Fluctuating Temperature Field

$|\Delta T_j|$ in Al-Si-Al composite beam of rectangular cross-section (V_f = 0.3) operated at selected frequencies are calculated for different locations along the positive Z

direction and plotted against the normalized z coordinates ($\xi = z/d_1$) in the positive Z direction in Figs. 5.10 and 5.11 for adiabatic and isothermal surface conditions respectively. Total size of composite or homogeneous beam in the bending direction is kept fixed to $2d_1$ = 2.22 μm. For an operating frequency ω, ΔT_j at any location along positive z direction is normalized by $|\Delta T_1|$ at $z = d_1$ for adiabatic surface condition (Fig. 5.10) while by $|\Delta T_1|$ at $z = d_2$ for isothermal surface condition (Fig. 5.11). Under both surface thermal condition, temperatures are continuous at the interfaces (Fig. 5.10) while the slopes of the temperature at the interfaces are discontinuous, which is the consequence of the requirement of continuity of heat flux at the interface. In Al-Si-Al composite beam, for both surface thermal conditions, higher fluctuations of temperature for all operating frequencies are always seen to occur in the outer layers. Under adiabatic condition, low operating frequencies produce higher temperature fluctuation all over the cross-section of Al-Si-Al composite beam. In case of isothermal condition, low operating frequencies produce higher temperature fluctuation only in inner layer of Al-Si-Al composite beam while the opposite is true for outer layer. It is to be noted that, as expected, gradient of temperature field at the outer boundary under adiabatic surface thermal condition is zero.

5.7.2 Lost Mechanical Work

In view of Eqs. (5.1), (5.7) and (5.8) lost mechanical work per unit volume per cycle in j^{th} layer can be given by

$$\Delta\Phi_j = -\pi\sigma_j\alpha_j Im\left(\Delta T_j\right) = -\pi E_j z\varphi_\circ\alpha_j Im\left(\Delta T_j\right) \tag{5.28}$$

Lost mechanical works ($\Delta\Phi_j$) in Al/Si/Al composite beam of rectangular cross-section (V_f = 0.3) are evaluated for selected operating frequencies and plotted

against the normalized z coordinates ($\xi = z/d_1$) in the positive Z direction in Figs. 5.12 and 5.13 for adiabatic and isothermal conditions respectively. For an operating frequency ω, lost mechanical works ($\Delta\Phi_j$) are normalized by $|\Delta\Phi_1|$ at $z = d_1$ for adiabatic condition (Fig. 5.12) while by $|\Delta\Phi_1|$ at $z = d_2$ for isothermal condition (Fig. 5.13). Irrespective of surface thermal condition, significant difference in lost mechanical works of the two constituent layers Al-Si-Al composite beam is observed at the interface where higher loss always occurs on the side of outer layer.

Negative values of lost mechanical works are observed for individual layer in composite beams of rectangular cross-section for both the surface thermal conditions (inset of Fig. 5.12). Negative values of lost mechanical work due to thermoelastic dissipation have also been observed in other studies, for example, in three-layered symmetric composite beams of rectangular cross-section (Bishop and Kinra 1997), layered semi-infinite rods of thermoelastically different materials (Kinra and Milligan 1994) and in the neighborhood of Griffith crack subjected to time harmonic loading in modes I, II and III (Kinra and Bishop 1996). Lost mechanical work in a closed thermodynamic system such as a thermoelastic beam is related to entropy generation, which is best described through Gouy-Stodola theorem (Nag 2005). Gouy-Stodola theorem asserts that lost mechanical energy is equal to the total entropy generated in the system and environment multiplied by the temperature of the environment, which implies that the lost mechanical work must be non-negative for an isolated system. However, Gouy-Stodola theorem is limited to special case where the system is only in contact with one environment at a fixed temperature. In a composite beam (with an adiabatic or an isothermal condition on boundary), the individual layers are not isolated systems. Thus, net change of entropy could be negative in individual layers although the total lost

mechanical work or the entropy generation in the entire composite beam is always non-negative.

5.8 Summary

Thermoelastic dissipation due to material interface is significant in layered composite beam resonators. The present work analyzes thermoelastic dissipation of composite beam resonators of rectangular and circular cross-sections with an emphasis on the role of material interface in thermoelastic dissipation. A perfect thermal contact is assumed at the interface between adjacent layers such that heat flux and temperature are continuous across the interface. The effects of volume fractions of the outer layer, material combination of layers and surface thermal conditions are numerically evaluated for composite beams of symmetric three-layered rectangular cross-section and axi-symmetric two-layered circular cross-section. Metal (Cu, Al, Ag, Au) coated ceramic (Si) beams are used for numerical analysis. All numerical calculations are based on same fixed total size of the two cross-sections of composite beam. Most interesting results obtained in this work include

i. Under any surface thermal conditions, volume fraction of the outer layer as low as 0.1 can cause significant thermoelastic dissipation in metal (Cu, Al, Ag, Au) coated ceramic (Si) composite beams of both rectangular and circular cross-sections compared to respective homogeneous beams (Si) of same size.

ii. Material combination for inner and outer layer is one of the most important factors in designing composite beam resonators and should be chosen carefully. For example, for both rectangular and circular cross-sections under any surface thermal condition, composite beam of ceramic inner layer (such as

Si) coated with Cu or Al outer layer creates very high thermoelastic dissipation compared to that with Ag or Au outer layer.

iii. Effects of cross-sectional shapes on thermoelastic dissipation of metal (Cu, Al, Ag, Au) coated ceramic (Si) composite beams are different for low and high frequencies. Under both surface thermal conditions, composite beams of three-layered rectangular cross-section are best to be operated at low frequencies while composite beams of two-layered circular cross-sections of same material combination are preferable to be operated at high frequencies if inner layers as well as outer layers of the two cross-sections have same size.

iv. Moreover, cross-sectional shapes strongly influence the frequency corresponding to maximum dissipation. Under any surface thermal condition, the frequencies corresponding to maximum dissipations in metal (Cu, Al, Ag, Au) coated ceramic (Si) composite beams of circular cross-section are always smaller than those for rectangular cross-section provided that the volume fraction of outer layer is same and both the cross-sections have same material combination.

v. Maximum dissipation and the frequency corresponding to maximum dissipation are strongly influenced by the volume fractions of outer layer. For composite beams of both cross-sections, specifically for Al coated Si beams under any surface thermal condition, the maximum thermoelastic dissipation increases, and frequency corresponding to maximum dissipation decreases as the volume fraction of outer layer increases.

vi. Surface thermal condition has a strong effect on the frequency corresponding to maximum dissipation. For example, for constant volume fraction of outer layer of Al coated Si beams of any cross-section, the frequencies corresponding

to maximum dissipations under adiabatic surface are always smaller than that under isothermal surface condition.

The above conclusions are drawn based on the analysis of ceramic (Si) beams coated with highly conductive metals (Cu, Al, Ag, Au). Different results may be obtained for other composites of different materials.

5.9 Figures and Illustrations

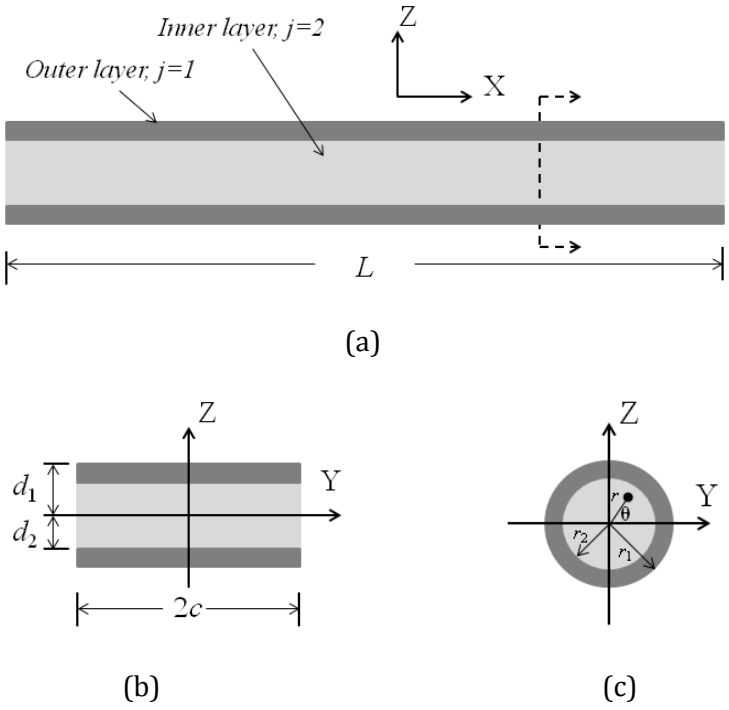

Fig. 5.1 Schematic diagram of (a) layered composite beam resonators, (b) three-layered symmetric rectangular cross-section and (c) two-layered axi-symmetric circular cross-section.

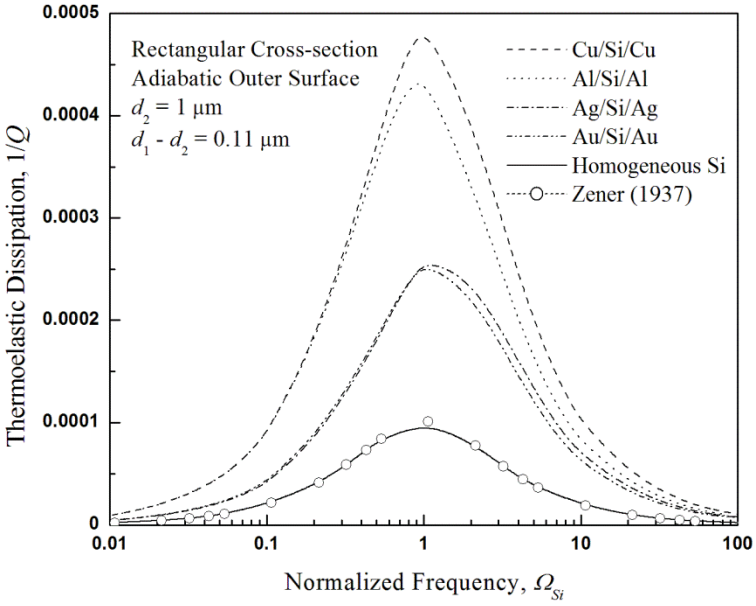

Fig. 5.2 Thermoelastic dissipation $(1/Q)$ in composite beams of three-layered rectangular cross-section with adiabatic outer surface for V_f = 0.1. Results are shown with respect to normalized frequency (Ω_{Si}) for beams having fixed total size $2d_1$ = 2.22 μm.

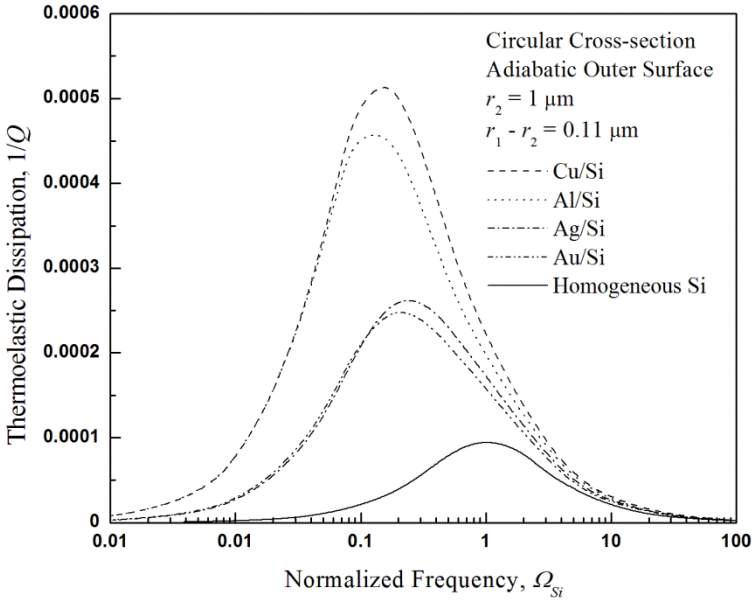

Fig. 5.3 Thermoelastic dissipation $(1/Q)$ in various composite beams of two-layered circular cross-section with adiabatic outer surface. Results are shown with respect to normalized frequency (Ω_{Si}) for beams having fixed total size $2r_1$ = 2.22 μm.

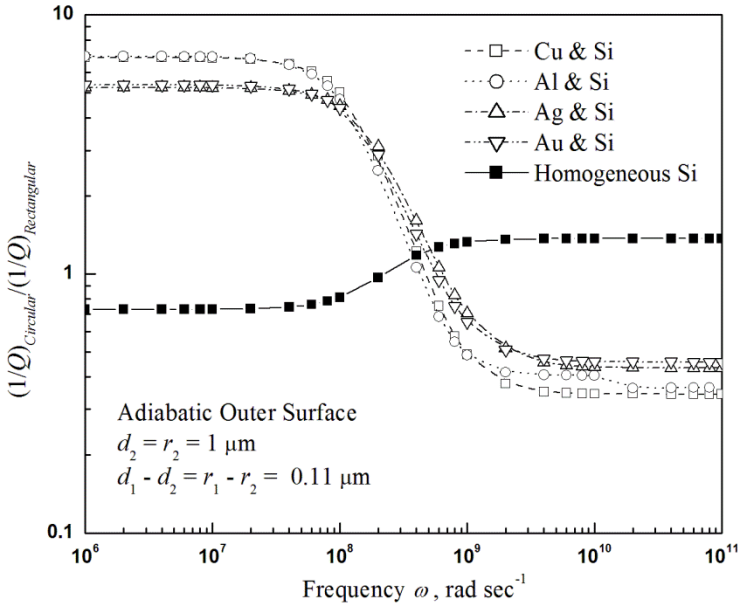

Fig. 5.4 Comparison of thermoelastic dissipation $(1/Q)$ between composite beams of three-layered rectangular and two-layered circular cross-section under adiabatic surface condition having same sizes of inner and outer layers ($d_2 = r_2$ and $d_1 - d_2 = r_1 - r_2$). Results are shown against operating frequency ω.

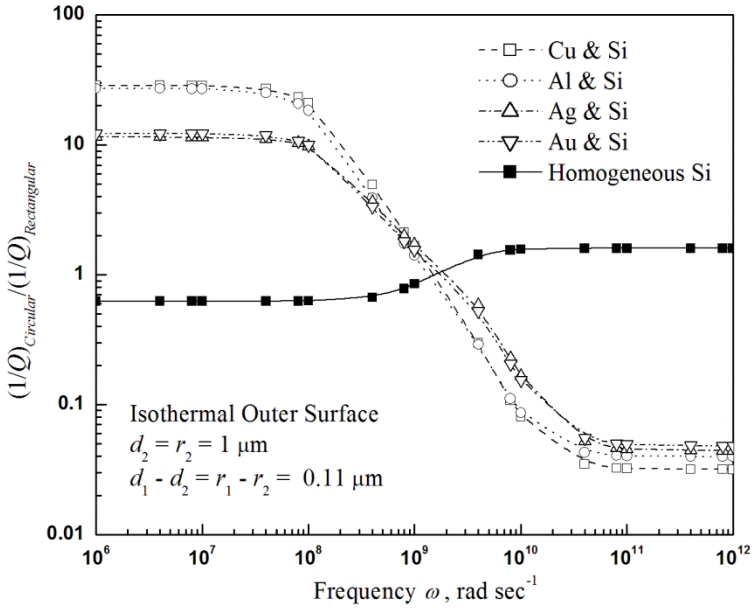

Fig. 5.5 Comparison of thermoelastic dissipation $(1/Q)$ between composite beams of three-layered rectangular and two-layered circular cross-section under isothermal surface condition having same sizes of inner and outer layers ($d_2 = r_2$ and $d_1 - d_2 = r_1 - r_2$). Results are shown against operating frequency ω.

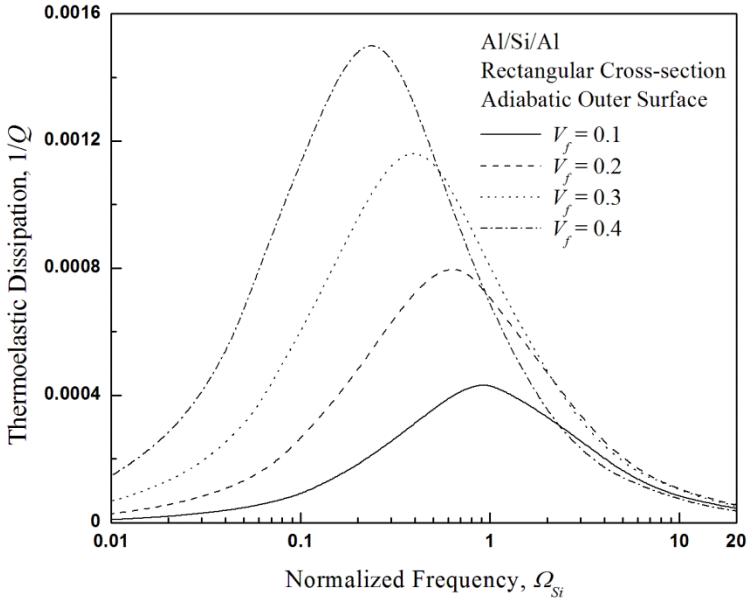

Fig. 5.6 Thermoelastic dissipation ($1/Q$) in three-layered composite beam (Al/Si/Al) of rectangular cross-section with adiabatic outer surface as a function of volume fractions (V_f) of outer layers. Results are shown with respect to normalized frequency (Ω) of inner layer for a beam having fixed cross-sectional size as d_1 = 1.11 μm.

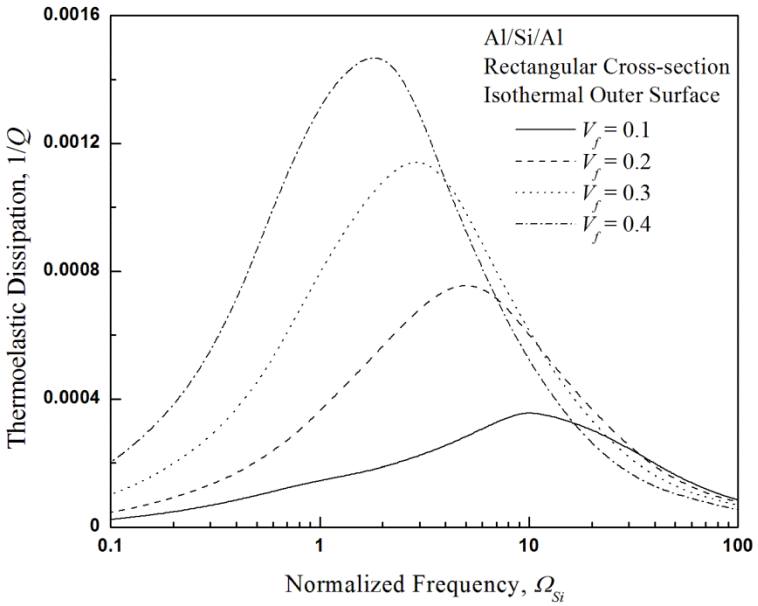

Fig. 5.7 Thermoelastic dissipation ($1/Q$) in three-layered composite beam (Al/Si/Al) of rectangular cross-section with isothermal outer surface as a function of volume fractions (V_f) of outer layers. Results are shown with respect to normalized frequency (Ω) of inner layer for a beam having fixed cross-sectional size as d_1 = 1.11 μm.

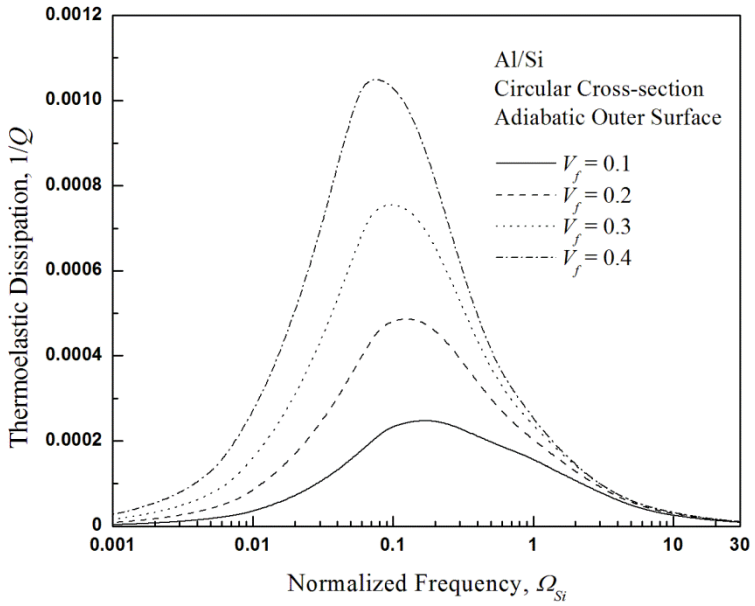

Fig. 5.8 Thermoelastic dissipation ($1/Q$) in two-layered composite beam (Al/Si) of circular cross-section with adiabatic outer surface as a function of volume fractions (V_f) of outer layers. Results are shown with respect to normalized frequency (Ω) of inner layer for a beam having fixed cross-sectional size as r_1 = 1.11 μm.

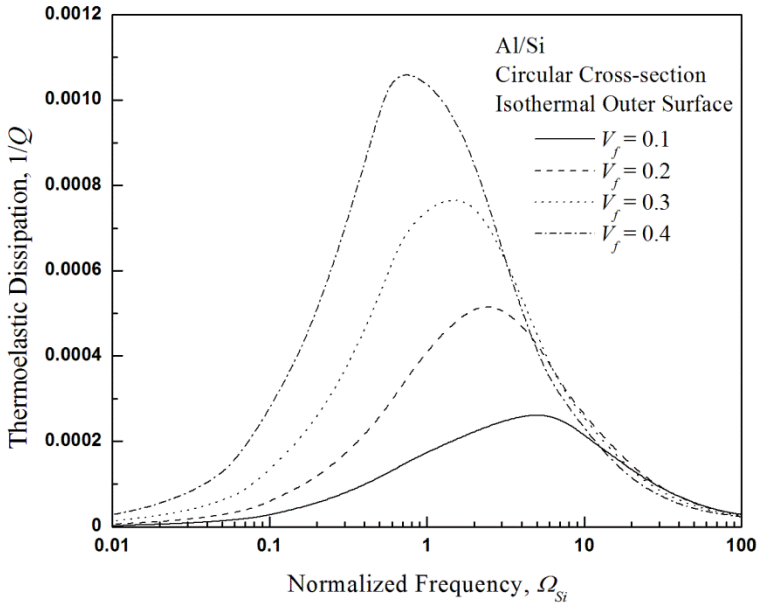

Fig. 5.9 Thermoelastic dissipation ($1/Q$) in two-layered composite beam (Al/Si) of circular cross-section with isothermal outer surface as a function of volume fractions (V_f) of outer layers. Results are shown with respect to normalized frequency (Ω) of inner layer for a beam having fixed cross-sectional size as r_1 = 1.11 μm.

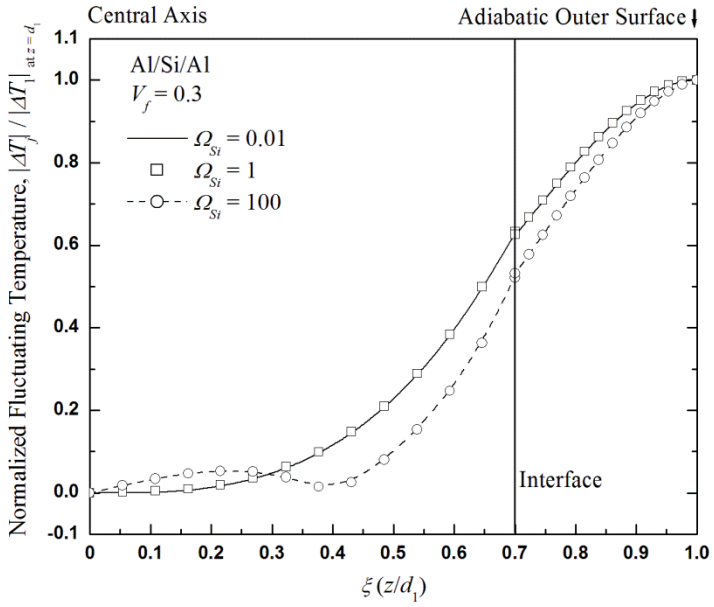

Fig. 5.10 Magnitude of the normalized fluctuating temperature $|\Delta T|$ vs. the normalized z coordinates ($\xi = z/d_1$) over the three-layered rectangular cross-section with V_f = 0.3 for outer layer. $|\Delta T|$ s' are shown as function of operating frequencies (ω) for adiabatic condition on outer surface.

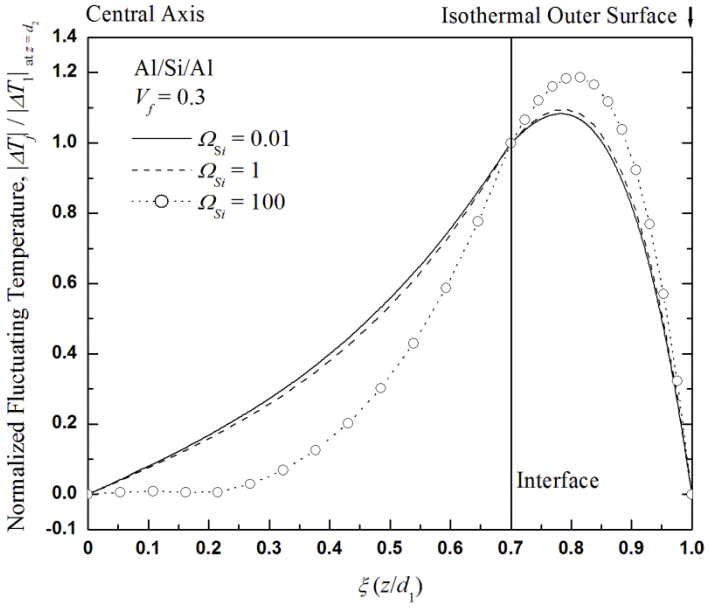

Fig. 5.11 Magnitude of the normalized fluctuating temperature $|\Delta T|$ vs. the normalized z coordinates ($\xi = z/d_1$) over three-layered rectangular cross-section with $V_f = 0.3$ for outer layer. $|\Delta T|$ s' are shown as function of operating frequencies (ω) for isothermal condition on outer surface.

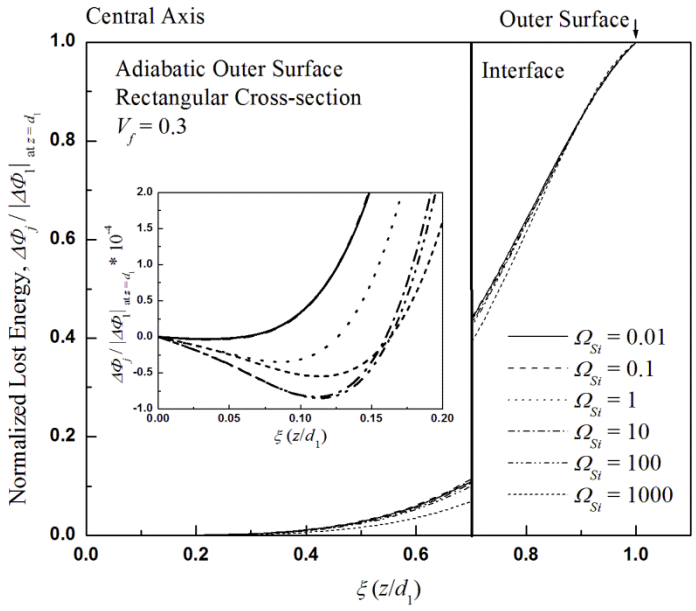

Fig. 5.12 Normalized lost mechanical energy per unit volume per cycle vs. the normalized z coordinates ($\xi = z/d_1$)over three-layered rectangular cross-section with V_f = 0.3 for outer layer. Lost mechanical energies are shown as function of selected operating frequencies for adiabatic condition on outer surface.

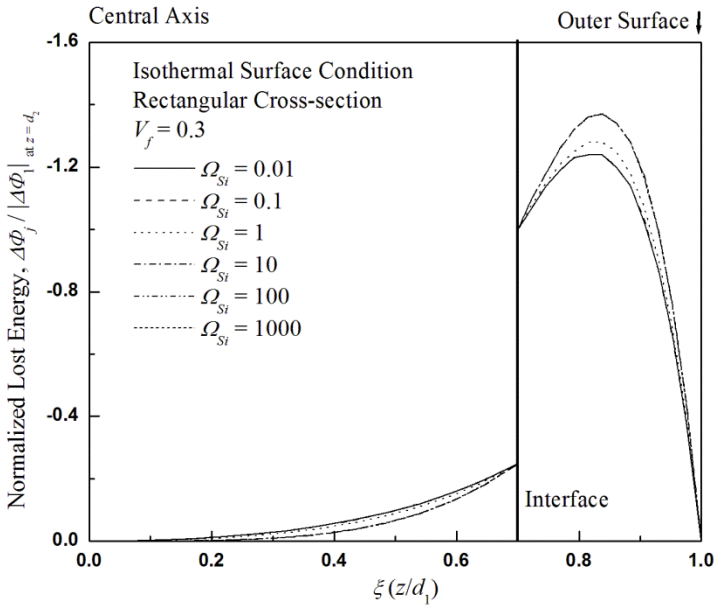

Fig. 5.13 Normalized lost mechanical energy per unit volume per cycle vs. the normalized z coordinates ($\xi = z/d_1$) over three-layered rectangular cross-section with V_f = 0.3 for outer layer. Lost mechanical energies are shown as function of selected operating frequencies for isothermal condition on outer surface.

5.10 References

Arslan I., Talin A. A., Wang G. T. 2008. Three-dimensional visualization of surface defects in core-shell nanowires. *Journal of Physical Chemistry C* **112** 11093-11097.

Bishop J. E. and Kinra V. K. 1993. Thermoelastic damping of a laminated beam in flexure and extension. *Journal of Reinforced Plastics and Composites* **12** 210.

Bishop J. E. and Kinra V. K. 1994. Elastothermodynamic damping in composite materials. *Mechanics of Composite Materials and Structures* **1** 75-93.

Bishop J. E. and Kinra V. K. 1997. Elastothermodynamic damping in laminated composites. *International Journal of Solids and Structures* **34** 1075-1092.

Cimalla V., Niebelschütz F., Tonisch K., Foerster Ch., Brueckner K., Cimalla I., Friedrich T., Pezoldt J., Stephan R., Hein M., Ambacher O. 2007. Nanoelectromechanical devices for sensing applications. *Sensors and Actuators B* **126** 24-34.

Czekalla C., Sturm C, Schmidt-Grund R, Cao B., Zúñiga Pérez J., Lorenz M., and GrundmannM. 2009. Optical characterization of zinc oxide microlasers and microwire core-shell heterostructures. *Journal of Vacuum Science Technology B* **27** 1780-1783.

Ekinci K. L., Roukes M. L. 2005. Nanoelectromechanical systems. *Review of Scientific Instruments* **76** 061101.

Huang L., Lau S. P., Yang H. Y., Yu S. F. 2006. Local measurement of secondary electron emission from ZnO-coated carbon nanotubes. *Nanotechnology* **17** 1564-1567.

Imboden M., Mohanty P., Gaidarzhy A., Rankin J., Sheldon B. W. 2007. Scaling of dissipation in megahertz-range micromechanical diamond oscillators. *Applied Physics Letters* **90** 173502.

Kim W. H., Lee W. J. and Shim S. H. 2008. Composite nanowires with MgO/ZnO core-sheath structures: study of thin ZnO shell layers. *Journal of Physics and Chemistry of Solids* **69** 1491-1494.

Kinra V. K. and Bishop J. E. 1996. Elastothermodynamic analysis of Griffith crack. *Journal Mechanics Physics and Solids* **44** 1305-1336.

Kinra V. K. and Milligan K. B. 1994. A second-law analysis of thermoelastic damping. *Journal of Applied Mechanics* **61** 71-76.

Lifshitz R., Roukes M. L. 2000. Thermoelastic damping in micro- and nanomechanical systems. *Physical Review B* **61** 5600-5609.

Liu J., Wang C., Xie Q., Cai J., Zhang J. 2010. Hierarchical Cd_4SiS_6/SiO_2 heterostructures nanowire arrays. *Nanoscale Research Letters* **5** 231-236.

Mohanty P., Harrington D. A., Ekinci K. L., Yang Y. T., Murphy M. J., Roukes M. L. 2002. Intrinsic dissipation in high-frequency micromechanical resonators. *Physical Review B* **66** 085416.

Nag P. K. 2005. Engineering Thermodynamics. Third Edition. Tata McGraw-Hill Publishing Company Limited.

Prabhakar S. and Vengallatore S. 2007. Thermoelastic damping in bilayered micromechanical beam resonators. *Journal of Micromechanics and Microengineering* **17** 532-538.

Ru C. Q. 2009. Thermoelastic dissipation of nanowire resonators with surface stress. *Physica E* **41** 1243-1248.

Sairam P. and Vengallatore S. 2009. Thermoelastic damping in hollow and slotted microresonators. *Journal of Microelectromechanical Systems* **18** 725-735.

Senthil K., Tak Y., Seol M., Yong K. 2009. Synthesis and characterization of ZnO nanowire-CdO composite nanostructures. *Nanoscale Research Letters* **4** 1329-1334.

Tunvir K., Ru C. Q. and Mioduchowski A. 2012. Effect of cross-sectional shape on thermoelastic dissipation of micro/nano elastic beams. *International Journal of Mechanical Sciences* **62** 77-88.

Tunvir K., Ru C. Q., Mioduchowski A. 2010. Thermoelastic dissipation of hollow micromechanical resonators. *Physica E* **42** 2341-2352.

Vengallatore S. 2005. Analysis of thermoelastic damping in laminated composite micromechanical beam resonators. *Journal of Micromechanics and Microengineering* **15** 2398-2404.

Wang C. Y. and Adhikari S. 2011. ZnO-CNT composite nanotubes as nanoresonators. *Physics Letters A* **375** 2171-2175.

Yang J., Ono T., Esashi M. 2002. Energy dissipation in submicrometer thick single-crystal silicon cantilevers. *Journal of Microelectromechanical Systems* **11** 775-783.

Yasumura K. Y., Stowe T. D., Chow E. M., Pfafman T., Kenny W. T., Stipe B. C., Rugar D. 2000. Quality factor in micros- and submicron-thick cantilevers. *Journal of Microelectromechanical Systems* **9** 117-125.

Yoneoka S., Roper C.S., Candler R.N., Chandorkar S.A., Graham A.B., Provine J., Maboudian R., Howe R.T., Kenny T.W. 2010. Characterization of encapsulated micromechanical resonators sealed and coated with polycrystalline SiC. *Journal of Microelectromechanical Systems* **19** 357-366.

Zener C. 1937. Internal Friction in Solids. I. Theory of Internal Friction in Reeds. *Physical Review* **52** 230-235.

Chapter 6

Thermoelastic Dissipation of Stepped-Beam Resonators[4]

6.1 Overview

In recent years, stepped-beam resonators have found broad application in MEMS/NEMS devices. A beam resonator with an undercut at the support, produced due to isotropic etching of the supporting substrate during fabrication, has also been characterized as stepped-beam in the literature. The present study deals with thermoelastic dissipations of clamped-clamped stepped-beam resonators under adiabatic surface thermal conditions having k (k = 1,2,….,n) number of sections defined by (k – 1) number of steps along the length. Numerical results are obtained for three different types of stepped-beams of rectangular cross-section having single step such as beams with cross-sectional change at the step only in lateral direction (type-1), in bending direction (type-2), and in both lateral and bending directions (type-3) where the section on the right of the step possesses smaller cross-sectional size compared to the other. The obtained results show that *Q-factor*s vary

[4]*A version of this chapter has been published. Tunvir K. 2012. Microsystem Technologies. Published Online as Online First Articles. DOI: 10.1007/s00542-012-1676-9. In Press.*

significantly with step positions in all the three types of stepped-beams. For constant length, the *Q-factor* increases in the type-1 while it decreases in other two types of stepped-beams as the step position moves from the left support to the right along the length. Moreover, *Q-factor*s in a type-1 stepped-beam depend on the widths of different sections and can be higher than a uniform beam of same thickness for some particular step positions. For most common lengths of stepped-beams in real applications with the step close to the left support, type-1 stepped-beams provide higher quality factors than the other stepped-beams if they have the same cross-sectional area.

6.2 Introduction

Beam resonators have broad application in a wide range of MEMS/NEMS (Ekinci and Roukes 2005; Cimalla *et al.* 2007). A relevant research topic of current interest is energy dissipation of beam resonators at the micro/nano scale (Imboden *et al.* 2007). Total dissipation of mechanical devices in MEMS/NEMS includes dissipation due to extrinsic causes (such as surrounding environment, clamping, etc.) and intrinsic causes (such as thermoelasticity, surface dissipation, etc.). While dissipation due to extrinsic causes can be avoided by the proper choice of environment and improved design, intrinsic thermoelastic dissipation and surface dissipation, etc. are often inevitable as they arise from interior defects of materials. Among various dissipation processes, thermoelastic dissipation has been identified as a major dissipation mechanism for energy loss in a large range of micro/nano mechanical resonators (Lifshitz and Roukes 2000; Yasumura *et al.* 2000; Mohanty *et al.* 2002).

Beams having change in cross-sectional area at various locations along the length are known as stepped-beams. As time goes on and new technologies evolve for designing MEMS/NEMS resonators, advanced structural geometries such as resonators with stepped-beam are increasingly being considered for their enhanced properties and real applications. Examples would include in sensing mechanical motion to allow MEMS sensors to be capable of measuring high frequency (Mamin 2007), in estimation of material properties (Behreyni and Shafai 2006), as nano-resonators for RF communication application (Wang *et al.* 2006), in detecting protein (Varshney *et al.* 2009) and viruses (Ilic *et al.* 2004) as MEMS/NEMS resonators, as nanomechanical resonant structure (Cleland *et al.* 2001; Sekaric *et al.* 2002), as higher-mode free-free micromechanical beam resonators (Hsu *et al.* 2000, 2001; Wang *et al.* 2000; Demirci *et al.* 2003) and so on. Besides as designed stepped-beam resonators, beams with an undercut at the clamped ends have also been distinguished as stepped-beams (Gavan *et al.* 2009a, b; Herrera-May *et al.* 2011). An undercut in a beam resonator of MEMS/NEMS is produced during fabrication when the supporting substrate is isotropically etched as a part of the release process of the beam. Due to an undercut at the clamped end, a uniform beam is converted to a stepped-beam possessing two different cross-sectional sizes at the step and the original length of the beam is changed depending on the position of the undercut.

Despite their technical relevancies, till to date, no systematic study of thermoelastic dissipation has been carried out for stepped-beam resonators. However, modal analysis of stepped-beam is heavily studied in the literature, for example, by Jang and Bert (1989), Naguleswaren (2002), Koplow *et al.* (2006), etc. Recently, especially for structures at micro/nano scale, Herrera-May *et al.* (2011) developed an analytical model for the bending resonant frequency of sensors based

on micro and nano resonators with complex structural geometry consisting of a number of beams having a number of steps along the length. Gavan *et al.* (2009a) investigated the effect of an undercut at the clamped end of silicon-nitride beam resonator on resonance frequency and found that the undercut increases the length of the original beam and this increment depends on the undercut distance and resonance mode shape of the beam, but not on the length of the beam. In another work, Herrera-May *et al.* (2010) developed an analytical model to estimate the first bending resonant frequency of MEMS beam resonator having undercuts at both clamped ends. In their work, the influences of both etched support and intrinsic stress were considered. Their results showed that a resonator beam with undercut can be approximated as stepped-beam.

Zener (1937) initiated the analysis of thermoelastic dissipation of flexural beam resonators where damping in some mechanical resonators of rectangular cross-section was attributed to thermoelastic relaxation. In the last two decades, Zener's work was followed by many research groups, for example, Lifshitz and Roukes (2000), Yang *et al.* (2002), Ru (2009), Tunvir *et al.* (2010, 2012), Hoseinzadeh and Khadem (2011), and so on. Among them, Lifshitz and Roukes (2000) studied an exact solution of thermoelastic dissipation for resonator beams of thin rectangular cross section, and their results showed that the simplified classical results of Zener (1937) is very close to the exact solution under reasonably fair conditions. However, all these works were limited to uniform homogeneous beams.

In the present work, thermoelastic dissipation of stepped-beams is studied at fundamental frequencies. Adiabatic surface condition is considered, with an emphasis on the effect of step positions on thermoelastic dissipation. Three different configurations of stepped-beam are considered in this study such as cross-sectional

change at the step in lateral direction only (type-1), in bending direction only (type-2), and in both lateral and bending directions (type-3). This paper is organized in the following way. The basic thermoelasticity model and formulation for thermoelastic dissipation of stepped-beam are described in section 6.3. Mode shapes and surface thermal conditions for stepped-beams with single step are described in section 6.4. Obtained numerical results for stepped-beams of rectangular cross-section are discussed and compared with FE analysis in section 6.5. Finally, all results are summarized in section 6.6.

6.3 Theoretical Model

6.3.1 Basic Thermoelasticity Model for Stepped-Beam

Thermoelastic dissipation is a relevant dissipation mechanism in beam resonators at smaller scales (Lifshitz and Roukes 2000). In this chapter, thermoelastic dissipation of stepped-beams has been modeled through a continuum modeling approach. Continuum models are expected to work well for thermoelastic dissipation of stepped-beam resonators at micro/nano scales.

Let us consider a thin, elastic, homogeneous, Eular-Bernoulli stepped-beam with k (k = 1,2,3,….,n) number of sections of different cross-sectional sizes defined by (k − 1) steps along the length, L as shown in Fig. 6.1. In a Cartesian coordinate system, the beam has the X-axis along its axial direction, the Y-axis as the neutral axis over the cross-section and Z-axis along the bending direction. The axial strain for bending in the X-Z plane is $(\varepsilon_{xx})_k = z\varphi_k$ where z is the distance to the neutral Y-axis, $\varphi_k = \partial^2 w_k / \partial x^2$ and $w_k(x,t)$ are the created curvature and transverse deflection of the bent beam respectively. Assuming each section of the stepped-beam as

isotropic, homogeneous and thermoelastic, the bending moments contributed by the k^{th} section of stepped-beam is given by

$$\begin{aligned} M_k &= \int_{A_k} \sigma_k z dA \quad for\ L_{k-1} < x < L_k \\ \sigma_k &= E\left[(\varepsilon_{xx})_k - \alpha \Delta T_k\right] \end{aligned} \tag{6.1}$$

Here σ_k is the uniaxial stress in k^{th} section of the beam, ΔT_k is the deformation-induced temperature change from the initial uniform temperature T_{o} of the k^{th} section, and A_k is the area of the cross-section of the k^{th} section of the stepped-beam. The temperature field $T_k(x,y,z,t) = T_{\text{o}} + \Delta T_k(x,y,z,t)$ is coupled with the deformation through heat equation (Lifshitz and Roukes 2000; Ru 2009) by

$$C_V \frac{\partial T_k}{\partial t} + \frac{E \alpha T_\circ}{1-2\nu} \frac{\partial \varepsilon_k}{\partial t} = \kappa \nabla^2 T_k \tag{6.2}$$

where C_V is the heat capacity per unit volume, $\varepsilon_k = (\varepsilon_{xx})_k + (\varepsilon_{yy})_k + (\varepsilon_{zz})_k$ is the mean strain, κ is the thermal conductivity, α is the thermal expansion coefficient, and E and ν are the Young's modulus and Poisson's ration of the bulk material. For uniaxial stress-state, the two lateral strains for the k^{th} section of the stepped-beam are $\left(\varepsilon_{yy}\right)_k = \left(\varepsilon_{zz}\right)_k = -\left(\nu \sigma_k / E\right) + \alpha \Delta T_k$. Because the axial wavelength of bending deformation is usually much larger than the dimension of the cross-section, heat conductions along axial x-direction is negligible (Lifshitz and Roukes 2000). Thus, Eq. (6.2) becomes

$$\left[C_V + 2(1+\nu)\frac{E\alpha^2 T_\circ}{1-2\nu}\right]\frac{\partial \Delta T_k}{\partial t} + E\alpha T_o z \frac{\partial \varphi_k(x,t)}{\partial t} = \kappa\left[\frac{\partial^2}{\partial y^2} + \frac{\partial^2}{\partial z^2}\right]\Delta T_k \tag{6.3}$$

6.3.2 Thermoelastic Dissipation in Stepped-Beam

Thermoelastic dissipation in a stepped-beam, defined by the ratio of mechanical energy loss per cycle in all the sections to total strain energy stored, can be calculated by the net mechanical work per cycle in all the sections of the stepped-beam for a periodic harmonic motion (Ru 2009; Tunvir *et al.* 2010, 2012). It is seen from Eq. (6.3) that for harmonic vibration, the temperature field ΔT_k for the k^{th} section must have the form $\Delta T_k(x,y,z,t) = \Theta_k(x,t) f_k(y,z)$. It follows from Eqs. (6.1) and (6.3) that

$$\begin{aligned} &M_k(x,t) = EI_k\,\varphi_k(x,t) - \alpha E S_k\,\Theta_k(x,t) \qquad \textit{for}\ \ L_{k-1} < x < L_k \\ &C_V S_k \frac{\partial}{\partial t}\Theta_k(x,t) + E\alpha T_\circ I_k \frac{\partial \varphi_k(x,t)}{\partial t} + \kappa \Theta_k(x,t) P_k = 0 \end{aligned} \tag{6.4}$$

where S_k, P_k and I_k are defined as

$$\begin{aligned} S_k &\equiv \int_{A_k} z f_k(y,z)\,dA \\ P_k &\equiv -\int_{A_k} z\left(\frac{\partial^2}{\partial y^2} + \frac{\partial^2}{\partial z^2}\right) f_k(y,z)\,dA \\ I_k &\equiv \int_{A_k} z^2\,dA \end{aligned} \tag{6.5}$$

Here second equation of Eq. (6.4) is the simplified first order average form of Eq. (6.3) over the cross-section of k^{th} section. Assuming $M_k(x,t) = \left[M_\circ(x)\right]_k e^{-i\omega t}$ and $\varphi_k(x,t) = \varphi_k(x) e^{-i\omega t}$, where $\varphi_k(x)$ is a real quantity and ω is the (circular) vibration frequency, $M_k(x,t)$, in view of Eq. (6.4), can be given by

$$M_k(x,t) = \left(EI_k + \frac{\omega^2 C_V E^2 \alpha^2 S_k^{\,2} I_k T_\circ}{P_k^{\,2}\kappa^2 + \omega^2 C_V^{\,2} S_k^{\,2}} - \frac{i\omega\kappa E^2 \alpha^2 P_k S_k I_k T_\circ}{P_k^{\,2}\kappa^2 + \omega^2 C_V^{\,2} S_k^{\,2}} \right) \varphi_k(x,t) \qquad \textit{for}\ \ L_{k-1} < x < L_k \tag{6.6}$$

The required energy supply for an infinitesimal bending element dx of the beam located at a point x on k^{th} section over a period, $t = 0 \sim 2\pi/\omega$, is equal to the

work done by the external force (stress) over a period. Notifying that the cross-section is symmetric about z and ΔT_k is anti-symmetric about z (Eq. (6.3)), it can be verified from (Eq. (6.1)) that the stress work on the element dx over a period is $dx \int_0^{2\pi/\omega} Re[M_k] Re[d\varphi_k/dt] dt$. The total strain energy stored in element dx of k^{th} section is $Re[(M_\circ)_k][\varphi_k(x)]dx/2$. Thus using Eq. (6.6), total lost energy per cycle and strain energy in stepped-beam having k number of sections can be given as

$$\sum_{k=1}^{n}\left[(Lost\ energy)/cycle\right]_k = \sum_{k=1}^{n} \pi \frac{\omega\kappa E^2 \alpha^2 P_k S_k I_k T_\circ}{P_k^{\,2}\kappa^2 + \omega^2 C_V^{\,2} S_k^{\,2}} \int_{L_{k-1}}^{L_k} [\varphi_k(x)]^2 dx \tag{6.7}$$

$$\sum_{k=1}^{n}\left[Total\ Stored\ Strain\ Energy\right]_k = \frac{1}{2}\sum_{k=1}^{n}\left[EI_k + \frac{\omega^2 C_V E^2 \alpha^2 S_k^{\,2} I_k T_\circ}{P_k^{\,2}\kappa^2 + \omega^2 C_V^{\,2} S_k^{\,2}} \right] \int_{L_{k-1}}^{L_k} [\varphi_k(x)]^2 dx \tag{6.8}$$

Thermoelastic dissipation or the inverse of the *Q-factor* for the stepped-beam having k number of sections is given by

$$\left[\frac{1}{Q}\right]_{Stepped\ Beam} = \frac{1}{2\pi} \frac{\sum_{k=1}^{n}\left[(Lost\ energy)/cycle\right]_k}{\sum_{k=1}^{n}\left[Total\ Stored\ Strain\ Energy\right]_k} \tag{6.9}$$

With the present method described above, the two constants P_k and S_k are independent of operating frequency ω. Therefore, for calculating the dissipation $1/Q$, it is enough to calculate the two constants S_k and P_k defined by the integrals of $f(y,z)$ over the cross-section of the k^{th} section (Eqs. (6.4) and (6.5)). The validity of the present method in case of uniform beam of thin-walled rectangular cross-section (Tunvir *et al.* 2012) was confirmed by excellent agreement with the well-known classical results (Zener 1937) under adiabatic surface condition.

6.4 Stepped-Beam of Rectangular Cross-Section with Single Step

For numerical analysis a clamped-clamped stepped-beam of rectangular cross-section with single step (k = 2) have been considered as shown in Fig. 6.2 where section on the right of the step possesses smaller cross-sectional size than the other. The width and thickness of the rectangular cross-section of the k^{th} section are $2c_k$ and $2d_k$ respectively.

6.4.1 Mode Shape of Stepped-Beam with Single Step

Following Eq. (6.9), thermoelastic dissipation ($1/Q$) for stepped-beam with single step (k = 2) can be written as

$$\frac{1}{Q}=\frac{B_1+B_2\left\{\int_{L_1}^{L_2}\left(\frac{d^2w_2(x)}{dx^2}\right)^2dx_2\Big/\int_{L_0}^{L_1}\left(\frac{d^2w_1(x)}{dx^2}\right)^2dx\right\}}{D_1+D_2\left\{\int_{L_1}^{L_2}\left[\frac{d^2w_2(x)}{dx^2}\right]^2dx\Big/\int_{L_0}^{L_1}\left[\frac{d^2w_1(x)}{dx^2}\right]^2dx\right\}}=\frac{B_1+B_2\zeta}{D_1+D_2\zeta} \tag{6.10}$$

where

$$\zeta=\int_{L_1}^{L_2}\left[\frac{d^2w_2(x)}{dx^2}\right]^2dx\Big/\int_{L_0}^{L_1}\left[\frac{d^2w_1(x)}{dx^2}\right]^2dx \tag{6.11}$$

and

$$L_0=0,\ B_1=\frac{\omega\kappa E^2\alpha^2P_1S_1I_1T_\circ}{P_1^{\,2}\kappa^2+\omega^2C_V^{\,2}S_1^{\,2}},\ B_2=\frac{\omega\kappa E^2\alpha^2P_2S_2I_2T_\circ}{P_2^{\,2}\kappa^2+\omega^2C_V^{\,2}S_2^{\,2}},\ D_1=\left[EI_1+\frac{\omega^2C_VE^2\alpha^2S_1^{\,2}I_1T_\circ}{P_1^{\,2}\kappa^2+\omega^2C_V^{\,2}S_1^{\,2}}\right],$$

$$D_2=\left[EI_2+\frac{\omega^2C_VE^2\alpha^2S_2^{\,2}I_2T_\circ}{P_2^{\,2}\kappa^2+\omega^2C_V^{\,2}S_2^{\,2}}\right]$$

To determine the ratio ζ of Eq. (6.11), the small displacement fields for the two sections (Fig. 6.2) of uniform cross-section are approximated by individual functions (Gorman 1975) such as

$$\begin{aligned} w_1(\xi') &= \eta_1 \sin\beta_1\xi' + \eta_2 \cos\beta_1\xi' + \eta_3 \sinh\beta_1\xi' + \eta_4 \cosh\beta_1\xi' \\ w_2(\xi') &= \eta_5 \sin\beta_2\xi' + \eta_6 \cos\beta_2\xi' + \eta_7 \sinh\beta_2\xi' + \eta_8 \cosh\beta_2\xi' \end{aligned} \tag{6.12}$$

where η_1, η_2, η_3, η_4, η_5, η_6, η_7, η_8 are constant coefficients to be determined upon application of boundary conditions at the clamped ends and continuity conditions at the steps; ξ' is the normalized coordinate ($\xi' = x/L$); β_1, β_2 are mode constants and are given by

$$\beta_1^{\,4} = \frac{\rho A_1}{E I_1}\omega^2 L^4, \quad \beta_2^{\,4} = \frac{\rho A_2}{E I_2}\omega^2 L^4, \quad L = L_1 + L_2 \tag{6.13}$$

The clamped-clamped boundary conditions at O', O'' and continuity conditions at O_1 (Fig. 6.2) are summarized in table 6.1. Using clamped-clamped boundary conditions for Eq. (6.12), the displacement functions are obtained as

$$\begin{aligned} w_1(\xi') &= \eta_1\left(\sin\beta_1\xi' - \sinh\beta_1\xi'\right) + \eta_2\left(\cos\beta_1\xi' - \cosh\beta_1\xi'\right) \\ w_2(\xi') &= \eta_5\left(\sin\beta_1\theta'\xi' - \sinh\beta_1\theta'\xi'\right) + \eta_6\left(\cos\beta_1\theta'\xi' - \cosh\beta_1\theta'\xi'\right) \end{aligned} \tag{6.14}$$

where

$$\theta' = \frac{\phi'}{\alpha'}, \quad \alpha' = \left(\frac{I_2}{I_1}\right)^{1/4} \text{ and } \quad \phi' = \left(\frac{A_2}{A_1}\right)^{1/4} \tag{6.15}$$

Upon application of continuity conditions (table 6.1) to Eq. (6.14), the following equations are obtained (Gorman 1975)

$$\begin{aligned} &\eta_1(\sin\beta_1\mu - \sinh\beta_1\mu) + \eta_2(\cos\beta_1\mu - \cosh\beta_1\mu) \\ &\quad + \eta_5(-\sin\beta_1\theta'\gamma + \sinh\beta_1\theta'\gamma) + \eta_6(-\cos\beta_1\theta'\gamma + \cosh\beta_1\theta'\gamma) = 0 \\ &\eta_1(\cos\beta_1\mu - \cosh\beta_1\mu) + \eta_2(-\sin\beta_1\mu - \sinh\beta_1\mu) \\ &\quad + \eta_5\,\theta'(\cos\beta_1\theta'\gamma - \cosh\beta_1\theta'\gamma) + \eta_6\,\theta'(-\sin\beta_1\theta'\gamma - \sinh\beta_1\theta'\gamma) = 0 \\ &\eta_1(-\sin\beta_1\mu - \sinh\beta_1\mu) + \eta_2(-\cos\beta_1\mu - \cosh\beta_1\mu) \\ &\quad + \eta_5\alpha'^4\theta'^2(\sin\beta_1\theta'\gamma + \sinh\beta_1\theta'\gamma) + \eta_6\alpha'^4\theta'^2(\cos\beta_1\theta'\gamma + \cosh\beta_1\theta'\gamma) = 0 \\ &\eta_1(-\cos\beta_1\mu - \cosh\beta_1\mu) + \eta_2(\sin\beta_1\mu - \sinh\beta_1\mu) \\ &\quad + \eta_5\alpha'^4\theta'^3(-\cos\beta_1\theta'\gamma - \cosh\beta_1\theta'\gamma) + \eta_6\alpha'^4\theta'^3(\sin\beta_1\theta'\gamma - \sinh\beta_1\theta'\gamma) = 0 \end{aligned} \tag{6.16}$$

where $\mu = L_1/L$ and $\gamma = 1 - \mu = L_2/L$ are normalized lengths of the two sections of the stepped-beam (Fig. 6.2). The eigenvalues β_1 can be determined from the vanishing coefficient matrix of Eq. (6.16). However, as the main focus of the present study is to investigate the effect of step positions of stepped-beam on thermoelastic dissipation of stepped-beam, β_1 for different values of μ along the length of the stepped-beam of particular size are collected from (Gorman 1975). To obtain the modal shapes (Eq. (6.14)) for the two sections of stepped-beam, arbitrarily one of the constants of Eq. (6.16), say η_1, is set to 1 to make a non-homogeneous set of three equations which for particular sizes of the sections and step position of a stepped-beam will provide the solutions for η_2, η_5 and η_6.

6.4.2 Thermal Boundary Condition

Surface thermal conditions depend on heat transfer between the beam and the surrounding medium. In the present case study, the outer surfaces of the rectangular cross-section are considered insulated i.e. adiabatic. An adiabatic condition (Cimalla *et al.* 2007) can be expected in vacuum (ignoring radiation losses). Adiabatic surface condition requests that normal gradient of the temperature field vanishes on the surface. Thus for adiabatic surface condition, normal derivative of ΔT i.e. $\partial \Delta T/\partial n$ vanishes along the given boundary curve $F(y,z) = 0$ of the cross-section in the Y-Z plane which means that

$$\frac{\partial f(y,z)}{\partial z}\Big|_{F(y,z)=0} = 0 \tag{6.17}$$

Here $f(y,z)$ for arbitrary rectangular cross-section is approximated by assuming a polynomial series in y and z with constant coefficients (Tunvir *et al.*

2012). P_k and S_k for k^{th} section of stepped-beam of arbitrary rectangular cross-section are readily obtained from previous research (Tunvir *et al.* 2012) such that

$$P_k = \frac{8}{3} c_k d_k$$
$$S_k = \frac{16}{15} c_k d_k^{\,3} \tag{6.18}$$

6.5 Numerical Results and Discussion

Eqs. (6.10), (6.13) and (6.18) are used to analyze the step position dependency of thermoelastic dissipation in clamped-clamped stepped-beams of rectangular cross-section with adiabatic surface thermal condition. In all the numerical results, equilibrium temperature of the stepped-beam was considered to be T_{o} = 300 K. Single crystal polysilicon was used as the beam material. Material and thermal properties of single crystal polysilicon are taken from (Vengallatore 2005).

6.5.1 FE Modeling

To support the theoretical findings of stepped-beams, 3-dimensional finite element simulations were carried out using ANSYS® for uniform and stepped-beams of rectangular cross-section. A 20-node 3-dimensional coupled-field (structural-thermal) solid element (solid226) was used in the simulation. All translational degrees of freedom were set to zero at the clamped ends of the beam and an insulated surface thermal condition was applied to all surfaces of the model. The size of each element was 1 μm. The structural-thermal harmonic analyses were performed in the desired frequency ranges that span the first six resonant modes of the beam. However, for a stepped-beam, only fundamental frequencies corresponding to various step positions along the beam length were of interest. The

accuracies of the present theoretical model and the FE analysis of thermoelastic dissipation were verified by comparing the results of $1/Q$ for a uniform slender beam of rectangular cross-section with the classical results of Zener (1937). It must be mentioned here that for a uniform beam $1/Q$ does not depend on the mode shape of the beam (Eq. (6.10)). However, the length dependency of $1/Q$ is manifested through the equation of natural frequency. Fig. 6.3 shows a plot of $1/Q$ against operating frequency $f' = \omega/2\pi$ for a uniform beam of rectangular cross-section (c = 6 μm, d = 2 μm, L = 240 μm) obtained from the present study, Zener (1937) and the FE modeling. They show good agreement to each other over a wide range of operating frequencies. Moreover, the lowest *Q-factor*s from all the calculations are about 10^4, which is almost the minimum *Q-factor* requested for many applications to MEMS/NEMS (Sepulveda *et al.* 2006). The temperature distribution in the deformed uniform beam of rectangular cross-section of Fig. 6.3 is shown in Fig. 6.4. It can be seen that compressed zones of the beam develop higher temperature while the zones under tension lose temperature.

6.5.2 Thermoelastic Dissipation of Stepped-Beams with Single Step

Three different configurations of stepped-beams with a single step as shown in Fig. 6.5 have been considered for the numerical analysis, such as, stepped-beams having a change in width at the step with constant thickness all over the beam (type-1, Fig. 6.5-a), change in the thickness at the step with constant width all over the beam (type-2, Fig. 6.5-b) and cross-sectional changes in both thickness and width at the step (type-3, Fig. 6.5-c). A type-1 stepped-beam of this study with step position close

to the left support represents a beam with undercut at the support. Numerical analysis of thermoelastic dissipations of various stepped-beams is carried out only for fundamental frequencies corresponding to various step positions of the stepped-beam. Total lengths of various stepped-beam is kept fixed to L = 280 μm in all calculations unless otherwise specified.

A plot of *Q-factor*s against various step positions μ for type-1 stepped-beam of two different sizes (c_1 = 7 μm, c_2 = 1.68 μm, $d_1 = d_2$ = 1.5 μm; c_1 = 7 μm, c_2 = 4.6 μm, $d_1 = d_2$ = 1.5 μm) operated at fundamental frequencies is shown in Fig. 6.6. To verify the accuracy of the present model of thermoelastic dissipation for stepped-beam, results obtained from the FE analysis for the same stepped-beams are included in Fig. 6.6. *Q-factor*s of type-1 stepped-beams are also compared with the results of uniform beams of the same thickness for μ = 1 and γ = 1 in the same plot (Fig. 6.6) where μ and γ point to the beam sections of larger and smaller cross-sections respectively. It is to be noted here that under adiabatic surface thermal condition, thermoelastic dissipation in a beam of uniform rectangular cross-section is independent of width, *c*, of the cross-section while it is dependent on thickness, *d* (Ru 2009; Tunvir *et al.* 2010, 2012). However thermoelastic dissipation in a type-1 stepped-beam depends on the width of two sections (c_1, c_2) of stepped-beam. Higher variation of *Q-factor*s is observed for type-1 stepped-beam having lower value of width c_2 for the section corresponding to γ. It is seen from Fig. 6.6 that *Q-factor*s of the type-1 stepped-beam of particular size are different for low and high values of μ. In particular, *Q-factor*s in type-1 stepped-beam are lower than the uniform beam for μ up to 0.42 while higher for μ > 0.42. Type-1 stepped-beam resonator having step position within $\mu = 0.1 \sim 0.3$, which may be produced due to an undercut in beam resonators of MEMS (Gavan *et al.* 2009a, 2009b; Herrera-May

et al. 2010), are less efficient than uniform beams. *Q-factor*s vary significantly over a range of step positions of μ = 0.25 ~ 0.65. However, different results may be obtained for other sizes of stepped-beam. All results for the type-1stepped-beam from the present study follow the results from FE modeling with reasonable accuracy. Temperature distribution of a type-1 stepped-beam with step at μ = 0.45 obtained from FE modeling is shown in Fig. 6.7. The compressed zone develops higher temperature, which is continuous across the step.

On the other hand, behaviors of thermoelastic dissipation of a type-2 (c_1 = c_2 = 7 μm, d_1 = 3 μm, d_2 = 1.5 μm) and a type-3 (c_1 = 7 μm, c_2 = 5.1 μm, d_2 = 5 μm, d_2 = 2.9 μm) stepped-beams are similar for various step positions as shown in Figs. 6.8 and 6.10. *Q-factor*s decrease for ranges of μ = 0.15~0.35 *and* μ = 0.60~0.85 while in between *Q-factor*s increase. For the particular size considered, *Q-factor*s in type-2 stepped-beam decreases about one order of magnitude as the step position moves from μ = 0.15 to μ = 0.85 Figs. 6.9 and 6.11 are showing the temperature distributions of type-2 and type-3 stepped-beam respectively for the step position at μ = 0.45. In both the stepped-beams, the compressed zone experiences higher temperature and temperature is continuous across the step of the beams.

6.5.3 Comparison among Different Types of Stepped-Beams

Relative comparison among the different types of stepped-beams with a constant step position is studied for the condition of same cross-sectional areas of the sections corresponding to μ as well as γ among different types of stepped-beams. Thus, the sizes of the stepped-beams are chosen in such a way that the sections corresponding to μ in all the three types of stepped-beam possess the same cross-sectional size while the section corresponding to γ in each stepped-beam possesses

a half of the cross-sectional area of the section corresponding to μ of that stepped-beam. Satisfying the above condition, the size of the stepped-beams are considered as, type-1: c_1 = 7 μm, c_2 = 3.5 μm, $d_1 = d_2$ = 3 μm; type-2: $c_1 = c_2$ = 7 μm, d_1 = 3 μm, d_2 = 1.5 μm; type-3: c_1 = 7 μm, c_2 = 5 μm, d_1 = 3 μm, d_2 = 2.1 μm. Thermoelastic dissipations of the three types of stepped-beams are compared with each other and with uniform beam in Fig. 6.12. The step position is kept fixed to μ = 0.15, which is selected based on the most common step position that formed due to undercut at the support of the beam during fabrication. The cross-sectional size of the uniform beam is chosen to be composed of the highest width and the lowest thickness among the stepped-beams such that c = 7 μm, d = 1.5 μm. Fundamental frequencies of the beams are varied by varying the total lengths of the stepped-beams and *Q-factor*s are plotted against total length of the stepped-beams (Fig. 6.12). It can be seen from Fig. 6.12 that *Q-factor*s in type-1 stepped-beams are always higher than the other types of stepped-beams and the uniform beams for lengths up to 100 μm. Moreover, *Q-factor*s in type-2 and type-3 stepped-beams are always higher than uniform beam for beams' length up to 60 μm. It is revealed that *Q-factor*s in a type-1 stepped-beams with μ = 0.15 can be one order of magnitude times higher than uniform beams for length, L = 20 μm. Actually, there is a specific "transition length" for each stepped-beam, below which the *Q-factor* decreases with increasing length and above which the *Q-factor* increases with increasing length. The transition length for the type-2 stepped-beam is of the order of a few tens of micrometers while that for the type-1 and type-3 stepped-beams is about one hundred of micrometer. It is revealed that the type-1 stepped-beams provide higher quality factors than the other stepped-beams for most common lengths (20 ~ 80μm) of stepped-beams as found in the literature (Wang *et al.* 2006; Varshney *et al.* 2009; Ilic *et al.* 2004; Sekaric *et al.*

2002; Cleland *et al.* 2001; Demirci *et al.* 2003; Wang *et al.* 2000; Hsu *et al.* 2000, 2001; Gavan 2009a, 2009b; Herrera-May *et al.* 2010, 2011).

6.6 Summary

The present work analyzes thermoelastic dissipation in stepped-beams under adiabatic surface thermal condition with an emphasis on the role of step positions along the length of the stepped-beams. Recently, beam resonators in MEMS/NEMS devices are designed with stepped configuration for their enhanced performances in real applications. Besides as designed stepped-beam resonators, resonator beams in MEMS with an undercut at the clamped end, produced due to isotropic etching of the supporting substrate during fabrication process to release the beam, are also identified as stepped-beams.

Conclusions are made based on stepped-beams of rectangular cross-section with a single step, where the section on the left of the step possesses larger cross-sectional size than the one on the right. Three different configurations of rectangular cross-section have been considered such as beams having cross-sectional changes only in lateral direction (type-1), only in the bending direction (type-2), and in both lateral and bending directions (type-3) at the step. For a fixed length, *Q-factor* in a type-1 stepped-beam of particular cross-sectional size for sections increases as the step position moves from the left support to the right along the length while opposite is true for the other two types of stepped-beams provided that the stepped-beams are slender. *Q-factor*s in a type-1 stepped-beam can be higher than a uniform beam of the same size along bending direction for some particular step positions only. *Q-factor*s in a type-2 stepped-beam can be decreased one order of magnitude as the step position moves to the right. However, these results are for

some particular sizes of stepped-beam and different results may be obtained for other sizes. For most common lengths of the clamped-clamped stepped-beams in real applications with step close to the left support, the type-1 stepped-beams provide higher quality factors than the other stepped-beams provided that they have same cross-sectional area. Thus, to design a stepped-beam of a particular type, total length, and step position should be chosen carefully to achieve higher quality factor.

6.7 Figures and Illustrations

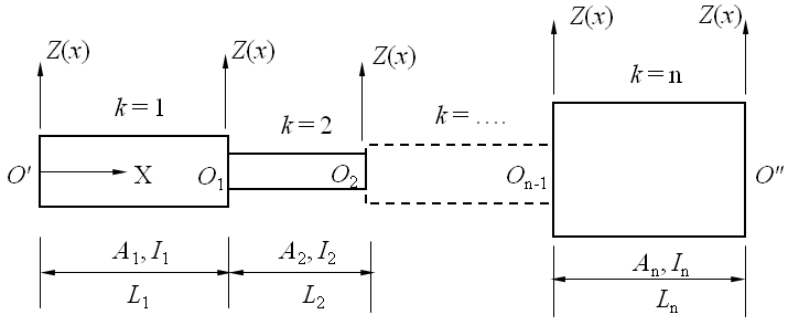

Fig. 6.1 Schematic diagram of stepped-beam having *k* number of sections.

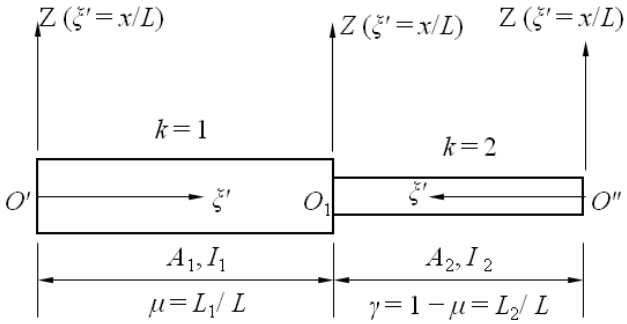

Fig. 6.2 Schematic diagram of stepped-beam with single step along the length that used for numerical analysis.

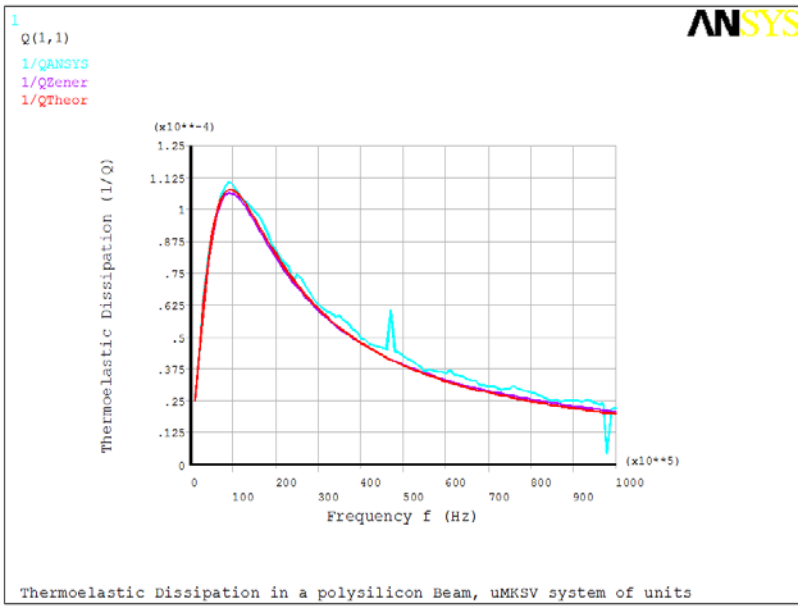

Fig. 6.3 Thermoelastic dissipation ($1/Q$) vs. operating frequency for uniform beam resonator of rectangular cross-section. Results from the present study are compared with the results obtained from FE modeling and Zener (1937).

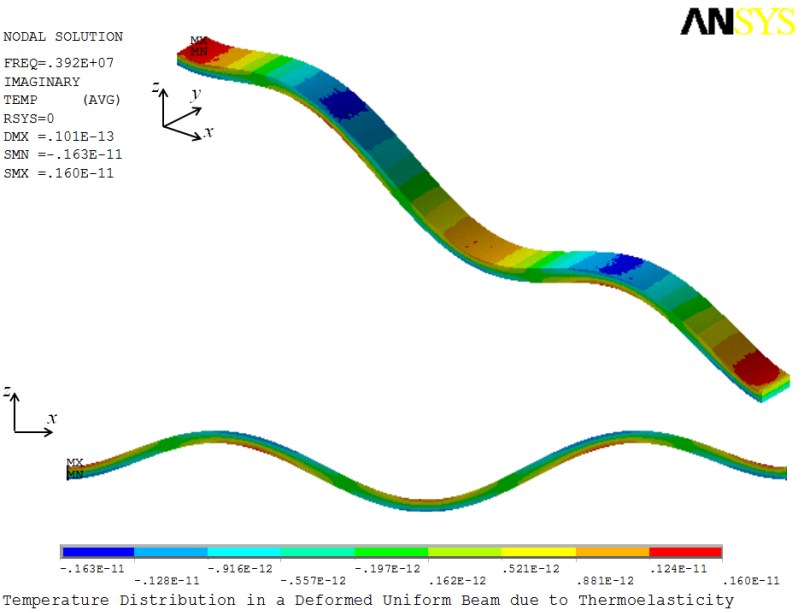

Fig. 6.4 Temperature distribution in deformed uniform beam resonator of rectangular cross-section having thickness, d = 2 μm and width, c = 6 μm.

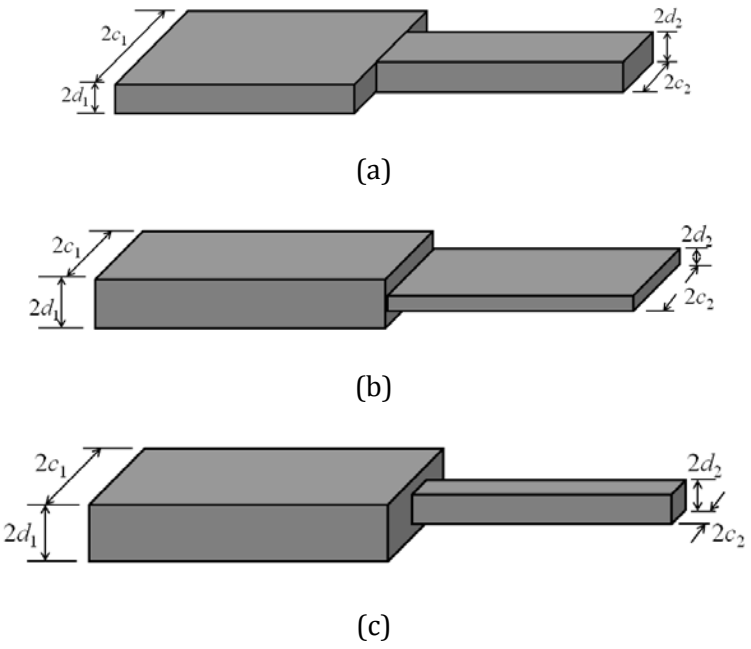

Fig. 6.5 Orientations of rectangular cross-section for different sections of a stepped-beam with single step; (a) type-1, (b) type-2 and (c) type-3.

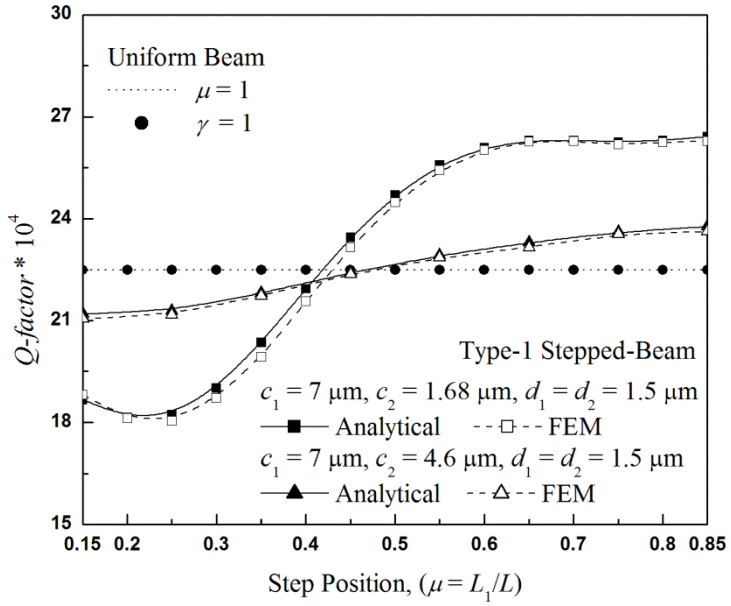

Fig. 6.6 *Q-factor* as a function of the step position μ in type-1 stepped-beam of total length, L = 280 μm. *Q-factor*s are calculated at fundamental frequencies corresponding to different step positions.

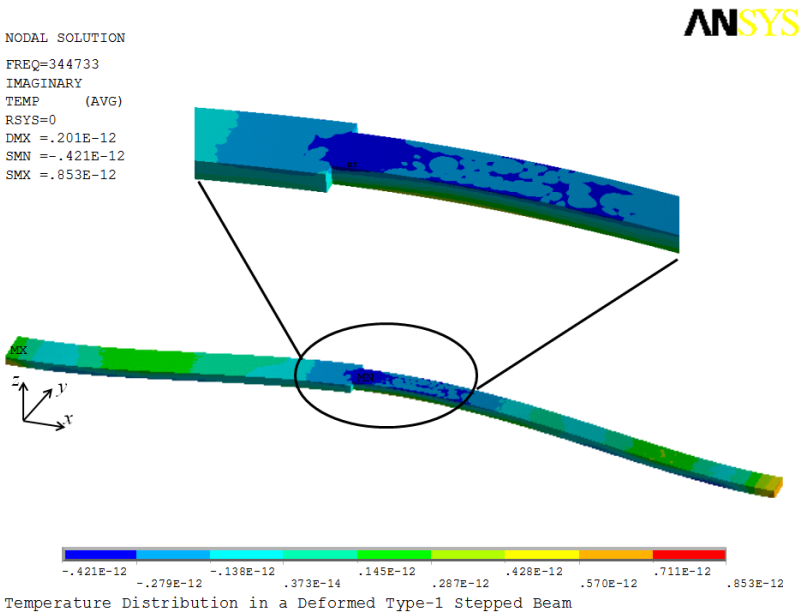

Fig. 6.7 Contour plot of temperature distribution of type-1 stepped-beam (μ = 0.45) vibrating at fundamental frequency. The size of the beam is L = 280 μm, c_1 = 7 μm, c_2 = 4.6 μm, $d_1 = d_2$ = 1.5 μm.

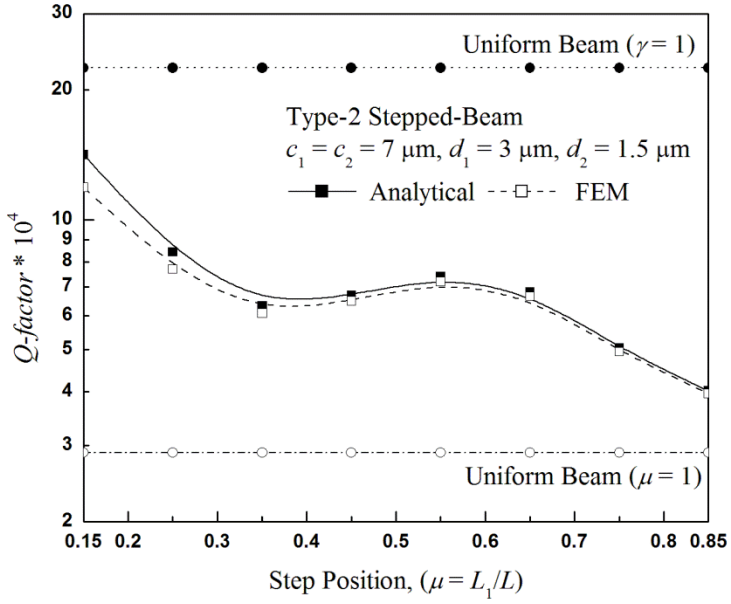

Fig. 6.8 *Q-factor* as a function of the step position μ in type-2 stepped-beam of total length, L = 280 μm. *Q-factor*s are calculated at fundamental frequencies corresponding to different step positions.

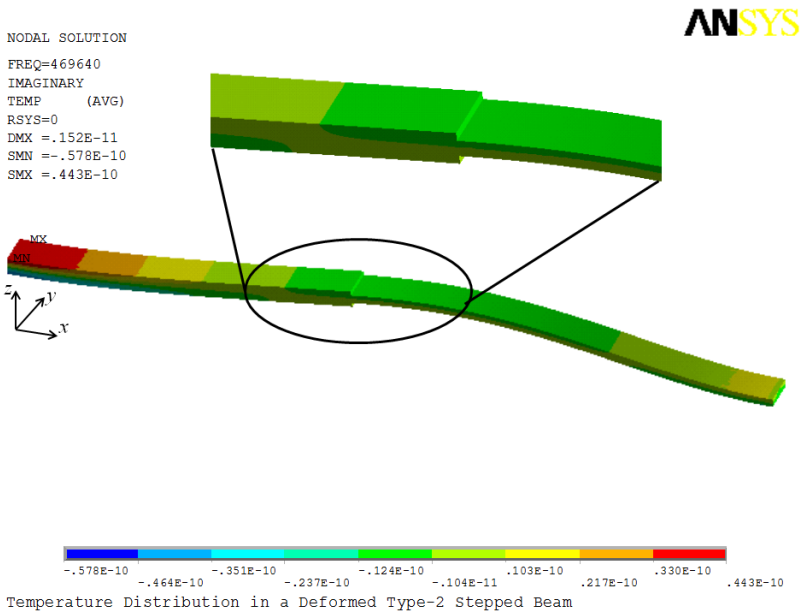

Fig. 6.9 Contour plot of temperature distribution of type-2 stepped-beam (μ = 0.45) vibrating at fundamental frequencies. The size of the beam is as L = 280 μm, $c_1 = c_2$ = 7 μm, d_1 = 3 μm, d_2 = 1.5 μm.

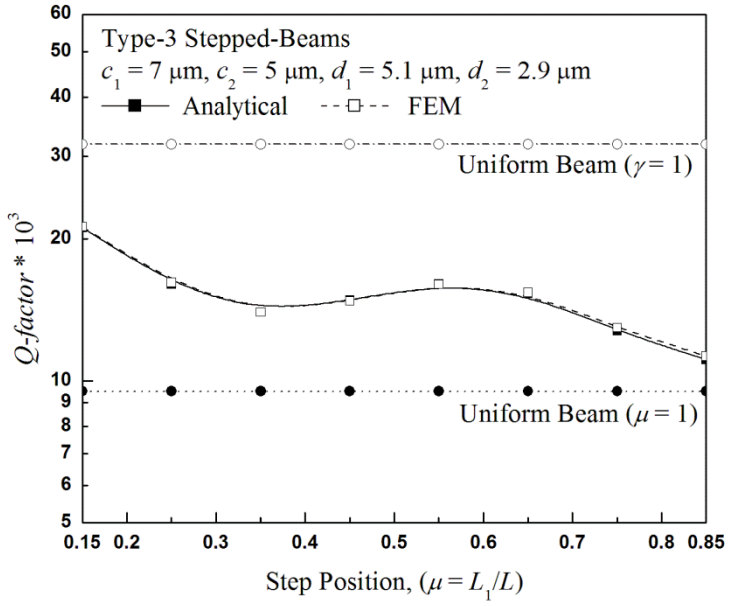

Fig. 6.10 *Q-factor* as a function of the step position μ in stepped-beam of type-3 of total length, L = 280 μm. *Q-factor* is calculated at fundamental frequencies corresponding to different step positions.

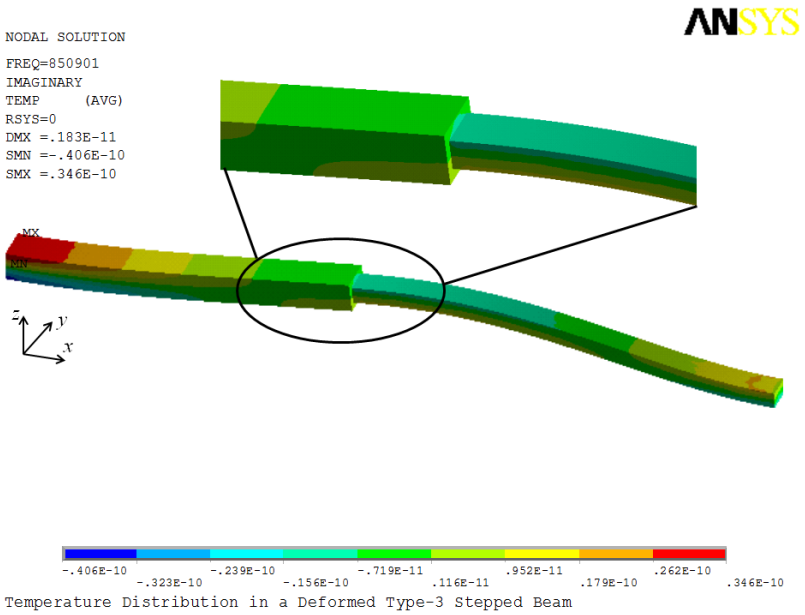

Fig. 6.11 Contour plot of temperature distribution of type-3 stepped-beam (μ = 0.45) vibrating at fundamental frequency. The size of the beam is as L = 280 μm, c_1 = 7 μm, c_2 = 5.1 μm, d_1 = 5 μm, d_2 = 2.9 μm.

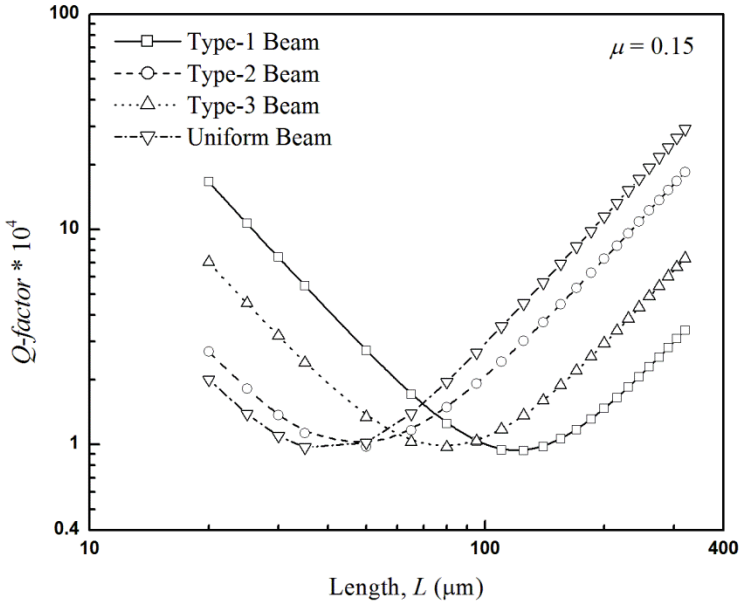

Fig. 6.12 *Q-factor* as a function of total length, L of different types of stepped-beams for a constant step position μ = 0.15. The sizes of the beams, Type-1: c_1 = 7 μm, c_2 = 3.5 μm, $d_1 = d_2$ = 3 μm; Type-2: $c_1 = c_2$ = 7 μm, d_1 = 3 μm, d_2 = 1.5 μm; Type-3: c_1 = 7 μm, c_2 = 5 μm, d_1 = 3 μm, d_2 = 2.1 μm; Uniform beam: c = 7 μm, d = 1.5 μm.

6.8 Tables

Table 6.1 Boundary and continuity conditions for stepped-beam with single step.

Conditions (Fig. 6.2)	**Expressions**
At clamped ends (*O′*, *O″*)	
Displacement	$w_1(\xi') = w_2(\xi') = 0\big\vert_{\xi'=0}$
Slope	$\dfrac{dw_1(\xi')}{d\xi'} = \dfrac{dw_2(\xi')}{d\xi'} = 0\Big\vert_{\xi'=0}$
Continuity at O_1	
Displacement	$w_1(\mu) = w_2(\gamma)$
Slope	$\dfrac{dw_1(\xi')}{d\xi'}\Big\vert_{\xi'=\mu} = -\dfrac{dw_2(\xi')}{d\xi'}\Big\vert_{\xi'=\gamma}$
Bending Moment	$\dfrac{d^2w_1(\xi')}{d\xi'^2}\Big\vert_{\xi'=\mu} = \alpha'^4 \dfrac{d^2w_2(\xi')}{d\xi'^2}\Big\vert_{\xi'=\gamma}$
Shear force	$\dfrac{d^3w_1(\xi')}{d\xi'^3}\Big\vert_{\xi'=\mu} = -\alpha'^4 \dfrac{d^3w_2(\xi')}{d\xi'^3}\Big\vert_{\xi'=\gamma}$

$\mu = L_1/L$, $\gamma = 1-\mu = L_2/L$

6.9 References

Behreyni B., Shafai C. 2006. Application of twin-beam structures for estimation of material properties and sensor fabrication. *Canadian Journal of Electronics and Computer Engineering* **31** 85-88.

Cimalla V., Niebelschütz F., Tonisch K., Foerster Ch., Brueckner K., Cimalla I., Friedrich T., Pezoldt J., Stephan R., Hein M., Ambacher O. 2007. Nanoelectromechanical devices for sensing applications. *Sensors and Actuators B* **126** 24-34.

Cleland A. N., Pophristic M., Ferguson I. 2001. Single-crystal aluminum nitride nanomechanical resonators. *Applied Physics Letters* **79** 2070.

Demirci M. U., Nguyen C. T. C. 2003. Higher-mode free-free beam micromechanical resonators. *Proceedings of IEEE International Frequency Control Symposium*, Tampa, Florida 810-818.

Ekinci K. L., Roukes M. L. 2005. Nanoelectromechanical systems. *Review of Scientific Instruments* **76** 061101.

Gavan K. B., Drift E. W. J. M. van der, Venstra W. J., Zuiddam M. R., Zant H. S. J. van der 2009a. Effect of undercut on the resonant behavior of silicon nitride cantilevers. *Journal of Micromechanics and Microengineering* **19** 035003.

Gavan K. B., Westra H. J. R., Drift E. W. J. M. van der, Venstra W. J., Zant H. S. J. van der 2009b. Impact of fabrication technology on flexural resonances of silicon nitride cantilevers. *Microelectronics Engineering* **86** 1216-1218.

Gorman D. J. 1975. Free vibration analysis of beams and shafts, 1st Ed., John Wiley & Sons, New York.

Herrera-May A. L., Aguilera-Cortés L. A., García-Ramírez P. J., Plascencia-Mora H., Torres-Cisneros M. 2010. Modeling of the intrinsic stress effect on the

resonant frequency of NEMS resonators integrated by beams with variable cross-section. *Microsystems Technology* **16** 2067-2074.

Herrera-May A. L., García-Ramírez P. J., Aguilera-Cortés L. A., Plascencia-Mora H., García-González L., Manjarrez E., Narducci M., Figueras E. 2011. Analytical Modeling for the Bending Resonant Frequency of Sensors Based on Micro and Nanoresonators With Complex Structural Geometry. *IEEE Journal of Sensors* **11** 1361.

Hoseinzadeh S., Khadem S. E. 2011. Thermoelastic vibration and damping analysis of double-walled carbon nanotubes based on shell theory**.** *Physica E* **43** 1146-1154.

Hsu W. T., Clark J. R., Nguyen C. T. C. 2000. Mechanically temperature-compensated flexural-mode micromechanical resonators. *Technical Digest*, *IEEE International Electronics Device Meeting* 399-402.

Hsu W. T., Clark J. R., Nguyen C. T. C. 2001. A sub-micron capacitive gap process for multiple-metal-electrode lateral micromechanical resonators. *Technical Digest, IEEE International Microelectromechanical Systems* 349-352.

Ilic B., Yang Y., Craighead H. G. 2004. Virus detection using nanoelectromechanical devices. *Applied Physics Letters* **85** 2604.

Imboden M., Mohanty P., Gaidarzhy A., Rankin J., Sheldon B. W. 2007. Scaling of dissipation in megahertz-range micromechanical diamond oscillators. *Applied Physics Letters* **90** 173502.

Jang S. K., Bert C. W. 1989. Free vibration of stepped-beams: exact and numerical solutions. *Journal of Sound and Vibration* **130** 342-346.

Koplow M. A., Bhattacharyya A., Mann B. P. 2006. Closed form solutions for the dynamic response of Eular-Bernoulli beams with step changes in cross-section. *Journal of Sound and Vibration* **295** 214-225.

Lifshitz R., Roukes M. L. 2000. Thermoelastic damping in micro- and nanomechanical systems. *Physical Review B* **61** 5600-5609.

Mamin J. 2007. Nanosensors: small strains, big gains. *Nature Nanotechnology* **2** 81-82.

Mohanty P., Harrington D. A., Ekinci K. L., Yang Y. T., Murphy M. J., Roukes M. L. 2002. Intrinsic dissipation in high-frequency micromechanical resonators. *Physical Review B* **66** 085416.

Naguleswaren S. 2002. Natural frequencies, sensitivity and mode shape details of an Eular-Bernoulli beam with one-step change in cross-section and with ends on classical supports. Journal of Sound and Vibration **252** 751-767.

Ru C. Q. 2009. Thermoelastic dissipation of nanowire resonators with surface stress. *Physica E* **41** 1243-1248.

Sekaric L., Parpia J. M., Craighead G. H., Feygelson T., Houston B. H., Butler J. E. 2002. Nanomechanical resonant structures in nanocrystalline diamond. *Applied Physics Letters* **81** 4455-4457.

Sepulveda N., Aslam D., Sullivan J. P. 2006. Polycrystalline diamond MEMS resonator technology for sensor applications. *Diamond Related Materials* **15** 398-403.

Tunvir K., Ru C. Q., Mioduchowski A. 2010. Thermoelastic dissipation of hollow micromechanical Resonators. *Physica E* **42** 2341-2352.

Tunvir K., Ru C. Q., Mioduchowski A. 2012. Effect of cross-sectional shape on thermoelastic dissipation of micro/nano elastic beams. *Intlernational Journal of Mechanical Sciences* **62** 77-88.

Varshney M., Waggoner P. S., Montagna R. A., Craighead H. J. 2009. Prion protein detection in serum using micromechanical resonator arrays. *Talanta* **80** 593-599.

Vengallatore S. 2005. Analysis of thermoelastic damping in laminated composite micromechanical beam resonators. *Journal of Micromechanics and Microengineering* **15** 2398-2404.

Wang K., Wong A. C., Nguyen C. T. C. 2000. VHF Free–Free Beam High-Q Micromechanical Resonators. *Journal of Microelectromechanical Systems* **9** 347.

Wang L., Phillips S. M., Branicky M. S., Bayraktar B. 2006. Nano-resonators for RF-enabled networked-control. *J of Physics: Conference Series* **38** 158-162.

Yang J., Ono T., Esashi M. 2002. Energy dissipation in submicrometer thick single-crystal silicon cantilevers. *Journal of Microelectromechanical Systems* **11** 775-783.

Yasumura K. Y., Stowe T. D., Chow E. M., Pfafman T., Kenny W. T., Stipe B. C., Rugar D. 2000. Quality factor in micros- and submicron-thick cantilevers. *Journal of Microelectromechanical Systems* **9** 117-125.

Zener C. 1937. Internal Friction in Solids. I. Theory of Internal Friction in Reeds. *Physical Review* **52** 230-235.

Chapter 7

Thermoelastic Dissipation of Beam Resonators under Non-Linear Large-Amplitude Vibration[5]

7.1 Overview

In real applications, beam resonators in MEMS/NEMS often vibrate beyond the linear regime. Here it is aimed to study the effect of large-deflection on thermoelastic dissipation of doubly-clamped microbeam resonators. Detailed formulas are derived for *Q-factor* due to thermoelastic dissipation, which depends on the amplitude of vibration deflection. Under adiabatic or isothermal surface conditions, the non-linear effect of large-deflection on thermoelastic dissipation is demonstrated with a comparison to the results based on linearized small deflection vibration. Numerical results show that thermoelastic dissipation is reduced monotonically with increasing amplitude of vibration deflection under adiabatic

[5]*A version of this chapter has been published. Tunvir K., Ru C. Q., Mioduchowski A. 2012. Journal of Thermal Stresses* ***35*** (*12*) *1076-1094.*

surface condition, while thermoelastic dissipation is increased monotonically with increasing amplitude under isothermal surface condition. Under both adiabatic and isothermal surface conditions, the large-deflection effect on thermoelastic dissipation becomes more significant for higher vibration frequencies than lower ones. For the first time to the best of author's knowledge, these results reveal that large-deflection has a significant effect on thermoelastic dissipation of microbeam resonators and surface thermal condition plays an important role in the large-deflection effect.

7.2 Introduction

Beam resonators have broad application in a wide range of MEMS/NEMS (Ekinci and Roukes 2005; Cimalla *et al.* 2007; Li *et al.* 2007.). A resonator is a device that violently oscillates at some specific frequencies, called its resonant frequencies, and is used either to generate waves of specific frequencies or to detect specific frequencies from a signal. Microbeam resonators often are driven into non-linear regime with larger amplitude in order to store enough energy (Mestrom *et al.* 2009; Husain *et al.* 2003). The amplitude of vibration increases with the frequency of vibration (Husain *et al.* 2003). A relevant research topic of beam resonators is energy dissipation at the micro/nano scales (Zener 1937, 1938; Yasumura *et al.* 2000; Ekinci and Roukes 2005; Khisaeva and Ostoja-Starjewski 2006; Sharma 2011). In particular, thermoelastic dissipation has been identified as a major energy dissipation mechanism for a large range of micro/nano mechanical resonators (Zener 1937, 1938; Lifshitz and Roukes 2000; Yasumura *et al.* 2000; Khisaeva and Ostoja-Starjewski 2006; Ru 2009; Tunvir *et al.* 2010) where almost all previous studies were limited to linearized vibration of microbeam resonators with small

vibration deflection. Thus, thermoelastic dissipation of microbeams for non-linear large-deflection vibration is a research topic of practical significance.

Recent studies showed that in next generation ultrahigh-frequency resonators of MEMS/NEMS, non-linear large-deflection vibration is practically evident (Peng *et al.* 2006; Bunch *et al.* 2007; Masmanidis *et al.* 2007; Eom *et al.* 2011; Husain *et al.* 2003). Ultrahigh-frequency beam resonators often vibrate in the non-linear regime to store high potential energy and amplitude of vibration increases with the frequency. Moreover, sensitivity of mass detection of micro/nano beam resonators can be improved by geometric nonlinearity induced nonlinear large-vibration, since the detection sensitivity is highly correlated with the resonant frequency (Eom *et al.* 2011). Though geometrical non-linearity is practically evident in ultrahigh-frequency resonators of MEMS/NEMS, almost no study has focused on large-deflection effect on thermoelastic dissipation.

Non-linear effects in microbeam resonators can arise from different sources including large-deflection (geometrical non-linearity) or material non-linearity etc. In a microbeam resonator, typically, geometrical non-linearity due to axial stretching is most significant for large-deflection vibration (Singh *et al.* 1990; Rao 1992; Rao and Raju 2003). Geometrical non-linearity due to large-deflection has been seen to occur in eletrostatically actuated microbeam resonators. Thermoelastic dissipation in electrostatically actuated micro beam/plate structure have been studied by Nayfeh and Younis (2004), Vahdat and Rezazadeh (2011), De and Aluru (2006), Hajnayeb *et al.* (2011), Zamanian and Khadem (2010) where axial pre-stretch of the midplane usually occurs in resonator structure due to the large-deflection generated by the attraction force of capacitive voltage. Nayfeh and Younis (2004) studied the effect of electrostatic magnitude on the *Q-factor* of the system by

considering the electrostatic actuation as a linear function of microbeam deflection but neglected the midplane stretching due to large-deflection. De and Aluru (2006) considered the non-linear effect of electrostatic actuation, but neglected the midplane stretching term. Both the works concluded that *Q-factor* due to thermoelastic dissipation in electrostatically actuated beam resonator decreases with the increase of actuating capacitive voltage. Later Vahdat and Rezazadeh (2011) carried out similar works but with the consideration of constant static pre-stretching of the midplane. They analyzed thermoelastic dissipation based on linearized small-amplitude vibration around the largely deflected static equilibrium position. Zamanian and Khadem (2010) studied the same problem for the solution of thermoelastic dissipation in two-layered beam structure, however, without considering any thermal contact between the beam layers. More similar examples include (Hajnayeb *et al.* 2011) in which thermoelastic damping of carbon nanotube resonators is investigated based on linearized small-amplitude vibration around a large-deflection static equilibrium position. Besides thermoelastic dissipation, some researchers studied non-linear large-deflection dynamics of MEMS resonators (Xie *et al.* 2003; Méndez *et al.* 2009; Mestrom *et al.* 2010). For example, Méndez *et al.* (2009) studied non-linear large-deflection effect on resonance frequencies and the decay rate of amplitude of cantilever microbeams with damping, without studying the effect of large-deflection vibration on thermoelastic dissipation. In spite of practical relevance of non-linear large-deflection vibration on MEMS/NEMS resonators (Peng *et al.* 2006; Bunch 2007; Masmanidis *et al.* 2007; Eom *et al.* 2011; Husain *et al.* 2003), up to date, no theoretical studies has been carried out to examine the effect of non-linear large-deflection on thermoelastic dissipation of microbeam resonators.

Here in this chapter it is attempted to analyze non-linear large-deflection effect on thermoelastic dissipation of doubly-clamped microbeam resonators under adiabatic or isothermal surface thermal condition. Thermoelasticity model and thermoelastic dissipation under non-linear large-deflection vibration are formulated in the section 7.3 and 7.4 respectively. Detailed analysis for a microbeam resonator of rectangular cross-section under adiabatic or isothermal surface thermal condition is demonstrated and discussed in sections 7.5 and 7.6. Finally, all results are summarized in 7.7.

7.3 Thermoelasticity Model with Large-Deflection

Thermoelastic dissipation is a relevant dissipation mechanism in beam resonators at smaller scales (Yasumura *et al.* 2000). Thermoelastic dissipation occurs in all elastic material subjected to cyclic deformation, especially when the period of cycle is close to the material's thermal relaxation time (Zener 1938; Lifshitz and Roukes 2000). For example when an elastic flexural beam vibrates, although most of the mechanical work is converted to elastic energy, some part of the work is converted to thermal energy. While the elastic energy is recoverable, the thermal energy is irreversible due to thermal conduction. The lost mechanical work due to thermal conduction defines thermoelastic dissipation. Thermoelasticity models are expected to work well for thermoelastic dissipation analysis of beam resonators at micro scales.

Consider an isotropic, homogeneous, thermoelastic slender beam, clamped at both ends, vibrating in the *X*-*Z* plane of a Cartesian coordinate system as shown in Fig. 7.1. The *Y* and *Z*-axes lie along the two perpendicular symmetric axes of the

cross-section, see Fig. 7.1. For bending with large-deflection, the non-linear axial strain is

$$\varepsilon_{xx} = (\varepsilon_{xx})_{stretching} + (\varepsilon_{xx})_{bending} = \left[\frac{\partial u}{\partial x} + \frac{1}{2}\left(\frac{\partial w}{\partial x}\right)^2\right] + \left[z\frac{\partial^2 w}{\partial x^2}\right] \tag{7.1}$$

where z is the distance to the neutral Y-axis, $u(x,t)$ and $w(x,t)$ are the axial displacement and transverse deflection of the beam respectively. The total uni-axial stress is

$$\sigma_{xx} = E[\varepsilon_{xx} - \alpha\,\Delta T] = E\left[\frac{\partial u}{\partial x} + \frac{1}{2}\left(\frac{\partial w}{\partial x}\right)^2\right] + E\,z\frac{\partial^2 w}{\partial x^2} - E\alpha\,\Delta T \tag{7.2}$$

where ΔT is the deformation-induced temperature change from the initial uniform temperature T_o, α is the linear thermal expansion coefficient, and E is the Young's modulus. For uni-axial stress-state, the two lateral strains of the beam are $\varepsilon_{yy} = \varepsilon_{zz} = -(\nu\,\sigma_{xx}/E) + \alpha\,\Delta T$. The temperature field $T(x,y,z,t) = T_o + \Delta T(x,y,z,t)$ is coupled with the deformation (Lifshitz and Roukes 2000; Yasumura *et al.* 2000; Ru 2009; Tunvir *et al.* 2010) by

$$C_V\frac{\partial T}{\partial t} + \frac{E\,\alpha\,T_o}{1-2\nu}\frac{\partial \varepsilon}{\partial t} = \kappa\nabla^2 T \tag{7.3}$$

where C_V is the heat capacity per unit volume, $\varepsilon = \varepsilon_{xx} + \varepsilon_{yy} + \varepsilon_{zz}$ is the mean strain, κ is the thermal conductivity, ν is the Poisson's ratio. Because the axial wave-length of bending deformation is usually much larger than the dimension of the cross-section, heat conduction along axial x-direction is negligible compared to heat conduction over the cross-section (Lifshitz and Roukes 2000). Moreover $E\alpha^2 T_o/C_V$ is negligible comparing to unity (Lifshitz and Roukes 2000). It follows from Eq. (7.3) that

$$C_V\frac{\partial \Delta T}{\partial t} + E\alpha T_o\frac{\partial}{\partial t}\left[\frac{\partial u}{\partial x} + \frac{1}{2}\left(\frac{\partial w}{\partial x}\right)^2\right] + E\alpha T_o z\frac{\partial}{\partial t}\left(\frac{\partial^2 w}{\partial x^2}\right) = \kappa\left(\frac{\partial^2}{\partial y^2} + \frac{\partial^2}{\partial z^2}\right)\Delta T \tag{7.4}$$

The present work focuses on the effect of large-deflection on deformation-induced temperature change and related thermoelastic dissipation. It follows from Eq. (7.4) that the deformation induced temperature, ΔT determined by Eq. (7.4) in terms of the deflection $w(x,t)$, can be decomposed into the bending and stretching related parts as

$$\Delta T(x,y,z,t)=(\Delta T)_1 + (\Delta T)_2 = \Theta_1(x,t)f_1(y,z)+\Theta_2(x,t)f_2(y,z) \tag{7.5}$$

where $\Theta_1(x,t)$ and $\Theta_2(x,t)$ are determined by the following two equations respectively

$$C_V f_1(y,z)\frac{\partial}{\partial t}\Theta_1(x,t)+E\alpha T_\circ \frac{\partial}{\partial t}\left[\frac{\partial u}{\partial x}+\frac{1}{2}\left(\frac{\partial w}{\partial x}\right)^2\right]-\kappa\Theta_1(x,t)\left(\frac{\partial^2}{\partial y^2}+\frac{\partial^2}{\partial z^2}\right)f_1(y,z)=0 \tag{7.6}$$

$$C_V f_2(y,z)\frac{\partial}{\partial t}\Theta_2(x,t)+E\alpha T_\circ z\frac{\partial}{\partial t}\left(\frac{\partial^2 w}{\partial x^2}\right)-\kappa\Theta_2(x,t)\left(\frac{\partial^2}{\partial y^2}+\frac{\partial^2}{\partial z^2}\right)f_2(y,z)=0 \tag{7.7}$$

It is seen from Eqs. (7.6) and (7.7) that for resonator beams of doubly symmetric cross-section (with two perpendicular axes of symmetry), because the non-homogeneous terms in Eqs. (7.6) and (7.7) are, respectively, symmetric and anti-symmetric about the neutral Y-axis, $(\Delta T)_1 = \Theta_1(x,t)f_1(y,z)$ must be symmetric about z, while $(\Delta T)_2 = \Theta_2(x,t)f_2(y,z)$ must be anti-symmetric about z. Therefore $f_1(y,z)$ should be even in z while $f_2(y,z)$ should be odd in z. As the problem is symmetric about the Z axis, $f_1(y,z)$ and $f_2(y,z)$ both should be even in y. It follows from Eqs. (7.6) and (7.7) that

$$C_V\frac{\partial\Theta_1(x,t)}{\partial t}S_1+E\alpha T_\circ A\frac{\partial}{\partial t}\left[\frac{\partial u}{\partial x}+\frac{1}{2}\left(\frac{\partial w}{\partial x}\right)^2\right]+\kappa\Theta_1(x,t)P_1=0 \tag{7.8}$$

$$C_V\frac{\partial\Theta_2(x,t)}{\partial t}S_2+E\alpha T_\circ I\frac{\partial}{\partial t}\left(\frac{\partial^2 w}{\partial x^2}\right)+\kappa\Theta_2(x,t)P_2=0 \tag{7.9}$$

where I is the cross-sectional moment of inertia ($I \equiv \int_A z^2 dA$) and the four constants S_1, P_1, S_2 and P_2 are defined as

$$\begin{aligned} S_1 &\equiv \int_A f_1(y,z)dA \\ P_1 &\equiv -\int_A \left(\frac{\partial^2}{\partial y^2} + \frac{\partial^2}{\partial z^2} \right) f_1(y,z)dA \\ S_2 &\equiv \int_A z f_2(y,z)dA \\ P_2 &\equiv -\int_A z \left(\frac{\partial^2}{\partial y^2} + \frac{\partial^2}{\partial z^2} \right) f_2(y,z)dA \end{aligned} \tag{7.10}$$

Here, A is the cross-sectional area of the beam. On the other hand, it follows from Eq. (7.2) that the resultant axial force and bending moment are given by

$$N_x = \int_A \sigma_{xx} dA = EA\left[\frac{\partial u}{\partial x} + \frac{1}{2}\left(\frac{\partial w}{\partial x} \right)^2 \right] - E\alpha S_1 \Theta_1(x,t) \tag{7.11}$$

$$M = \int_A \sigma_{xx} z dA = EI \frac{\partial^2 w}{\partial x^2} - E\alpha S_2 \Theta_2(x,t) \tag{7.12}$$

The present work is limited to doubly-clamped beam resonators with axially immovable end condition. As usual, it is assumed that axial displacement u is negligible and the resultant axial force N_x is spatially uniform along the beam. Thus, the resultant axial force N_x can be written as

$$N_x = \frac{EA}{2L} \int_0^L \left(\frac{\partial w}{\partial x} \right)^2 dx - \frac{E\alpha S_1}{L} \int_0^L \Theta_1(x,t)dx \tag{7.13}$$

where L is the length of the beam. Eq. (7.13) describes the axial stretching force over the length of the beam, which is uniform along x but dependent on time (t). Finally, the equation for deflection is

$$EI \frac{\partial^4 w}{\partial x^4} - N_x \frac{\partial^2 w}{\partial x^2} + \rho A \frac{\partial^2 w}{\partial t^2} = 0 \tag{7.14}$$

with boundary conditions $w = 0$ and $(\partial w / \partial x) = 0$ at $x = 0, L$.

Assuming a simple harmonic oscillation and linear vibration mode for non-linear vibration will simplify the problem in hand, however, will provide the upper bound of the exact solution of non-linear frequency by satisfying only the equation of motion at an instant of maximum deflection (Singh *et al.* 1990). Moreover this assumption has been adopted frequently in previous studies of vibration problem, for example, Ray and Bert (1969), Tseng and Dugundji (1970), Bennouna and White (1984). As the focus of the present study is to determine the effect of large-deflection on deformation-induced temperature change, the simplest harmonic vibration of the form $w(x,t)=w_{\circ}(x)e^{-i\omega t}$ has been considered where ω is the circular frequency, and $w_{\circ}(x)$ is approximated by the linear vibration mode. Here, due to non-linear large-deflection, the operating frequency ω may depend on the amplitude of vibration deflection, as to be discussed later. Therefore, since $w(x,t)=w_{\circ}(x)e^{-i\omega t}$, it is seen from Eqs. (7.8), (7.9), (7.11) and (7.12) that $N_x \sim e^{-2i\omega t}$, $\Theta_1 \sim e^{-2i\omega t}$ and $M \sim e^{-i\omega t}$, $\Theta_2 \sim e^{-i\omega t}$. Furthermore, integrating Eq. (7.8) over the beam length, it follows from Eqs. (7.8) and (7.13) that

$$N_x = \frac{D'_{\omega}}{L}\int_0^L \left(\frac{\partial w}{\partial x}\right)^2 dx \tag{7.15}$$

where the complex axial rigidity (D'_{ω}) depends on the frequency ω and is given by

$$D'_{\omega} = \frac{EA\left(\kappa^2 {P_1}^2 + 4\omega^2 {C_V}^2 {S_1}^2\right) + 4\omega^2 E^2 \alpha^2 {S_1}^2 AT_{\circ} C_V}{2\left(\kappa^2 {P_1}^2 + 4\omega^2 {C_V}^2 {S_1}^2\right)}\left[1 - \frac{i2\omega E^2 \alpha^2 AT_{\circ}\kappa S_1 P_1}{EA\left(\kappa^2 {P_1}^2 + 4\omega^2 {C_V}^2 {S_1}^2\right) + 4\omega^2 E^2 \alpha^2 {S_1}^2 AT_{\circ} C_V}\right] \tag{7.16}$$

Similarly, eliminating Θ_2 from Eqs. (7.9) and (7.12), the following relation is obtained

$$M(x,t) = D''_{\omega}\left(\frac{\partial^2 w}{\partial x^2}\right) \tag{7.17}$$

where the complex bending rigidity (D''_{ω}) depends on the frequency ω and is given by

$$D''_{\omega} = \frac{EI\left(\kappa^2 {P_2}^2 + \omega^2 {C_V}^2 {S_2}^2\right) + \omega^2 E^2 \alpha^2 T_\circ I C_V {S_2}^2}{\kappa^2 {P_2}^2 + \omega^2 {C_V}^2 {S_2}^2}\left[1 - \frac{i\omega E^2 \alpha^2 T_\circ I \kappa S_2 P_2}{EI\left(\kappa^2 {P_2}^2 + \omega^2 {C_V}^2 {S_2}^2\right) + \omega^2 E^2 \alpha^2 T_\circ I C_V {S_2}^2}\right] \tag{7.18}$$

7.4 Thermoelastic Dissipation for Non-Linear Large-Amplitude Vibration

Thermoelastic dissipation, defined by the ratio of mechanical energy loss per cycle to total strain energy stored, can be calculated by the required energy supply for each cycle to keep a periodic harmonic motion (Zener 1937, 1938; Lifshitz and Roukes 2000; Ru 2009; Tunvir *et al.* 2010). The required energy supply for an infinitesimal element *dx* of the beam located at a point *x* over a period, $t = 0 \sim 2\pi/\omega$, is given by

$$dx \int_0^{2\pi/\omega}\int_A \sigma_{xx}\,\dot{\varepsilon}_{xx}\,dA\,dt = dx \int_0^{2\pi/\omega} N_x \frac{d}{dt}\left[\frac{\partial u}{\partial x} + \frac{1}{2}\left(\frac{\partial w}{\partial x}\right)^2\right]dt + dx \int_0^{2\pi/\omega} M \frac{d}{dt}\left(\frac{\partial^2 w}{\partial x^2}\right)dt \tag{7.19}$$

where $\left(\partial^2 w/\partial x^2\right)$ is the curvature of bending deformation. Substituting the expressions for N_x and M into Eq. (7.19) gives

$$
\begin{aligned}
\left[Lost\ Energy\right]_{Strecthing} &= \int_0^{L}\int_0^{2\pi/\omega} N_x \frac{d}{dt}\left[\frac{1}{2}\left(\frac{\partial w}{\partial x}\right)^2\right]dt\,dx \\
&= \int_0^{L}\int_0^{2\pi/\omega} Re[N_x]Re\left[\frac{d}{dt}\left(\frac{1}{2}\left(\frac{\partial w}{\partial x}\right)^2\right)\right]dt\,dx \\
&= -\pi\, Im[D'_\omega]\frac{1}{L}\left[\int_0^{L}\left(\frac{dw_\circ}{dx}\right)^2 dx\right]^2
\end{aligned}
\tag{7.20}
$$

$$
\begin{aligned}
\left[Lost\ Energy\right]_{Bending} &= \int_0^{L}\int_0^{2\pi/\omega} M\frac{d}{dt}\left(\frac{\partial^2 w}{\partial x^2}\right)dt\,dx \\
&= \int_0^{L}\int_0^{2\pi/\omega} Re[M]Re\left[\frac{d}{dt}\left(\frac{\partial^2 w}{\partial x^2}\right)\right]dt\,dx \\
&= -\pi\, Im[D''_\omega]\int_0^{L}\left(\frac{d^2 w_\circ}{dx^2}\right)^2 dx
\end{aligned}
\tag{7.21}
$$

These indicate that the imaginary parts of the complex axial (D'_ω) and bending (D''_ω) rigidities determine the lost mechanical energy. Total stored strain energy due to stretching and bending deformation is given by the integral of $Re[N_x]\left[(1/2)(\partial w/\partial x)^2\right]/2$ and $Re[M_\circ]\left(\partial^2 w_\circ/\partial x^2\right)/2$ over the beam length. Therefore, using Eqs. (7.20) and (7.21), the general expression for thermoelastic dissipation, or the inverse of the *Q-factor* due to thermoelastic dissipation, is given by

$$
\left(\frac{1}{Q}\right)_{Non-linear} = \frac{(Energy\ loss)/cycle}{2\pi(Total\ energy\ stored)} = \frac{-Im[D''_\omega]\int_0^{L}\left(\frac{d^2 w_\circ}{dx^2}\right)^2 dx - \frac{1}{L}Im[D'_\omega]\left[\int_0^{L}\left(\frac{dw_\circ}{dx}\right)^2 dx\right]^2}{Re[D''_\omega]\int_0^{L}\left(\frac{d^2 w_\circ}{dx^2}\right)^2 dx + \frac{Re[D'_\omega]}{2L}\left[\int_0^{L}\left(\frac{dw_\circ}{dx}\right)^2 dx\right]^2}
\tag{7.22}
$$

As usual, large-deflection effect on vibration mode is assumed secondary and thus negligible, and the vibration mode is approximated by the linear mode of doubly-clamped beam as (Gorman 1975; Hao *et al.* 2003)

$$
w_\circ(x) = \left(\frac{W}{J}\right)\left[\cosh\left(\frac{\beta x}{L}\right) - \cos\left(\frac{\beta x}{L}\right) + \psi\left\{\sinh\left(\frac{\beta x}{L}\right) - \sin\left(\frac{\beta x}{L}\right)\right\}\right]
\tag{7.23}
$$

where W is the real (maximum) amplitude of vibration mode, ψ is the mode shape factor, β is the mode constant, and J, is determined so that W represents the real amplitude. The mode shape factor, ψ and mode constant, β are given by

$$\psi_n = \frac{\sin\beta_n + \sinh\beta_n}{\cos\beta_n - \cosh\beta_n} \quad \text{and} \quad \beta_n^{\,4} = \frac{\rho A \omega_n^{\,2} L^4}{EI} \tag{7.24}$$

where subscript n denotes mode numbers (n = 1, 2, 3,.....). It is found that J_n (J_1, J_2, J_3……..) = 1.6, 1.44, 1.39 and so. Therefore $(1/Q)_{Non\text{-}linear}$ becomes

$$\left(\frac{1}{Q}\right)_{Non-linear} = \frac{-Im\left[D''_\omega\right]\beta_n U_n - \dfrac{W^2}{8J_n^{\,2}} Im\left[D'_\omega\right]V_n}{Re\left[D''_\omega\right]\beta_n U_n + \dfrac{W^2}{16J_n^{\,2}} Re\left[D'_\omega\right]V_n} \tag{7.25}$$

Here, U_n and V_n depend on the mode shape factor and mode constant. Details of U_n and V_n are given in Appendix: A (Chapter 9, Section 9.1).

7.5 Temperature Field under Non-Linear Large-Amplitude Vibration

Let us consider a beam resonator of rectangular cross-section with length (L), width ($2c$) and thickness ($2d$), as shown in Fig. 7.1 where Y-axis coincides with the neutral axis of the cross-section. The equation of the boundary of the cross-section is

$$F(y,z) = \left(y^2 - c^2\right)\left(z^2 - d^2\right) \tag{7.26}$$

7.5.1 Adiabatic Surface Condition

Let us first consider adiabatic surface condition which requires that normal derivative $\partial\Delta T/\partial n$ (or $\partial f/\partial n$) vanishes along the given boundary curve $F(y,z)$ = 0 in

the *Y-Z* plane. It can be easily verified that ($\partial f/\partial n = 0$) on the curve $F(y,z) = 0$ means that

$$\left(\frac{\partial f_\upsilon}{\partial y}\frac{\partial F}{\partial y}+\frac{\partial f_\upsilon}{\partial z}\frac{\partial F}{\partial z}\right)\Big|_{F(y,z)=0}=0 \tag{7.27}$$

where υ = 1,2 represent functions $f_1(y,z)$ and $f_2(y,z)$ for stretching and bending deformation respectively. It is noticed that under adiabatic condition, $P_1 = 0$ is a general consequence of the divergence theorem for arbitrary cross-section shapes. As discussed previously that $f_1(y,z)$, representing temperature field due to stretching deformation, should be even in y and z. If $f_1(y,z)$ is expanded in z up to the second power of z, the coefficient of the second power must be zero, in order to meet the adiabatic surface condition. Thus, because deformation due to stretching is independent of z, it follows that

$$f_1(y,z)=q_1 \tag{7.28}$$

where q_1 is a constant. As the definition of $f_1(y,z)$ is arbitrary within a constant factor, q_1 = 1 can be chosen always to simplify the problem. Thus, constants S_1 and P_1 are given by

$$S_1 = 4dc\ ,\ P_1 = 0$$

(7.29)

For $f_2(y,z)$, representing temperature field due to bending deformation, it follows from author's previous works (Tunvir *et al.* 2012) for rectangular cross-section that

$$f_2(y,z)=z\left[1-\frac{z^2}{3d^2}\right] \tag{7.30}$$

which gives S_2 and P_2 as

$$S_2 = \frac{16}{15} cd^3 , \quad P_2 = \frac{8}{3} cd \tag{7.31}$$

7.5.2 Isothermal Surface condition

An isothermal surface requests $\Delta T = 0$ along the given boundary curve $F(y,z) = 0$ in the *Y-Z* plane, such that

$$(\Delta T)_v \big|_{F(y,z)=0} = 0 \tag{7.32}$$

Therefore $f_1(y,z)$, which satisfies the above required condition, is given by

$$f_1(y,z) = \left(y^2 - c^2\right)\left(z^2 - d^2\right) \tag{7.33}$$

which gives S_1 and P_1 as

$$S_1 = \frac{16}{9} c^3 d^3 , \; P_1 = \frac{16}{3} cd\left[c^2 + d^2\right] \tag{7.34}$$

On the other hand, for $f_2(y,z)$ should be odd in z and even in y, in view of Eq. (7.26), $f_2(y,z)$ can be approximated as

$$f_2(y,z) = z\left(y^2 - c^2\right)\left(z^2 - d^2\right) \tag{7.35}$$

which gives S_2 and P_2 as

$$S_2 = \frac{16}{45} c^3 d^5 , \; P_2 = \frac{16}{3} c^3 d^3 + \frac{16}{15} cd^5 \tag{7.36}$$

7.6 Result and Discussion

Now let us examine the effect of large-deflection on thermoelastic dissipation of a doubly-clamped beam resonator of rectangular cross-section under adiabatic or isothermal surface thermal condition. An adiabatic condition can be expected in vacuum (ignoring radiation losses) while isothermal condition can be

expected in a denser external medium. In what follows, the formulas derived in the last two sections will be used to examine the dependence of thermoelastic dissipation on the ratio of deflection amplitude (W) to thickness ($2d$). Calculation of thermoelastic dissipation is carried out for beam resonators of typical fine-grained polysilicon and the material constants are taken from (Srikar and Senturia 2002) such as coefficient of thermal expansion, $\alpha = 2.6\times10^{-6}$ K^{-1}, bulk elastic modulus, $E = 160\times10^{9}$ Nm^{-2}, thermal conductivity, $\kappa = 148$ Wm^{-1}K^{-1} and heat capacity per unit volume, $C_V = 1.66\times10^{6}$ Jm^{-3}K^{-1}, mass density, $\rho = 2330$ Kgm^{-3}. *Q-factor*s based on the present non-linear large-deflection model and the previous linear model (Ru 2009; Tunvir *et al.* 2010), will be called $Q_{Non\text{-}linear}$ and Q_{Linear} respectively.

7.6.1 Effect of Large-Deflection on Thermal Field

Fig. 7.2 shows the magnitudes of $(\Delta T)_1$ and $(\Delta T)_2$ at various locations along the positive Z-axis of the rectangular cross-section of beam resonator (a beam resonator of typical size: L = 300 μm, $2c$ = 56 μm and $2d$ = 2.1 μm) that vibrating at fundamental frequency with different real amplitudes, W. As can be seen from Fig. 7.2-a that under adiabatic condition, $|(\Delta T)_1|$ remains same over the positive z coordinates, while under isothermal condition $|(\Delta T)_1|$ (Fig. 7.2-b) is maximum at neutral axis (z = 0) and gradually decreases to zero at the surface for vibration of any amplitude. On the other hand, $|(\Delta T)_2|$ under adiabatic surface condition (Fig. 7.2-c) is found zero at z = 0 for any amplitude which increases monotonically to a maximum value at the surface. It is to be noted here that as expected, under adiabatic surface thermal condition, gradients of temperature field at the outer surface for both stretching and bending deformation are zero at any amplitude of vibration. Under isothermal surface condition, $|(\Delta T)_2|$ is zero at both z = 0 and the

surface for any amplitude (Fig. 7.2-d); and the maximum occurs at some mid location between them. Moreover amount of $|(\Delta T)_1|$ and $|(\Delta T)_2|$ are found to increase as the amplitude of vibration increases. Nevertheless, rate of change in ΔT (except $|(\Delta T)_1|$ under adiabatic condition) over the cross-section increases as the amplitude of vibration increases. Because of constant $|(\Delta T)_1|$ under adiabatic surface, there is no loss of mechanical energy due to axial stretching deformation, while it does increase the total elastic energy. As a result, axial stretching deformation will increase the *Q-factor* for thermoelastic dissipation under adiabatic surface condition.

7.6.2 Thermoelastic Dissipation at Linear Natural Frequencies under Adiabatic Surface Condition

First, let us consider linear natural frequencies of beam resonator. The formula for thermoelastic dissipation of small amplitude linear vibration is given by (Ru 2009; Tunvir *et al.* 2010, 2012)

$$\left(\frac{1}{Q}\right)_{Linear} = -\frac{Im\left[D''_{\omega}\right]}{Re\left[D''_{\omega}\right]} \tag{7.37}$$

Fig. 7.3 shows the effect of large-deflection amplitude on thermoelastic dissipation under adiabatic surface condition. $Q_{Non\text{-}linear}$s' are normalized by Q_{Linear} and shown against various values of the amplitude (W) to thickness ($2d$) ratio. For example, for the fundamental mode of vibration, $Q_{Non\text{-}linear}$ is about 9.87 times Q_{Linear} for the amplitude-to-thickness ratio ($W/2d$) of 5. It should be mentioned here that because $\left(E\alpha^2 T_{\circ}\right)/C_V$ is negligible compared to unity (Zener 1938; Lifshitz and Roukes 2000), under adiabatic surface thermal condition, the ratio $Q_{Non\text{-}linear}/Q_{Linear}$ is

independent of material constants and the size of the beam's cross-section for any vibration mode and can be expressed as

$$\left(\frac{Q_{Non-linear}}{Q_{Linear}}\right)_{Adia} = 1 + \frac{3}{8}\frac{V_n}{U_n \beta_n J_n^{\,2}}\left(\frac{W}{2d}\right)^2 \tag{7.38}$$

It is also observed that the large-deflection effect on thermoelastic dissipation is more significant for higher-order vibrational modes. In particular, for adiabatic surface condition, there is no loss of mechanical energy due to axial stretching deformation (as P_1 = 0 for adiabatic surface), which indicates that axial stretching deformation does not contribute to thermoelastic dissipation while it does increase the total elastic energy. As a result, axial stretching deformation increases *Q-factor* for thermoelastic dissipation. This conclusion seems consistent with some recent works, which confirmed that tensile axial pre-stress will increase *Q-factor* for thermoelastic dissipation (Kumar and Haque 2010; Unterreithmeier *et al.* 2010; Zamanian and Khadem 2010; Kim and Kim 2011).

Fig. 7.4 shows the *Q-factor* for a beam resonator of typical size: L = 300 μm, $2c$ = 56 μm and $2d$ = 2.1 μm (Ahn and Guckel 2000; Srikar and Senturia 2002). It is seen that $Q_{Non\text{-}linear}$s' and Q_{Linear}s' decrease with increasing frequency whereas $Q_{Non\text{-}linear}/Q_{Linear}$ always increases with increasing frequency. It could suggest that doubly-clamped beam resonators with adiabatic surface should be better driven at higher frequencies with larger vibration amplitude.

7.6.3 Thermoelastic Dissipation at Linear Natural Frequencies under Isothermal Condition

On the other hand, opposite effect of large-deflection on thermoelastic dissipation is predicted for isothermal surface condition (Figs. 7.5 and 7.6). Under isothermal surface condition, considering $\left(E\alpha^2 T_\circ\right)/C_V$ is negligible compared to unity (Yasumura *et al.* 2000), $Q_{Non\text{-}linear}/Q_{Linear}$ can be expressed as

$$\left(\frac{Q_{Non-linear}}{Q_{Linear}}\right)_{Iso} = \left[1+\frac{3}{8}\frac{V_n}{U_n \beta_n {J_n}^2}\left(\frac{W}{2d}\right)^2\right] \Bigg/ \left[1+\frac{3}{2}\frac{V_n}{U_n \beta_n {J_n}^2}\frac{S_1 P_1\left(\kappa^2 {P_2}^2+\omega^2 {C_V}^2 {S_2}^2\right)}{S_2 P_2\left(\kappa^2 {P_1}^2+\omega^2 {C_V}^2 {S_1}^2\right)}\left(\frac{W}{2d}\right)^2\right] \tag{7.39}$$

Thus it is seen that under isothermal surface condition $Q_{Non\text{-}linear}/Q_{Linear}$ is dependent on the material constants and the size of the beam's cross-section. For all the modes of vibration considered, $Q_{Non\text{-}linear}$ is lower than Q_{Linear}, as much as 20 times when the amplitude-to-thickness ratio ($W/2d$) = 5. This degradation of *Q-factor* with increasing amplitude is substantial for the ratio $W/2d$ up to 3 while after that the degradation of *Q-factor* with increasing amplitude becomes less significant. The increased thermoelastic dissipation under isothermal surface condition is attributed to the lost mechanical energies due to stretching deformations as shown in Fig. 7.7. As showed in Fig. 7.6, the lost mechanical energy due to stretching deformation is considerably larger than that due to bending deformation, which causes total lost mechanical energy to increase with amplitude especially when the ratio $W/2d$ exceeds 0.3.

7.6.4 Thickness Dependence of Thermoelastic Dissipation at Linear Natural Frequencies

For a particular application in MEMS/NEMS it is of interest to know the non-linear large-deflection effect on the maximum dissipation $(1/Q)_{max}$ with respect to the size of beam resonators. To this end, *Q-factor*s ($Q_{Non\text{-}linear}$ and Q_{Linear}) have been calculated for doubly-clamped beam resonators of various thicknesses, $2d$ (ranging from 2 μm to 16 μm) at the linear fundamental frequency (Figs. 7.8 and 7.9). The length, L and width, $2c$ of the beams are kept constant at L = 300 μm and $2c$ = 20 μm. *Q-factor*s are obtained for several values of vibration amplitudes, for example, W = 4, 8, 12 μm. Under adiabatic surface thermal condition (Fig. 7.8), though $Q_{Non\text{-}linear}$ always higher than Q_{Linear} for all the sizes considered, the maximum thermoelastic dissipation seems to occurs around ($2d$ = 11.5 μm) for both the linear and non-linear vibration. The specific size of the beam resonator corresponding to maximum-dissipation is almost the same for linear and non-linear vibration, because in both the cases, thermoelastic dissipations are dominated by lost mechanical energy due to bending deformation. Under isothermal surface condition, however, it is seen from Fig. 7.9 that the maximum dissipation occurs at two different sizes for non-linear and linear cases respectively. In this case, thermoelastic dissipation for non-linear vibration depends on lost mechanical energies due to both bending and stretching deformations. This result indicates that non-linear large-deflection affects not only the amount of energy dissipation but also the specific size at which the maximum thermoelastic dissipation occurs.

Finally, as found from a simple FEM analysis (Kaajakari *et al.* 2004), *Q-factor* and the maximum stored energy for a single crystal silicon bridge (doubly-clamped)

resonator (dimension as L = 52 μm, 2c = 10 μm, 2d = 4 μm) vibrating at an operating frequency of 13 MHz with an amplitude of W = 65 nm are: Q = 10000 and 2.6E-11 J, respectively. From this example, the present solution predicts that the *Q-factor* due to thermoelastic dissipation and the maximum stored energy are: Q = 13000 and 2.03E-11 J respectively (material constants are taken from (Pourkamali *et al.* 2003; Kaajakari *et al.* 2004)). Evidently, theoretical predictions of this study are comparable to FEA results of (Kaajakari *et al.* 2004).

7.6.5 Thermoelastic Dissipation at Non-Linear Natural Frequencies

The effect of large-amplitude on resonant frequencies can be easily estimated by Eq. (7.14). For a slender beam resonator of rectangular cross-section having thickness 2d, the non-linear fundamental frequency is related to the linear (Rao *et al.* 2008) one by

$$\frac{\omega_{NL}^2}{\omega_L^2} = 1 + \frac{9}{16}\left(\frac{W}{2d}\right)^2 \tag{7.40}$$

where ω_{NL}, ω_L are non-linear fundamental frequency and linear fundamental frequency respectively, and W is the vibration amplitude of the beam. It is noted here that the tensile load that develops during large-deflection vibration in doubly-clamped a beam with immovable ends is treated as a uniform axial force which depends on the amplitude ratio $W/2d$.

The effect of non-linear large-deflection on thermoelastic dissipation of a typical doubly-clamped fine-grained polysilicon (Srikar and Senturia 2002) beam resonator of L = 300 μm, 2c = 56 μm, 2d = 2.1 μm (Srikar and Senturia 2002), which is vibrating at non-linear natural frequencies, is shown in Figs. 7.10 and 7.11 for

adiabatic and isothermal surface conditions respectively. In both the figures, $Q_{Non\text{-}linear}$ is calculated based on non-linear natural frequencies given by Eq. (7.40) and Q_{Linear} is obtained for the same beam resonator using the linear natural frequencies. It is stated here that considering the amplitude effect on natural frequency makes the ratio $Q_{Non\text{-}linear}/Q_{Linear}$ to be dependent on both material constants and cross-sectional size of the beam. It is found that $Q_{Non\text{-}linear}$ is about 2.5 times of Q_{Linear} for the amplitude-to-thickness ratio ($W/2d$) of 5, which is much lower than the ratio $Q_{Non\text{-}linear}/Q_{Linear}$ = 9.87 given in Fig. 7.3 based on linear natural frequency. On the other hand, under isothermal surface condition, it can be seen from Fig. 7.10 that $Q_{Non\text{-}linear}/Q_{Linear}$ = 0.014 for the amplitude-to-thickness ratio ($W/2d$) of 5, which is much lower than 0.054 obtained with linear natural frequency as shown in Fig. 7.5. Due to lack of relevant known data in the existing literature on the non-linear large-deflection effect on thermoelastic dissipation, it is not possible to compare the present results with any available experimental or simulation results.

7.7 Summary

The present work analyzes the effects of non-linear large-deflection on thermoelastic dissipation of doubly-clamped beam resonators. Detailed results are demonstrated for beam resonators of rectangular cross-sections. It is found that non-linear large-deflection has a significant effect on thermoelastic dissipation, and this effect is very sensitive to adiabatic or isothermal surface thermal conditions. More explicitly, the large-deflection significantly increases the *Q-factor* for adiabatic surface conditions, while it considerably decreases the *Q-factor* for isothermal surface condition. This conclusion is mainly attributed to the fact that stretching deformation does not contribute to loss of mechanical energy under adiabatic

surface condition while it has a significant contribution to loss of mechanical energy under isothermal surface condition. These results suggest that doubly-clamped beam resonators should be better driven with larger amplitude under adiabatic surface condition while small-amplitude vibration is preferable for isothermal surface condition.

7.8 Figures and Illustrations

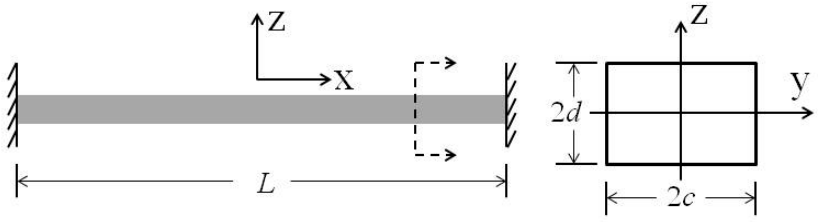

Fig. 7.1 Schematic diagram of doubly-clamped beam resonator.

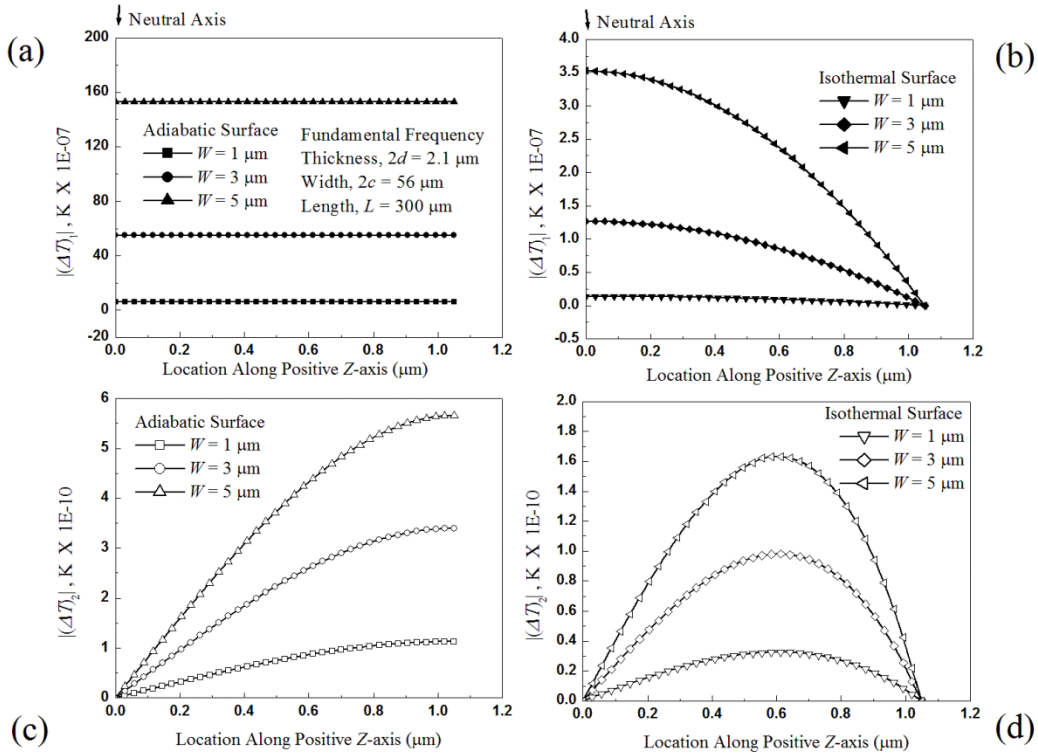

Fig. 7.2 $|(\Delta T)_1|$ and $|(\Delta T)_2|$ along the positive z locations of the cross-section of a beam resonator vibrating at fundamental frequencies with different amplitude.

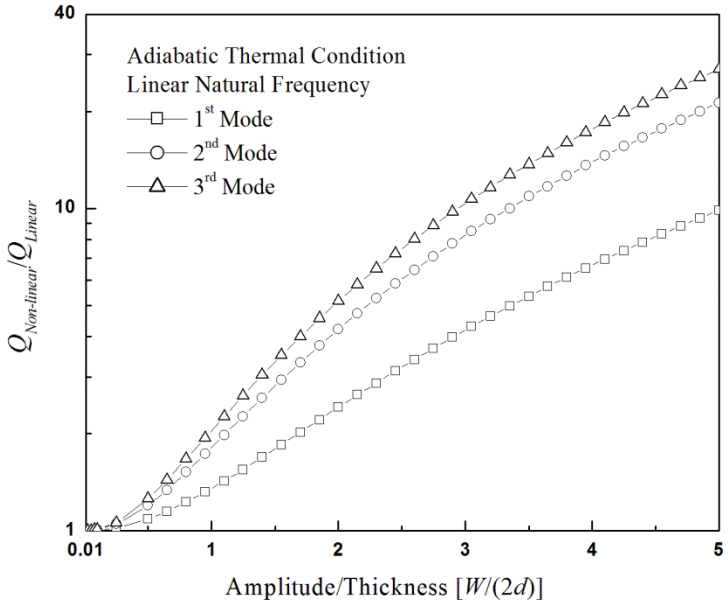

Fig. 7.3 $Q_{Non\text{-}linear}$ due to thermoelastic dissipation for a doubly-clamped beam resonator normalized by Q_{Linear} of the same resonator. Results are plotted for the first three linear frequencies and modes against different amplitude/thickness ratio under adiabatic surface thermal condition.

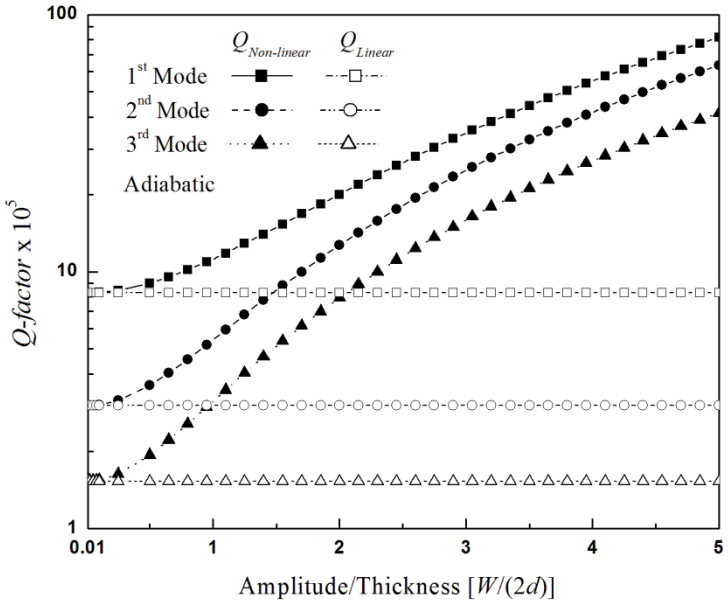

Fig. 7.4 *Q-factor* due to thermoelastic dissipation for a beam resonator for the first three vibration modes at linear natural frequencies. Results are shown against different amplitude/thickness ratio for a particular beam (L = 300 μm, $2c$ = 56 μm, $2d$ = 2.1 μm (Srikar and Senturia 2002)) of fine-grained polysilicon (Srikar and Senturia 2002) under adiabatic surface thermal condition.

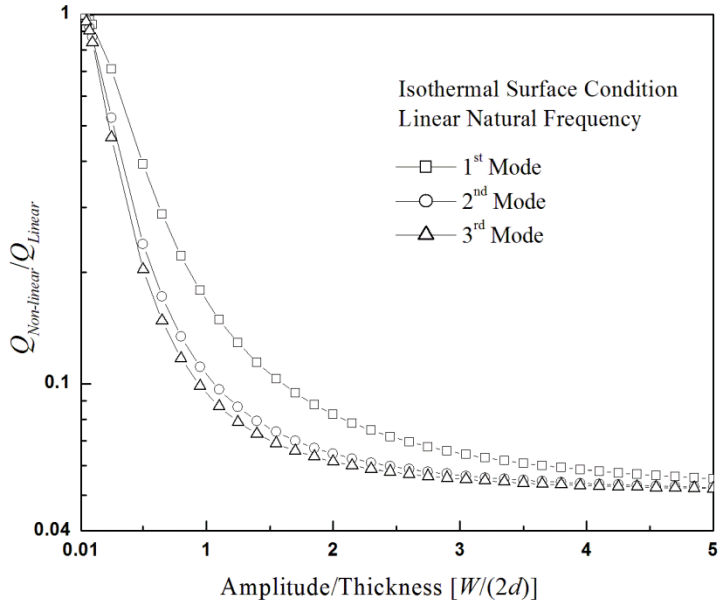

Fig. 7.5 $Q_{Non\text{-}linear}$ due to thermoelastic dissipation normalized by Q_{Linear} for the same resonator for a doubly-clamped beam resonator (L = 300 μm, $2c$ = 56 μm, $2d$ = 2.1 μm (Srikar and Senturia 2002)) of fine-grained polysilicon (Srikar and Senturia 2002). Results are plotted for the first three linear frequencies and modes against different amplitude/thickness ratio under isothermal surface condition.

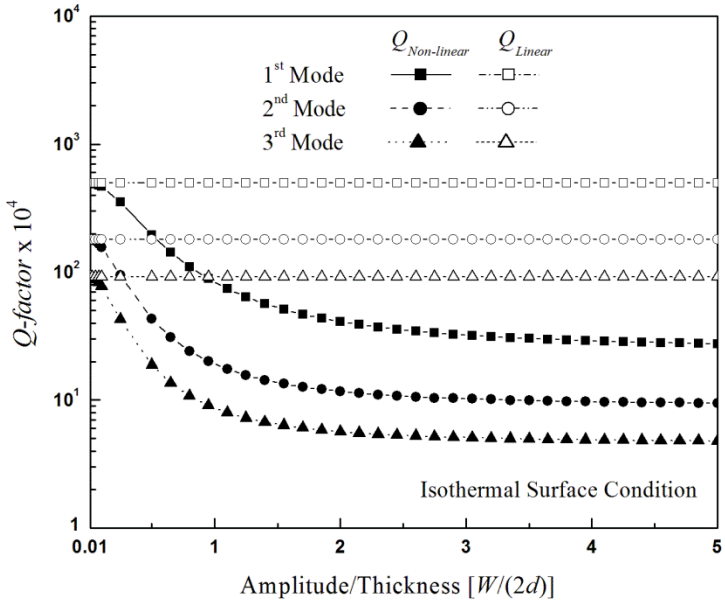

Fig. 7.6 *Q-factor* due to thermoelastic dissipation for a beam resonator for the first three vibration modes at the linear natural frequencies. Results are shown against different amplitude/thickness ratio for a particular beam (L = 300 μm, $2c$ = 56 μm, $2d$ = 2.1 μm (Srikar and Senturia 2002)) of fine-grained polysilicon (Srikar and Senturia 2002) under isothermal surface condition.

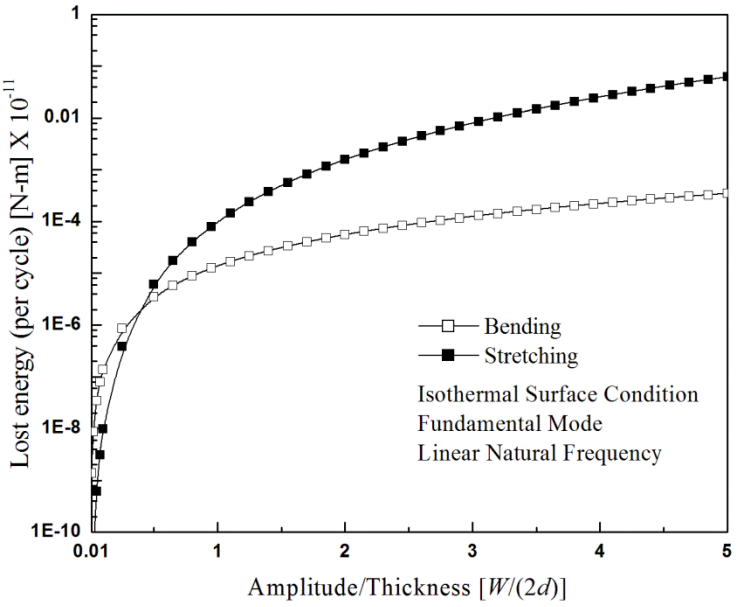

Fig. 7.7 Lost mechanical energies per cycle due to bending and stretching under isothermal surface condition at the linear natural frequency for fundamental mode. Results are shown for different amplitude to thickness ratio ($W/2d$) for a typical beam (L = 300 μm, $2c$ = 56 μm, $2d$ = 2.1 μm (Srikar and Senturia 2002)) of fine-grained polysilicon (Srikar and Senturia 2002).

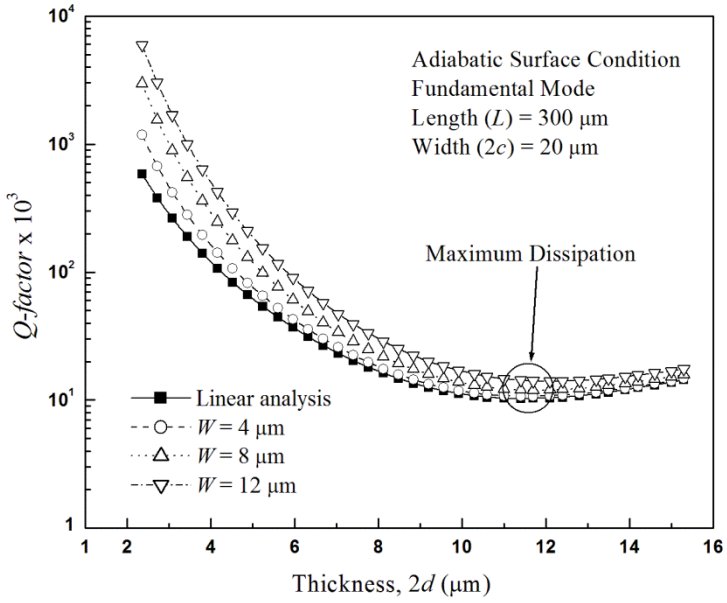

Fig. 7.8 *Q-factor* due to thermoelastic dissipation for beam resonators of fine-grained polysilicon (Srikar and Senturia 2002) under adiabatic surface condition against different thicknesses of the beams for various amplitudes. *Q-factor* are calculated for both linear and non-linear vibration using the linear natural frequencies of the beams.

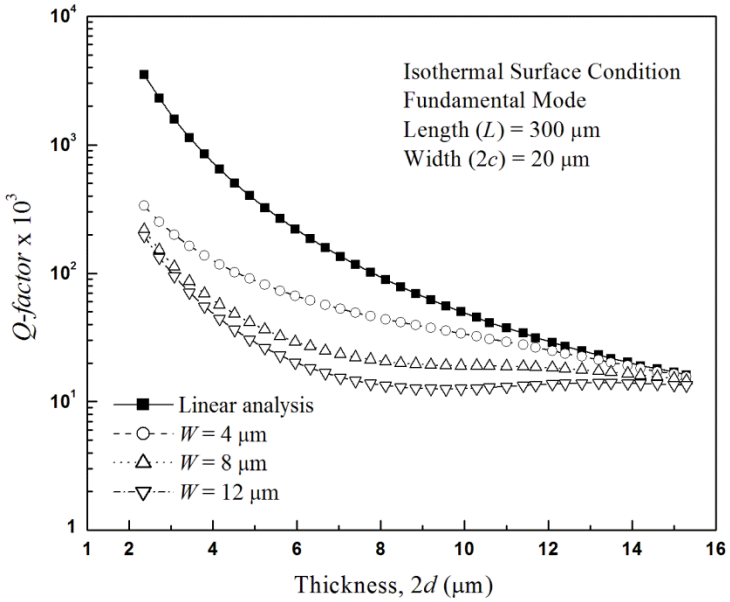

Fig. 7.9 *Q-factor* due to thermoelastic dissipation for beam resonators of fine-grained polysilicon (Srikar and Senturia 2002) under isothermal surface condition against different thicknesses of the beams for various amplitudes. *Q-factor* are calculated for both linear and non-linear vibration using the linear natural frequencies of the beams.

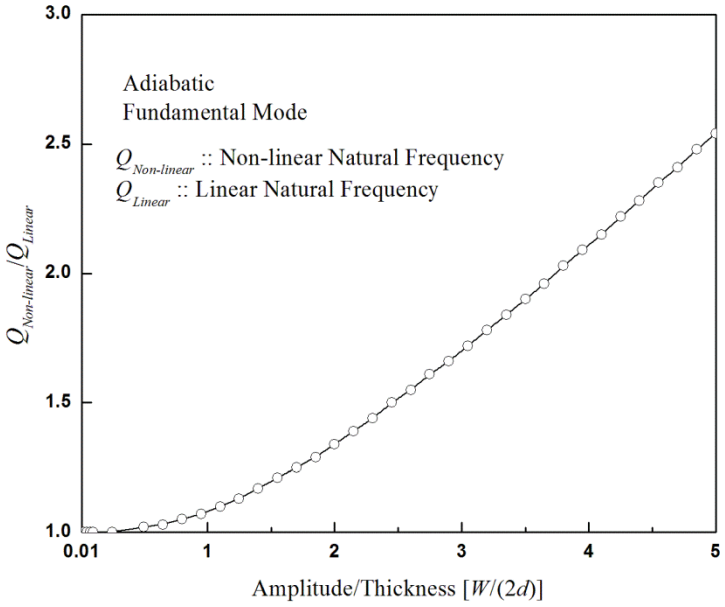

Fig. 7.10 $Q_{Non\text{-}linear}$ (calculated using non-linear natural frequency) due to thermoelastic dissipation for a typical beam resonator (L = 300 μm, $2c$ = 56 μm, $2d$ = 2.1 μm (Srikar and Senturia 2002)) of fine-grained polysilicon (Srikar and Senturia 2002) normalized by Q_{Linear} (calculated using linear natural frequency) under adiabatic surface condition.

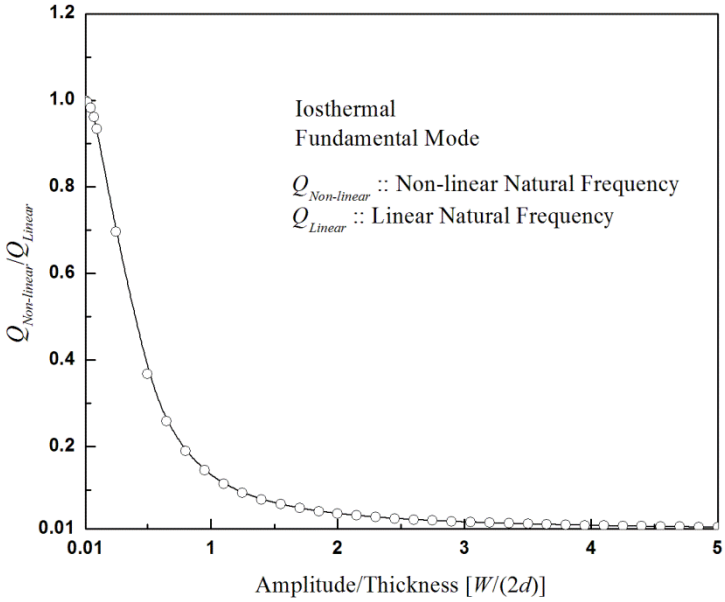

Fig. 7.11 $Q_{Non\text{-}linear}$ (calculated using non-linear natural frequency) due to thermoelastic dissipation for a typical beam resonator (L = 300 μm, $2c$ = 56 μm, $2d$ = 2.1 μm (Srikar and Senturia 2002)) of fine-grained polysilicon (Srikar and Senturia 2002) normalized by Q_{Linear} (calculated using linear natural frequency) under isothermal surface condition.

7.9 References

Ahn Y. and Guckel H. 2000. Fabrication process for high Q polysilicon beam resonators. *Sensors Materials* **12** 143-162.

Bennouna M. M., White R. G. 1984. The effects of large-vibration amplitude on the fundamental mode shape of a clamped-clamped uniform beam. *Journal of Sound and Vibration* **96**(3) 309-331.

Bunch J. S. 2007. Electromechanical resonators from graphene sheets. *Science* **315** 490.

Cimalla V., Niebelschütz F., Tonisch K., Foerster Ch., Brueckner K., Cimalla I., Friedrich T., Pezoldt J., Stephan R., Hein M. and Ambacher O. 2007. Nanoelectromechanical devices for sensing applications. *Sensors and Actuators B* **126** 24-34.

De S. K. and Aluru N. R. 2006. Theory of thermoelastic damping in electrostatically actuated microstructures. *Physical Review B* **74** 14305.

Ekinci K. L. and Roukes M. L. 2005. Nanoelectromechanical systems. *Review of Scientific Instruments* **76** 061101.

Eom K., Park H. S., Yoon D. S. and Kwon T. 2011. Nanomechanical resonators and their applications in biological/chemical detection: nanomechanics principles. *Physics Reports* **503** 115-163.

Gorman D. J. 1975. *Free Vibration Analysis of Beams and Shafts*. John Wiley & Sons, New York.

Hajnayeb A., Khadem S. E. and Zamanian M. 2011. Thermoelastic damping of a double-walled carbon nanotube under electrostatic force. *Micro & Nano Letters* **6** 698-703.

Hao Z., Erbil A. and Ayazi F. 2003. An analytical model for support loss in micromachined beam resonators with in-plane flexural vibrations. *Sensors and Actuators A* **109** 156-164.

Husain A., Hone J., Henk W., Ch. Postma, Huang X. M. H., Drake T., Barbic M., Scherer A., Roukes M. L. 2003. Nanowire-based very-high-frequency electromechanical resonator. *Applied Phyiscs Letters* **83**(6), 1240.

Kaajakari V., Mattila T., Oja A. and Seppä H. 2004. Non-linear limits for single-crystal silicon microresonators. *Journal of Microelectromechanical Systems* **13** 715-724.

Khisaeva Z. F. and Ostoja-Starjewski M. 2006. Thermoelastic damping in nanomechanical resonators with finite wave speeds. *Journal of Thermal Stresses* **29** 201-216.

Kim S. B. and Kim J. H. 2011. Quality factors for the nanomechanical tubes with thermoelastic damping and initial stress. *Journal of Sound and Vibration* **330** 1393-1402.

Kumar S. and Haque M. A 2010. Stress-dependent thermal relaxation effects in micro-mechanical resoantors. *Acta Mechanica* **212** 83-91.

Li M., Tang H. X. and Roukes M. L. 2007. Ultra-sensitive NEMS-based cantilevers for sensing, scanned probe and very high-frequency applications. *Nature Nanotechnology* **2** 114-120.

Lifshitz R. and Roukes M. L. 2000. Thermoelastic damping in micro- and nanomechanical systems. *Physical Review B* **61** 5600-5609.

Masmanidis S. C., Rassul B. K., Iwijn D. V., Gustaaf B., Mark R. F. and Roukes M. L. 2007. Multifunctional nanomechanical systems via tunably coupled piezoelectric actuation. *Science* **317** 780.

Méndez C., Paquay S., Klapka I. and Raskin J. P. 2009. Effect of geometrical non-linearity on MEMS thermoelastic damping. *Non-linear Analysis: Real World Applications* **10** 1579-1588.

Mestrom R. M. C., Fey R. H. B., Phan K. L. and Nijmeijer H. 2010. Simulations and experiments of hardening and softening resonances in a clamped-clamped beam MEMS resonator. *Sensors and Actuators A: Physical* **162** 225-234.

Nayfeh A. H., Younis M. I. 2004. Modeling and simulations of thermoelastic damping in microplates. *Journal of Micromechanics and Microengineering* **14** 1711.

Peng H. B., Chang C. W., Aloni S., Yuzvinsky T. D. and Zettl A. 2006. Ultrahigh frequency nanotube resonators. *Physical Review Letters* **97** 087203.

Pourkamali S., Hashimura A. and Abdolvand R., Ho G.-K., Erbil A. and Ayazi F. 2003. High-Q single crystal silicon HARPSS capacitive beam resonators with self-aligned sub-100-nm transduction gaps. *Journal of Microelectromechanical Systems* **12** 487-496.

Rao B. N. 1992. Large-amplitude free vibrations of simply supported uniform beams with immovable ends. *Journal of Sound and Vibration* **155** 523-527.

Rao G. V. and Raju K. K. 2003. Large-amplitude free vibrations of beams – an energy approach. *Z. Angew. Math. Mech.* **83** 493-498.

Rao G. V., Saheb K. M. and Janardhan G. R. 2008. Simple formula to study the large-amplitude free vibrations of beams and plates. *Journal of Applied Mechanics* **75** 014505-10.

Ray J. D., Bert C. W. 1969. Non-linear vibrations of a beam with pinned ends. *Journal of Engineering for Industries* **91B** 997-1004.

Ru C. Q. 2009. Thermoelastic dissipation of nanowire resonators with surface stress. *Physica E* **41** 1243-1248.

Sharma J. N. 2011. Thermoelastic damping and frequency shift in micro/nanoscale anisotropic beam. *Journal of Thermal Stresses* **34** 650-666.

Singh G., Sharma A. K. and Rao G. V. 1990. Large-amplitude free vibrations of beams – a discussion on various formulations and assumptions. *Journal of Sound and Vibration* **142** 77-85.

Srikar V. T. and Senturia S. D. 2002. Thermoelastic damping in fine-grained polysilicon flexural beam resonators. *Journal of Microelectromechanical Systems* **11** 499-504.

Tseng W. Y., Dugundji J. 1970. Non-linear vinration of a beam under harmonic excitation. *Journal of Applied Mechanics* **37** 292-297.

Tunvir K., Ru C. Q. and Mioduchowski A. 2010. Thermoelastic dissipation of hollow micromechanical resonators. *Physica E* **42** 2341-2352.

Tunvir K., Ru C. Q., Mioduchowski A. 2012. Effect of cross-sectional shape on thermoelastic dissipation of micro/nano elastic beams. *Intlernational Journal of Mechanical Sciences* **62** 77-88.

Unterreithmeier Q. P., Faust T. and Kotthaus J. P. 2010. Damping of nanomechanical resonators. *Physical Review Letters* **105** 027205.

Vahdat A. S. and Rezazadeh G. 2011. Effect of axial and residual stresses on thermoelastic damping in capacitive micro-beam resonators. *Journal of the Franklin Institute* **348** 622-639.

Xie W. C., Lee H. P. and Lim S. P. 2003. Non-linear dynamic analysis of MEMS switches by non-linear modal analysis. *Non-linear Dynamics* **31** 243-256.

Yasumura K. Y., Stowe T. D., Chow E. M., Pfafman T., Kenny W. T., Stipe B. C. and Rugar D. 2000. Quality factor in micros- and submicron-thick cantilevers. *Journal of Microelectromechanical Systems* **9** 117-125.

Zamanian M. and Khadem S. E. 2010. Analysis of thermoelastic damping in microresonators by considering the stretching effect. *International Journal of Mechanical Sciences* **52** 1366-1375.

Zener C. 1937. Internal Friction in Solids. I. Theory of Internal Friction in Reeds. *Physical Review* **52** 230-235.

Zener C. 1938. Internal friction in solids II. General theory of thermoelastic internal friction. *Physical Review* **53** 90-99.

Chapter 8

General Discussion and Conclusions

8.1 Discussion and Conclusion

High *Q-factor* of beam resonator in MEMS/NEMS devices is always the primary concern for uninterrupted performance. Thermoelastic dissipation is a major dissipation mechanism for loss of mechanical energy in MEMS/NEMS beam resonators. Prior to the present study, analyses of thermoelastic dissipation in beam resonators were mainly focused on thin rectangular cross-section. These studies mainly emphasized the effects of size, operating frequency, temperature, and material properties of the beam on thermoelastic dissipation. Dependency of thermoelastic dissipation in beam resonator on size of the beam is found crucial as seen from the experimental studies of Roszhart (1990), Yasumura *et al.* (2000), Yang *et al.* (2002) and Duwel *et al.* (2003). Very few studies explored for ideas that useful in reducing thermoelastic dissipation in beam resonator, for example, Abdolvand *et al.* (2003, 2006), Sairam and Vengallatore (2009) who introduced trench and slots in the body of the beam resonator of thin rectangular cross-section

to change their resonance frequencies and to alter the mechanical and thermal eigenmodes respectively. However, analysis of thermoelastic dissipation for various geometries of beam resonators other than beam resonator of uniform thin rectangular cross-section has never been a topic so far. Nevertheless, practical operating and surface thermal conditions for beam resonators such as non-linear large-vibration (Eom *et al.* 2011; Husain *et al.* 2003), adiabatic and isothermal surface conditions have never been considered in the analysis of thermoelastic dissipation for a system. Therefore, in this dissertation, the effects of various cross-sections of homogeneous and layered composite beam resonators and various operating conditions on thermoelastic dissipation have been studied. The goal is to find better designs and operating conditions for next generation high frequency beam resonators of MEMS/NEMS that offer high performance. Geometries for beam resonators that considered for the study of thermoelastic dissipation are selected from the practically available beam structures at micro/nano scale. Examples would include hollow tubular beams; solid beams of different doubly symmetric and non-doubly symmetric solid cross-sections such as elliptical, triangular, arbitrary rectangular cross-sections; layered composite beam resonators of circular and rectangular cross-sections, and stepped-beam of rectangular cross-section. On the other hand, non-linear large-vibration and small linear vibration are chosen as operating conditions based on the practical relevancies. Nevertheless, for the first time in literature, each aforementioned problem has been solved for two practical surface thermal conditions such as adiabatic and isothermal conditions. The following conclusions are made from this dissertation –

i. Hollow tubular beam resonators are better than solid beam resonators of same size

Thermoelastic dissipation of hollow tubular beam resonators is studied in comparison to beams of solid circular and solid rectangular cross-sections under adiabatic and isothermal surface conditions (Tunvir *et al.* 2010). Thermal field, which is coupled to the deformation fields due to thermoelastic effect, in hollow tubular beam resonator is different from that in solid beam resonators of circular and rectangular cross-sections. In a hollow tubular beam resonator, two boundary-surfaces (inner and outer surfaces) of the cross-section are exposed to the environment, which make its thermal transport behavior different from others. Thermoelastic dissipation strongly depends on the hollow geometry and surface thermal conditions, and the *Q-factor* due to thermoelastic dissipation can be increased by almost two orders of magnitude as compared to a solid circular beam of same outer diameter. Hollow tubular beam resonators, under adiabatic surface thermal condition, have been identified to be better members for next generation gigahertz ($f' \geq 10^9$ Hz) resonators (Peng *et al.* 2006; Gaidarzhi *et al.* 2007; Husain *et al.* 2003) for any wall thickness as compared to solid circular or rectangular cross-section of same cross-sectional area and width. On the other hand, under isothermal surface condition, to achieve a higher *Q-factor* compared to beam resonators of solid rectangular cross-section of same cross-sectional area and width, hollow tubular resonators are best for operating at low frequencies. Similar results are achieved for beam resonator of any wall thickness when compared to a beam resonator of solid circular cross-section. It is suggested that in case of

high frequency applications, a beam resonator with solid rectangular or circular cross-section should be replaced with a hollow tubular beam resonator with appropriate wall thickness. It is believed that these results offer new insight and useful data for the effect of hollow geometry on thermoelastic dissipation of tubular mechanical resonators at micro/nano scales.

ii. Cross-sectional shape have great influence on the thermal field and Q-factor

Beam resonators of elliptical, triangular and arbitrary rectangular cross-section have strong influence on thermoelastic dissipations depending on surface thermal conditions (Tunvir *et al.* 2012a). Replacing a beam of elliptical cross-section by a rectangular beam of same cross-sectional area and width can cause a few tens of percentages in relative error for the cross-sectional aspect ratio up to 10. To achieve a higher *Q-factor*, beam resonators with elliptical or triangular cross-sections are best to operate at high frequencies while beams of rectangular cross-sections of same cross-sectional area and width are best to operate at low frequencies. In particular, for wide ranges of frequencies, beam resonators of elliptical and triangular cross-sections can be the superior members for next generation gigahertz ($f' \geq 10^8$ Hz) resonators. Nevertheless, for the frequencies higher than gigahertz, *Q-factor* of a beam resonator of square cross-section can be as high as 10 times of that for thin rectangular cross-section ($Thickness = Width/10$) of same cross-sectional area under any surface thermal conditions.

iii. A circular cross-section is better than a rectangular one for layered composite beams

At present, layered composite beam structure of circular cross-section is practically available through various fabrication processes as found in the literature (Huang *et al.* 2006; Kim *et al.* 2008; Arslan *et al.* 2008; Czekalla *et al.* 2009; Senthil *et al.* 2009; Liu *et al.* 2010; Wang and Adhikari 2011). Therefore, thermoelastic dissipation in metal-coated ceramic beam resonators of two-layered circular cross-section has been studied in this dissertation in comparison with symmetric three-layered rectangular cross-section of same layer size and materials (Tunvir *et al.* 2012b). Thermoelastic dissipation in layered composite beam resonators of rectangular cross-section always increases with the increasing volume fraction of outer layers under adiabatic surface condition and is always higher than that in homogeneous beam of same size (Bishop and Kinra 1993, 1994, 1997; Vengallatore 2005; Prabhakar and Vengallatore 2007) which is also true for layered composite beam of circular cross-section. However, for any surface thermal condition, a circular cross-section is a better geometry for a high performance layered composite beam resonator. A result supporting the statement shows that for the same total size and material combination, a two-layered circular cross-section with a volume fraction for outer layer of 0.3 suffers equal, if not less, thermoelastic dissipation to a three-layered rectangular cross-section with volume fraction for outer layer of 0.2. For any surface thermal condition, a composite beam of three-layered rectangular cross-section is best for operating at low frequencies while a composite

beam of two-layered circular cross-sections of same material combination and layer size is best for operating at high frequencies. Surface thermal condition has a strong influence on thermoelastic properties of layered composite beam resonator of any cross-section, especially on the frequency corresponding to maximum dissipation. For example, for any particular volume fraction of the outer layer in any cross-section, the frequencies corresponding to maximum dissipations under adiabatic surface condition are always smaller than that under isothermal surface condition.

Another noticeable phenomenon in layered composite beam is the negative values of the lost mechanical works that resulted for individual layer in composite beams. Lost mechanical work in a closed thermodynamic system such as a thermoelastic beam is related to entropy generation. In an isolated system of composite beam (with adiabatic condition on boundary), the individual layers are not isolated systems to each other. Thus during loading of one cycle, total entropy change in a system, say the inner layer, is the combination of entropy generations by itself and entropy exchange with the outer layer which may result in a negative net change of entropy in any layer. On the other hand, composite beam with isothermal boundary condition on outer surface is a closed thermodynamic system in which in addition to generating entropy, individual layers can exchange entropy among them as well as with the surrounding environment. Thus, net change of entropy in individual layers can be negative although the total lost mechanical work or the entropy generation in the entire composite beam is always non-negative.

iv. Stepped-beams are better member for resonators than uniform beams

Thermoelastic dissipation in beam resonators of rectangular cross-section with variation in cross-sectional size at various locations along the length of the beam, also known as stepped-beam, has been studied under adiabatic surface thermal condition because of the presence of these structures in practical applications (Tunvir 2012c). Stepped-beams, either designed or produced by an undercut at the clamped end, are frequently present in various MEMS devices (Gavan *et al.* 2009a, 2009b; Herrera-May *et al.* 2010, 2011). An undercut in beam resonators of MEMS/NEMS is produced during fabrication when the supporting substrate is isotropically etched as a part of the release process of the beam. The doubly-clamped stepped-beams that considered in this dissertation have two sections defined by a single step and section on the left of the step possesses larger cross-sectional size than the other. Three different configurations of stepped-beams with a single step have been considered, such as, stepped-beams having a change in width at the step with constant thickness all over the beam (type-1), change in the thickness at the step with constant width all over the beam (type-2) and cross-sectional changes in both thickness and width at the step (type-3). A type-1 stepped-beam of this study with step position close to the left support represents a beam with an undercut at the support (Gavan *et al.* 2009a, 2009b; Herrera-May *et al.* 2010, 2011). A slender type-1 stepped-beam provides higher *Q-factor* than a uniform beam of same thickness for some particular position of step along the length. For most common lengths of stepped-beams of real applications, the type-1 stepped-beam with step close

to the left support provides higher *Q-factor* than the other stepped-beams of same cross-sectional area and step position. It is to be noted that resonance frequency of a type-1 stepped-beam of a constant length changes with step position without even having change in thickness of the beam and therefore affects the thermoelastic dissipation in them. On the other hand, thermoelastic dissipation under adiabatic surface thermal condition and resonance frequency of a uniform beam resonator of a constant length strictly depends only on the thickness of the beam. Thus in the real applications where a uniform beam resonator of particular length has a constraint in the size of thickness, thermoelastic dissipation in that beam can be reduced by adopting a type-1 stepped feature. Here, the conclusions are made based on the results of doubly-clamped stepped-beam of rectangular cross-section. However, stepped-beams with other end conditions and cross-sectional geometries such as circular cross-section may offer higher quality factor.

v. Non-linear large-amplitude vibration is a better operating condition for doubly-clamped beam resonators

Discussion on operating conditions for beam resonator is one of the main agendas of this dissertation. Analysis of thermoelastic dissipation under non-linear large-vibration is essential for a next generation high frequency beam resonator (Tunvir *et al.* 2012d) since high frequency microbeam resonators are often driven into non-linear regime with larger amplitude in order to store enough energy (Eom *et al.* 2011). In a doubly-clamped beam resonator with non-linear large-vibration, large-deflection creates an axial

stretch of the midplane of the beam due to the clamped condition. Temperature field over the cross-section of a doubly-clamped beam resonator can be changed under non-linear large-vibration depending on surface thermal conditions. Therefore, non-linear large-deflection in a doubly-clamped beam resonator has a significant influence on thermoelastic dissipation, and this effect is very sensitive to surface thermal conditions. More explicitly, the large-deflection significantly increases the *Q-factor* for adiabatic surface conditions, while it considerably decreases the *Q-factor* for isothermal surface condition. This conclusion is mainly attributed to the fact that stretching deformation does not contribute to the loss of mechanical energy under adiabatic surface condition while it has a significant contribution to the lost mechanical energy under isothermal surface condition. These results suggest that doubly-clamped beam resonators should be better driven with larger amplitude under adiabatic surface condition while small-amplitude vibration is preferable for isothermal surface condition. The conclusions are limited to the beam resonator of rectangular cross-section; however, different conclusions may be achieved for beam resonators of other doubly symmetric and non-doubly symmetric cross-sections.

vi. Effect of size of beam resonator on thermoelastic dissipation is non-monotonic

Effect of cross-sectional size of beam resonators on thermoelastic dissipation is one of the most important factors that needed to be understood carefully to design high performance beam resonators for

MEMS/NEMS. For any cross-sectional geometry and any surface thermal condition, a change in the absolute size of the cross-section results in a shift of the frequency corresponding to maximum dissipation under both small linear vibration and non-linear large-vibration which in result affects the thermoelastic dissipation of beam resonator. Moreover, for any cross-sectional geometry, thermoelastic dissipation is a non-monotonic function of the absolute size of the cross-section for both the operating conditions of beam resonators such as linear small vibration and non-linear large-vibration. At least for examples discussed, under any surface thermal condition and linear small vibration, thermoelastic dissipation increases with decreasing cross-sectional size within the micron scale while it decreases with decreasing size within the nano scale and the maximum dissipation appears at a specific size of the order of a few hundreds of nanometers. Under adiabatic surface thermal condition, the specific size of the beam resonator corresponding to maximum-dissipation is almost the same for linear and non-linear vibration, however, under isothermal surface condition, the maximum dissipation occurs at two different sizes for non-linear and linear cases. This result indicates that non-linear large-deflection affects not only the amount of energy dissipation but also the specific size at which the maximum thermoelastic dissipation occurs. These results provide a complete view of size-effect on thermoelastic dissipation of beam resonators of uniform cross-section compared to the partial observations from experimental studies such that decrease in *Q-factor* with decreasing thickness of the resonator indicates the domination of thermoelastic

dissipation (Roszhart 1990; Yasumura *et al.* 2000; Yang *et al.* 2002; Duwel *et al.* 2003).

Effect of size of stepped-beam resonators on thermoelastic dissipation is also non-monotonic. Interestingly, thermoelastic dissipation in a type-1 stepped-beam, which has variation of cross-sectional size at the steps in lateral (width) direction only, depends on the widths of sections of stepped-beam. For example, higher variation of *Q-factor*s for various step positions is observed in a type-1 single-step stepped-beam with higher value of the ratio of widths for the sections (width of left section/width of right section).

This dissertation ends with the conclusion that hereafter for applications at high frequencies, for example close to gigahertz range, beam resonators (homogeneous or layered composite) of solid circular, elliptical, triangular and arbitrary rectangular cross-sections should be used as replacements for beam resonators of rectangular cross-section of equivalent size to achieve high *Q-factor*. Hollow tubular beam resonator may be a perfect replacement for solid circular or solid rectangular cross-section of same size depending on surface thermal conditions for a wide range of operating frequencies. A particular type of stepped-beams that have cross-sectional changes only in widths at the step are better members for beam resonators than beams of uniform cross-section for some particular step positions. Non-linear large-vibration of beam resonator with moderate to large-amplitude of deflection is useful to beam resonators under adiabatic surface thermal condition to achieve high performance. Surface thermal condition is one of the most important factors in the determination of thermoelastic dissipation in beam resonators. Therefore, surface thermal condition in a system should be identified correctly and be used accordingly for numerical calculation.

8.2 Ideas for Future Works

This dissertation shares various novel ideas for designing beam resonators in MEMS/NEMS based on real structures and suggests various practical operating conditions that are in favor of reducing thermoelastic dissipation in beam resonators. Hollow tubular beams, stepped-beams of rectangular cross-section, solid beams of various cross-sections such as elliptical, triangular, and arbitrary rectangular cross-sections, layered composite beams of circular cross-section are found better in performance for wide frequency range than the existing beam resonators of thin rectangular cross-section of equivalent size. Thermoelastic dissipation in the aforementioned beam structures is studied for linear small vibration or non-linear large-amplitude vibration, for adiabatic and isothermal surface conditions. However, some further works are recommended for understanding their applicability to particular jobs. Such recommendations include

i. In the present study, hollow tubular beam resonator, beam resonators of solid arbitrary rectangular, elliptical and triangular cross-section are found superior than the beam resonators of thin rectangular cross-section especially under high frequencies, making them suitable for next generation gigahertz resonator (Peng *et al.* 2006; Gaidarzhi *et al.* 2007) for MEMS/NEMS devices. However, experimental investigation of thermoelastic dissipation at high frequencies should be carried out on these structures to determine their response at high frequencies and to validate the results of the present study.

ii. Thermoelastic dissipation under non-linear large-vibration in this study is done by assuming a simple harmonic oscillation $w(x,t)=w_{\circ}(x)e^{-i\omega t}$ and linear vibration mode $w_o(x)$ to simplify the problem. The assumption is justified based on the view that the focus of the study is to determine the effect of large-deflection on deformation-induced temperature. Though this assumption had been adopted frequently in previous studies of vibration problem, for example, Ray and Bert (1969), Tseng and Dugundji (1970), Bennouna and White (1984), it provides the upper bound on the exact solution of non-linear frequency by satisfying only the equation of motion at the instant of maximum deflection. Therefore, under non-linear large-vibration, effect of non-linear mode shape and higher harmonics on thermoelastic dissipation should be studied to determine the difference from the results of present study.

iii. Microbeam resonators often are driven into non-linear regime with larger amplitude in order to store enough energy (Eom *et al.* 2011; Husain *et al.* 2003). Analysis of thermoelastic dissipation for non-linear large-vibration is a crucial and time demanding work as done in this dissertation. However, in present work, the solution is shown only for doubly symmetric beam resonators (such as arbitrary rectangular cross-section). Thus as an extension of the present work, thermoelastic dissipation for beam resonator of non-doubly symmetric cross-sections such as triangular cross-section should be studied under non-linear large-vibration. The combination of beam resonator of triangular cross-section and non-linear large-vibration may provide a very high performance resonator for MEMS/NEMS.

iv. A type-1 stepped-beam with a single step (having variation only in the width of rectangular cross-section at the step), which is found to be the best in respect of less thermoelastic dissipation among various types of doubly-clamped stepped-beams, possesses two sections. Of the two sections, one has smaller length and larger width than the other, and is attached to one support. Due to large width and small length for this section at the support, the stepped-beam may suffer energy dissipation due to support since loss of energy due to support is directly proportional to the width while inversely proportional to the length of the beam resonator (Judge *et al.* 2007; Hosaka *et al.* 1995). On the other hand, thermoelastic dissipation of the type-1 stepped-beam resonators depends on the width of different sections and positions of the step along the length of the beam. Therefore, dissipation due to support in stepped-beam should be investigated along with thermoelastic dissipation to determine an optimum size for type-1 stepped-beam. Nevertheless, based on the results of previous studies of cross-sectional effect on thermoelastic dissipation, stepped-beam with circular cross-section can be analyzed for possible member of beam resonator with higher *Q-factor* than rectangular cross-section.

v. Thermoelastic dissipation in layered composite beams of rectangular and circular cross-sections has been studied in this dissertation under the assumption of a perfect thermal contact at the interfaces of two adjacent layers. The assumption requires the temperature and the heat flux to be continuous across the interface given by the following equations

$$\Delta T_j = \Delta T_{j+1} \qquad \text{at} \quad z = z_{Interface} \tag{8.1}$$

$$\kappa_j \frac{\partial(\Delta T_j)}{\partial z} = \kappa_{j+1} \frac{\partial(\Delta T_{j+1})}{\partial z} \qquad \text{at} \quad z = z_{Interface} \tag{8.2}$$

However, in real engineering problem, the adjacent layers may not always have perfect thermal contact at the interface due to delamination, cracks etc. (Lin *et al.* 2003; Yan *et al.* 2009; Misra *et al.* 2009) and thus may produce a thin film of interface layer. In this case, Eqs. (8.1) and (8.2) are needed to be revised considering the properties of the thin film of interface layer. The solution of thermoelastic dissipation incorporating this problem is needed to be investigated in future.

8.3 References

Abdolvand R., Ho G. K., Erbil A. and Ayazi F. 2003. Thermoelastic damping in trench-refilled polysilicon resonators. *Transducer '03: The 12th International Conference on Solid State Sensors, Actuators and Micro Systems* 324-327.

Abdolvand R., Johari H., Ho G. K., Erbil A. and Ayazi F. 2006. Quality factor in trench-refilled polysilicon beam resonators. *Journal of Microelectromechanical Systems* **15** 471-478.

Alblas J. B. 1961. On the general theory of thermo-elastic friction. *Applied Science Research* **10** 349-362.

Arslan I., Talin A. A., Wang G. T. 2008. Three-dimensional visualization of surface defects in core-shell nanowires. *Journal of Physical Chemistry C* **112** 11093-11097.

Bennouna M. M., White R. G. 1984. The effects of large-vibration amplitude on the fundamental mode shape of a clamped-clamped uniform beam. *Journal of Sound and Vibration* **96**(3) 309-331.

Bishop J. E. and Kinra V. K. 1993. Thermoelastic damping of a laminated beam in flexure and extension. *Journal of Reinforced Plastics and Composites* **12** 210.

Bishop J. E. and Kinra V. K. 1994. Elastothermodynamic damping in composite materials. *Mechanics of Composite Materials and Structures* **1** 75-93.

Bishop J. E. and Kinra V. K. 1997. Elastothermodynamic damping in laminated composites. *International Journal of Solids and Structures* **34** 1075-1092.

Czekalla C., Sturm C, Schmidt-Grund R, Cao B., Zúñiga Pérez J., Lorenz M., and GrundmannM. 2009. Optical characterization of zinc oxide microlasers and microwire core-shell heterostructures. *Journal of Vacuum Science Technology B* **27** 1780-1783.

Duwel A., Gorman J., Weinstein M., Borenstein J., Ward P. 2003. Experimental study of thermoelastic damping in MEMS gyros. *Sensors and Actuators A* **103** 70-75.

Eom K., Park H. S., Yoon D. S. and Kwon T. 2011. Nanomechanical resonators and their applications in biological/chemical detection: nanomechanics principles. *Physics Reports* **503** 115-163.

Gaidarzhy A.**,** Imboden M., Mohanty P.,Rankin J., Sheldon B. W. 2007**.** High quality factor gigahertz frequencies in nanomechanical diamond resonators. *Applied Physics Letters* **91** 203503.

Gavan K. B., Drift E. W. J. M. van der, Venstra W. J., Zuiddam M. R., Zant H. S. J. van der 2009a. Effect of undercut on the resonant behavior of silicon nitride cantilevers. *Journal of Micromechanics and Microengineering* **19** 035003.

Gavan K. B., Westra H. J. R., Drift E. W. J. M. van der, Venstra W. J., Zant H. S. J. van der 2009b. Impact of fabrication technology on flexural resonances of silicon nitride cantilevers. *Microelectronics Engineering* **86** 1216-1218.

Herrera-May A. L., Aguilera-Cortés L. A., García-Ramírez P. J., Plascencia-Mora H., Torres-Cisneros 2010. Modeling of the intrinsic stress effect on the resonant frequency of NEMS resonators integrated by beams with variable cross-section. *Microsystems Technology* **16** 2067-2074.

Herrera-May A. L., García-Ramírez P. J., Aguilera-Cortés L. A., Plascencia-Mora H., García-González L., Manjarrez E., Narducci M., Figueras E. 2011. Analytical Modeling for the Bending Resonant Frequency of Sensors Based on Micro and Nanoresonators With Complex Structural Geometry. *IEEE Journal of Sensors* **11** 1361.

Hosaka H., Itao K., Kuroda S. 1995. Damping characteristics of beam-shaped micro oscillators. *Sensors and Actuator A* **49** 87-95.

Huang L., Lau S. P., Yang H. Y., Yu S. F. 2006. Local measurement of secondary electron emission from ZnO-coated carbon nanotubes. *Nanotechnology* **17** 1564-1567.

Husain A., Hone J., Henk W., Ch. Postma, Huang X. M. H., Drake T., Barbic M., Scherer A., Roukes M. L. 2003. Nanowire-based very-high-frequency electromechanical resonator. *Applied Phyiscs Letters* **83**(6), 1241.

Imboden M., Mohanty P., Gaidarzhy A., Rankin J., Sheldon B. W. 2007. Scaling of dissipation in megahertz-range micromechanical diamond oscillators. *Applied Physics Letters* **90** 173502.

Judge J. A., Photiadis D. M., Vignola J. F., Houston B. H., Jarzynski J. 2007. Attachment loss of micromechanical and nanomechanical resonators in the limits of thick and thin support structures. *Journal of Applied Physics* **101**(1) 013521.

Kim W. H., Lee W. J. and Shim S. H. 2008. Composite nanowires with MgO/ZnO core-sheath structures: study of thin ZnO shell layers. *Journal of Physics and Chemistry of Solids* **69** 1491-1494.

Lifshitz R. and Roukes M. L. 2000. Thermoelastic damping in micro- and nanomechanical systems. *Physical Review B* **61** 5600-5609.

Lin S., Narita F., Shindo Y. 2003. Comparison of energy release rate and energy density criteria for a piezoelectric layered composite with a crack normal to interface. *Theoretical and Applied Fracture Mechanics* **39** 229–243.

Liu J., Wang C., Xie Q., Cai J., Zhang J. 2010. Hierarchical Cd_4SiS_6/SiO_2 heterostructures nanowire arrays. *Nanoscale Research Letters* **5** 231-236.

Misra A., Zhang X, Demkowicz M. J., Hoagland R. G., Nastasi M. 2009. Design of Nano-composites for ultra-high strengths and radiation damage tolerance. *Materials Research Society Symposium Proceedings - Cambridge University Press* **1188** 1188-LL06-01.

Mohanty P., Harrington D. A., Ekinci K. L., Yang Y. T., Murphy M. J., Roukes M. L. 2002. Intrinsic dissipation in high-frequency micromechanical resonators. *Physical Review B* **66** 085416.

Peng H. B., Chang C.W., Aloni S., Yuzvinsky T. D., Zettl A. 2006. Ultrahigh frequency nanotube resonators. *Physical Review Letters* **97** 087203.

Prabhakar S. and Vengallatore S. 2007. Thermoelastic damping in bilayered micromechanical beam resonators. *Journal of Micromechanics and Microengineering* **17** 532-538.

Ray J. D., Bert C. W. 1969. Non-linear vibrations of a beam with pinned ends. *Journal of Engineering for Industries* **91B** 997-1004.

Roszhart T. V. 1990. The effect of thermoelastic internal friction on the Q of micromachined silicon resonators. *IEEE Sensors* 13-16.

Sairam P. and Vengallatore S. 2009. Thermoelastic damping in hollow and slotted microresonators. *Journal of Microelectromechanical Systems* **18** 725-735.

Senthil K., Tak Y., Seol M., Yong K. 2009. Synthesis and characterization of ZnO nanowire-CdO composite nanostructures. *Nanoscale Research Letters* **4** 1329-1334.

Tseng W. Y., Dugundji J. 1970. Non-linear vinration of a beam under harmonic excitation. *Journal of Applied Mechanics* **37** 292-297.

Tunvir K., Ru C. Q., Mioduchowski A. 2010. Thermoelastic dissipation of hollow micromechanical resonators. *Physica E* **42** 2341-2352.

Tunvir K., Ru C. Q., Mioduchowski A. 2012a. Effect of cross-sectional shape on thermoelastic dissipation of micro/nano elastic beams. *Intlernational Journal of Mechanical Sciences* **62** 77-88.

Tunvir K., Ru C. Q. and Mioduchowski A 2012b. Thermoelastic dissipation in micromechanical composite beam resonators (Submitted to *Composites Part B: Engineering*, Under Review).

Tunvir K. 2012c. Thermoelastic dissipation in stepped-beam resonators. *Microsystem Technologies.* Published Online as Online First Articles. DOI: 10.1007/s00542-012-1676-9.

Tunvir K., Ru C. Q. and Mioduchowski A. 2012. "Large-deflection Effect on Thermoelastic Dissipation ofMicrobeam Resonators." *Journal of Thermal Stresses* (Proof submitted; Expected online publication date November 08, 2012)

Vengallatore S. 2005. Analysis of thermoelastic damping in laminated composite micromechanical beam resonators. *Journal of Micromechanics and Microengineering* **15** 2398-2404.

Wang C. Y. and Adhikari S. 2011. ZnO-CNT composite nanotubes as nanoresonators. *Physics Letters A* **375** 2171-2175.

Yan W., Cai J. B., Chen W. Q. 2009. Monitoring interfacial defects in a composite beam using impedance signatures *Journal of Sound and Vibration* **326** 340–352.

Yang J., Ono T., Esashi M. 2002. Energy dissipation in submicrometer thick single-crystal silicon cantilevers. *Journal of Microelectromechanical Systems* **11** 775-783.

Yasumura K. Y., Stowe T. D., Chow E. M., Pfafman T., Kenny W. T., Stipe B. C., Rugar D. 2000. Quality factor in micros- and submicron-thick cantilevers. *Journal of Microelectromechanical Systems* **9** 117-125.

Zener C. 1937. Internal friction in solids. I. Theory of internal friction in reeds. *Physical Review* **52** 230-235.

Zener C. 1938. Internal friction in solids II. General theory of thermoelastic internal friction. *Physical Review* **53** 90-99.

Chapter 9

Appendices

9.1 Appendix A

In chapter 7, expression for mode shape $w_o(x)$ is used to determine $\int_0^L \left(\frac{d^2 w_o}{dx^2}\right)^2 dx$ and

$\left[\int_0^L \left(\frac{dw_o}{dx}\right)^2 dx\right]^2$ of Eq. (7.22) for any vibration mode such that

$$\int_0^L \left(\frac{d^2 w_o}{dx^2}\right)^2 dx = \frac{W^2 \beta_n^{\,3}}{8 J_n^{\,2} L^3}\left[K'_1 + K'_2 \cos\beta_n + K'_3 \sin\beta_n + K'_4 \sin\beta_n \cos\beta_n\right] = \frac{W^2 \beta_n^{\,3} U_n}{8 J_n^{\,2} L^3} \qquad \text{(A9.1)}$$

$$\left[\int_0^L \left(\frac{dw_o}{dx}\right)^2 dx\right]^2 = \frac{W^4 \beta_n^{\,2}}{64 q_n^{\,4} L^2}\left[K'_5 + K'_6 \cos\beta_n + K'_7 \sin\beta_n + K'_8 \sin\beta_n \cos\beta_n\right]^2 = \frac{W^4 \beta_n^{\,2} V_n}{64 J_n^{\,4} L^2} \qquad \text{(A9.2)}$$

where,

$$U_n = K'_1 + K'_2 \cos\beta_n + K'_3 \sin\beta_n + K'_4 \sin\beta_n \cos\beta_n$$

$$V_n = \left[K'_5 + K'_6 \cos\beta_n + K'_7 \sin\beta_n + K'_8 \sin\beta_n \cos\beta_n\right]^2$$

$$K'_1 = 8\beta_n + 4\psi_n + e^{2\beta_n}\left(1 + 2\psi_n + \psi_n^{\,2}\right) - e^{-2\beta_n}\left(1 - 2\psi_n + \psi_n^{\,2}\right)$$

$$K'_2 = -8\psi_n \cos\beta_n + e^{\beta_n}\left(4 - 4\psi_n^{\,2}\right) - e^{-\beta_n}\left(4 - 4\psi_n^{\,2}\right)$$

$$K'_3 = e^{\beta_n}\left(4 + 8\psi_n + 4\psi_n{}^2\right) + e^{-\beta_n}\left(4 - 8\psi_n + 4\psi_n{}^2\right)$$

$$K'_4 = 4 - 4\psi_n{}^2$$

$$K'_5 = 8\beta_n\psi_n{}^2 + 4\psi_n + e^{2\beta_n}\left(1 + 2\psi_n + \psi_n{}^2\right) - e^{-2\beta_n}\left(1 - 2\psi_n + \psi_n{}^2\right)$$

$$K'_6 = 8\psi_n \cos\beta_n - e^{\beta_n}\left(4 + 8\psi_n + 4\psi_n{}^2\right) + e^{-\beta_n}\left(4 - 8\psi_n + 4\psi_n{}^2\right)$$

$$K'_7 = \left(4 - 4\psi_n{}^2\right)\left(e^{\beta_n} + e^{-\beta_n}\right)$$

$$K'_8 = 4\psi_n{}^2 - 4$$